A high energy electron-photon detector employing flash tube arrays

Tait, I. D.

A HIGH ENERGY ELECTRON-PHOTON DETECTOR

EMPLOYING FLASH TUBE ARRAYS

by

I.D. TAIT B.Sc.

A thesis submitted to the University of Durham

for the Degree of Doctor of Philosophy

Being an account of the work carried out

at the University of Durham

during the period October 1973 to September 1976

ACKNOWLEDGEMENTS

The author would like to thank Professor A.W. Wolfendale for his support of this work and the use of his laboratory facilities.

He is indebted to his supervisor, Dr. J.M. Breare, for his encouragement and guidance throughout the work.

Dr. B.C. Nandi, W. El Disouki, J.E. Chaney and P.J. Doe are thanked for their collaboration in part of this work, and the members of the Nuclear Instrumentation Group are thanked for their useful discussions.

Dr. R.J. Stubbs is thanked for his most useful criticisms, and his wife Dr. F.W. Stubbs for the typing of the thesis.

He would also like to thank the staff of the Daresbury Laboratory for their continued interest and help, and for the use of facilities.

Mr. R. McDermott and Mr. J. Webster are thanked for building most of the experimental apparatus, and the International Research and Development Co. are acknowledged for manufacturing the flash tubes.

The Science Research Council is thanked for providing a research studentship.

Lastly, but by no means least, the author would like to thank his wife, Ruthie, for her continuous encouragement and patience.

CONTENTS

ABSTRACT

The development of a high energy electromagnetic shower detector for use in high energy electron or photon detection, particularly in machine experiments, is described. The detector is a modified version of a prototype chamber, which was successfully tested, and which is described briefly in this thesis. The detector gives fully digitised information from which incident particle energies and trajectories can be estimated.

The detector consists of twelve flash tube arrays sandwiched between lead target. A total of 768 tubes are employed. They have an internal diameter of 0.8 cm., a wall thickness of 0.03 cm. and are filled with a gas mixture of Ne(70%)-He(30%) + 2% CH_4 at 2.3 atmospheres pressure. The operation of these tubes under various working conditions has been extensively studied and the results are presented in the thesis.

The detector has been tested in the positron beam at the Daresbury Laboratory, where digitised information was obtained using a computerised data acquisition system.

The energies of the positrons used ranged from 0.5 to 3.5 GeV. Analysis of the data showed that the chamber operated satisfactorily in high backgrounds of radiation and was very capable in the detection of electromagnetic showers, giving energy and spatial resolutions comparable to those obtained by the conventional, more complex and more expensive detecting systems.

However, the use of the detector was restricted to working at several events per minute, due to the build up of large induced clearing fields inside the flash tubes.

The build up of these fields is shown to be greatly reduced by the use of a modified pulsing system, and further tests are to be carried out using this pulsing system, with the view of increasing the working rate of the chamber to 50 Hz.

CHAPTER ONE

INTRODUCTION

Flash tubes were first developed at Pisa (1) during 1954-55 where they were used by Conversi and Gozzini in the study of cosmic rays. A flash tube consists of a sealed glass tube filled with an inert gas positioned between two parallel-plate electrodes. On the passage of an ionizing particle through the tube, the plates are pulsed by an electric field of magnitude a few kilovolts per centimetre. The electrons left by the primary ionizing particle are accelerated towards the anode plate and gain sufficient energy to produce secondary electrons. The avalanches generated produce luminous discharges which may be photographed, or digitised information may be obtained from probes placed on the tube windows.

Several arrays of these parallel-plate electrodes filled with flash tubes constitute a flash tube hodoscope which may be used to define particle trajectories.

Flash tubes, because of their very long sensitive and recovery times were mainly confined to cosmic ray research, whereas the spark chamber, a later development of the flash tube principle, had a number of characteristics which justified its use in many experiments with particle accelerators. These included a short and adjustable sensitive time, a greater efficiency in detecting single ionizing particles, a short recovery time and a smaller volume of insensitive material. This meant that spark chambers were used exclusively in the fast rate accelerator experiments. Development in the field of flash tubes greatly declined and a lot of their

versatile characteristics were overlooked. However, the work done by several groups on their development, notably the recent work at Durham and Rome, has opened up new possibilities for their use in accelerator experiments

One important way in which flash tubes could greatly contribute in the high energy physics field is in the detection of high energy photons and electrons, and this thesis describes the development of such a detector.

Some detectors that have been used recently in the detection of high energy photons or electrons in accelerator experiments are described in the following paragraphs.

The present method of detecting high energy photons or electrons in the GeV energy range is by the detection of the electromagnetic showers they produce in suitable targets such as lead, lead glass or lead/scintillator sandwiches. Detectors which give both spatial and energy information usually utilize several different detecting techniques. The trajectories of the secondaries produced in a shower are normally studied by spark chambers, proportional counters or lead scintillator hodoscopes, and the energy of the incident particle is obtained mainly from a total absorption device such as a lead glass hodoscope or a lead/scintillator sandwich placed behind the trajectory detectors. However, some energy information may be obtained from the trajectory detectors.

A detector which has been used recently at the CERN Intersecting Storage Rings to detect photons and electrons in the 1 - 10 GeV range consisted of a spark chamber-lead glass combination (2). Track location was given by ten planes of wire spark chambers with magnetic core readout and energy measurements were given by

two walls of lead-glass Cherenkov counters consisting of 76 glass blocks, each viewed by a photomultiplier.

A similar detecting technique ~~has been~~ will be used on the Omega experiment (3) at CERN where the positions and momenta of π^0 s having energies up to 100 GeV will be measured from the detection of the gammas produced from the $\gamma\gamma$ decay mode of the π^0 s.

Spark chambers and lead/scintillator sandwich combinations have also been used for photon and electron detection (4,5,6), the most recent by Basile et al. (5) where photons and electrons in the energy range of 1 GeV were measured. The detector consisted of two six-gap, thin plate spark chambers followed by nine sandwiched elements, each element consisting of a spark chamber and a plastic scintillator. Most of the information obtained from the detector was recorded by photographic methods. The trajectories of the secondaries produced in a shower were studied by the thin plate spark chambers and energy information was obtained from the total number of sparks counted in the rear spark chambers together with pulse height measurements from the scintillators.

Allkofer et al. (7) used 21 glass spark chambers interspaced with iron targets in the detection of electromagnetic showers. The glass spark chambers had a much greater multitrack efficiency than conventional spark chambers employing metal plate electrodes, however, the repetition rate of the detector was restricted to several events per minute.

A detector has recently been proposed for photons in the energy range 1 - 100 GeV on a Super Proton Synchrotron experiment at CERN (8). It consists of a pre-shower detector comprising a lead-scintillator sandwich with crossed scintillator hodoscopes, a three plane proportional chamber, and finally two lead glass hodoscopes each containing 240 glass blocks.

The use of a drift chamber lead glass combination to give spatial information in shower development has been proposed by Rosny (17).

A method has recently been persued where the electromagnetic showers are detected by a sandwich of lead targets and orthogonally placed flash tube arrays (9, 10). This method could provide a simple and inexpensive alternative to the very complex and expensive systems used at present. In this method, three dimensional information about the development of a shower is recorded by flash tubes. Using this information, an estimate can be made of the primary particle trajectory, and measurements of its energy can also be achieved from the total number of tubes that ignite. This number gives a sampled measure of the number of secondaries produced in the shower, which is proportional to the energy of the incident particle. (see chapter 3)

Flash tubes have a number of features which make them very suitable for the detection of high energy photons and electrons in accelerator experiments. The most important is high multitrack efficiency, which enables them to be used in the detection of showers. This high multitrack efficiency results from the use of glass as the tube material; the high resistance limits the current flowing in a tube so that all the available energy is not taken by any one tube. Spark chambers on the other hand, have low multi-track efficiency (11) due to the robbing of available energy by one or more sparks.

The high multitrack efficiency of flash tubes has been fully exploited in the past in the field of cosmic rays by many workers, the most striking example being that of the large scale flash tube hodoscope chambers used by the air shower group at Kiel (12).

A simple and inexpensive method of digitising flash tube information has recently been developed (13) and has been successfully used on several computer linked flash tube experiments (see chapter 2, section 2.6.3).

Flash tubes are also very robust, unlike many of the wire chambers used in shower detection, and they are found to give reliable and reproducible results after many years in service (14). Also they do not possess the added complications of operation such as a gas flow system or accurately positioned mirror systems present in spark chamber experiments.

They are very flexible in that they can be made into any required shape, hence 4π geometry detection is possible using circular tubes. They can also be dismantled and re-assembled into arrays of different configurations and hence utilised in other experiments requiring different areas or geometries of detection.

Another advantage in using flash tubes is that they are relatively inexpensive and the cost of a flash tube is independent of its length. Recent estimates (1976 prices) (15) have given an average cost of £7.00 per tube. This price includes the cost of an associated pulsing system and a data aquisition system as far as a computer interface. This enables larger detecting areas to be covered by flash tubes than by conventional detecting systems for the same cost.

The following chapter describes the operation of flash tubes and some of the recent developments that have taken place in their design resulting in shorter sensitive and recovery times.

A prototype flash tube chamber designed by Chaney et al. (16) for use in the detection of high energy electrons or photons

in accelerator experiments is described briefly in chapter 3. The analysis of the results obtained from testing this chamber in a positron beam was carried out by Chaney and the author, and the analysis procedure and results obtained are described in detail. The subsequent development of a modified flash tube chamber designed by Chaney et al. has been carried out by the author, and is described in the following chapters.

REFERENCES

1. Conversi, M., Gozzini, A. (1955) Nuovo Cim. 2 189
2. Beale, J.S. et al. (1974) Nucl. Inst. & Meth. 117 501
3. Dowell, J.D., Sloan, T. (1972) Internal Report, Birmingham University, 72-06
4. Massam, T. et al. (1965) Nuovo Cim. 41 464
5. Basile, M. et al. (1972) Nucl. Inst. & Meth. 101 433
6. Agrinier, B. et al. (1965) Nuovo Cim. 36 1077
7. Allkofer, O.C. et al. (1973) Proc. Int. Conf. Cosmic Rays. Denver. 2761
8. Proposed Experiments and Equipment for a Programme of Muon Physics at the S.P.S. (1974) CERN/SPSC/74-78 206
9. Chaney, J.E. et al. (1975) Nucl. Inst. & Meth. 125 189
10. Conversi, M. (1973) Riv. del Nuovo Cim. 3 274
11. Cronin, J.W. et al. (1962) Rev. Sci. Inst. 33 946
12. Bagge, E. et al. (1965) Proc. Int. Conf. Cosmic Rays London. 2 738
13. Ayre, C.A., Thompson, M.G. (1969) Nucl. Inst. & Meth. 69 106
14. Coxell, H., Wolfendale, A.W. (1960) Proc. Roy. Soc. 75 378
15. Breare, J.M. (1976) Private Communication, University of Durham
16. Chaney, J.E., Breare, J.M. (1975) Nucl. Inst. & Meth. 124 61
17. De Rosny, G. (1975) E-γ Symposium, Glasgow University, 7

CHAPTER TWO

THE OPERATION OF FLASH TUBES

2.1 REQUIREMENTS

The satisfactory operation of flash tubes requires the application of a pulsed electric field across them on the traversal of an ionizing particle. If the time delay between the traversal of the ionizing particle and the application of the pulsed field is short enough, and the operating conditions are correct, then free electrons remaining in the gas produce localised avalanches under the accelerating effect of the field. Subsequent photon emission causes the discharge to spread very quickly and this results in a bright, visible discharge along the length of the tube.

2.2 EXPERIMENTAL ARRANGEMENTS

A very effective, and the most frequently used method of applying the pulsed electric fields was first developed by Conversi (1). This entails the formation of a parallel plate electrode system with flash tubes sandwiched between them. Alternate plates are connected to ground, the remaining plates being connected to a high voltage pulsing system (see figure 2.1).

Pulsed electric fields transverse to the tube length are usually employed, however, when very small diameter (2) or short length tubes are used (3) the applied field is in the longitudinal

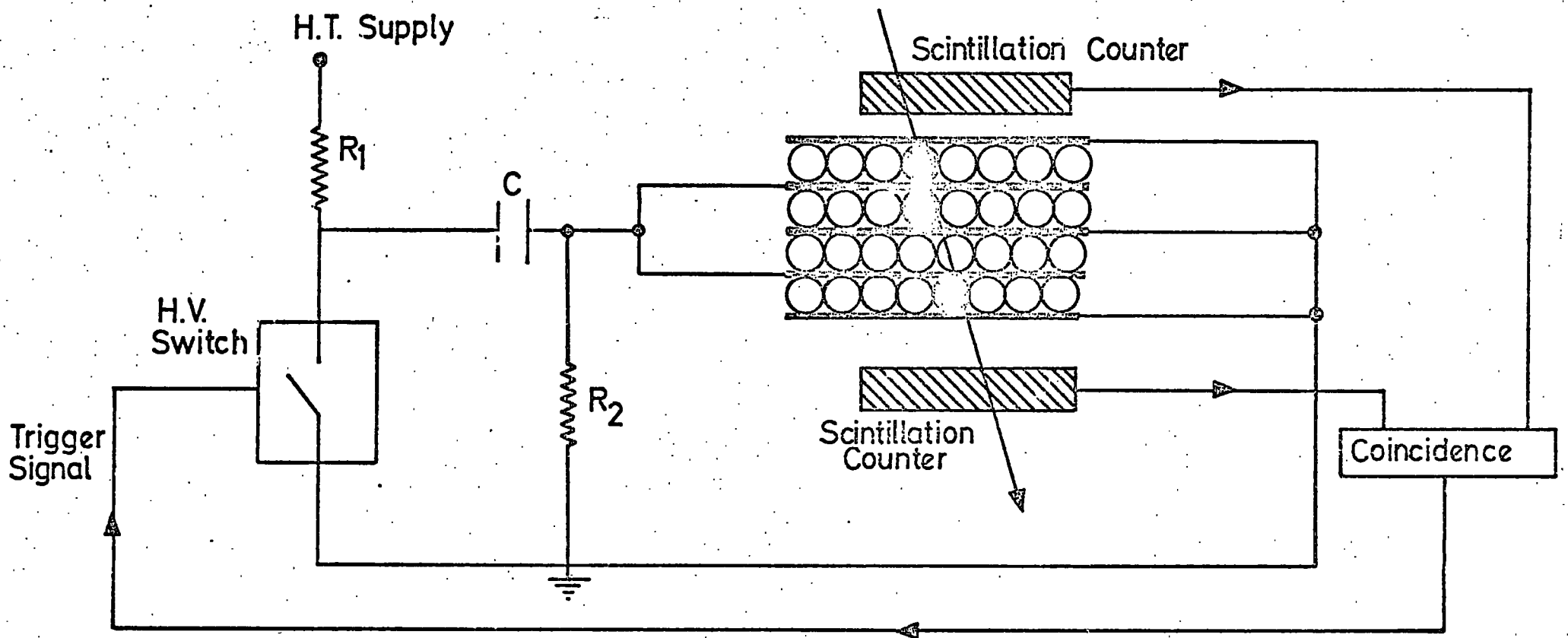

Fig. 2.1 A pulsing circuit for flash tubes.

direction.

In most applications the high voltage electrodes are flat metal sheets or grids, however in some applications where 4π geometry is a necessity then concentric circular plates or grids are used (4).

The area of the electrodes and the number of flash tubes used depends on the experimental requirements, however, the size of the array in a CR decay high voltage pulsing system is limited by its capacitance which determines the rise time of the applied electric field (5). Chambers of up to 0.1 μF have been operated satisfactorily (6).

The flash tube spacing and plane separation have been extensively studied by Bull et al. (7) and by Ashton (8) who have found optimum values for locating single particle trajectories and for ionization measurements for single particles passing through a flash tube array.

2.3 GAS MIXTURE AND PRESSURE

The gas mixture used in conventional flash tubes has varied considerably, however, all have been mixtures of the noble gases (9, 10, 11, 12). Noble gases are used for several reasons which include their high stability, low breakdown voltages and copious visible and ultraviolet emission during discharge. The once predominantly used mixture of Ne(98%)-He(2%) has now been superseded by the Ne(70%)-He(30%) mixture which has similar characteristics but is cheaper and more readily available commercially.

The pressure of the gas mixture has been studied by several authors (9, 13, 14) and the optimum working pressures are found to

depend to a large extent on the diameter of the flash tubes. The pressure should be such that a sufficient mass of gas is traversed by the ionizing particle to produce adequate numbers of secondaries, ensuring that several remain in the gas on the application of the pulsed electric field. There should also be sufficient matter in the tube volume to produce satisfactory avalanches on the application of the pulsed electric field.

The majority of flash tubes in use at present are either about two centimetres in diameter and filled at 600 torr, or about one centimetre in diameter and filled at 2.3 atmospheres.

2.4 FLASH TUBE CHARACTERISTICS

2.4.1 EFFICIENCY

The most important and convenient parameter specifying the performance of a flash tube is its efficiency, or the probability that it will discharge after the passage through it of an ionizing particle.

Because of the inherent insensitive material present in a flash tube array two efficiency parameters have been defined. These are the internal efficiency η, which is defined as the probability of a tube flashing if an ionizing particle passes through the gas of the tube, and the layer efficiency η_L, which represents the probability of a tube flashing and hence registering the passage of an ionizing particle through a layer of tubes.

The layer efficiencies of tubes are normally measured experimentally, from which the internal efficiencies can be obtained

using the relation;

$$\eta = \eta_L \frac{D}{d} \cos\Theta$$

where D is the distance between tube centres, d is the internal diameter of the tubes, and Θ is the angle between the particle trajectories and the perpendicular to the flash tube planes. The efficiency of flash tubes is a function of many factors and these have been extensively studied by many authors. Factors include high voltage pulse characteristics such as magnitude, rise time, width and delay (9, 10, 15, 16), gas mixtures (see sections 2.3, 2.7.3) temperature (17) and flashing rates (14, 18, 19, 20).

The fundamental factor affecting the efficiency is the magnitude of the applied field. In correctly functioning tubes the efficiency is found to increase with magnitude of the applied field until a plateau region is reached corresponding to an internal efficiency of about 100%. Further increase in the magnitude of the field beyond the plateau region then produces spurious flashing. The magnitude of the field used under normal working conditions is on this plateau.

Spurious flashing can be caused by several factors, the most common being the application of too large a field across the tubes; this can then produce ionization via field emission which leads to spurious flashing.

Another cause of spurious flashing is a factor which is always present in flash tubes, that is, ionization produced in the tubes resulting from background radiations. This effect cannot be removed but can almost always be estimated and taken into account in efficiency measurements.

The most serious cause of spurious flashing is the contamin-

ation of the inside walls of the tubes or of the gas mixture. The most common contaminants are minute particles of dirt which give rise to field emission and hence discharging of the tubes. These effects cannot usually be removed and tubes exhibiting them must be re-cleaned and re-filled.

2.4.2 SENSITIVE TIME

Another important flash tube parameter is the sensitive time, t_s. This is defined as the time delay between the passage of an ionizing particle and the application of the pulsed field such that the internal efficiency of the flash tubes falls to 50%. Conventional flash tubes have sensitive times of the order of tens of microseconds.

A considerable amount of theoretical work has been done by several authors on this topic, notably by Lloyd (21), however, discrepancies between theoretical and experimental results were observed, which have since been attributed to induced clearing fields (18, 19, 20, 22,23, 24, 25, 26). Clearing fields are discussed in the following section.

2.4.3 INDUCED CLEARING FIELDS

After the discharge of a flash tube, charges are deposited on the inside surfaces of the tube. These charges produce an induced field in an opposite direction to that of the applied field. Because of the high resistance of the glass the induced fields can take a relatively long time to decay. Fields of about 10^{-2} V cm^{-1}

may remain for tens of minutes after the discharge of a tube (23, 27). These fields have the effect of sweeping to the walls any ionization left by an ionizing particle passing through the tube. This means that on the application of the pulsed electric field fewer electrons remain in a 'formative region', that is, a region over which the electrons can form suitable avalanches before collision with the tube walls. The sensitive times of the tubes are therefore reduced, giving lower values than those predicted from theoretical considerations based on simple electron diffusion.

The magnitude and decay time of clearing fields have been studied by several authors (23, 24, 25, 27), and is a subject of study in this thesis (see chapter 7, section 7.2.2).

2.4.4 RECOVERY TIME

After an initial discharge a finite time is taken for the gas plasma to disperse making the tube ready for further detection of ionizing particles. This gives rise to another flash tube parameter, the recovery time t_r, defined such that a flash tube subject to a pulsed electric field t_r seconds after a discharge has a reignition probability of 50%. Conventional flash tubes have recovery times of the order of hundreds of milliseconds.

A theoretical study of recovery times has been done by Brosco (28), but the values he obtained for t_r were much smaller than those found experimentally. No full explanation has been found for these discrepancies, however, metastable atoms or molecules present in a tube after a discharge are thought to play some part in the lengthening of t_r.

2.5 THE PULSING SYSTEM

There are two common methods of generating high voltage pulses for flash tubes. The simpler one, which is used for the work in this thesis, is the CR discharge technique. In this case a high voltage capacitor of value C is charged to a potential V_o, and then quickly discharged over a resistor of value R, in parallel with the flash tubes of capacity C_1. This produces a high voltage pulse, decaying with time, of the form $V = -V_o \exp(-t/R(C + C_1))$ (see figure 2.1). The capacitor is discharged by the closing of a fast high voltage switch on receiving a trigger signal.

The second method is by the discharging of a lumped circuit transmission line which has been charged to a potential V_o. The line can either be discharged into its characteristic impedance Z_o, or the Blumlein method can be used, where two coupled lines, each of characteristic impedance Z_o, are discharged. Both methods produce rectangular pulses, the former rising to $-V_o/2$, with no delay, and the latter to $-V_o$, with an intrinsic delay equal to half the pulse width.

The applied pulsed fields must have fast rise times so that electrons left by the ionizing particle are not swept out of the gas before avalanches are produced. This requires the use of fast high voltage switching techniques.

The high voltage switches employed in flash tube work are usually trigatron spark gaps (29), which are themselves triggered by EG & G HV100 trigger supplies (30), or hydrogen thyratron pulsing units. The latter are three stage devices which work from NIM standard signals. The first stage consists of a single transistor

(MPS6530) working in avalanche mode, triggered by the NIM signal. The second stage consists of a small Xenon thyratron (Mullard 2021W), which is used as a buffer between the transistor input stage and the output stage which consists of a hydrogen thyratron. This is a ceramic device manufactured by English Electric Ltd. (CX1157).

Trigger signals, signifying the passage of an ionizing particle through a stack of flash tubes, are usually obtained as coincidence signals from several sets of scintillator-phototube arrangements, forming a particle telescope (see figure 2.1). In most applications the time delay between the coincidence signal and the application of the pulsed field is as short as possible, however delays are often introduced to obtain estimates of the charge of the ionizing particles (31), and to suppress discharges due to knock on electrons accompanying multiply charged nuclei (32).

2.6 OUTPUT INFORMATION

2.6.1 OPTICAL METHODS

As described in section 2.1 the passage of an ionizing particle through a flash tube is accompanied by the discharge of the tube, the light output of which has been extensively studied by Coxell et al. (33). Emission is predominantly in the yellow-red region due to the Ne and He present in the tube, and is sufficiently intense to be easily seen by eye or recorded on most fast red-sensitive films such as Ilford Mark V, HP3 and Kodak Trix. Photography, using mirror systems, is standard practice on many extensive air shower arrays employing flash tubes (3, 34).

Cadmium selenide light cells placed on the tube windows have been used successfully where photography proves difficuly (35). However, such systems are quite expensive and complex, and simpler systems employing light activated silicon controlled rectifiers have been proposed by Evans and Baker (36). A method of scanning flash tube arrays by a vidicon system giving digitised information has been developed by Harrison and Rastin (37), and later, the scanning, by vidicon methods, of optical fibres coupled to the flash tubes was proposed by Conversi et al. (4).

The possibility of viewing large air shower arrays of flash tubes by several phototubes has also been suggested by Coxell et al. (33), the outputs from the photomultipliers giving a measure of the total number of tubes that ignite.

2.6.2 PLASMA PROBES

Several groups (4, 38) have used metal probes projecting inside the flash tubes. The plasma formed during a discharge produces a pulse on the probe. Such systems have the advantage that information both from light output and probes can be utilised (4).

2.6.3 EXTERNAL PROBES

A very simple and effective method of digitising flash tube information was developed by Ayre and Thompson (39). This method involves the positioning of well screened external probes on the flash tube windows. Signals of several hundred volts are then obtained on these probes when the tubes discharge. These signals

result from the capacitive coupling between the plasma formed in the tube and the probe. They can be reduced by a resistive potential divider and used to drive conventional electronics without the need for any amplifier interfacing, thus forming an inexpensive means of digitisation. This method has been used successfully on the M.A.R.S. spectrograph (40) where digitised information is stored via an "on line" computer system. This method has been used sucessfully in sending digital data from flash tubes at rates up to 50 Hz (14).

2.7 THE DEVELOPMENT OF FLASH TUBES FOR ACCELERATOR EXPERIMENTS

2.7.1 CRITERIA

For satisfactory operation of flash tubes in accelerator experiments the tubes must be able to function correctly in relatively high backgrounds of radiation, possibly in the region of 10^5 particles/tube/second, and they must be able to work at repetition rates in excess of 50 Hz. It would also be a great advantage if the flash tube information were in digitised form, as this would greatly facilitate data handling, enabling the use of computer "links" for experiments and allowing computational methods of analysis to be used "on" or "off" line.

2.7.2 REDUCTIONS IN FLASH TUBE SENSITIVE TIMES

The high backgrounds of radiation associated with accelerator experiments necessitate flash tube sensitive times to be less than the mean time between background particles, this requires sensitive

times in the one microsecond region whereas, as has been stated, conventional flash tubes have sensitive times of the order of tens of microseconds.

The method of externally applied DC clearing fields had been used successfully in reducing the sensitive times of spark chambers (41) however, this technique proved inadequate in flash tube operations (13). This was attributed to the movement of charges on the glass surfaces of the tubes thereby backing off the externally applied DC field. Further work at Durham and Rome (42, 43) lead to the development of externally applied AC clearing fields of 50 Hz or more. These frequencies proved too high for the charges to follow, and externally applied AC clearing fields of several volts per centimetre were found to reduce the sensitive time to the microsecond region (see figure 2.2).

The long tails present on the curves are due to events occurring in the lower voltages of the sinusoidal clearing fields, these tails are greatly reduced by using square wave clearing fields.

2.7.3 REDUCTIONS IN FLASH TUBE RECOVERY TIMES

The recovery times of flash tubes have been greatly reduced, enabling them to be used at the high repetition rates encountered in accelerator experiments. This has been achieved by the addition of certain impurity gases to the conventional noble gas mixture, these impurities include SF_6 (43), O_2 (44), H_2, CO_2, C_2H_6, C_4H_{10}, (24) and CH_4 (14). Workable tubes with recovery times of the order of a millisecond have been produced at Durham (14) by the addition of up to 2% Methane to the noble gas mixture, Ne(70%)-He(30%) (see figure 2.3).

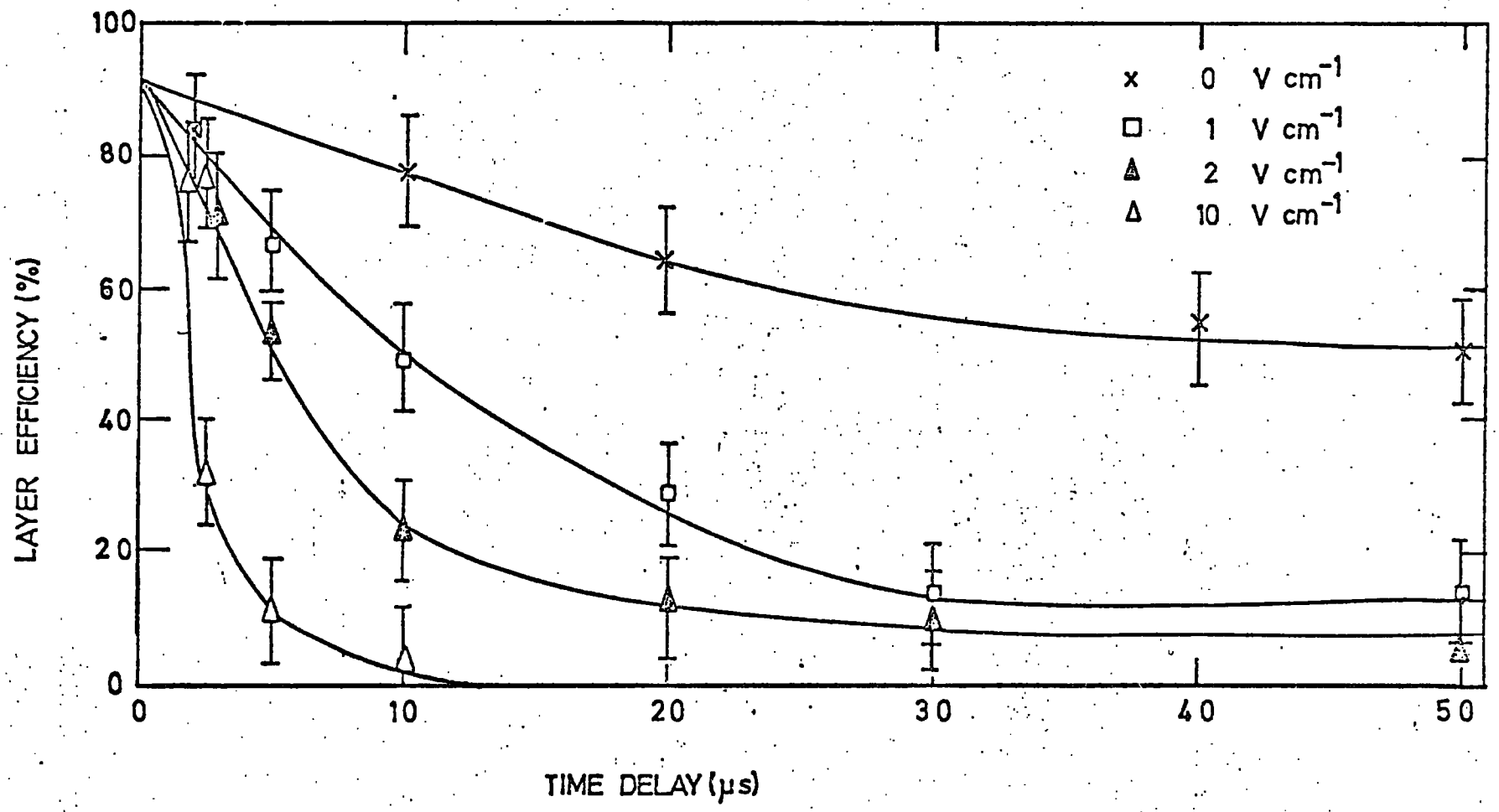

Efficiency versus Time Delay for several Sinusoidal Clearing Fields.

Fig. 2-2

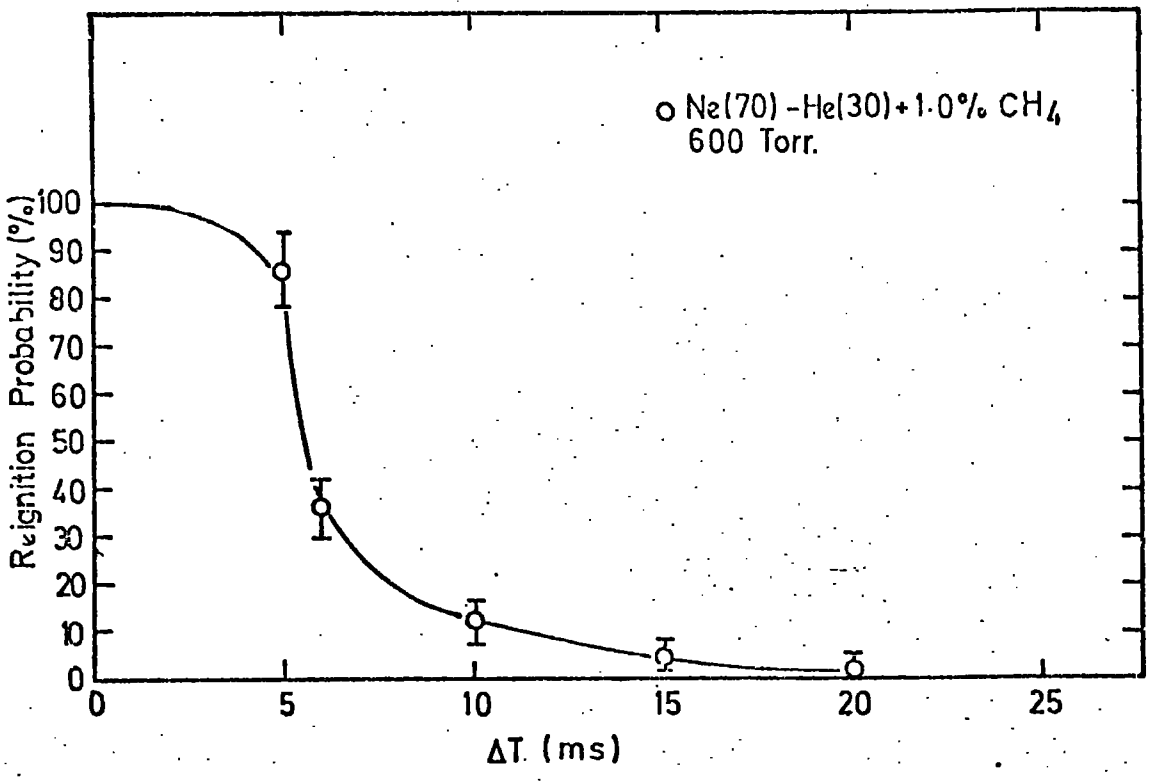

Reignition Probability versus Time Interval for 1·6cm. internal diameter tubes filled at 600 Torr.

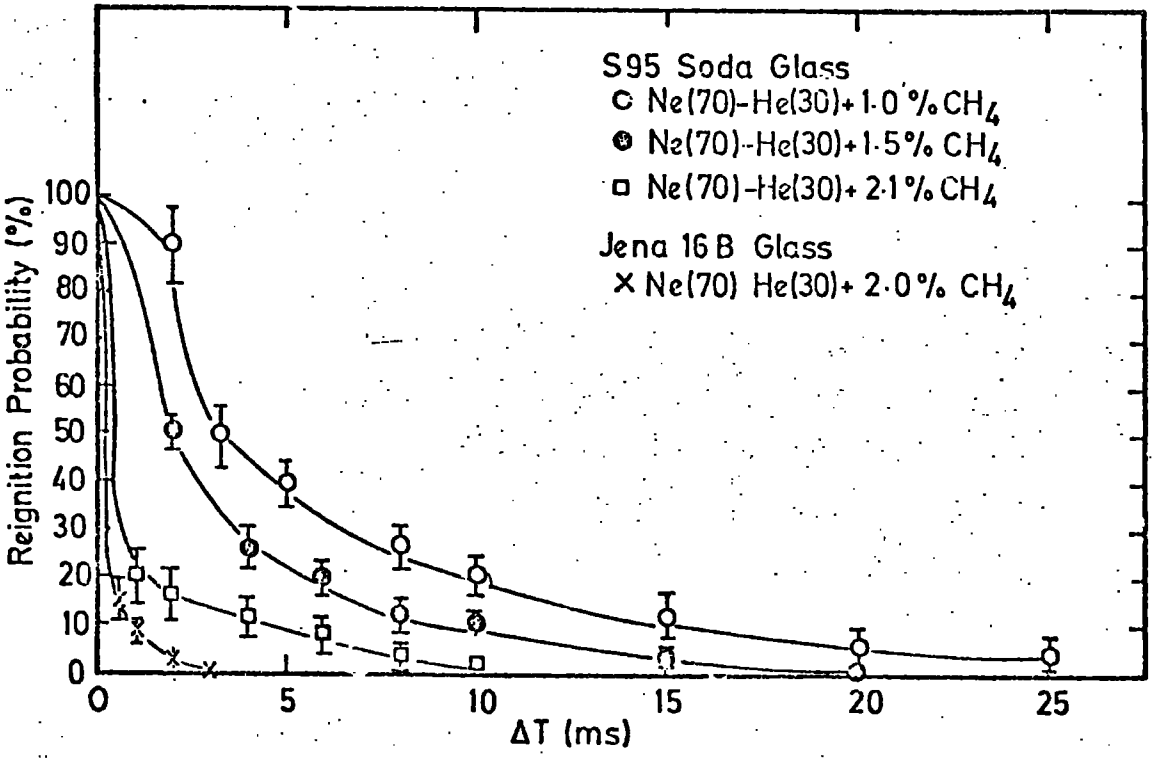

Reignition Probability versus Time Interval for 0·6 cm. internal diameter tubes filled at 2·3 atmospheres.

Fig. 2·3

The mechanism by which the methane reduces the recovery time of the tubes is not fully understood, however the reduction in the number of metastable atoms and molecules present in the gas via Penning de-excitation is thought to be a major effect.

2.7.4 REDUCTIONS IN INDUCED CLEARING FIELDS

Much work has been done on the possible uses of lower resistance glasses in flash tube manufacture (43, 45), thus facilitating the decay of internally induced clearing fields. This work has now resulted in flash tubes for use at high repetition rates being made from Jena 16B glass (14) whose resistivity at room temperature is $6 \times 10^{10} \Omega$ cm, (45), a factor of 80 less than the resistivity of S95 glass used in conventional flash tube manufacture.

Various forms of pulsing systems have also been used to reduce the induced clearing fields with some degree of success (22, 46, 47).

2.7.5 RECENTLY DEVELOPED FLASH TUBES FOR ACCELERATOR WORK

Several research groups have now produced flash tubes that have worked satisfactorily under accelerator conditions.

Flash tubes made of Jena G20 glass having an external diameter of 2 cms. and a filling of Ne(30%)-He(70%) at 375 torr were successfully tested at Adone, the Frascati storage ring, where data was recorded photographically from a flash tube hodoscope chamber at repetition rates up to 1 Hz, (12, 48).

A flash tube hodoscope chamber for use in high energy photon or electron detection has also been successfully tested at Frascati (4, 49). Tubes having an external diameter of one cm. were used, they were made from Jena 16B glass and filled with a mixture of Ne(30%)-He(70%) at 0.5 atmosphere.

A prototype flash tube chamber was built at Durham and was used successfully in the detection of positrons, sending fully digitised information at repetition rates up to 50 Hz without any deterioration in efficiency (14, 50). The tubes used had an external diameter of 1.8 cm., and were made of S95 soda glass filled with a mixture of Ne(30%)-He(70%) + 1% methane at 600 torr.

The flash tubes were manufactured by The International Research and Development Company of Newcastle-upon-Tyne, as were many of the flash tubes used both at Rome and at Durham.

A modified detector is now being developed at Durham employing tubes made of Jena 16B glass, having external diameters of 0.9 cm. and fillings of Ne(30%)-He(70%) + 2% methane at 2.3 atmospheres (15).

The following chapter describes the reults obtained from the testing of the prototype chamber built at Durham on a positron beam.

REFERENCES

1. Conversi, M., Gozzini, A. (1955) Nuovo Cim. 2 189
2. Breskin, A., Charpak, G. (1973) Nucl. Inst.& Meth. 108 27
3. Bagge, E. et al. (1965) Proc. Int. Conf. Cosmic Rays. London. 2 738
4. Conversi, M. (1973) Riv. del Nuovo Cim. 3 274
5. Lewis, I.A.D., Wells, F.W. Millimicrosecond Pulse Techniques. Pergamon Press
6. Ashton, F. et al. (1973) Proc. Int. Conf. Cosmic Rays. Denver. 4 3000
7. Bull, R.M. et al. (1962) Suppl. Nuovo Cim. 23 39
8. Ashton, F. Private Communication, University of Durham
9. Barsanti, G. et al. (1956) Proc. CERN Symp. 2 56
10. Gardener, M. et al. (1957) Proc. Phys. Soc. B70 687
11. Breare, J.M., Holroyd, F.W. (1972) Internal Report, University of Durham
12. Conversi, M. et al. (1972) Nuovo Cim. Lett. 3 483
13. Coxell, H., Wolfendale, A.W. (1960) Proc. Phys. Soc. 75 378
14. Chaney, J.E., Breare, J.M. (1975) Nucl. Inst. & Meth. 124 61
15. Breare, J.M. et al. (1976) Nucl. Inst. & Meth. 133 415
16. Holroyd, F.W. (1971) Ph. D. Thesis, University of Durham
17. Breare, J.M. et al. (1973) Proc. Int. Conf. on Inst. for High Energy Phys. Frascati. 415
18. Ferguson, H., Rastin, B.C. (1971) Nucl. Inst. & Meth. 96 405
19. Holroyd, F.W., Breare, J.M. (1972) Nucl. Inst. & Meth. 100 429
20. Breare, J.M. et al. Nucl. Inst. & Meth. In the Press
21. Lloyd, J.L. (1960) Proc. Phys. Soc. 75 387

22. Crouch, M.F. (1969) Internal Group Report. Case Western Reserve University

23. Ashton, F. et al.(1971) Lett. Nuovo Cim. 2 707

24. Chaney, J.E. (1973) Ph.D. Thesis, University of Durham

25. Breare, J.M., Doe, P.J. (1976) Nucl. Inst. & Meth. 133 247

26. Brosco, G. et al. (1973) Proc. Int. Conf. on Inst. for High Energy Phys. Frascati. 211

27. Holroyd, F.W., Breare, J.M. (1972) Nucl. Inst. & Meth. 100 227

28. Brosco, G. (1973) Proc. Int. Conf. on Inst. for High Energy Physics. Frascati. 207

29. Stubbs, R.J. (1971) Ph.D. Thesis, University of Durham

30. EG & G Inc. Instruction Manual No. B-3179A

31. Ashton, F. et al.(1971) J. Phys. A. Gen. Phys. 4 895

32. Funch, O, et al. (1973) Proc. Int. Conf. Cosmic Rays, Denver. 4 3023

33. Coxell, H. et al. (1961) Suppl. Nuovo Cim. 21 597

34. Hooke, J.R. (1973) Ph.D. Thesis, University of Durham

35. Reines, F. (1967) Proc. Roy. Soc. 301 125

36. Evans, W.M., Baker, J.C. (1971) Internal Report, Rutherford High Energy Laboratory, RHEL/M/H/4

37. Harrison, D.J., Rastin, B.C. (1970) Nucl. Inst. & Meth. 77 181

38. Bacon, D.F., Nash, W.F. (1965) Nucl. Inst. & Meth. 37 43

39. Ayre, C.A., Thompson, M.G. (1969) Nucl. Inst. & Meth. 69 106

40. Ayre, C.A. et al. (1972) Nucl. Inst. & Meth. 102 29

41. Meyer, M.A. (1963) Nucl. Inst. & Meth. 23 277

42. Chaney, J.E. et al. (1973) Lett. Nuovo Cim. 6 339

43. Brosco, G. et al. (1973) Nucl. Inst. & Meth. 111 477

44. Breare, J.M. et al. (1973) Proc. Int. Conf. on Inst. for High Energy Phys. Frascati. 215

45. Breare, J.M. et al. (1973) Proc. Int. Conf. on Inst. for High Energy Phys. Frascati. 221

46. Bemporad, C. et al. (1973) Proc. Int. Conf. on Inst. for High Energy Phys. Frascati. 193

47. Breare, J.M. et al. (1976) Nucl. Inst. & Meth. in the Press

48. Borgia, B. et al. (1971) Phys. Lett. 35 340

49. Brosco, G. (1972) Ph.D. Thesis, University of Rome

50. Chaney, J.E. et al. (1975) Nucl. Inst. & Meth. 125 189

CHAPTER THREE

THE OPERATION OF A PROTOTYPE FLASH TUBE CHAMBER IN A POSITRON BEAM

3.1 INTRODUCTION

The flash tubes developed by Chaney et al. (1) (see chapter 2, section 2.7.5) at Durham, containing a 1% addition of methane to the Ne(70%) - He(30%) mixture, were found to give characteristics suited to working in high backgrounds of radiation and at high repetition rates. Chaney et al. built a chamber containing these tubes in order to carry out a series of tests on the positron beam facility at the Daresbury Laboratory.

These tests were planned to verify the satisfactory operation of the tubes in high backgrounds of radiation, to register their efficiency for various working rates and to test their suitability for high energy photon and electron detection by the detection and study of electromagnetic showers produced in the chamber by positrons having energies of a few GeV.

The electromagnetic showers developed by high energy photons and electrons were found experimentally (2) and theoretically (3, 4) to be very similar, hence the positron beam could also be used to simulate high energy photon induced showers.

3.2 THE FLASH TUBE CHAMBER

A diagram of the flash tube chamber is shown in figure 3.1.

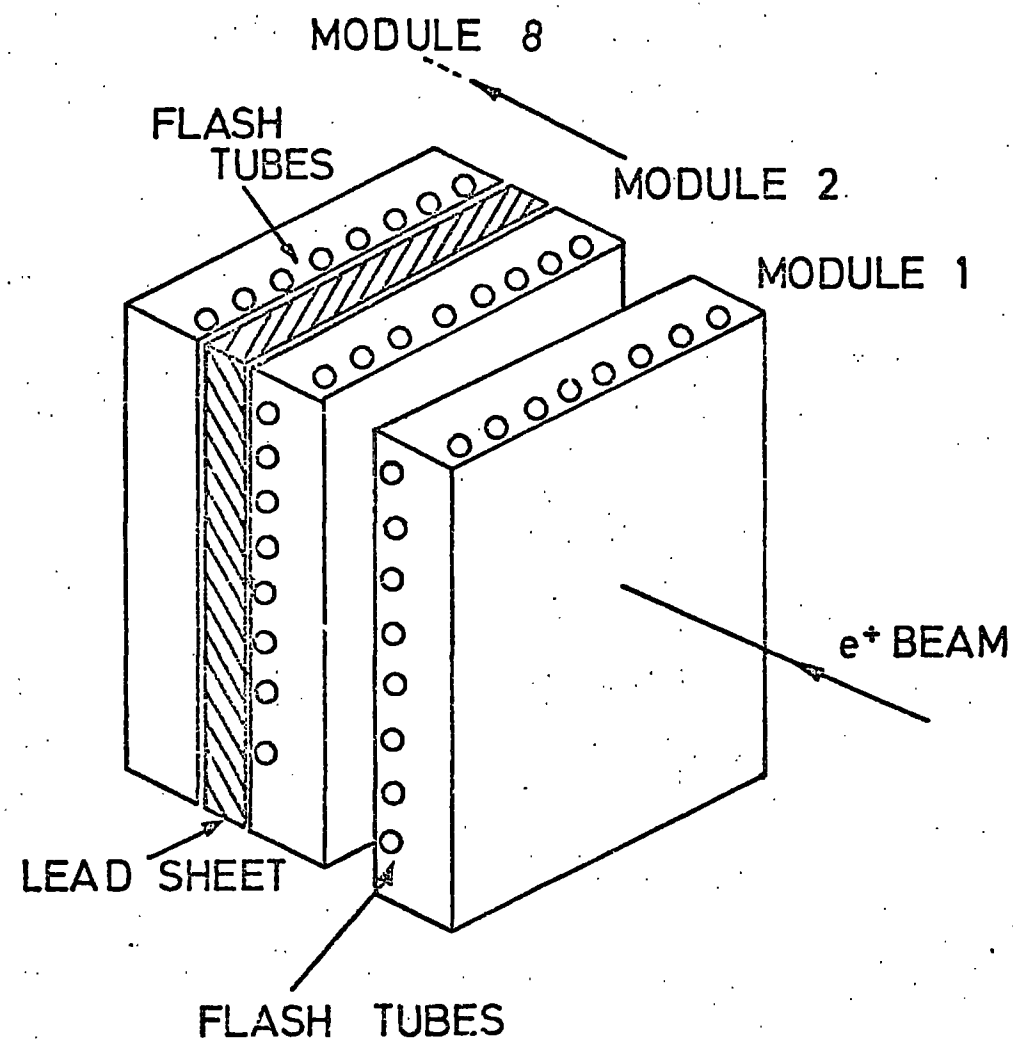

Fig. 3.1

The prototype flash tube chamber.

It consisted of eight separate, self contained electrode modules, each containing two sets of eight 1.6 cm. internal diameter flash tubes. Each set of tubes was positioned in orthogonal X-Y planes on either side of a central H.T. electrode. A space was provided between each module for accommodating up to two radiation lengths of lead target. The tubes were made to fit closely together and rested on digitisation probes which were supported in machined aluminium blocks. The blocks provided an earth screen for the probes against electrical interference from the high voltage pulsing unit which consisted of a CR decay system employing a trigatron spark gap (see chapter 2, section 2.5)

The flash tube chamber was exposed to an almost parallel positron beam, the energy resolution of which was $\pm$ 1% (5). The energy of the incident positrons was varied between 0.5 GeV and 4 GeV.

Output pulses were taken from the digitisation probes through two metres of doubly screened 50 Ω coaxial cable, without any electronic amplifier interfacing and fed directly into eight 16-bit CAMAC pattern units (16 P 2007), where the information was stored in address registers before being read by a PDP 11 computer. Several events were stored in the computer, then the data was copied to paper tape.

The flash tubes were made from type S 95 soda glass, of 1.6 cm. internal diameter, 0.1 cm wall thickness and filled with Ne(70%) He(30%) plus 1% methane at 600 torr pressure. They had a recovery time of about 7 ms. (1). A 30 V cm^{-1} square wave clearing field was applied, giving sensitive times of about 1.0 μ s. (6).

3.3 RESULTS TAKEN ON THE POSITRON BEAM

3.3.1 EFFICIENCY

The chamber was first tested on the positron beam without any lead target between the modules. Straight through positron tracks were then detected for various working rates.

The chamber functioned satisfactorily under the accelerator conditions and gave an overall layer efficiency of about 80% for various working rates between 5 and 50 Hz, the layer efficiency of every module remaining above 70% (1).

3.3.2 REIGNITION PROBABILITY

Because of the narrowly collimated positron beam there was a high probability of consecutive positrons passing through the same tube; this resulted in a value of about 25% for the measured reignition probability. However, when the dimensions of the beam profile were taken into account, zero value reignition probabilities were found at all working rates. (1).

3.3.3 ENERGY MEASUREMENTS

The chamber was then tested in the positron beam after placing a lead target between each of the modules. Two thicknesses of lead target were used, 1.0 and 2.0 radiation lengths. No target was placed in front of module one as this module was used to give a "true" position of an incident positron.

Data was taken for several thousand showers developed in the chamber for each selected incident positron energy.

3.3.4 ENERGY RESOLUTION

The Monte Carlo simulation of electromagnetic shower development from photons or electrons of a few Gev has been extensively studied by several authors (3, 4, 7, 8). Most of the results obtained are fairly consistent and show a fair agreement with experimental data (9, 10, 11, 12, 13, 14, 15, 16).

Some of the results obtained by Messel and Crawford, and Volkel at DESY on shower development in lead for high energy electrons are shown in figure 3.2. The threshold energy of the secondaries is 2 MeV.

From studying these shower development curves, one finds that the total sum of secondaries obtained by sampling the shower development at fixed radiation lengths, is proportional to the energy of the incident electron or photon (see figure 3.3). This provides a simple and effective method of determining the energy of an electron or photon, producing an electromagnetic shower in a detector which samples the shower development at various positions.

This method is well used on spark chamber experiments where the total number of sparks produced in an electromagnetic shower is summed, thus giving an estimate of the number of secondaries at various positions in the shower (10, 15, 16, 17, 18).

This method was extended to give estimates of the energies of the incident positrons in the flash tube chamber by counting the total number of ignited tubes in a shower, thus giving a sampled

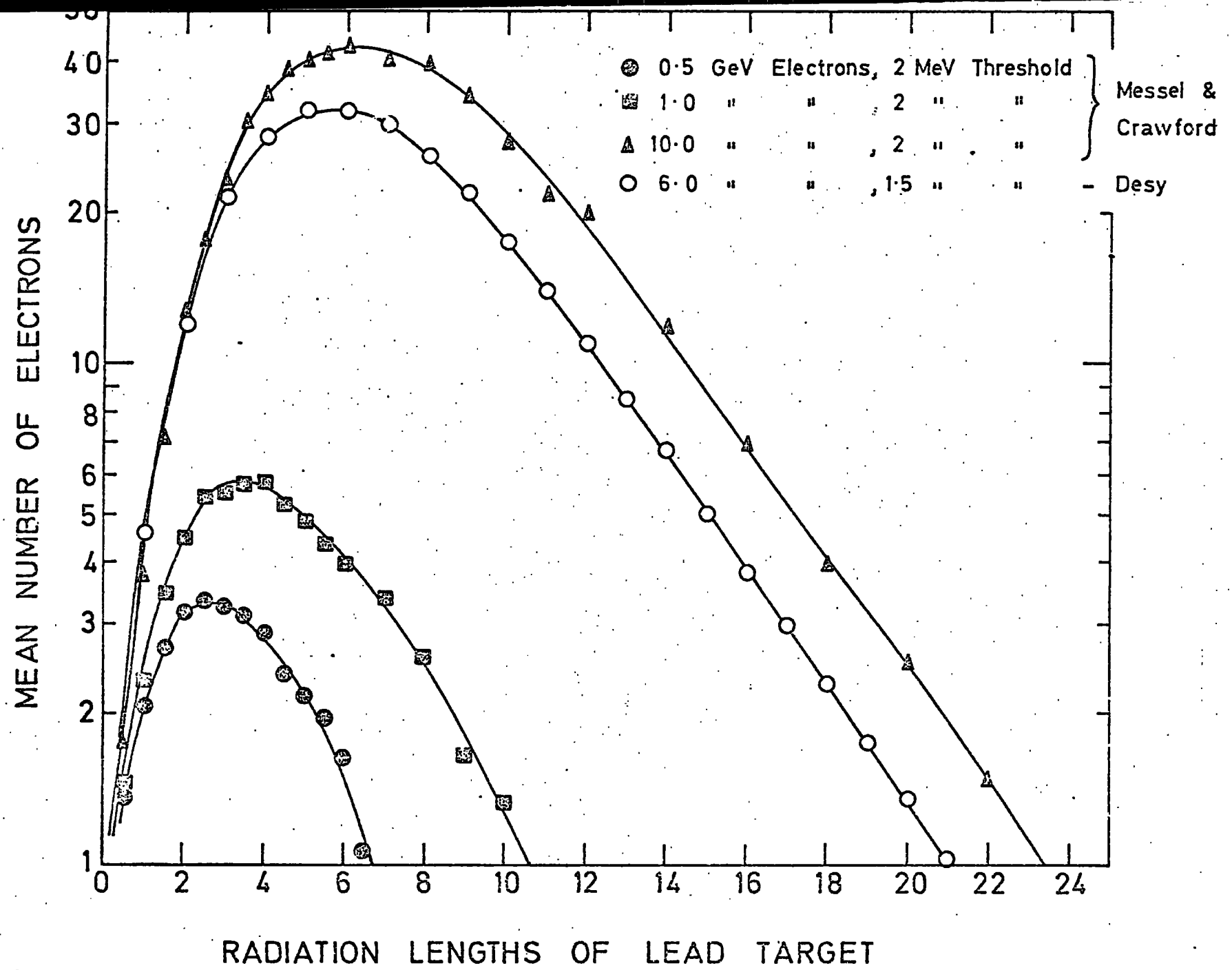

Fig. 3·2 Mean numbers of electrons produced vs target depth for various primary energies.

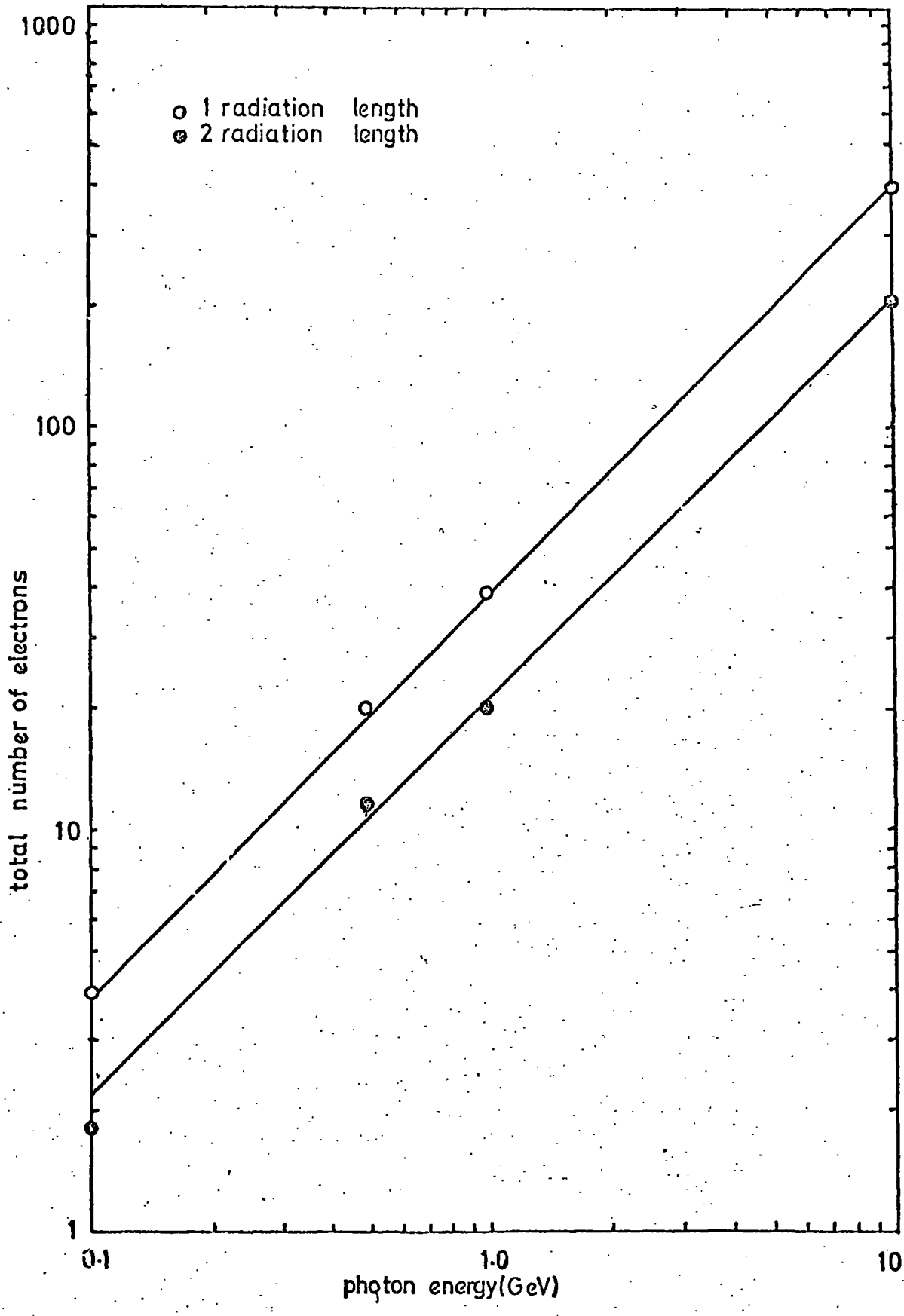

Fig: 3.3

total number of electrons expected by sampling at 1 and 2 radiation length intervals as a function of primary photon energy

estimate of the number of secondaries produced.

Frequency distributions of the total number of ignited tubes obtained with 1.0 and 2.0 radiation lengths of lead between each module for various positron energies are shown in figures 3.4 and 3.5.

From these distributions the mean total number of tube ignitions as a function of positron energy was obtained, a plot of which is shown in figure 3.6

The deviations of the curves from the linear relationships one expects are due to losses of the shower both in the lateral and longitudinal directions, and the inability of a flash tube to register the passage of more than one secondary at the same time.

The energy resolution was calculated by taking the full widths of the frequency distributions in figures 3.4 and 3.5 at a height given by half of the maximum frequency (FWHM).

The resulting resolutions are plotted in figure 3.7 for various incident positron momenta.

If n_i is the total number of secondaries sampled at module i, then an estimate of the total number of secondaries sampled throughout the chamber is given by N where $N = \Sigma_i n_i$

However, from Monte Carlo simulations we have, for a given target thickness between each module,

$$E \sim K \Sigma_i n_i = KN$$

where E is the incident positron energy and K is a constant of proportionality depending on the lead target configuration. Hence we have a statistical error on the measured energy given by

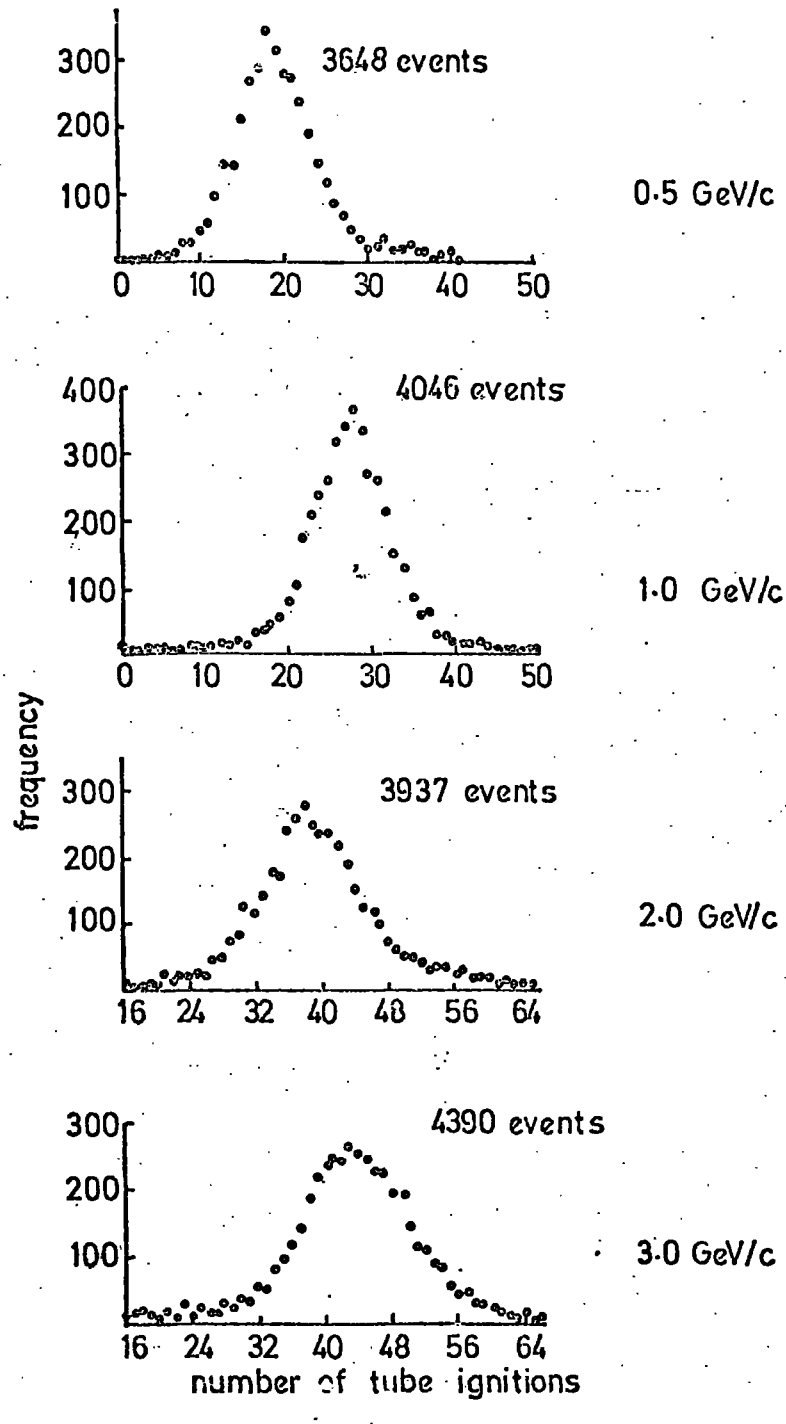

Fig. 3.4 frequency distributions of the total number of tube ignitions with 1.0 radiation length of lead between modules

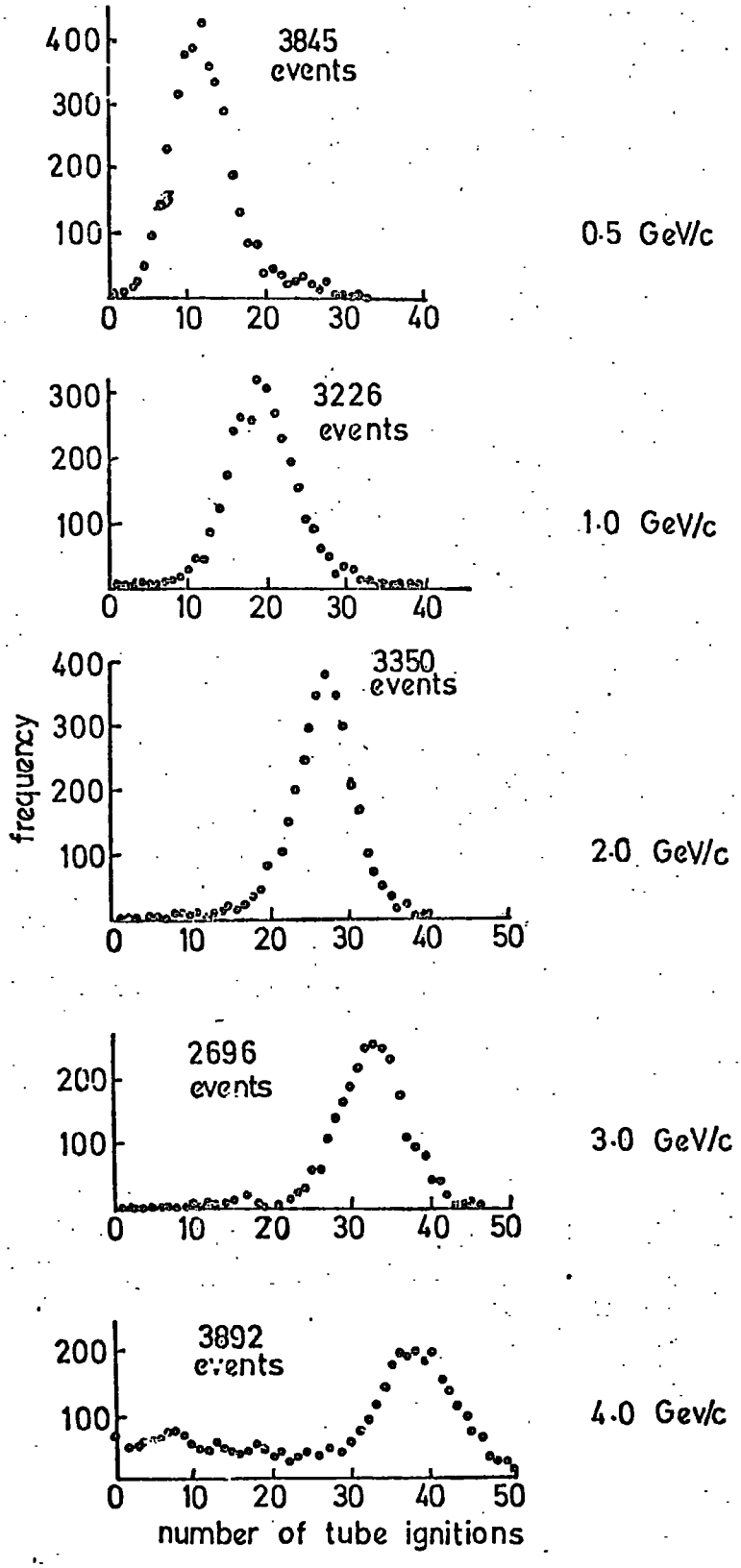

Fig. 3.5

frequency distributions of the total number of tube ignitions with 2·0 radiation lengths of lead between modules

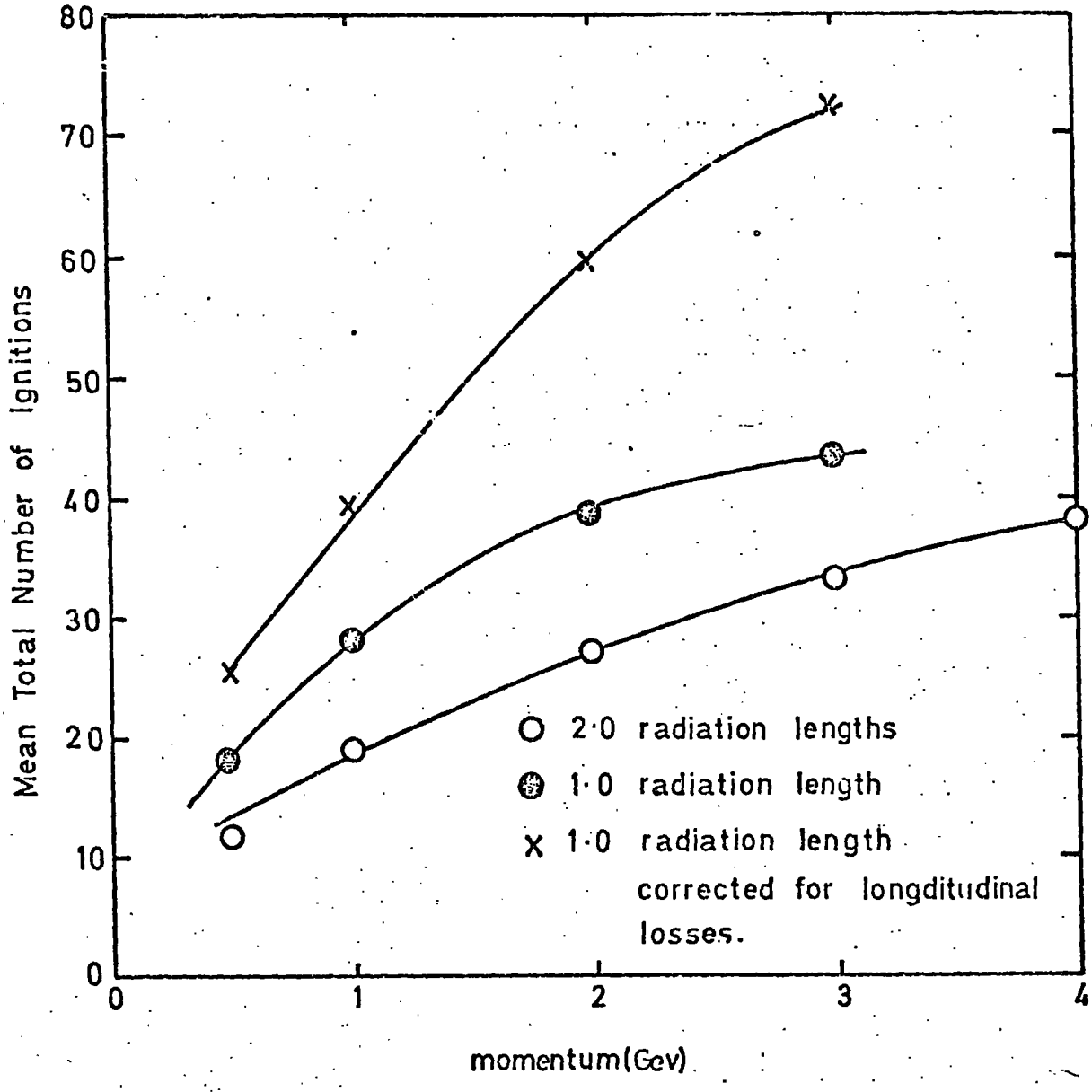

Fig. 3.6

Mean total number of tubes igniting versus positron energy.

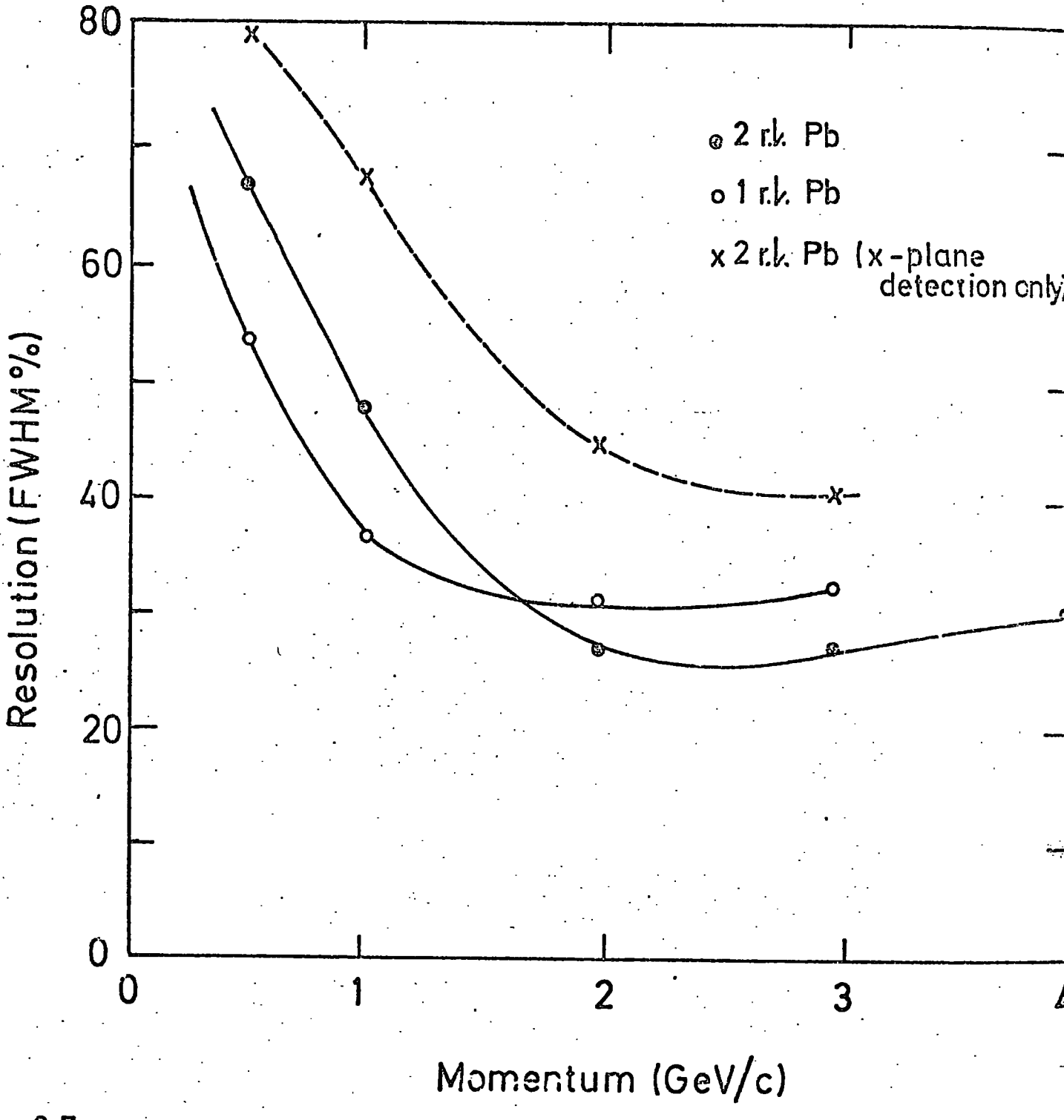

Fig. 3.7 Energy resolution as a function of positron momentum.

$$\frac{dE}{E} = \frac{dN}{N} = \frac{1}{\sqrt{N}} \quad \frac{\sqrt{K}}{\sqrt{E}}$$

one therefore expects the resolution to vary as $1/\sqrt{E}$. This variation is initially seen in figure 3.7, however, the resolution curve flattens off at higher momenta, due to shower leakage and multi-electron insensitivity of the flash tubes.

The resolution is also seen to improve for the 1 radiation length run for lower energies, before shower leakage and shower density become serious. This is what one would expect as the 1 radiation length target configuration would give a smaller value of K.

A great improvement in resolution is obtained if the sum of the X and the Y ignited tubes are used instead of using only one plane of ignited tubes.

The resolutions obtained experimentally are not as good as those expected from theoretical considerations, due to the inherent errors in detection of the chamber.

3.3.5 SHOWER LEAKAGE

Shower leakage took place both in the lateral and longitudinal directions. Leakage was especially noticable when using thin targets and high energy positrons.

Longitudinal leakage is very much in evidence in figure 3.8, where the mean number of tube ignitions in each of the X modules is shown for various positron momenta.

Lateral leakage is evident in figure 3.9 where the shower

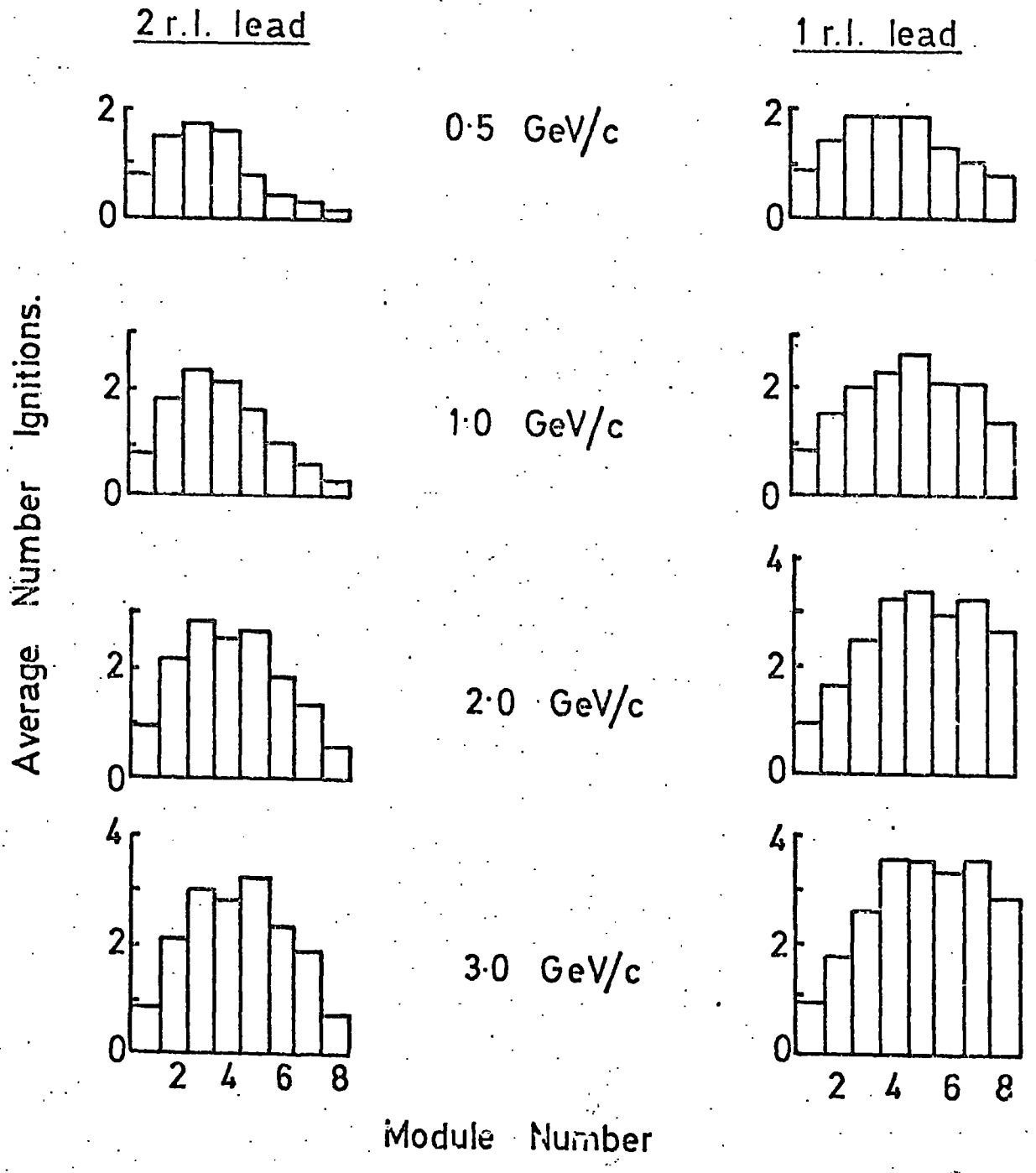

Fig. 3·8 The average number of ignitions in each module at various momenta.

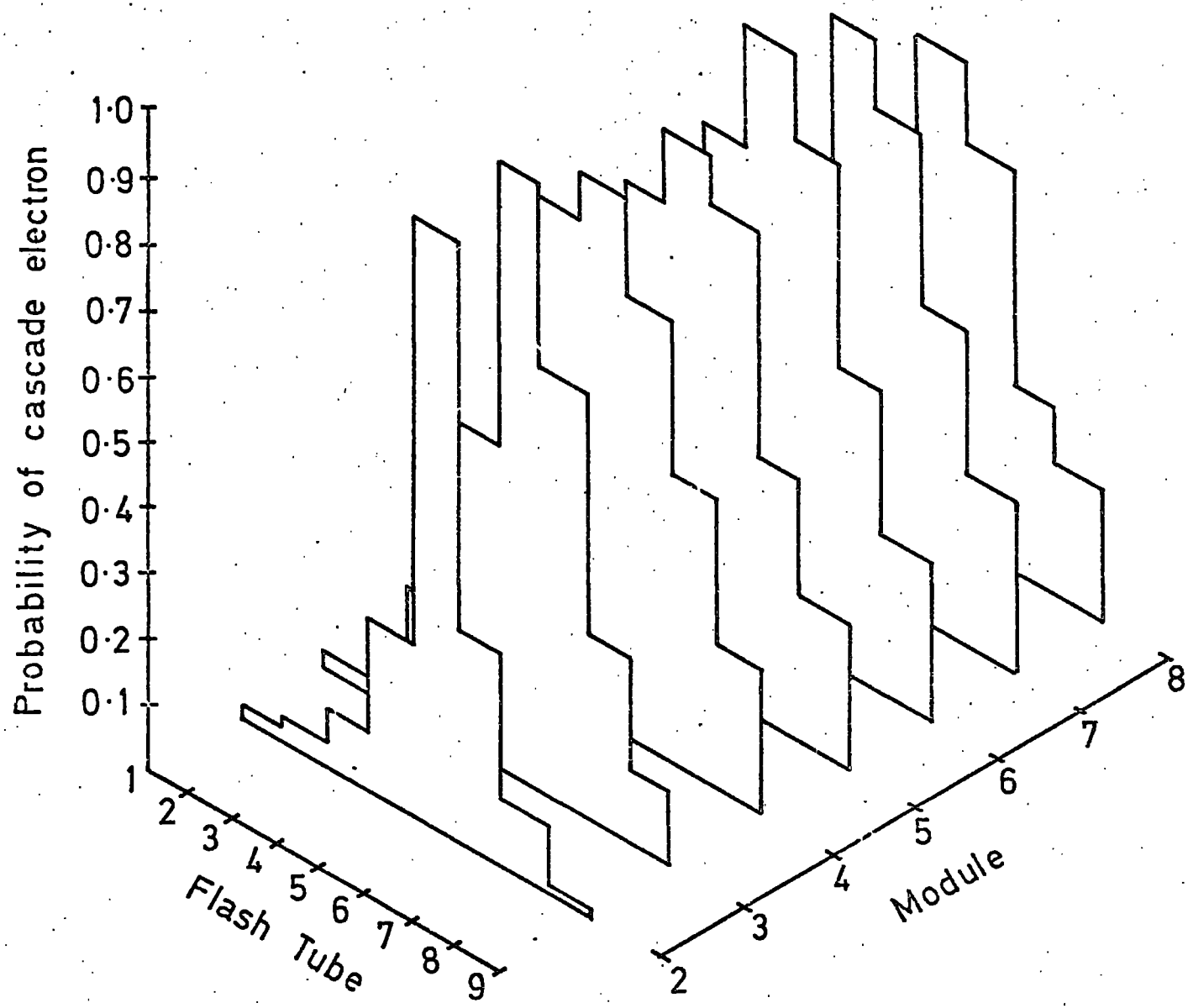

Fig.3.9 Average shower development for 3.0 GeV positrons using 1.0 r.l. of lead target between each module.

profile is drawn for 3 GeV incident positrons with 1 radiation length of target between each module.

Curves are drawn in figure 3.10 showing the total number of tube ignitions for various radiation lengths of target traversed. These curves show the same behaviour as those obtained from Monte Carlo simulations (figure 3.2). Using the curves drawn in figure 3.10 one can estimate, and correct for, longitudinal losses suffered in the chamber. Corrections for these losses have been made on runs with 1 radiation length of lead between the modules. These corrected runs are shown in figure 3.6. The corrected curve gives a much better linear agreement, however, deviations are still present due to the multi-electron insensitivity of one tube.

3.3.6 ELECTRON SENSITIVITY OF THE TUBES

As mentioned in sections 3.4 and 3.5, one of the main reasons for the deviation of the curve in figure 3.6 from the linear, is the inability of a flash tube to resolve more than one particle passing through it.

An estimate of the electron insensitivity of the tubes in the chamber was made by comparing the results obtained from the chamber for the total number of ignited tubes when using 0.5 GeV/c and 1.0 GeV/c momenta for positrons, with those obtained by Messel and Crawford (figure 3.3). The results are shown in table 1.

The electron sensitivity is seen to decrease with increasing positron momentum, due to the development of higher density showers.

The electron sensitivity depends very much on the diameter of the tubes used, and also on the separation between modules. The

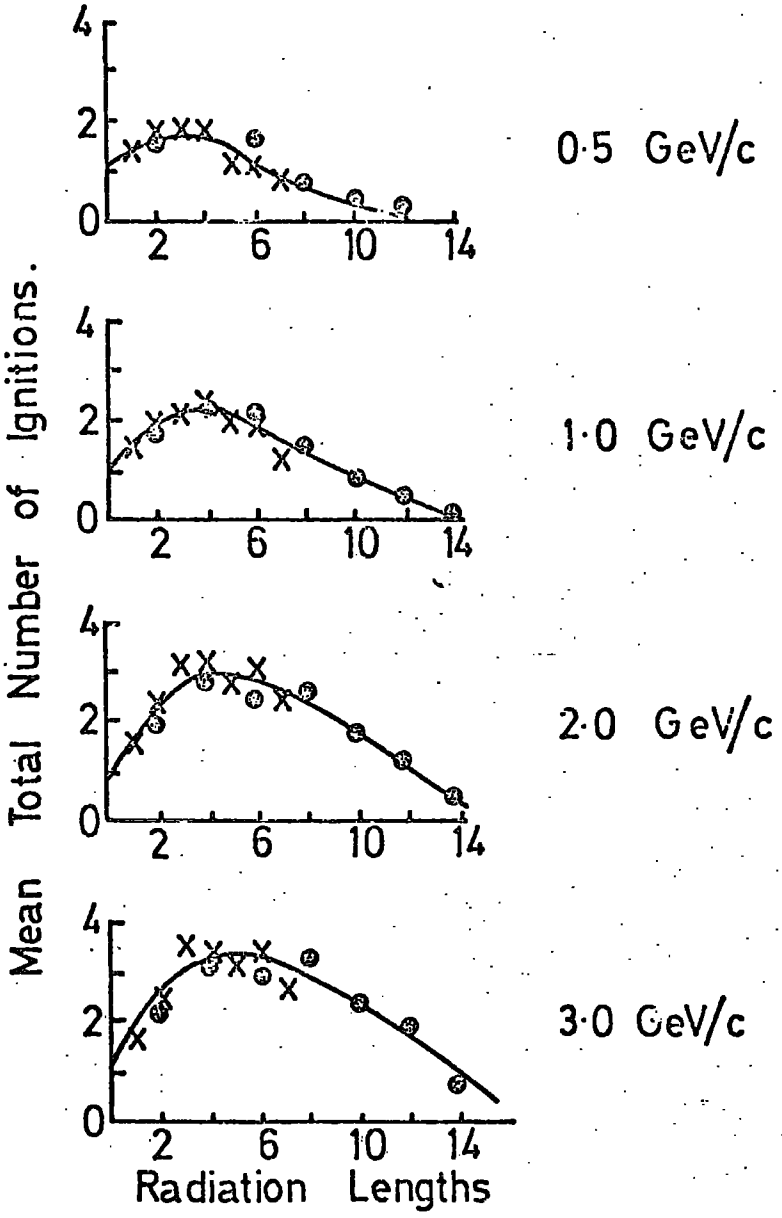

x Data from 1·0 r.l. between modules.

o " " 2·0 " " "

ig. 3.10

Mean total numbers of ignitions vs target depth for various momenta .

TABLE I

Positron momentum GeV/c	Radiation lengths of target between each module	Number of secondaries	Number of flash tube ignitions	Sensitivity (%)
0.5	1.0	16.7	9.7	58.1
0.5	2.0	10.0	6.4	63.9
1.0	1.0	31.4	13.4	42.8
1.0	2.0	20.2	9.8	48.7

latter is restricted by the physical size of the detector, but increased electron sensitivity may be obtained by using smaller diameter tubes.

3.3.7 SPATIAL MEASUREMENTS

The following section describes a computational method developed to give estimates of the spatial resolution of the chamber. Computational methods could be easily used as the shower data was in digitised form, unlike the shower data obtained from conventional detectors such as spark chambers, where most of the data is in photographic form and has to be analysed visually (15, 16, 18).

The shower data taken and analysed with respect to energy (section 3.3) was also analysed to give estimates of the spatial resolution of the chamber. However, in the shower analysis only events where one tube ignited in the first module were considered. The single ignited tube giving a "true" measure of the incident positron position.

3.3.8 SPATIAL RESOLUTION

Positrons incident on the chamber produced electromagnetic showers which propagated through the detector. It was assumed that a developing shower spread with circular symmetry about its core or axis, ie. the trajectory which the incident positron would have described had there been no target material in its path.

Using this assumption, an estimate of the shower axis may be determined by calculating the "centre of gravity" or "shower

centre" in each detecting plane. The centres may be found by calculating the following expression for each detector module.

$$\bar{Y}_i = \sum_{j=1}^{N} y_{ij}/n_i \qquad (i)$$

where $\bar{Y}_i$ is the coordinate of the shower centre in the i^{th} module.
y_{ij} is the coordinate of the j^{th} ignited tube in the i^{th} module.
n_i is the total number of ignited tubes in the i^{th} module.
N is the total number of tubes in a module.

In this way, coordinate points, which represent a series of shower centres, may be found in each modular plane along the length of the shower. From these points a straight line may be fitted representing the shower axis.

In the above method however, no account has been taken of the statistical fluctuations that occur in the shower development. A general widening of the shower occurs due to multiple scattering effects, producing fluctuations in electron positions and densities throughout the shower. This is illustrated in figure 3.11 where the shower development of 0.5 GeV positrons is seen. Electrons at the rear and edges of the shower have suffered severe multiple scattering and absorption, hence the data at the beginning and interior of the shower is most reliable. This means that a better estimate of the shower axis will be obtained if the data is weighted in the lateral direction according to position with respect to the shower core, in the calculation of the shower centres, and in the longitudinal direction when fitting a straight line through the shower centres.

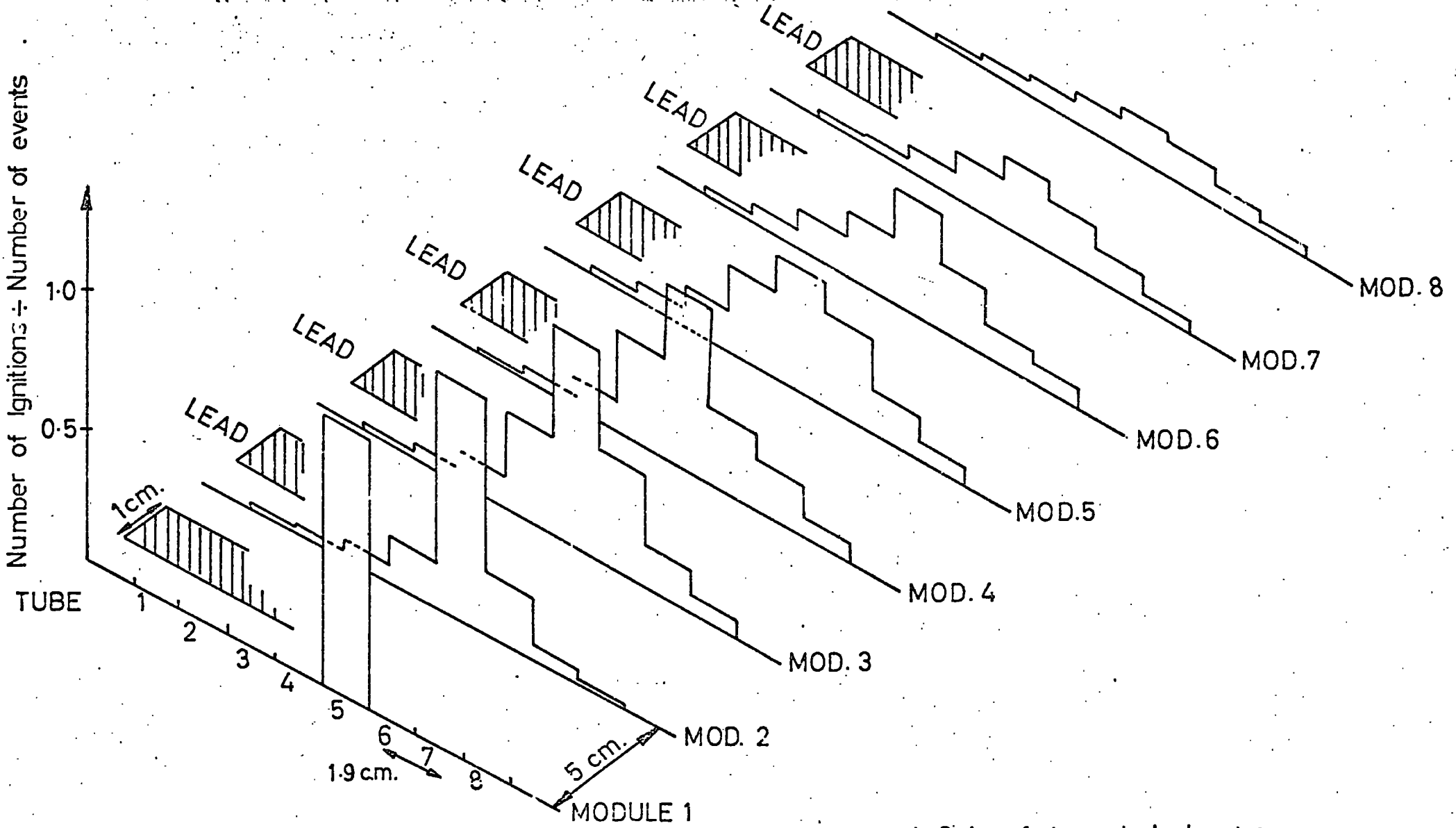

Fig.3.11 Average shower development for 0.5GeV positrons using 1.0r.l. of target between each module .

A method of analysis was therefore developed in which the data was weighted according to its position, and then an iterative fitting of the shower axis was made. The weighting in the lateral direction was achieved by using a weighting function of similar form to the mean lateral shower distribution in a given detecting plane, which may be represented by a Gaussian function (19). The frequency distribution and hence the weighting function for the i^{th} module and j^{th} tube were described by the following expression:-

$$W_{ij}(y_{ij}) = \exp(-(q_{ij})^2) \qquad \text{(ii)}$$

$$\text{where } q_{ij} = \frac{(y_{ij} - y_i)\cos\phi}{\sigma_i} \qquad \text{(iii)}$$

and y_{ij} is the coordinate of the j^{th} tube in the i^{th} module.

y_i is the distance of the shower axis in the i^{th} module from the base of the modules.

σ_i is a quantity representing the mean spread of the shower in the i^{th} module.

ϕ is the angle between the shower axis and the base of the modules.

These parameters are shown in figure 3.12

In the experiment, the showers were produced from positrons incident at angles of $\phi = 0 \pm 2^{o}$ (20), so the $\cos\phi$ term was removed from equation (iii).

Comparison between the fitted lateral shower distributions and the distributions obtained from the experimental data are shown

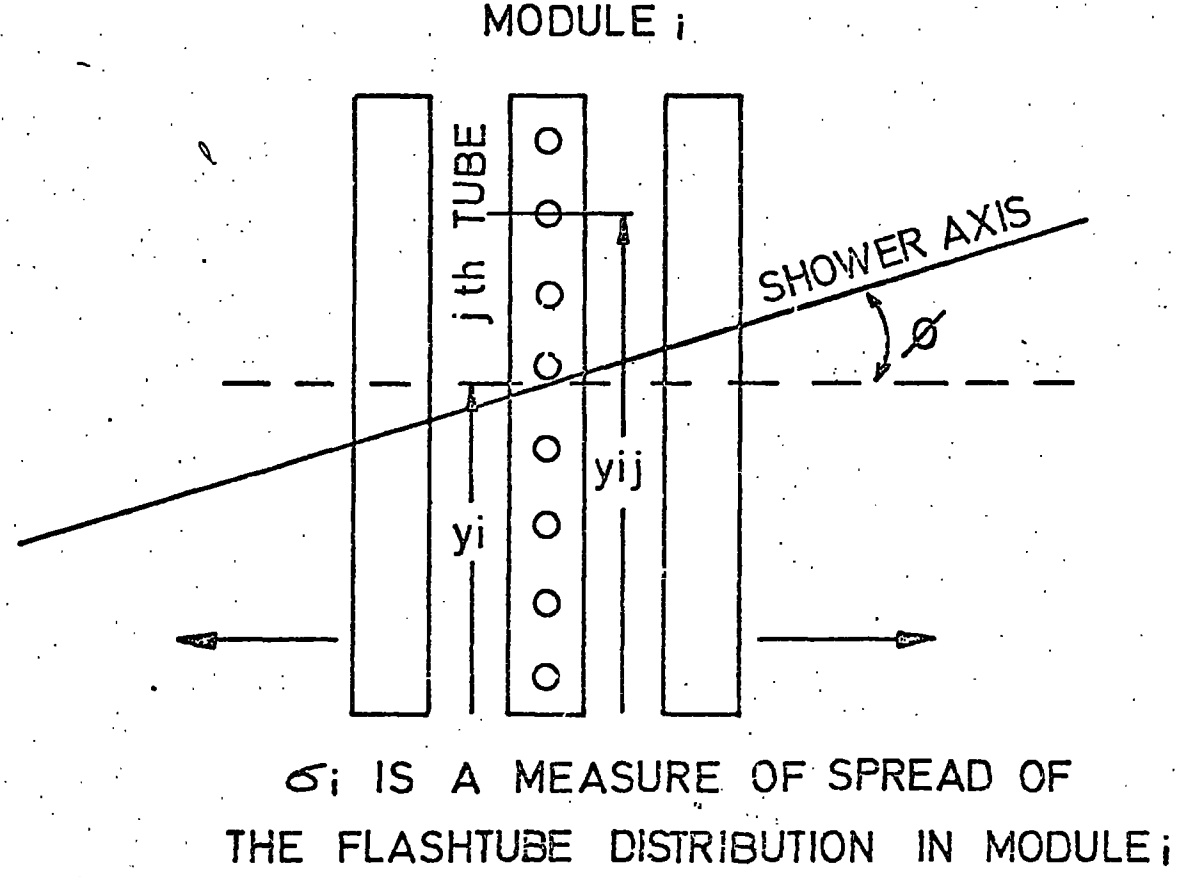

Fig. 3.12 Parameters used in the analysis of the shower data.

in figure 3.13.

In the longitudinal direction, a least squares fit was made to the shower centres, using weighting factors equal to $1/F_i$, where F_i gave a measure of the fluctuations in module i, and was taken as the standard deviation of the distribution of fluctuations of the calculated shower centres, obtained from equation (i), about the true centre in each detecting plane. The true shower centres were obtained from the position of the incident positron in the first module, knowing that the positrons were incident at $\phi = 0 \pm 2^{o}$.

The weighting factors F_i were found to give very good measures of spread of the lateral distributions in the modules, and were used as the σ_i's in fitting these distributions. The values of σ obtained are shown in table II.

The shower axis was calculated by an iterative process. An initial estimate was obtained by calculating the shower centre in each module using equation (i). A straight line representing the shower axis was then fitted to the seven centres using a least squares fit. The data was then weighted in the lateral direction with respect to this first estimate of the shower axis using equation (ii). Thus a new set of weighted shower centres was obtained for the seven modules, given by

$$\bar{Y}_i \text{ (weighted)} = \frac{\sum_{j=1}^{N} y_{ij} \times W_{ij}(y_{ij})}{\sum_{j=1}^{N} W_{ij}(y_{ij})} \qquad \text{(iv)}$$

A second and better estimate of the shower axis was then found by the least squares fitting of a line to these new centres, using

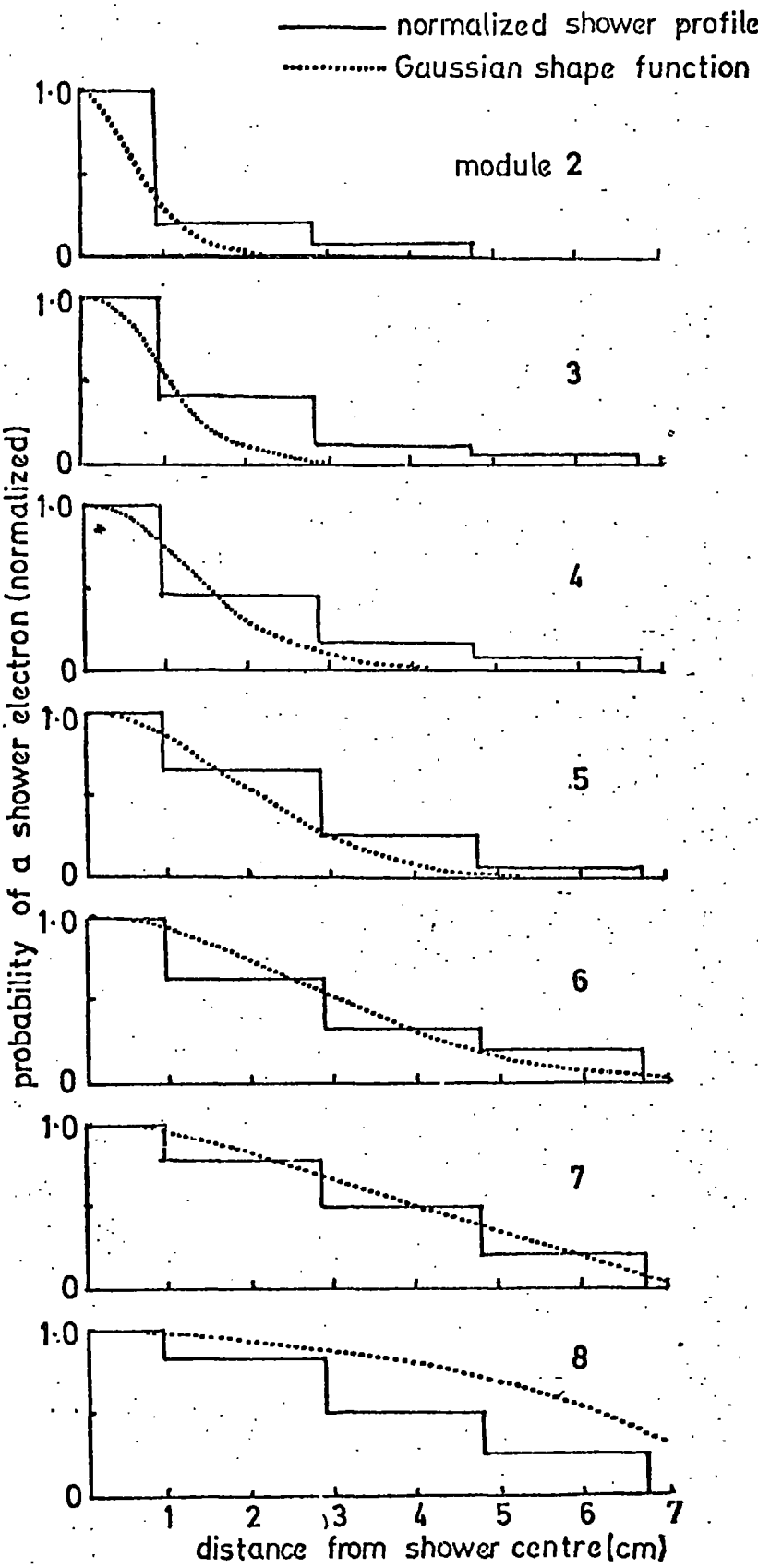

Fig. 3·13

normalized shower profiles at 0·5 GeV/c with 1·0 r.l. of lead compared with Gaussian shape functions

TABLE II

One radiation length of lead target							
	standard deviation (cm)						
	module						
E(GeV)	2	3	4	5	6	7	8
0.5	1.03	1.20	1.77	2.48	3.64	4.94	8.68
1.0	1.03	1.09	1.29	1.63	2.01	3.01	5.04
2.0	1.01	1.02	1.09	1.25	2.09	2.09	4.08
3.0	1.05	1.13	1.10	1.13	1.62	1.62	3.13

Two radiation lengths of lead target							
	standard deviation (cm)						
	module						
E(GeV)	2	3	4	5	6	7	8
0.5	1.11	1.26	1.35	1.59	2.11	2.22	2.63
1.0	1.09	1.10	1.19	1.24	1.41	1.61	2.14
2.0	1.23	1.27	1.32	1.29	1.39	1.42	1.63
3.0	1.29	1.28	1.30	1.27	1.35	1.33	1.61

longitudinal weighting factors $1/\sigma_i$. The data was then once more weighted in the lateral direction with respect to the better estimate of the shower axis. The values of the shower axis angle (ϕ) and the intercept of the shower axis on the first module (estimate of incident positron position) for a single shower were recorded for various numbers of iterations and were found to converge to constant values after about five iterative loops, hence in the final analysis ten iterative loops were performed on the data from each event.

Two parameters were obtained for each event in the chamber, the shower axis angle (ϕ) and the apex deviation (Δ) of the shower axis, defined as:

(the estimated position of the incident positron) -
(the "true" position of the incident positron)

The "true" position of an incident positron was taken as the position of the single flashed tube in module 1 (see figure 3.14).

From the measurements of these two parameters estimates of the chamber's spatial resolution and angular resolution were obtained.

The shower data obtained was also analysed using non-weighted methods in order to make a comparison between the two methods of analysis.

The apex deviation frequency distributions which give measures of the spatial resolutions of the chamber are shown in figures 3.15 and 3.16 for the 1 and 2 radiation length shower runs respectively. The distributions obtained using weighted iterative

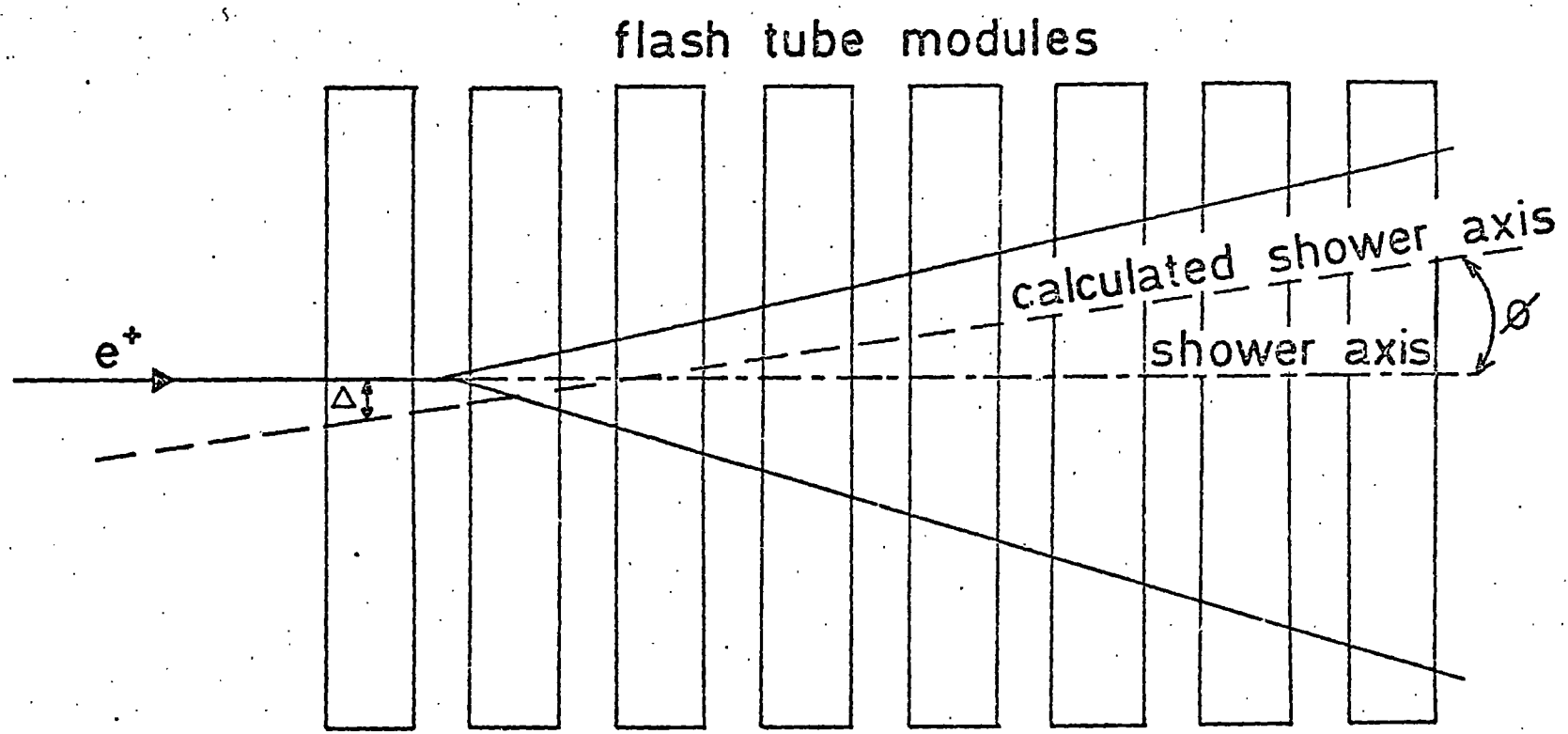

Fig. 3.14 The shower apex deviation(Δ) and shower axis angle(ø) .

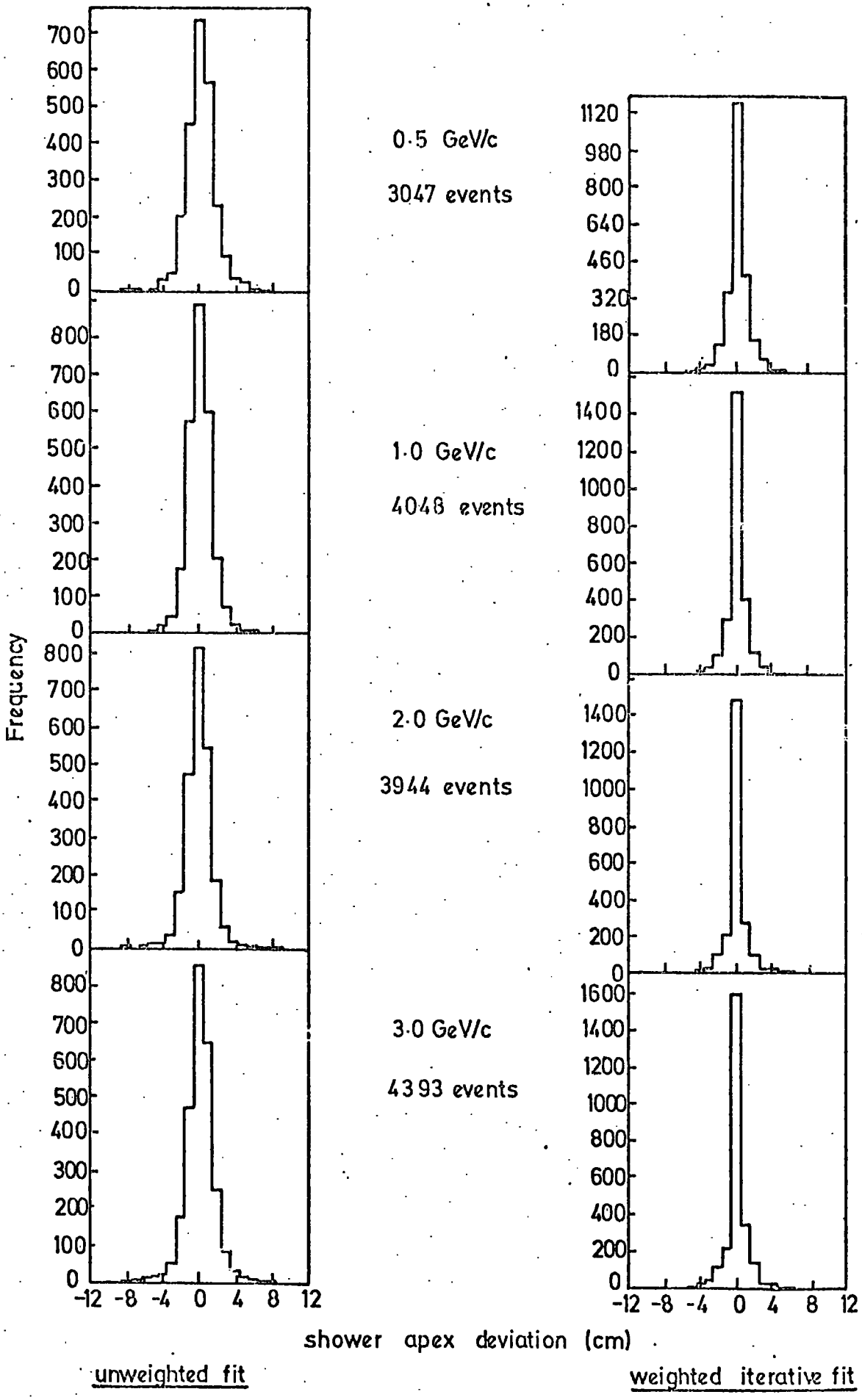

Fig.3.15 Frequency distribution for the shower axis deviation calculated by an unweighted and weighted iterative fit from 1·0 radiation length data.

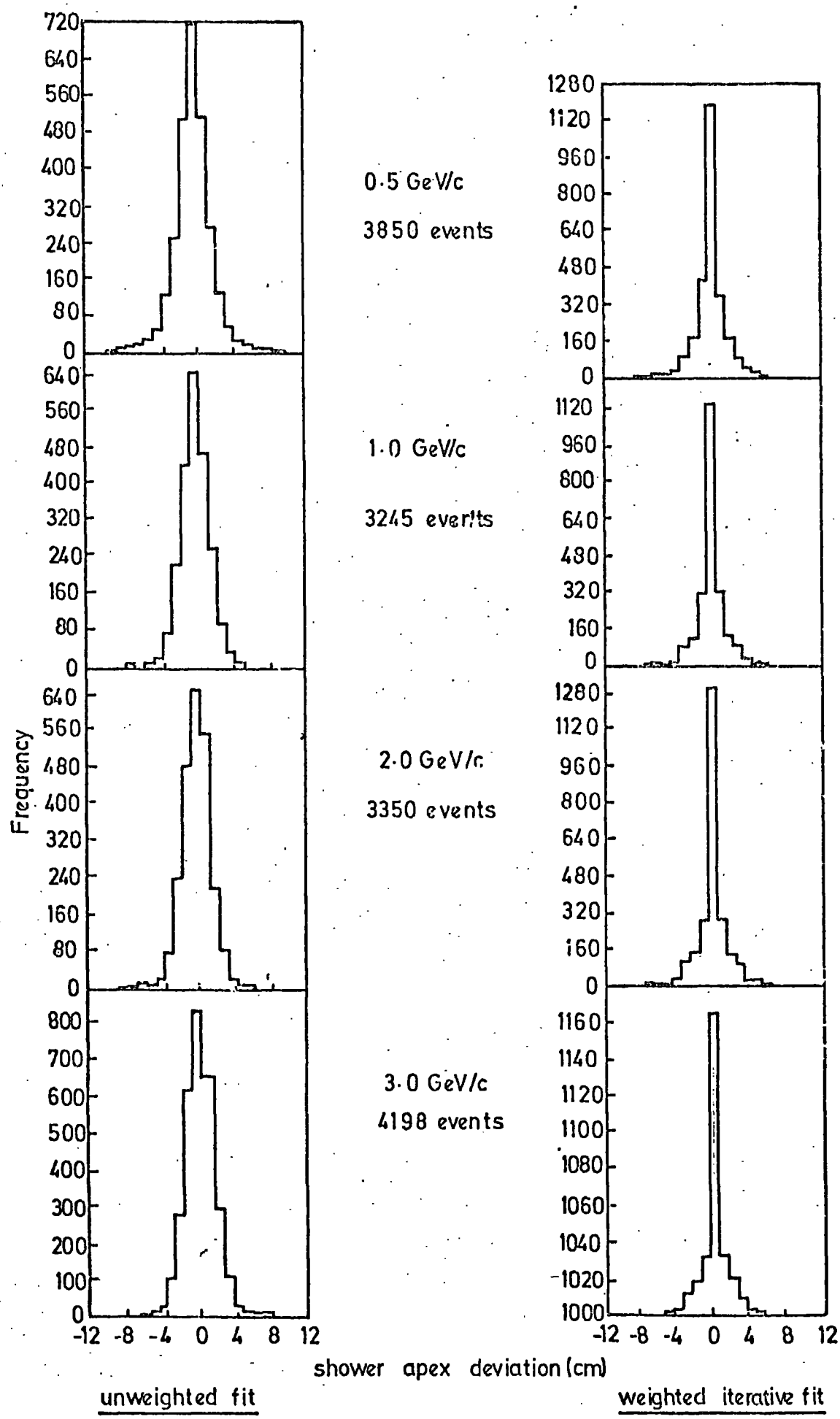

g. 3·16 Frequency distribution for the shower axis deviation calculated by an unweighted and weighted iterative fit from 2·0 radiation length data.

and unweighted methods are both shown. A considerable improvement in the chamber resolution is seen when using the weighted iterative method of analysis.

The frequency distributions of shower axis angles, giving measures of the angular resolution of the chamber, for the 1 and 2 radiation length shower runs are shown in figures 3.17 and 3.18 respectively. Once more a considerable improvement was found using weighted iterative methods of analysis.

The need for longitudinal weighting of the shower data is made evident from figure 3.19 where apex deviation frequency distributions are plotted after the data has been analysed using an unweighted method and using various numbers of modules. At first the spatial resolution of the chamber improves as the number of modules used in the analysis is increased, but deteriorates when the rear modules are used because of the large fluctuations in the positions of shower centres obtained from the rear modules. Similar results were found for the angular resolution of the chamber.

The frequency distributions obtained for the shower axis angles and apex deviations were not Gaussian like in shape and hence estimates of the resolutions of the chamber could not be obtained from the FWHM as had been done in the energy resolution measurements (see section 3.3.4).

In order to achieve a fair estimate of the resolution of the chamber, the percentage of data lying between fixed limits were found. These are shown in table III . An estimate of the resolution of the chamber was then obtained by finding the limits which contained about 75% of the data, analogous to the definition of the FWHM in a Gaussian like distribution (see table IV).

The widths obtained for the frequency distributions do not

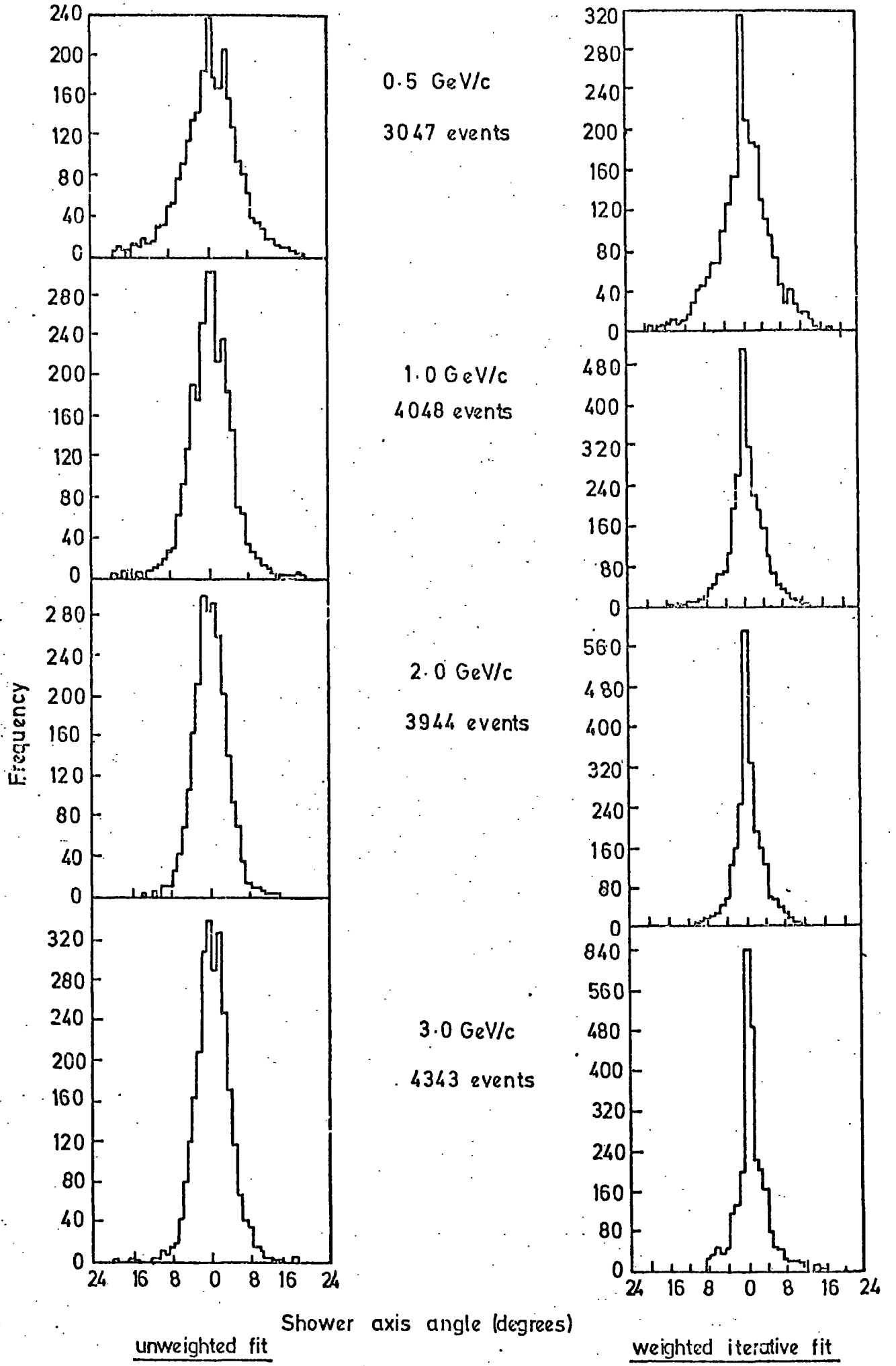

Fig. 3·17 Frequency distribution for the shower axis angle calculated by an unweighted and weighted iterative fit from 1·0 radiation length data.

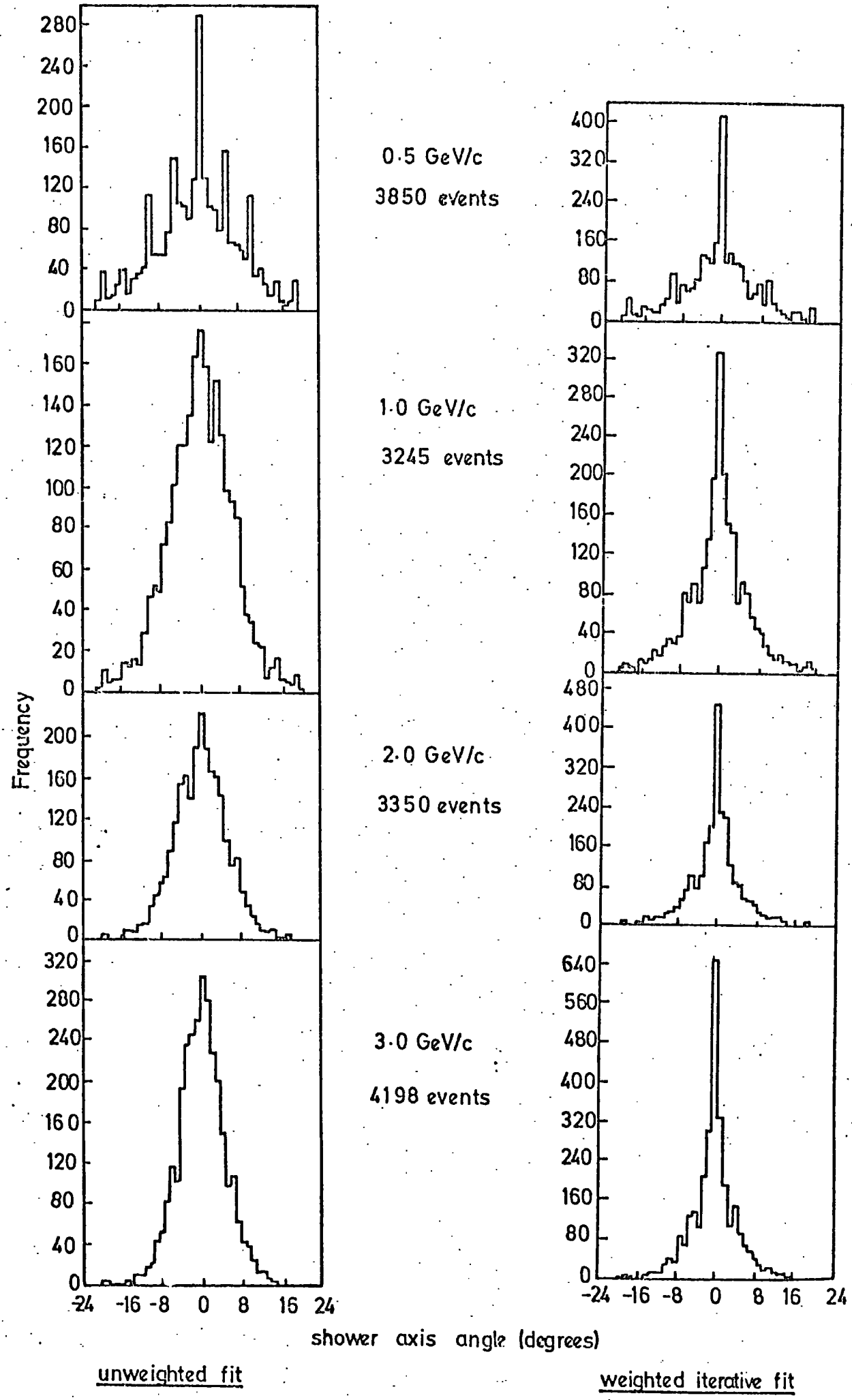

Fig. 3.18 Frequency distribution for the shower axis angle calculated by an unweighted and weighted iterative fit from 2·0 radiation length data.

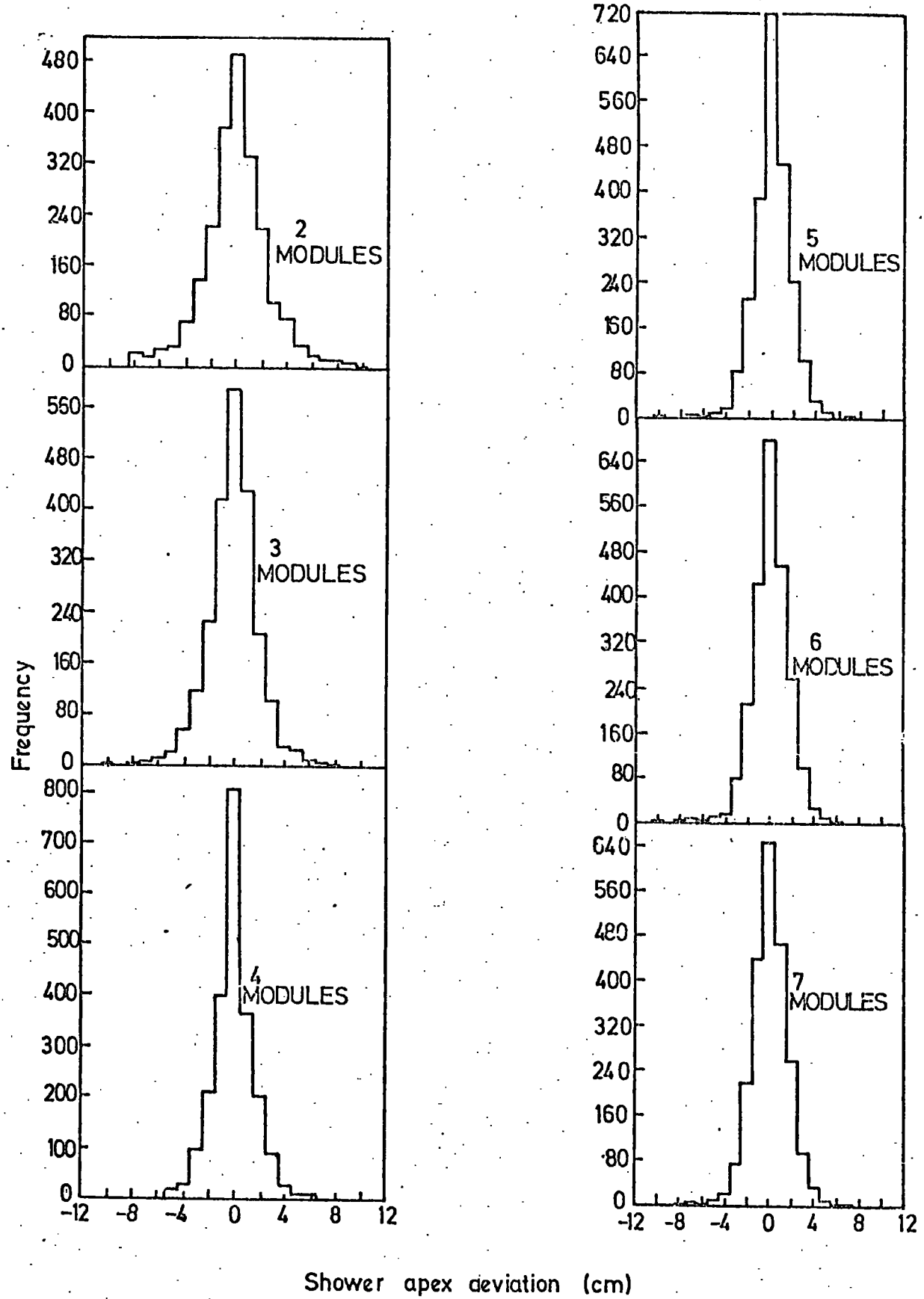

Fig.3.19 Shower apex deviation using different numbers of modules for 1·0 GeV/c positrons with 2 radiation lengths of lead target.

TABLE III

	E(GeV)	% data lying between fixed error limits							
		unweighted fit				weighted iterative fit			
		apex dev.		angle		apex dev.		angle	
		±0.5 cm.	±1.5 cm.	±1.5°	±2.5°	±0.5 cm.	±1.5 cm.	±1.5°	±2.5°
2 r.l. of lead target per module	0.5	26.5	64.2	20.5	35.1	44.4	73.4	35.7	44.1
	1.0	28.2	67.8	21.9	44.0	49.8	77.6	31.6	55.0
	2.0	27.3	71.1	25.0	51.3	54.2	78.0	36.8	62.2
	3.0	28.2	71.2	28.4	51.2	55.7	76.6	43.0	63.6
1 r.l. of lead target per module	0.5	33.9	71.5	20.0	50.9	58.3	79.7	40.1	54.3
	1.0	30.1	64.4	24.3	63.9	48.0	85.2	37.7	69.4
	2.0	34.9	78.4	37.5	73.3	63.6	84.5	49.9	82.1
	3.0	32.7	75.1	35.6	70.0	61.2	83.3	50.5	75.8

TABLE IV

Weighted iterative analysis

Estimates of limits containing ~ 75% of the data, and the resolutions of the chamber

	E(GeV)	Apex deviations (mm.)	Spatial resolution of chamber (mm.)	Shower axis angles (degrees)	Angular resolution of chamber (degrees)
2 r.l. of	0.5	± 16	± 14	± 6.0	± 5.6
target	1.0	± 14	± 12	± 3.4	± 2.7
per	2.0	± 14	± 12	± 3.0	± 2.2
module	3.0	± 15	± 13	± 3.1	± 2.4
1 r.l. of	0.5	± 13	± 10	± 4.0	± 3.7
target	1.0	± 13	± 10	± 2.7	± 1.8
per	2.0	± 11	± 8	± 2.3	± 1.1
module	3.0	± 12	± 9	± 2.5	± 1.5

give direct measures of the resolution of the chamber due to the intrinsic errors involved in the measures of the "true" incident positron positions and shower angles. The position of the incident positron was estimated from the position of a single flashed tube in the first module. Since the internal diameters of the tubes were about 1.6 cm. an error of about $\pm$ 0.8 cm. was involved in the measurement of this position.

Hence:

(spatial resolution obtained from apex deviation frequency distribution (mm.))^2

$\sim$ 64 + (spatial resolution of chamber (mm.))^2

Similarly for the shower angle distributions:

(angular resolution from shower angle frequency distribution (degrees))^2

$\sim$ 4 + (angular resolution of chamber (degrees))^2

Using these facts the different resolutions of the chamber were estimated and are shown in table IV, from which one can see that the spatial resolution over the energy range 0.5 to 3.0 GeV is of the order of one tube radius, and that the angular resolution over this energy range is of the order of a few degrees. It is noted that the resolutions of the chamber increase with increasing energy and decreasing target thickness, as under these conditions less absorption and scattering take place, hence more precise shower centres are obtained.

An estimate of the spatial resolutions expected can be obtained from the equations giving the error involved in intercept

values using a weighted fit (21). That is:

$$\sigma_s^2 \approx \frac{1}{\rho} \sum \frac{x_i}{\sigma_i^2}$$

$$\rho = \sum \frac{1}{\sigma_i^2} \sum \frac{x_i^2}{\sigma_i^2} - \left(\sum \frac{x_i}{\sigma_i^2} \right)^2$$

where σ_s is the spatial resolution of the chamber.
x_i's are the positions of the modules.

Substituting in values of σ_i and x_i obtained from the shower widths and chamber dimensions, one obtains a value of about ±1 cm. for the spatial resolution of the chamber, which agrees quite favourably with the resolutions obtained from the analysis of the data taken with the chamber.

3.3.9 CONCLUSIONS

The results obtained from testing the prototype chamber proved conclusively the usefulness of flash tubes for use in accelerator experiments.

The flash tube chamber operated satisfactorily in high background radiation conditions, and functioned without any deterioration in efficiency at repetition rates up to 50 Hz.

When used in the detection of electromagnetic showers produced by positrons in lead, then the energy, spatial and angular resolutions obtained were comparable to those obtained by conventional detecting techniques (22).

Motivated by the results obtained from the simple prototype detector using relatively large diameter flash tubes, Chaney et al. designed a modified flash tube chamber employing small diameter flash tubes and more detecting planes. A description of this modified detector is given in the following section.

3.4 THE MODIFIED FLASH TUBE CHAMBER

3.4.1 INTRODUCTION

The modified chamber used the same detecting technique as in the prototype chamber but was designed to give improved energy, spatial and angular resolutions when used in electromagnetic shower detection. It was also designed to function at working rates of up to 1 KHz.

It was hoped to improve energy, spatial and angular resolutions by:

a) Increasing the number of flash tube modules in order to increase the number of secondaries sampled in a shower, and decrease longitudinal shower leakage.
b) Increasing the width and breadth of the chamber and so minimise lateral shower leakage.
c) Decreasing the tube diameters and wall thicknesses in order to increase electron sensitivity and detecting efficiency.

It was hoped to increase the working rate of the chamber to the 1 KHz region by using a hydrogen thyratron pulsing system (see

chapter 2, section 2.5), and CH_4 doped flash tubes made of low resistance Jena 16B glass (1).

3.4.2 THE CHAMBER CONSTRUCTION

The chamber consists of twelve modules, each about 22 mm. wide, with a space of about 16 mm. between modules to accomodate lead target. Each module holds two orthogonal sets of thirty two flash tubes separated by an aluminium high voltage plane and contained between two aluminium earth plates secured to an aluminium earth block base (see figures 3.20 and 3.21). The tubes are located in accurately positioned holes in the aluminium block base and in a perspex plate parallel to it. The holes are 9.0 mm. in diameter and there is a spacing between hole centres of 9.5 mm. The aluminium blocks are positioned at 45° to the vertical so that the weight of the flash tubes ensures good contact with digitisation probes set in the blocks (see figure 3.21). Six integrated circuit boards are mounted beneath each module. The modules are held parallel in a steel framework and are accurately aligned by adjusting screws which pass through the framework and meet the bases of the aluminium earth blocks.

The modular design of the chamber is also included in the wiring associated with each module, so making it possible for each module and its associated wiring to be removed from the chamber without too much difficulty. This greatly facilitates the process of checking or modifying individual modules.

A perspex bar is suspended from the roof of the chamber and holds the capacitors and resistors used in pulsing the high voltage

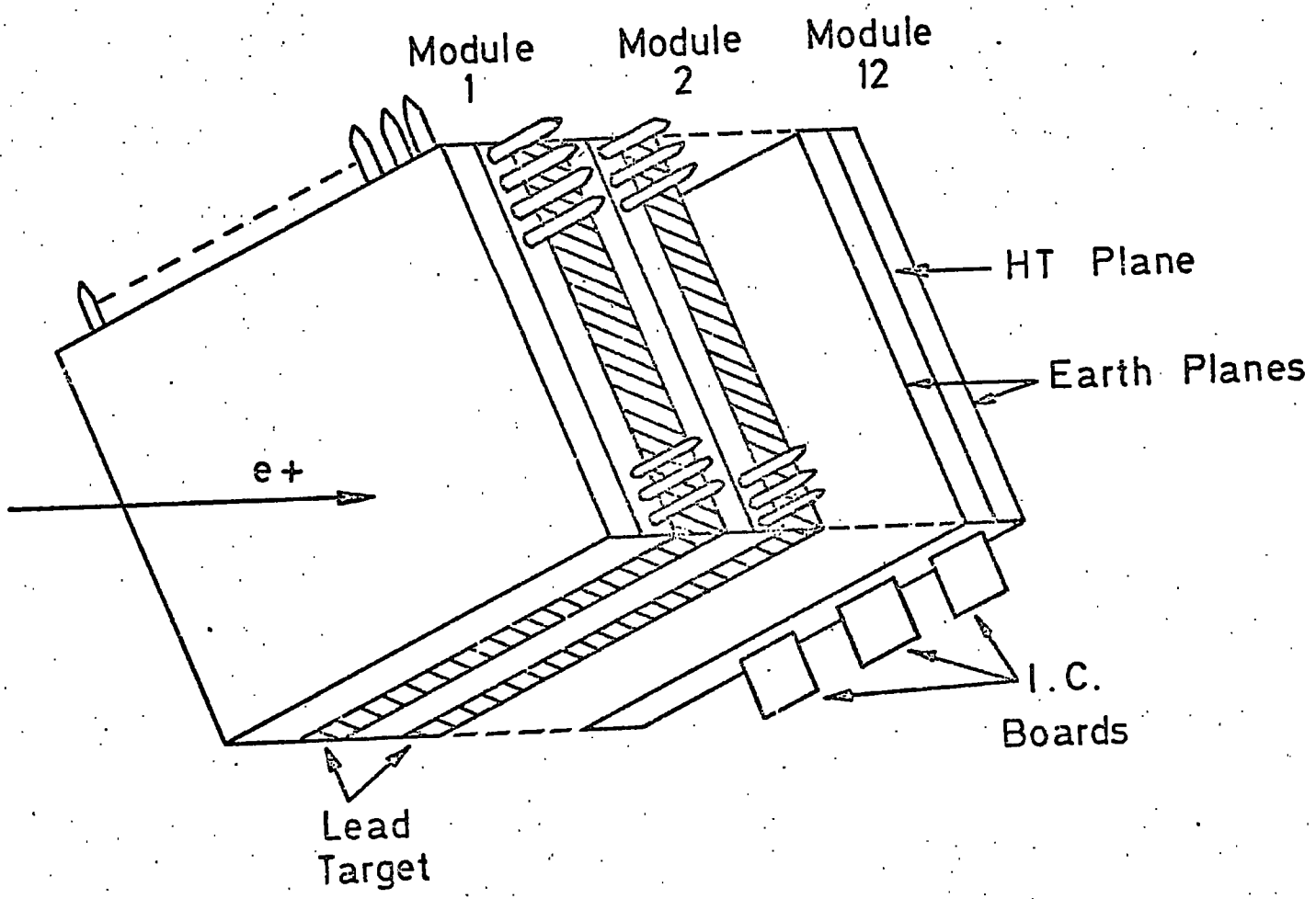

Fig. 3.20 The modified flash tube chamber.

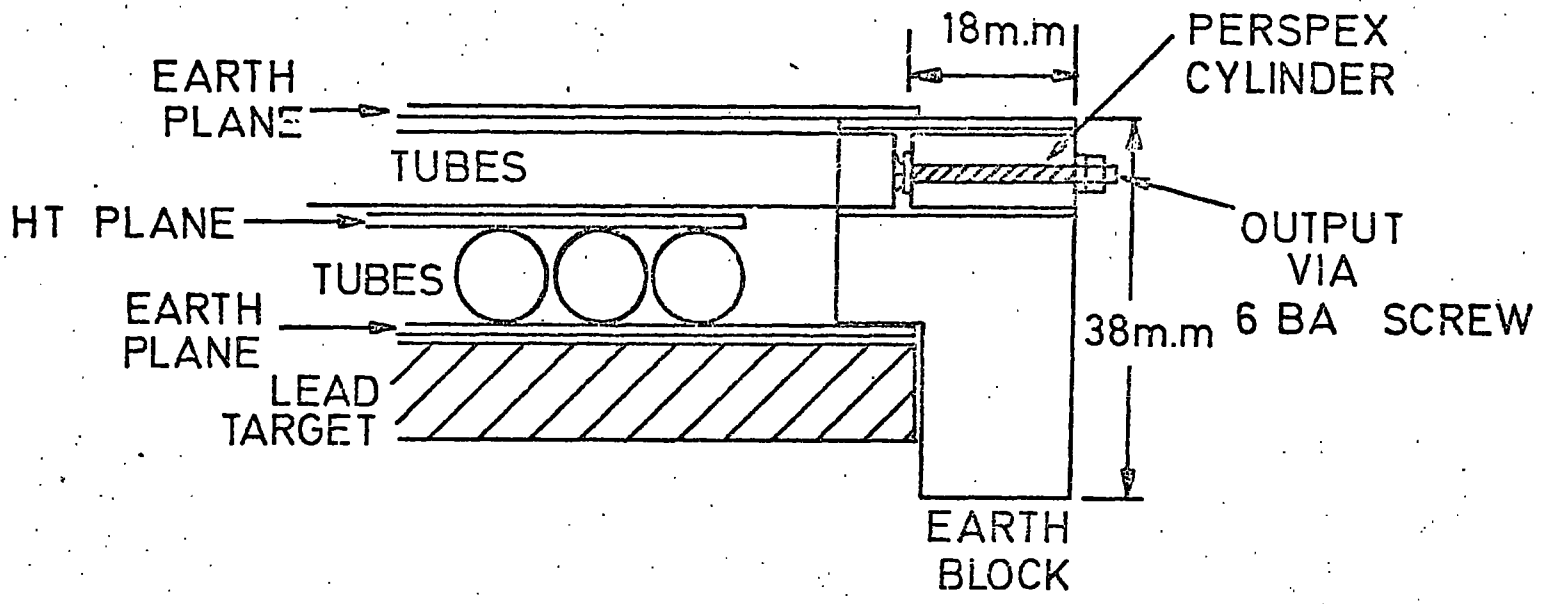

Fig. 3·21 The digitisation probe arrangement .

planes. The hydrogen thyratron pulsing unit is housed in an aluminium box and secured to the top of the chamber, together with the electronics for the A.C. clearing field arrangement.

Shielding is important because of the high frequency noise generated by the pulsing system. The chamber is completely cased in aluminium sheeting to exclude any such noise which may affect the integrated circuit boards mounted beneath the modules or any associated electronics used in the vicinity.

The photograph in figure 3.22 shows four of the modules removed from the chamber, and figure 3.23 shows the chamber with the aluminium shielding removed.

3.4.3 THE FLASH TUBES

The flash tubes to be used in the chamber were developed by Chaney et al. (1) for use in high backgrounds of radiation and at repetition rates up to 1 KHz. They have a recovery time of less than 0.6 ms. and a sensitive time of about 1.4 μs. (without any applied clearing field). 768 tubes are employed; these are made of Jena 16 B soda glass, and are filled with a mixture of Ne(70%)-He(30%) + 2% CH_4 at 2.3 atmospheres. They have an internal diameter of about 8 mm. and a wall thickness of about 0.3 mm. They are painted externally with a thin layer of white paint in order to help prevent the passage of photons from a discharging tube to neighbouring tubes.

3.4.4 THE HIGH VOLTAGE PULSING SYSTEM AND CLEARING FIELD ARRANGEMENT

The pulsing of the chamber is carried out by a simple CR

Fig.3.22 Four Modules of the Modified Flash Tube Chamber.

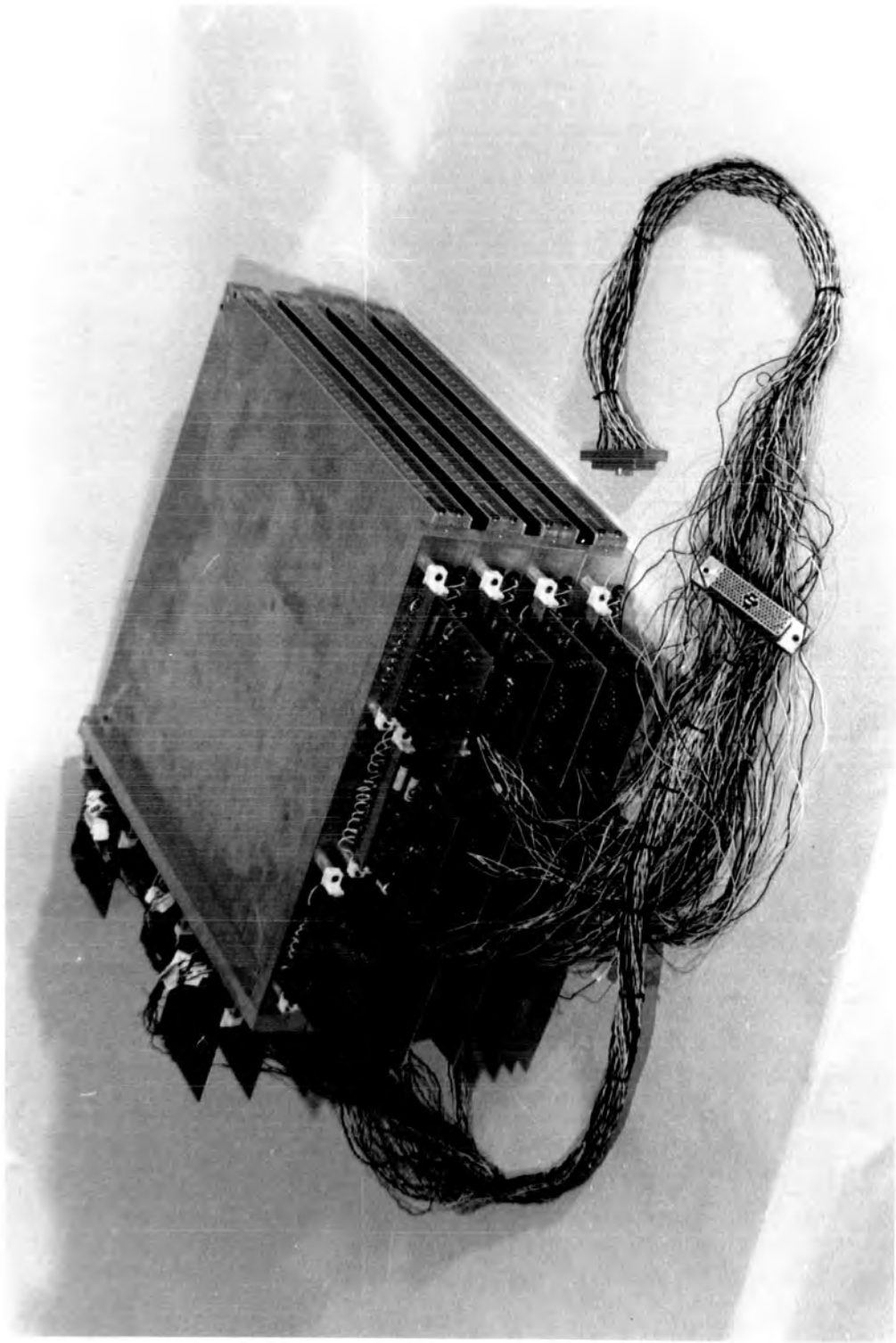

Fig. 3·23 The

Modified Flash Tube Chamber.

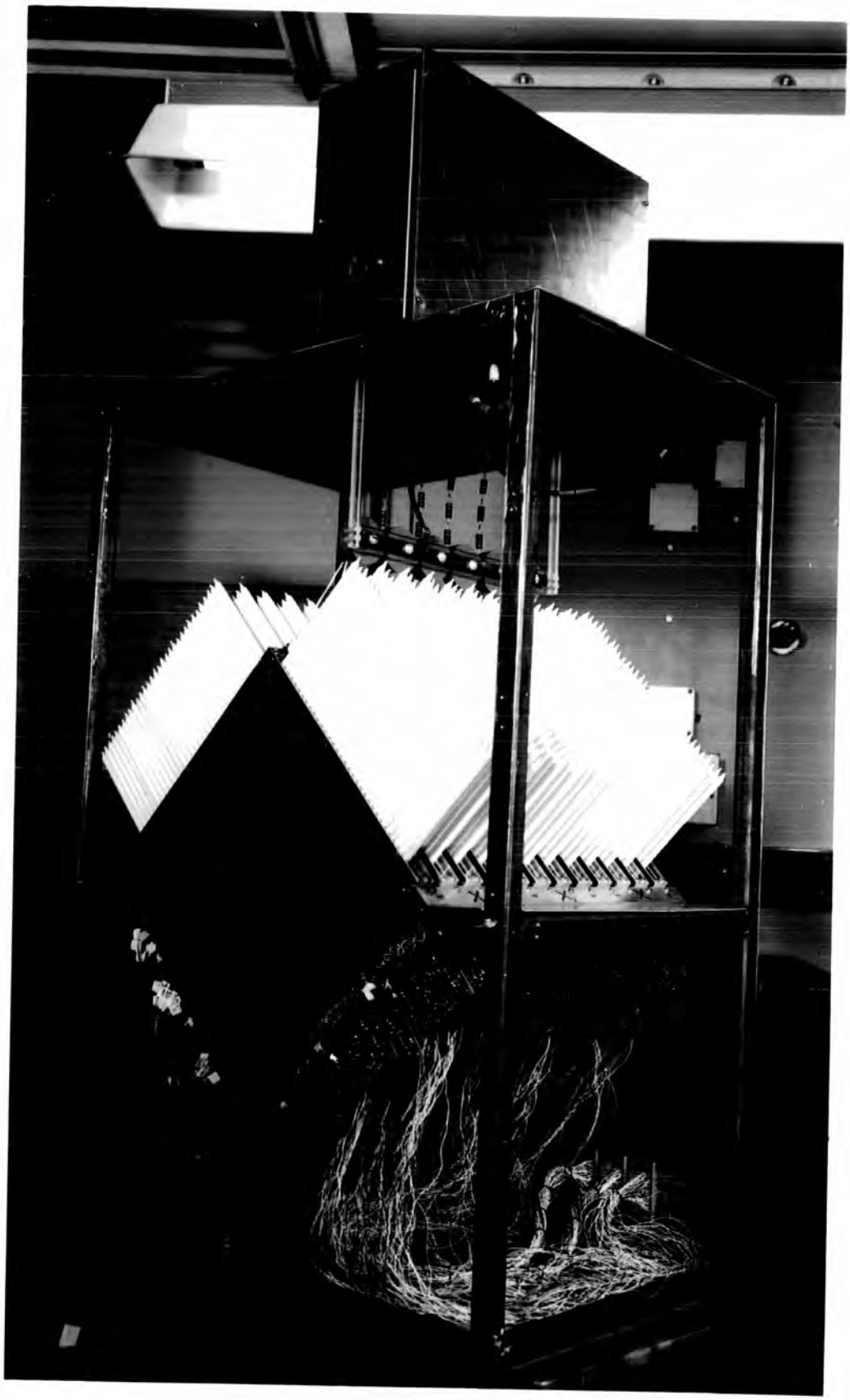

discharge system as described in chapter 2, section 2.5. A diagram of the pulsing system is shown in figure 3.24. Six high voltage 6000 pF capacitors are mounted above the modules, each capacitor being used to deliver a negative high voltage pulse to two modules. The capacitors are charged to a high positive potential via a charging resistor R_1 by a Universal Voltronics power supply (25 KV, 25 mA). Each capacitor can then be discharged through an associated discharge resistor R_2 by the switching of the hydrogen thyratron pulsing unit mounted on the roof of the chamber, producing a negative polarity high voltage CR decaying pulse on the high voltage planes.

An external clearing field arrangement is coupled to the high voltage planes (see figure 3.24) producing on them a field of frequency 100 Hz and variable peak to peak voltage.

3.4.5 DATA ACQUISITION

The discharge of a flash tube is recognised by a pulse on the digitisation probe set in the earth block beneath the tube (see figure 3.21). These probes consist of 6 BA brass screws secured in perspex cylinders. The outputs from them are fed into set-reset latches contained in the integrated circuit boards mounted beneath the modules. Each board contains two 6-input latches (type 74118) and a NAND buffer (type 7440) which provides a reset pulse for the latches on the board and an output reset pulse for the NAND buffer of a neighbouring board (see figure 3.25). The circuit boards were all powered from a +6 V, 10 A stabilized supply. The set output levels from the latches are taken to 6, 132 way EMIHUS sockets

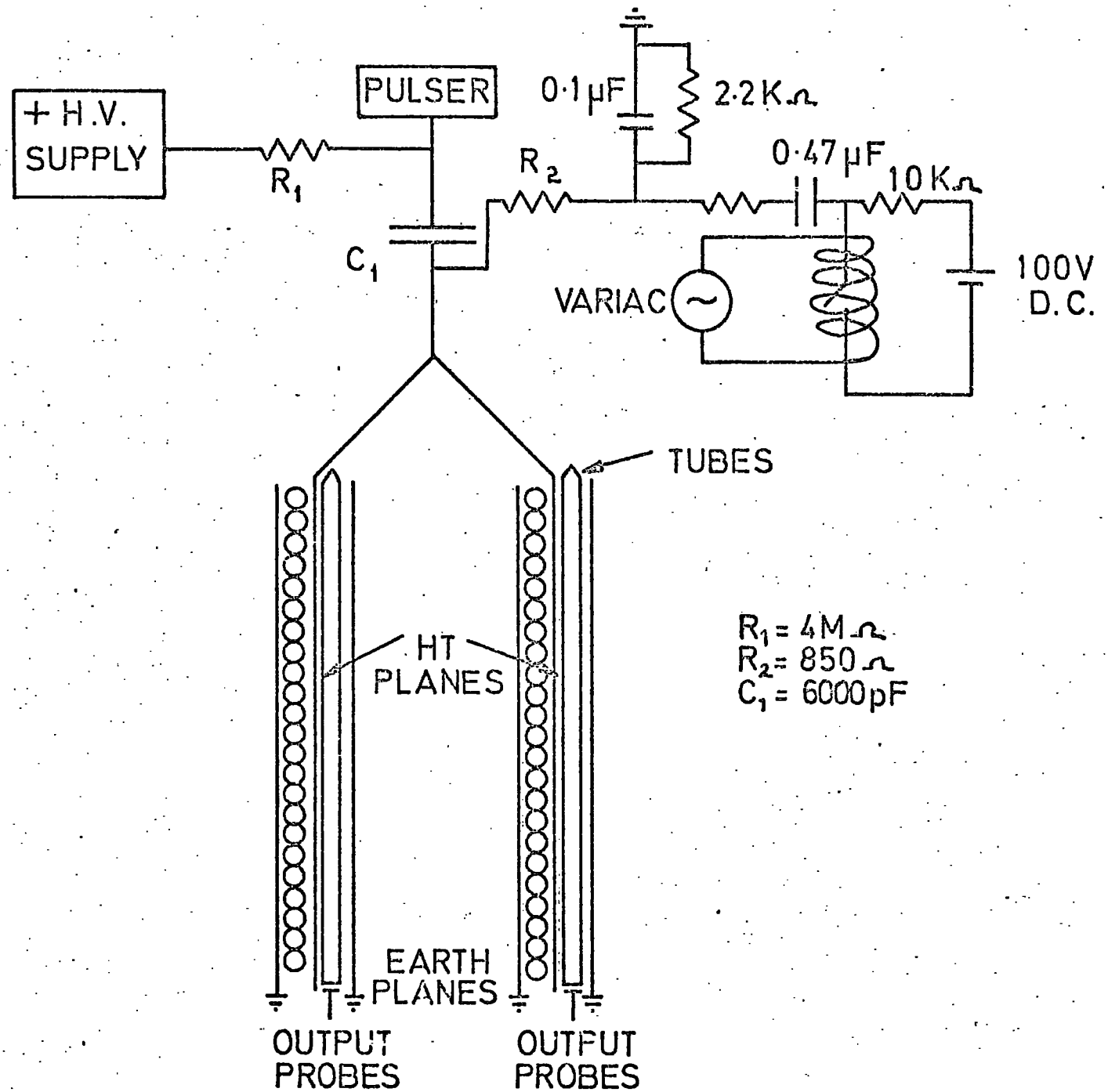

Fig. 3·24 The high voltage and clearing field arrangement.

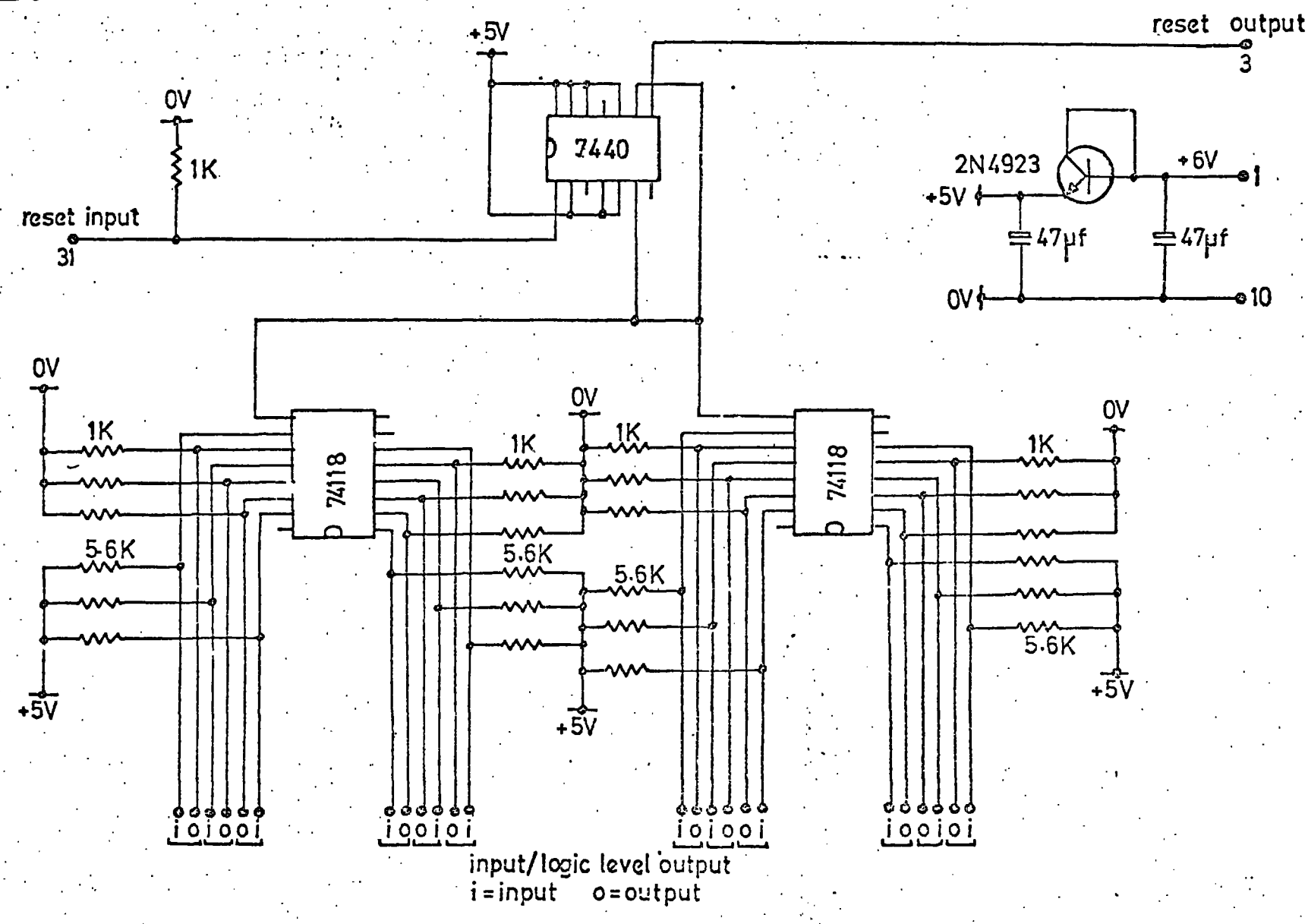

12-bit memory register

Fig. 3·25

mounted in the base of the chamber. These levels can then be read by a computer via a CAMAC interface and EMIHUS cable connections.

The inputs to the reset integrated circuits are combined and connected to a B.N.C. socket situated in the base of the chamber. All the latches can then be reset by the changing level of a CAMAC output level unit connected via a B.N.C. cable to the B.N.C. socket.

REFERENCES

1. Chaney, J.E., Breare, J.M. (1975) Nucl. Inst. & Meth. 124 61
2. McFarlane, W.K. et al. (1971) Nucl. Inst. & Meth. 91 85
3. Messel, H., Crawford, D.F. (1970) Electron Photon Shower Distribution Functions. Pergamon Press. New York
4. Volkel, U. (1965) Internal Report, DESY 65/6
5. Aitken, T.W. (1970) Daresbury Nuclear Physics Laboratory Report, DNPL/TM70
6. Chaney, J.E. et al. (1973) Lett. Nuovo Cim. 6 339
7. Wilson, R.R. (1958) Phys. Rev. 86 261
8. Tamura, M. (1965) Prog. Theor. Phys. 34 912
9. Muller, D. (1972) Phys. Rev. 5 2677
10. Allkofer, O.C. et al. (1973) Proc. Int. Conf. Cosmic Rays, Denver 2761
11. Kantz, A., Hofstadter, R. (1954) Nucleonics 12 36
12. Ohuchi, F. et al. (1975) Jap. Jour. Appl. Phys. 18 1197
13. Cronin, J.W. et al. (1962) Rev. Sci. Inst. 33 946
14. Hemmi, Y. et al. (1967) Nucl. Inst. & Meth. 56 213
15. Kajikawa, R. (1963) Jour. Phys. Soc. Japan. 18 1365
16. Agrinier, B. et al. (1965) Nuovo Cim. 36 1078
17. Basile, M. et al. (1972) Nucl. Inst. & Meth. 101 433
18. Bauer, A. et al. (1965) Proc. Int. Symp. Electron and Photon Interactions at High Energies, Hamburg, 2 401
19. Franzinetti, C., Gerber, H.J. (1964) NPA Internal Report 64-10
20. Browell, R., Short, K.A. Private Communication, University of Durham
21. Bevington. Data Reduction and Error Analysis for the Physical Sciences. McGraw Hill.

22. Chaney, J.E. et al. (1975) Nucl. Inst. & Meth. 125 189

CHAPTER FOUR

SOME CHARACTERISTICS OF HIGH PRESSURE Ne-He-CH_4 FILLED FLASH TUBES

4.1 INTRODUCTION

Investigations were carried out into the optimum working conditions of the Ne-He-CH_4 filled flash tubes developed by Chaney et al. (1) (see chapter 3, section 3.4.3). These working conditions would then be used in the testing of the modified 768 tube chamber on the positron beam at the Daresbury Laboratory.

The characterisics of the newly developed tubes were studied at low repetition rates at Durham using cosmic rays (2), and at higher repetition rates using the positron beam at the Daresbury Laboratory (3).

In the modified chamber, output information is digitised using the simple probe method (4) and made to set integrated circuit latches, (see chapter 3, section 3.4.5). Thus it is essential that the working conditions of the flash tubes are chosen so that the magnitude of the digitisation pulses remains above 4V in order to set the latches. Therefore the digitised output information from the tubes was investigated as well as the light output.

4.2 VARIATION IN EFFICIENCY OF THE TUBES WITH PARAMETERS OF THE APPLIED FIELD

Some of the tubes were arranged in an array of three layers

separated by H.T. and earth plates. The layer efficiency of the tubes was determined for single cosmic ray muons. The passage of the muon was registered by a two-fold coincidence of plastic scintillators placed above and below the array. The output from the coincidence was used to trigger a spark gap-CR high voltage pulsing system. The time delay between the passage of a particle through the array and the application of the pulsed field was about 200 nsec.

The rise time of the applied field was varied by connecting resistances in series with the H.T. plates. The layer efficiency of the tubes was then measured for various magnitudes and rise times of the applied field. The results obtained are shown in figure 4.1.

Without any resistance connected in the H.T. line the rise time of the applied field was about 70 nsec. Under this condition the plateau region of the layer efficiency was reached at about 9.5 KV cm^{-1}, where a value of 88% was obtained. This corresponds to an internal efficiency of about 100%. It was also observed that spurious flashing took place for applied fields greater than 9.5 KV cm^{-1}, and the number of spuriously flashing tubes increased with increasing applied field.

The value of 9.5 KV cm^{-1} obtained for the position of the plateau region in the efficiency versus applied field curve can be compared with values of about 7 KV cm^{-1} obtained by other workers (5, 6, 7), using conventional high pressure tubes filled with commercial neon. Higher applied fields are needed in the methane doped tubes because of the quenching action of the methane on both the primary ionisation and the actual discharge process in the tube.

A significant variation of layer efficiency with the rise

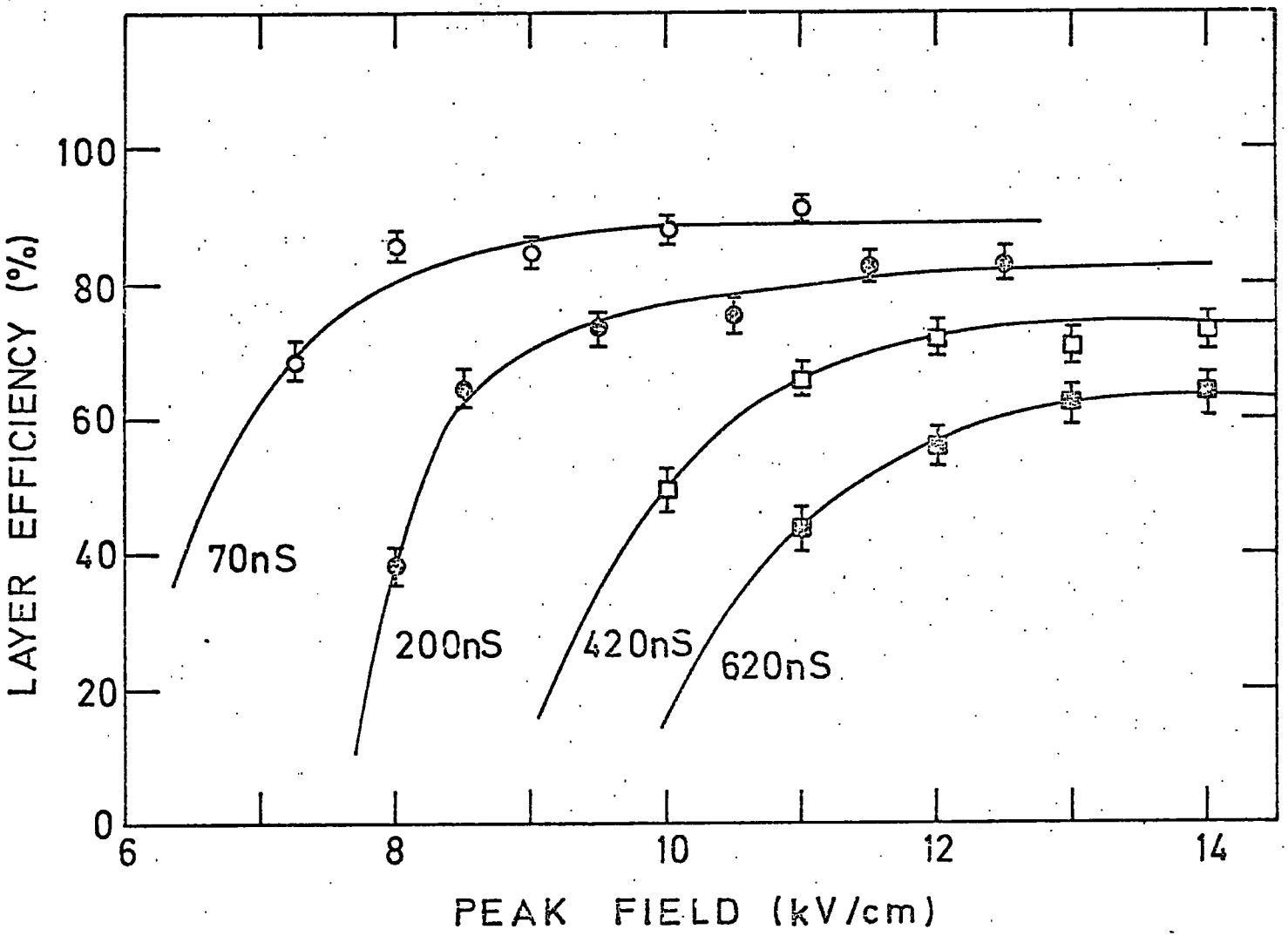

Fig.4-1

Efficiency versus peak field for several rise time values

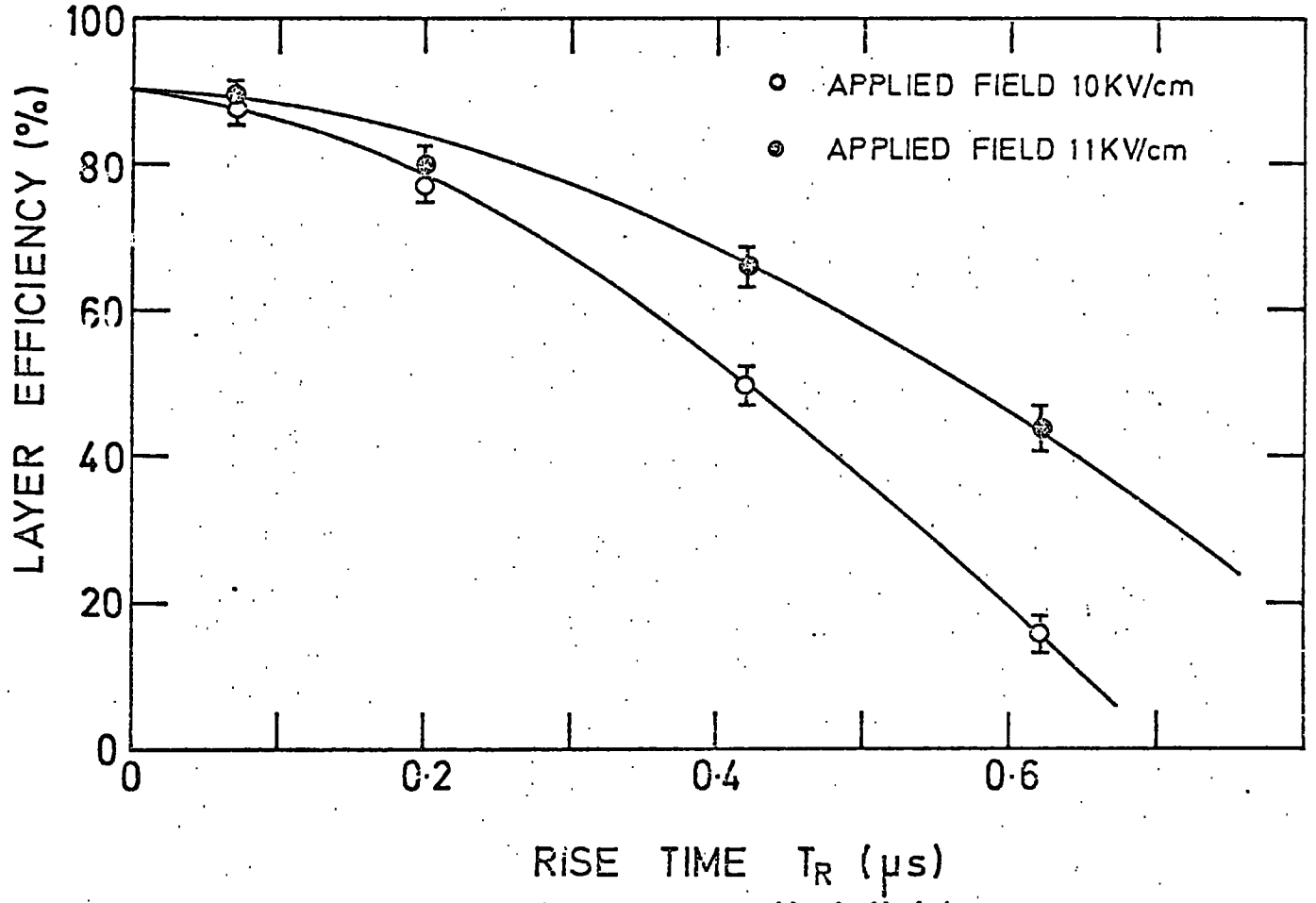

Fig. 4·2

Efficiency versus rise time for different applied fields .

time of the applied field is also indicated in figure 4.1. The layer efficiency of the tubes is plotted against the rise time of the applied field for two different applied field magnitudes in figure 4.2. The efficiency of the tubes is seen to be very dependent on the rise time of the applied field. This is another characteristic of the Ne-He-CH_4 filled tubes which makes them differ so much from conventional high pressure tubes filled with commercial neon, where rise times of 1 μsec. produce layer efficiencies of 70-80% (5, 6, 7). The discrepancies are again due to the quenching action of the methane.

Figure 4.3 shows the variation of layer efficiencies obtained for various widths of applied high voltage pulse, for an applied field of 9 KV cm^{-1}. This was achieved by varying the RC constant of the applied high voltage pulse.

A plateau in the efficiency was reached for an RC pulse width of about 1.5 μsec., however, for pulse widths less than 3 μsec. a dimmer discharge resulted.

4.3 INVESTIGATIONS INTO THE DIGITISATION PULSE HEIGHTS OBTAINED AT SLOW FLASHING RATES

In order to make a detailed study of the digitisation pulse heights obtained from a tube, a small test module was constructed. A diagram of the test module is shown in figure 4.4. The design and dimensions were almost the same as those of a module in the modified flash tube chamber, hence results obtained from the test module would be similar to those one would obtain from a module in the modified flash tube chamber.

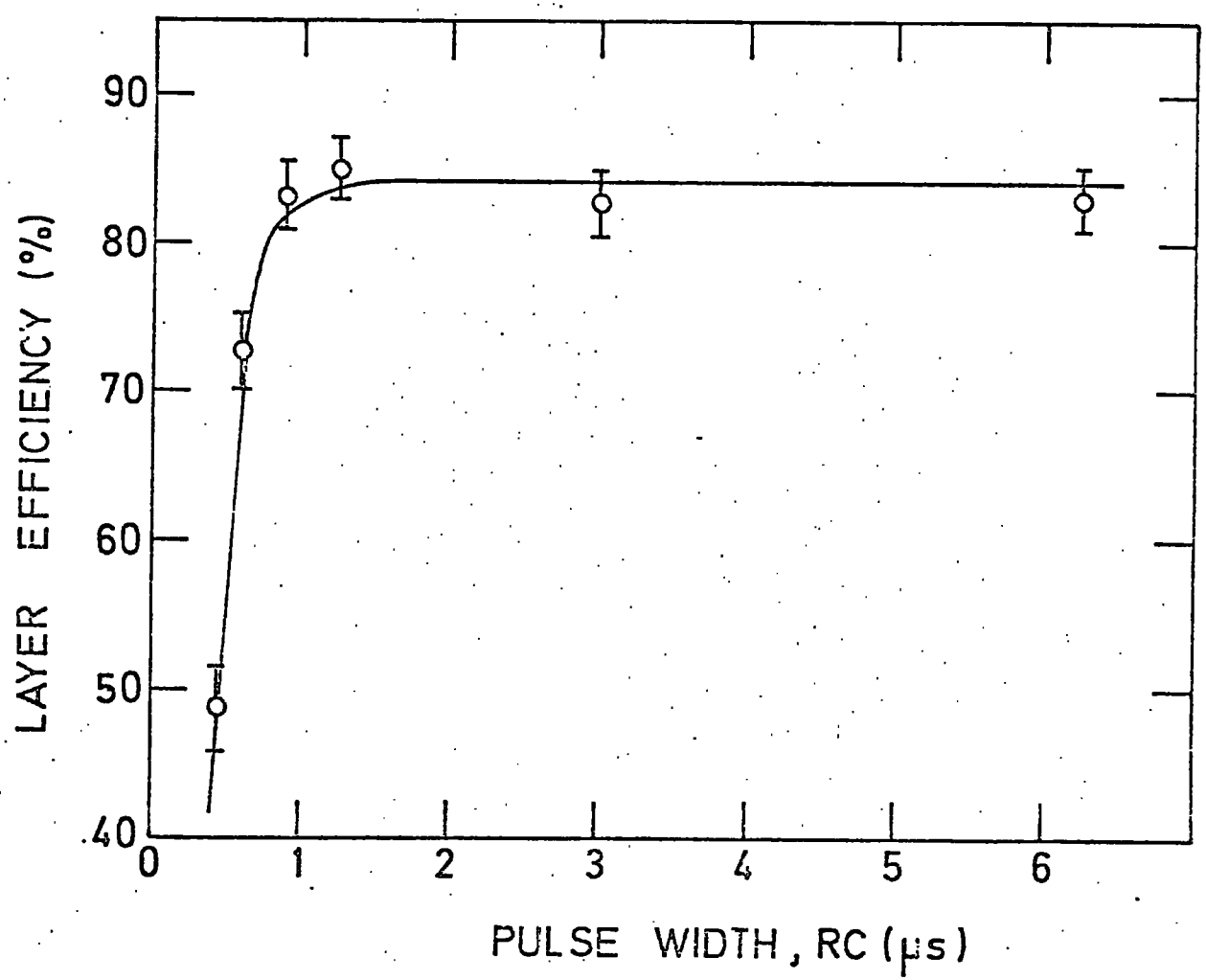

Fig. 4.3

Efficiency versus pulse width.

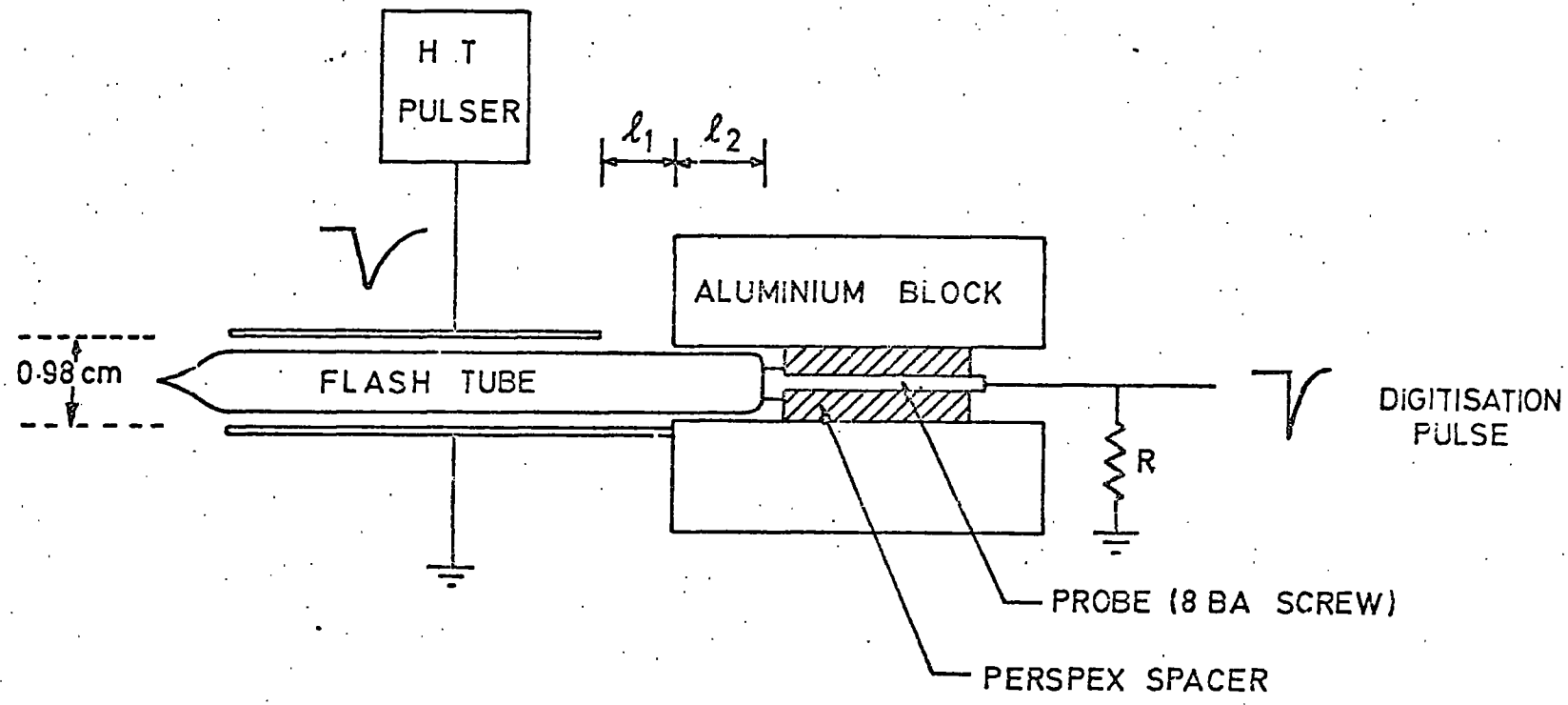

Fig.4-4

Digitisation probe arrangement .

The array of flash tubes used on the efficiency tests was replaced by the test module, and a high voltage pulse was applied for single muon traversals as had been done in previous tests.

The discharge of the tube was accompanied by a digitisation pulse across a resistor connected to a 4 mm. diameter probe placed next to the tube. The value of this resistor, R, could be varied, and digitisation pulses occurring across this resistance were observed on an oscilloscope. Noise produced across the resistor by the pulsed electric field was effectively screened by a surrounding aluminium block.

4.3.1 THE EFFECT ON THE DIGITISATION PULSE OF THE DISTANCE BETWEEN THE H.T. PLATE AND THE FLASH TUBE

It had been noticed by the author and others (8) that variations in distance between the flash tube and the H.T. plate caused large changes in digitisation pulse heights. This effect was investigated using the test module, by placing thin sheets of polythene between the flash tube on test and the H.T. plate. For each separation about 100 digitisation pulse heights were measured. From these pulse height distributions, positions of the most probable pulse height and the spread (standard deviation) of the distributions were measured. The most probable pulse heights are plotted against the separation of the tube and the H.T. plate in figure 4.5. The applied field was 12.0 KV cm^{-1} which may have caused some spurious flashing, but this would not affect the digitisation pulse. The CR decay time of the field was 3 μsec. and the probe resistance R was 5.6 KΩ. The tests were repeated

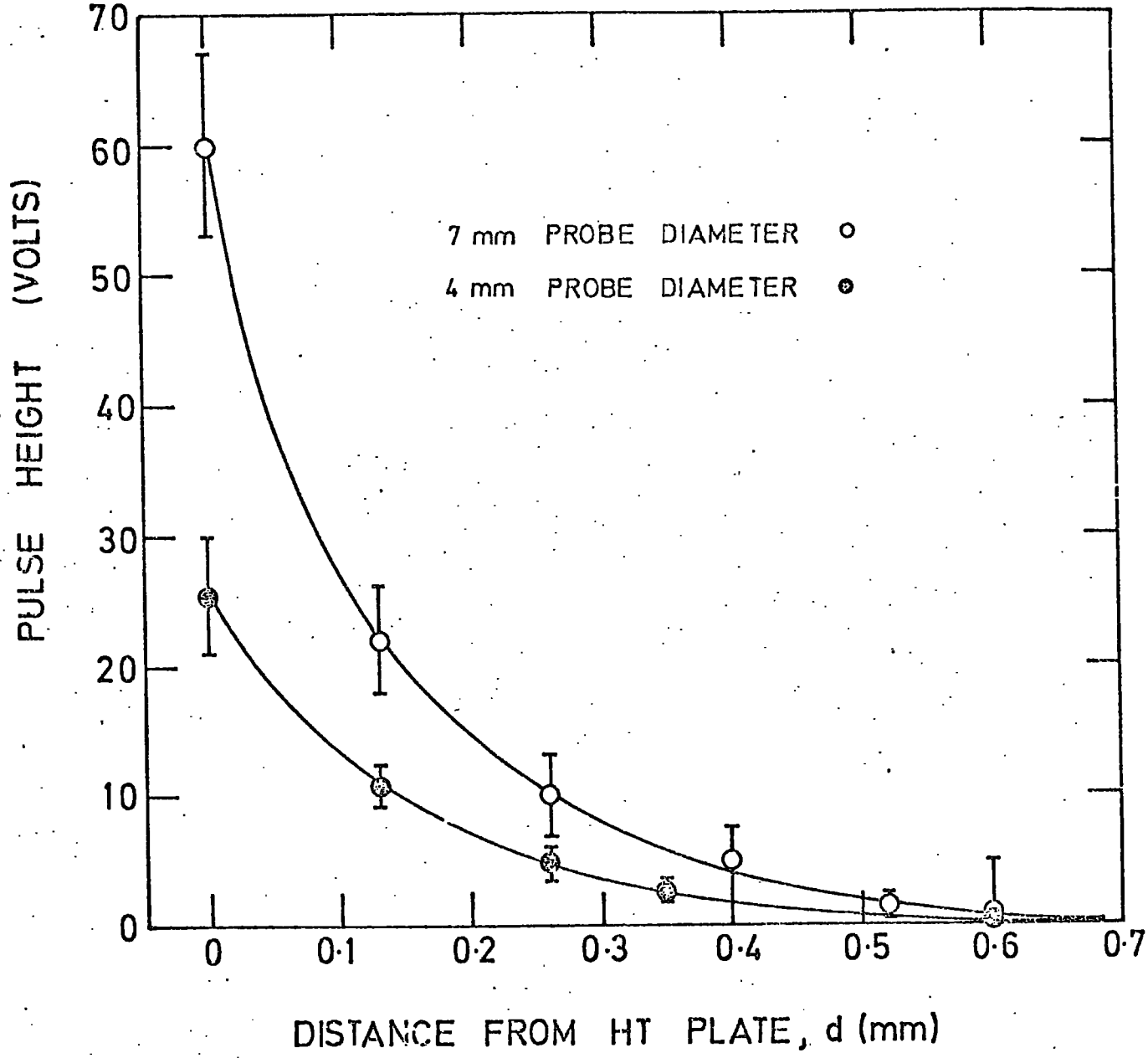

Fig.4·5

Pulse height versus tube–ht plate separation.

using the same tube, but the tube window was painted with a conducting silver paint in order to increase the effective probe diameter to 7 mm.; these results are also shown in figure 4.5. From this figure one can see that a separation (d) as small as 0.1 mm. reduced the pulse height considerably. The two curves are seen to have a similar shape and follow an approximate $1/d^2$ variation.

4.3.2 VARIATION OF DIGITISATION PULSE HEIGHT WITH APPLIED FIELD

About 100 digitisation pulse heights were observed for various applied fields, and the maxima of these distributions are plotted against the applied field in figure 4.6. The RC decay time of the applied fields was 3 μsec., the rise time about 60 nsec. and the delay time between a muon traversal and the application of the pulsed field was about 150 nsec. Results obtained using a 7 mm. diameter circle of conducting paint on the tube window are also shown. Lines drawn through the two sets of data points give two gradients, the ratio of which is found to be 2.5 ± 0.3. Assuming that a digitisation pulse is due to the capacitive pick up of the applied high voltage pulse through the gas plasma and glass by the probe (4), then an increased gradient is expected with an increase in the effective capacitance of the probe. The ratio of the effective areas of the digitisation probes is approximately 3, which agrees with the ratio of the two gradients obtained.

4.3.3 VARIATION OF DIGITISATION PULSE PARAMETERS WITH PROBE IMPEDANCE

Applying an electric field of 10 KV cm^{-1} with a CR decay

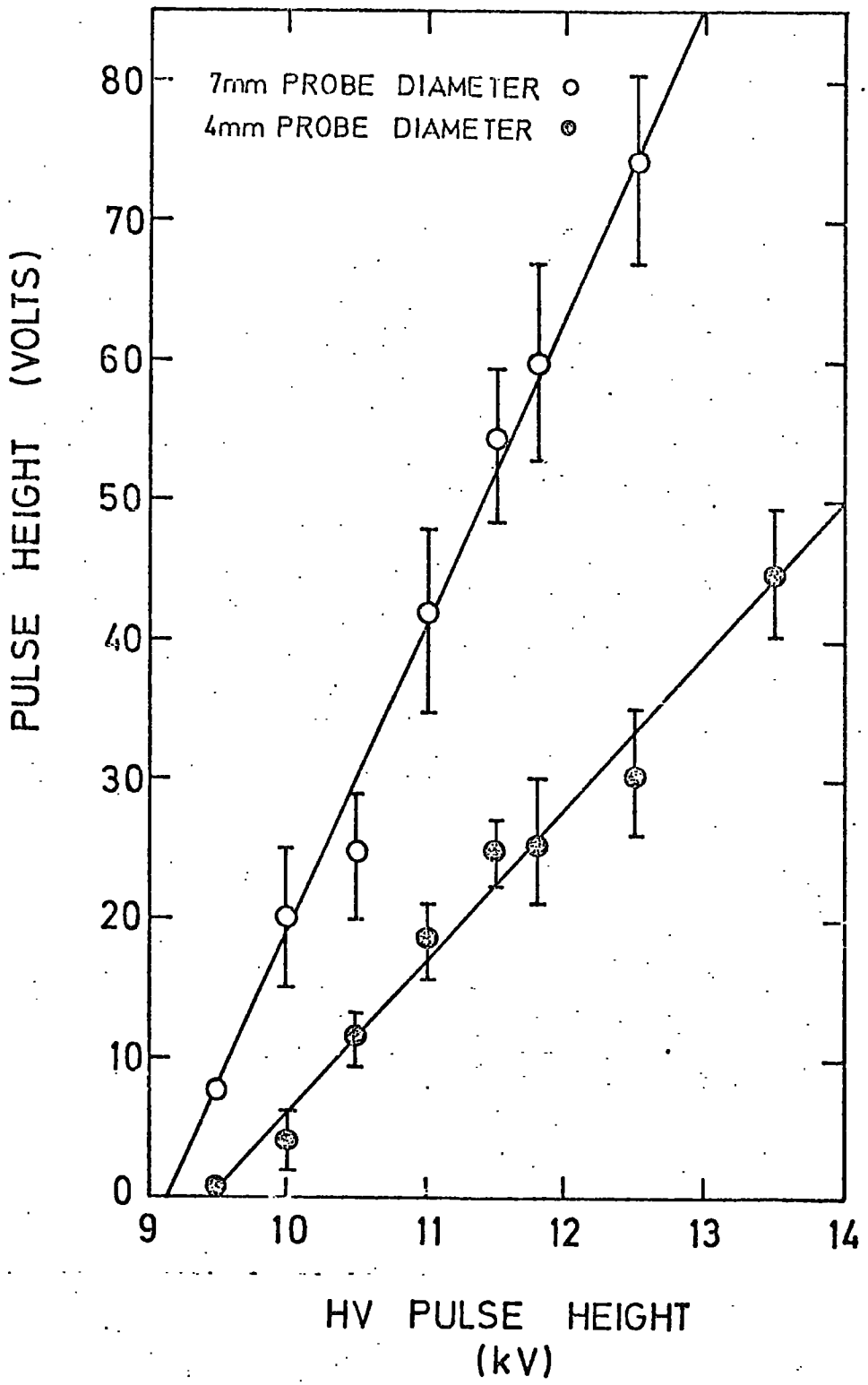

Fig.4.6

Digitisation pulse height versus applied high voltage pulse height .

time of 3 μ sec., the variations in digitisation pulse heights were observed for various probe impedances R (see figure 4.4). The results are shown in figure 4.7. The pulse heights are seen to rise initially with increasing probe impedance, then gradually become constant. This occurs when the probe impedance is high and the impedance due to the stray capacitance of wires etc. becomes similar in comparison; further increases in probe impedance, therefore, have little or no effect on the digitisation pulse height.

The variation of the digitisation pulse length and rise time with R are shown in figure 4.8. Similar trends in digitisation pulse length with probe impedance were found by Ayre and Thompson (4) using high pressure tubes filled with commercial neon.

4.3.4 VARIATIONS IN THE TIME DELAY BETWEEN THE APPLICATION OF THE APPLIED FIELD AND THE APPEARANCE OF THE DIGITISATION PULSE

The time delays between the application of the applied field and the appearance of the digitisation pulse were measured for different separations of the tube and the H.T. plate, and for two different applied fields. The positions of the maxima of the time delay distributions are plotted for different tube-H.T plate separations for the two different applied fields in figure 4.9. It can be seen that the time delay increases with increasing distance between tube and H.T. plate, but decreases with increasing applied field.

The average velocity of propagation of the discharge down the length of the flash tubes can be measured from the time delays between the application of the applied field and the appear-

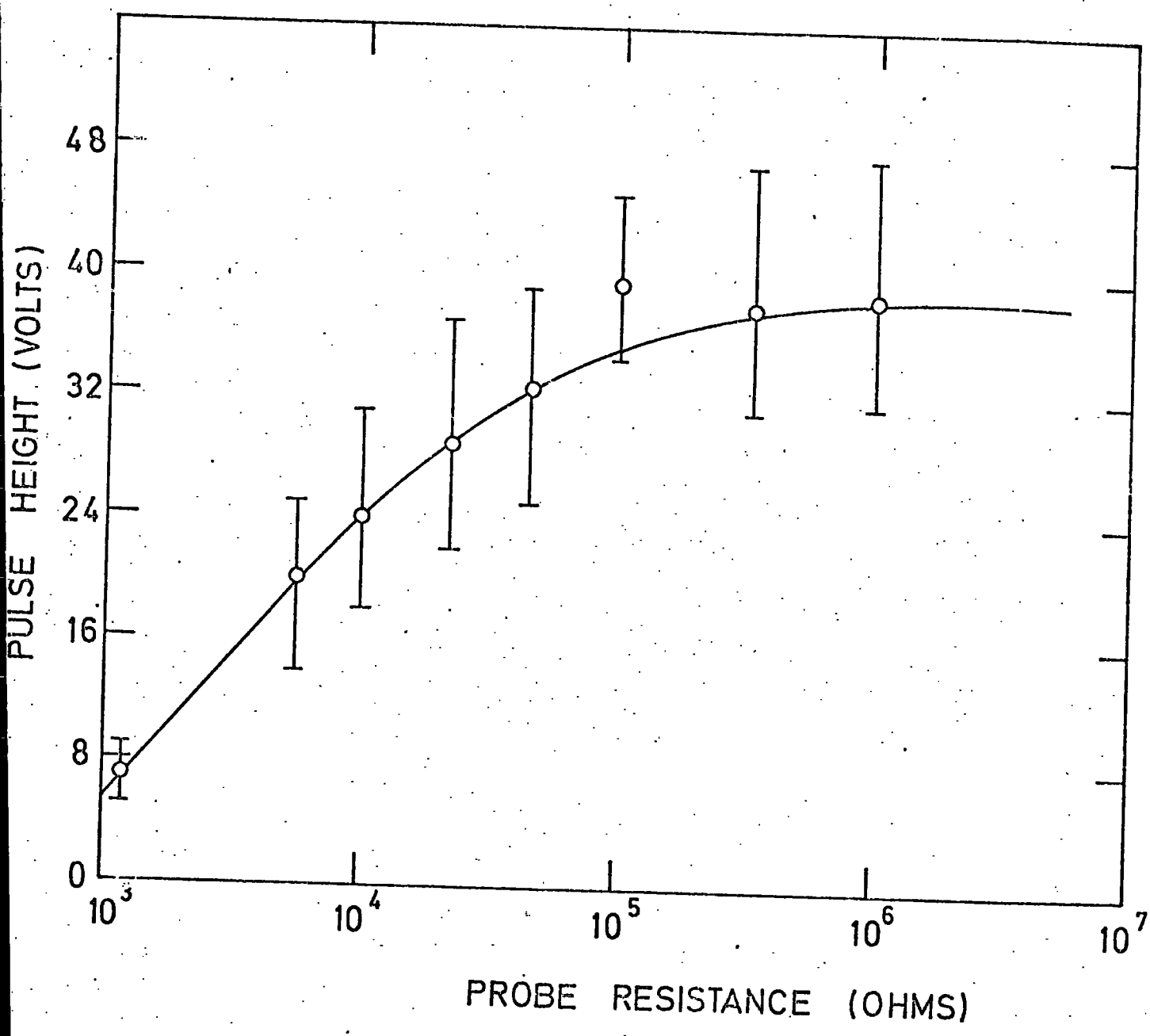

Fig.4.7

Digitisation pulse height versus digitisation probe resistance .

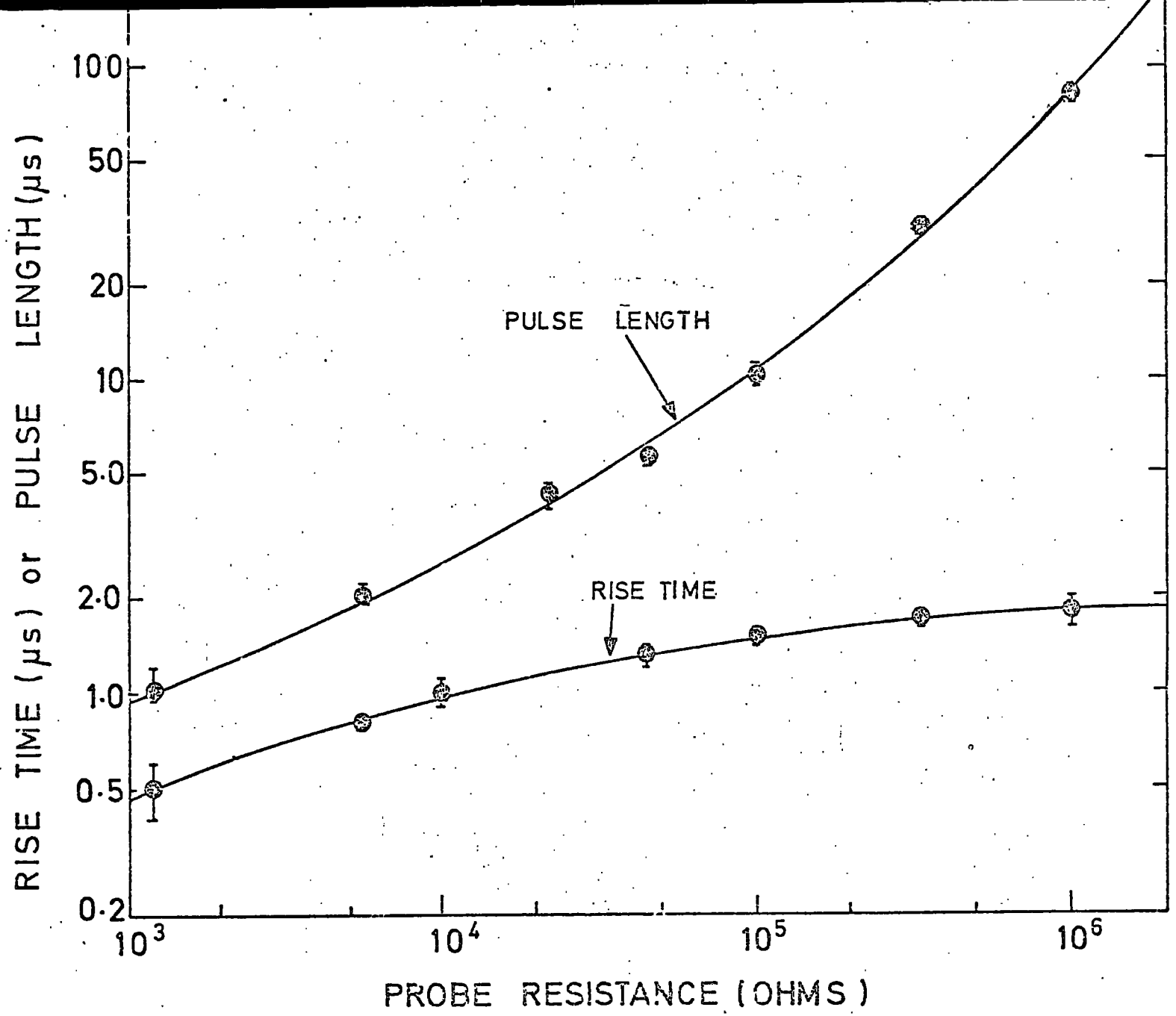

Fig.4.8 Digitisation pulse rise time and length versus digitisation probe resistance.

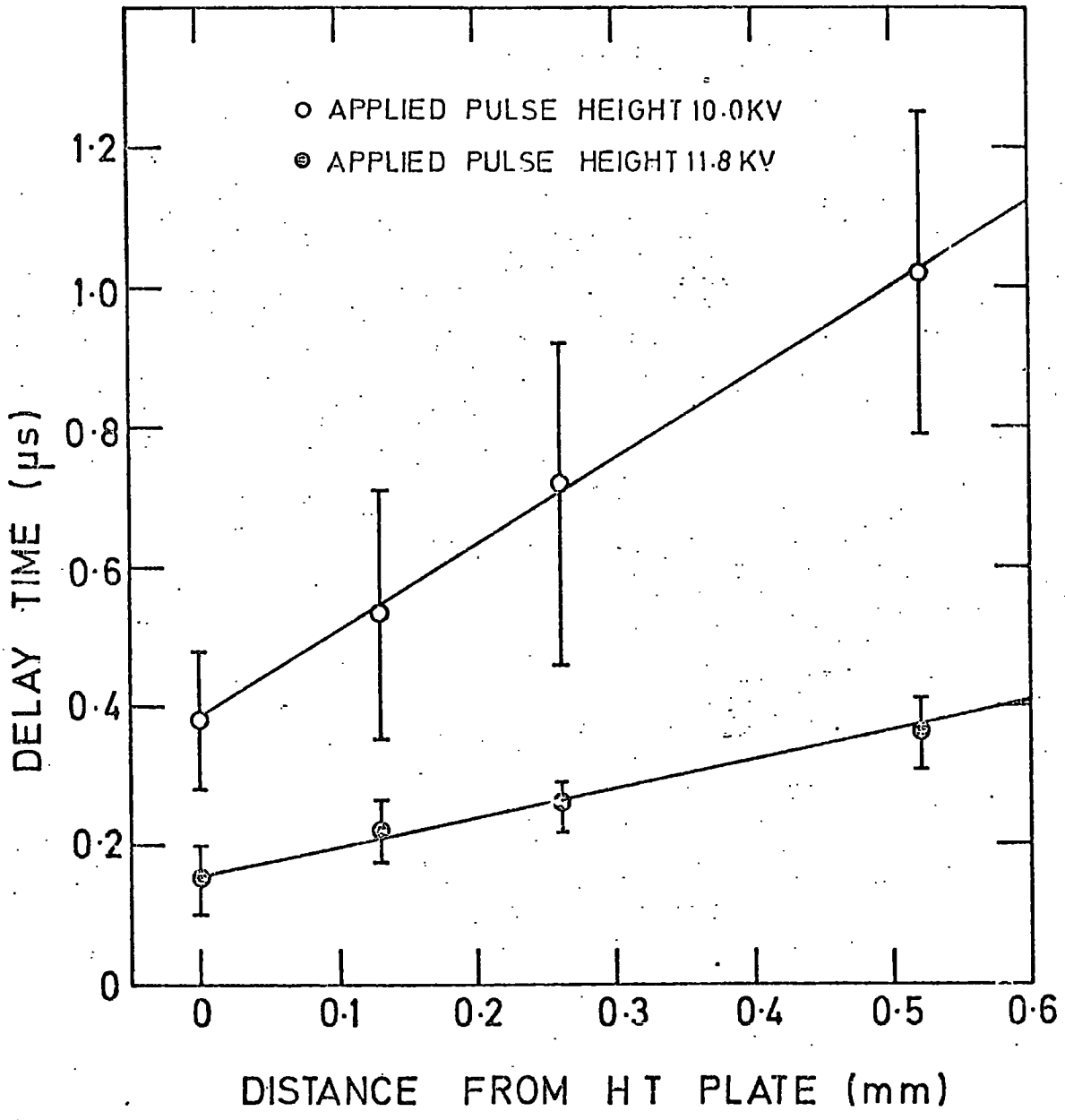

Fig.4·9

Delay time of digitisation pulse versus tube-ht plate separation .

ance of the digitisation pulse. For an applied field of 7.5 KV cm^{-1} across a tube touching the H.T. plate, an average velocity of propagation of about 2×10^5 m sec^{-1} has been estimated. This is about an order of magnitude smaller than the values obtained by other workers (9,10) using high pressure tubes filled with commercial neon.

The most significant mechanisms responsible for the rapid propagation of the discharge along the tube is by the production of ultraviolet photons from the walls of the flash tube. However, in the methane doped tubes a substantial absorption of photons takes place due to the very high and broad photoabsorption cross section of methane (11) resulting in smaller velocities of propagation of the discharge down the tube.

4.3.5 VARIATION OF DIGITISATION PULSE HEIGHT WITH LENGTH OF APPLIED ELECTRIC FIELD

The length of the applied electric field was varied by varying the discharge resistor in the high voltage CR discharge system. About 100 digitisation pulse heights were measured for each length of the applied field, the magnitude of which was 10 KV cm^{-1}. The results obtained are shown in figure 4.10. It can be seen that the digitisation pulse height is considerably increased by increasing the length of the applied field. However, increasing the width of the applied field is limited by the larger resulting induced fields that are built up (12, 13) which may become significant at higher flashing rates (3, 12, 13, 14).

The increase in the digitisation pulse height with the

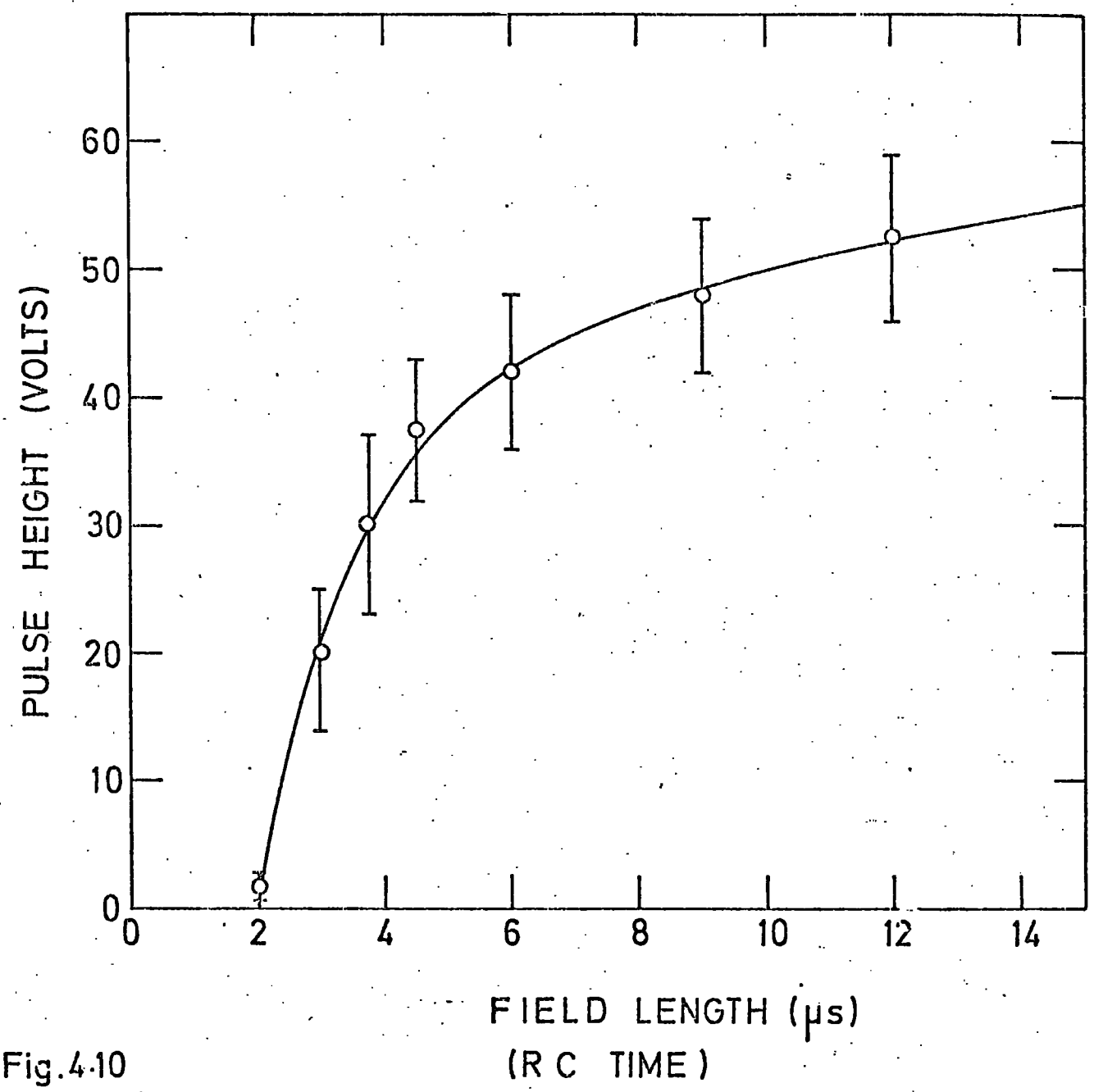

Fig.4.10

Digitisation pulse height versus length of applied field .

increase in length of the applied field, can be explained by considering the digitisation pulse to be due to the capacitive pick up of the H.T. pulse, via the plasma-digitisation probe arrangement. The height of the digitisation pulse should then depend on the state of the applied field at the moment of pick up by the probe, and should therefore depend on the characteristics of the applied field (ie. length, rise time etc.).

From the results shown in figures 4.6, 4.8 and 4.9, estimates of the expected digitisation pulse heights for various lengths of applied field were made using the assumptions above. For various applied H.T. pulses of different magnitudes, but the same RC decay constant of 3 μ sec., the effective magnitudes of the applied H.T. pulses were calculated at the moment of pick up by the probe, assuming the digitisation pulse rise times and delay times given by figures 4.8 and 4.9. Figure 4.6, which gives digitisation pulse heights for various applied fields of 3 μ sec. in length, was then modified to give digitisation pulse heights for various effective applied fields, and was used as a calibration graph.

The effective heights of applied H.T. pulses were calculated for a 10 KV applied H.T. pulse of varying lengths, and the corresponding digitisation pulse heights expected were obtained from the calibration graph. The results obtained for measured and calculated values of digitisation pulse heights for various H.T. pulse lengths are shown in table I.

A close agreement is seen between the measured and calculated digitisation pulse heights, supporting the belief that the digitisation pulse is formed by the close capacitive coupling between the H.T. plate and the digitisation probe.

TABLE I

MEASURED AND CALCULATED VALUES OF PULSE HEIGHTS

FOR DIFFERENT H.T. PULSE LENGTHS

Applied H.T. pulse height = 10 KV

Probe resistance = 5.6 K Ω

Probe diameter = 7 mm.

Tube-H.T. plate separation = 0 mm.

Applied H.T. pulse length (RC time in μsec.)	Effective H.T. pulse height (KV)	Measured digitisation pulse height (volts)	Calculated digitisation pulse height (volts)
2.0	7.0	1.5 ± 1.0	3.5
4.5	8.6	37.5 ± 5.5	32.0
6.0	8.9	42.0 ± 6.0	38.5
9.0	9.3	48.0 ± 6.0	45.0
12.0	9.4	52.5 ± 6.5	48.5

To find whether the increase in delay time due to increased tube-H.T. plate separation, could be the cause of the observed decrcase in digitisation pulse height shown in figure 4.5, digitisation pulse heights were calculated for different separations using the curves in figure 4.9 and the calibration graph.

It was found that the increase in time delay alone, due to the tube-H.T. plate separation, was not sufficient to cause the sharp decrease in digitisation pulse height observed. It is thought that some resistive coupling may be taking place between the H.T. plate, tube and probe.

4.4 INVESTIGATIONS INTO THE DIGITISATION PULSE HEIGHTS AT HIGH FLASHING RATES

In order to study the digitisation pulse heights obtained from the tubes at fast flashing rates, it was necessary to use the positron beam facility at the Daresbury Laboratory. A modified test module was constructed which was similar in design to the original test module, but with dimensions the same as those of a module in the modified 768 flash tube chamber. The digitisation probe was a 6 BA screw mounted in a perspex cylinder, and the probe impedance (R) was 5.6 KΩ. An aluminium disc of 7 mm. diameter was attached to the flash tube window giving an effectively larger area digitisation probe, in order to give larger digitisation pulses.

The modified test module was mounted in the positron beam as shown in figure 4.11. Single positrons were selected from the beam by means of a four-fold coincidence of scintillation counters

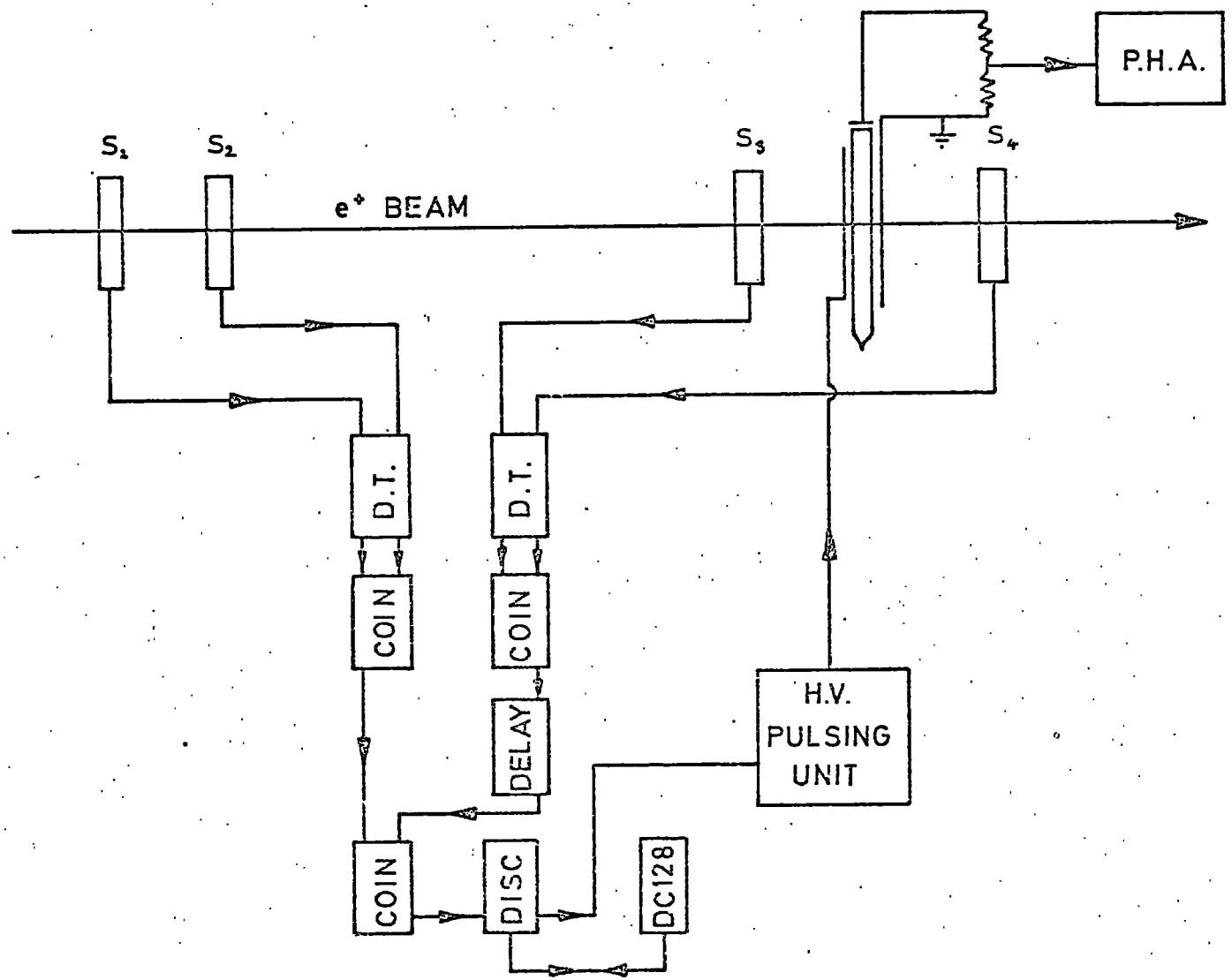

Fig.4.11

The data aquisition system .

S_1, S_2, S_3 and S_4, the coincidence signal of which was used to trigger the high voltage pulsing system.

A CR decaying high voltage pulse was used throughout the tests, the characteristics of the applied field being;- applied electric field 10.0 KV cm^{-1}, delay time 200 μsec., width (CR time) 4.5 μsec. and rise time 70 nsec.

A charging time (CR) of 15 msec. was used in the investigations, so as not to affect the magnitude of the applied field when working at fast flashing rates.

The flashing rate was varied by using the paralysis unit, which disabled the coincidence circuits of the scintillators for a fixed period of time after each coincidence.

The digitisation pulse heights obtained were stored in a pulse height analyser.

4.4.1 VARIATION OF DIGITISATION PULSE HEIGHT WITH FLASHING RATE

The flashing rate of a flash tube was varied between 0.5 per second and 4.6 per second, and about 1500 digitisation pulse heights were recorded for each flashing rate. The most probable values of the pulse heights were found from these pulse height distributions and are plotted as a function of flashing rate in figure 4.12. The digitisation pulse heights are seen to be very strongly dependent on the flashing rate of the tube, an increase in flashing rate from 0.45 per second to 1.1 per second, caused a decrease in digitisation pulse height from about 48 V to 13 V.

The rapid decrease in the digitisation pulse heights was due to the build up of very large induced clearing fields inside the

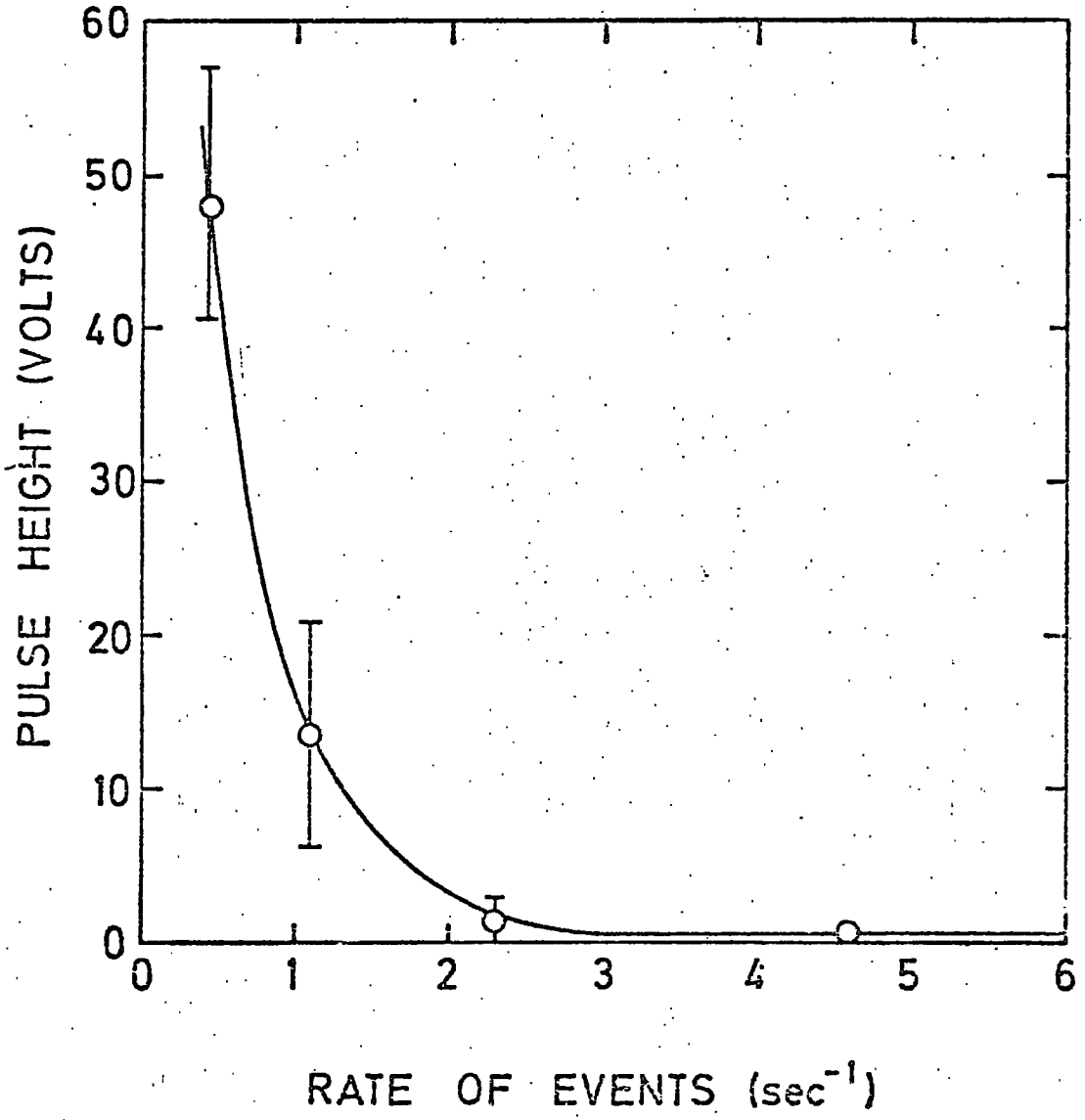

Fig. 4.12

Digitisation pulse height versus flashing rate .

tube at the higher flashing rates. The induced fields decay exponentially with time (15, 16, 17, 18, 19), the rates of decay depending on the resistance and capacitance of the glass flash tube. The direction of the induced field is in the opposite direction to that of the applied field, therefore at the faster flashing rates, when the induced fields have less time to decay, the effective applied fields are lower, hence the digitisation pulses resulting from the pick up of the high voltage pulses are lower.

However, a rapid decrease in digitisation pulse height with flashing rate was not observed by Chaney et al. (1) at flashing rates up to 50 Hz. This probably results from the fact that they were using larger diameter flash tubes and were applying much lower electric fields. Electric fields of 6 KV cm^{-1} were used, whereas it has been observed that applied electric fields in excess of 6 KV cm^{-1} build up substantially larger clearing fields (13).

4.4.2 VARIATION OF DIGITISATION PULSE HEIGHT WITH APPLIED FIELD AT HIGH FLASHING RATES

About 1500 digitisation pulse heights were recorded for each of several applied fields, at a flashing rate of 4.6 per second. The dependance of the digitisation pulse height on the applied high voltage pulse is shown in figure 4.13. This curve can be compared with that of digitisation pulse height versus applied field taken at low flashing rates (figure 4.6). At the lower flashing rates a linear rise of digitisation pulse height is seen with rising applied field, however at the faster flashing rates the relationship deviates from the linear. This is further evidence of

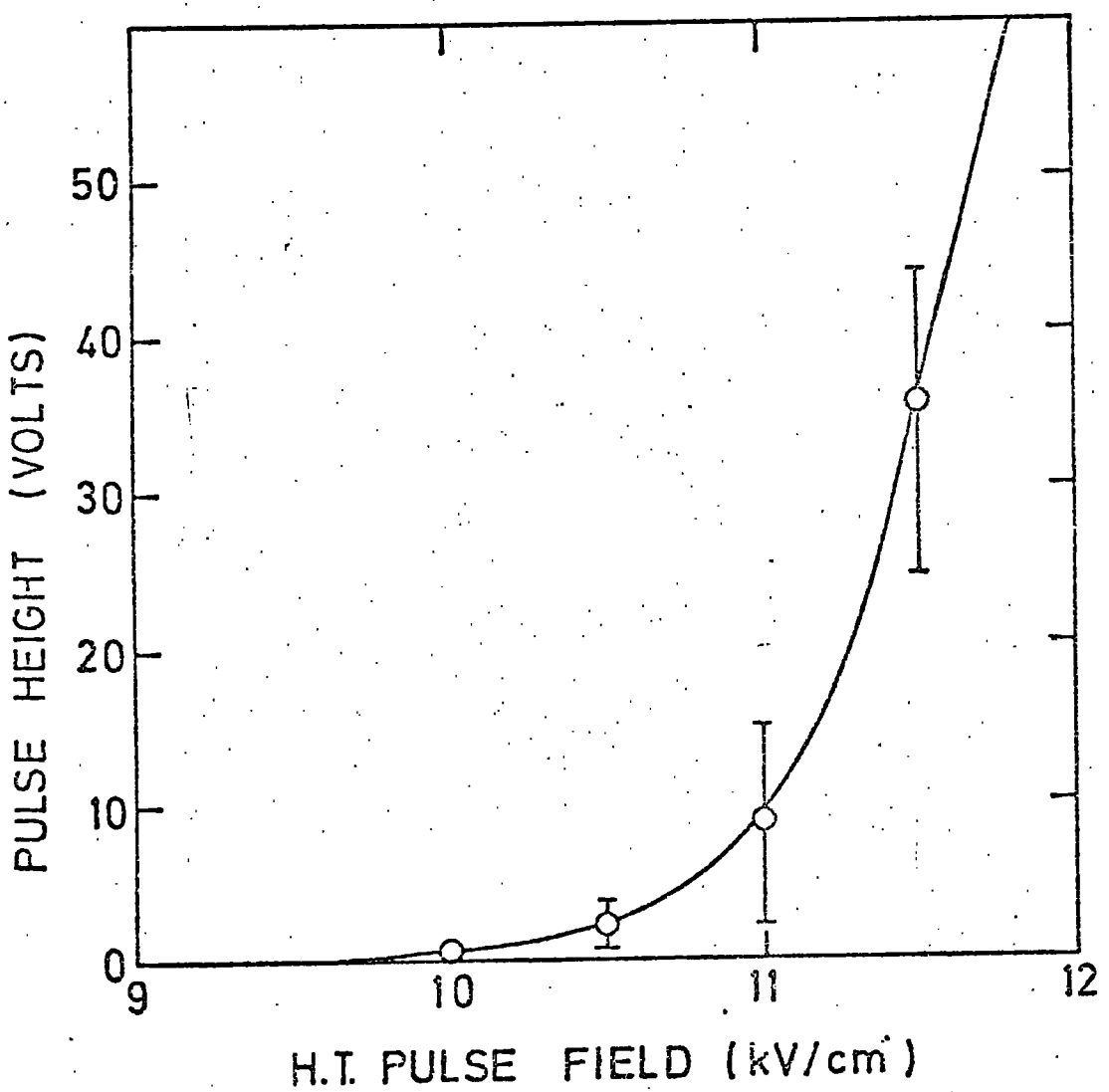

Fig. 4-13 Digitisation pulse height versus applied field.

the large induced clearing fields, which modify the applied field, at the higher flashing rates.

4.5 CONCLUSIONS

Unlike conventional high pressure flash tubes the Ne-He-CH_4 filled tubes must be operated under certain working conditions, to ensure that satisfactory digitised information is obtained. These conditions primarily arise due to the addition of methane to the gas mixture, which produces a marked quenching effect on the discharge process.

The Ne-He-CH_4 tubes require the application of pulsed electric fields at minimum delays, and having rise times of 70 nsec. or less. A high electric field, in the region of 9 - 10 KV cm^{-1}, is also required for the satisfactory functioning of the tubes, and a pulsed field width (CR) of about 3 - 5 μ sec. is necessary so as to minimise the build up of induced clearing fields in the tubes.

Due to this build up of clearing fields when working at rates of several events per second, the working rate of the tubes is restricted to a few events per minute only.

However, a high voltage pulsing system has recently been developed (19) which greatly reduces the build up of induced clearing fields, when applying high electric fields to small diameter flash tubes. This pulsing system is described in detail in chapter 7.

The digitisation pulses obtained from the Ne-He-CH_4 filled flash tubes can be greatly increased if the tubes are mounted in such a way that they are in good contact with the H.T. planes, and

if the areas of the digitisation probes are increased providing better coupling between the applied high voltage pulse and the digitisation probes.

The H.T. planes, digitisation probes and integrated circuit boards were modified in the 768 flash tube chamber, to ensure that digitisation pulse heights in excess of 4 V were obtained when working at flashing rates of several events per tube per minute. The modified 768 flash tube detector was then tested in the positron beam at the Daresbury Laboratory at slow flashing rates. The tests were in order to study the feasibility of the flash tube chamber in the detection of electromagnetic showers, produced by positrons of a few GeV in energy.

The set up of the chamber on the positron beam, and the results obtained from the chamber, are presented in the two following chapters.

REFERENCES

1. Chaney, J.E., Breare, J.M. (1975) Nucl. Inst. & Meth. 124 61
2. Breare, J.M. et al. (1976) Nucl. Inst. & Meth. 133 415
3. Breare, J.M. et al. (1976) Nucl. Inst. & Meth. In the Press
4. Ayre, C.A., Thompson, M.G. (1969) Nucl. Inst. & Meth. 69 106
5. Gardener, M. et al. (1957) Proc. Phys. Soc. B70 687
6. Coxell, H, Wolfendale, A.W. (1960) Proc. Phys. Soc. 75 378
7. Hampson, H.F., Rastin, B.C. (1971) Nucl. Inst. & Meth. 95 337
8. Thompson, M.G. et al. (1976) Private Communication, University of Durham
9. Ayre, C.A., Thompson, M.G., Whalley, M.R., Young, E.C.M. (1972) Nucl. Inst. & Meth. 103 49
10. Evans, W.M., Baker, J.C. (1971) Internal Report, Rutherford High Energy Laboratory, RHEL/M/H/4
11. Wainfan, N., Walker, W.C., Weissler, G.L. (1955) Phys. Rev. 99 542
12. Holroyd, F.W., Breare, J.M. (1972) Nucl. Inst. & Meth. 100 429
13. Brosco, G., Cialdea, R., Conversi, M., Zolesi, B. (1973) Proc. Int. Conf. on Inst. for High Energy Physics, Frascati, 211
14. Ferguson, H., Rastin, B.C. (1971) Nucl. Inst. & Meth. 96 405
15. Ashton, F. et al. (1971) Lett. Nuovo Cim. 2 707
16. Holroyd, F.W., Breare, J.M. (1972) Nucl. Inst. & Meth. 100 277
17. Chaney, J.E. (1973) Ph.D. Thesis, University of Durham
18. Breare, J.M., Doe, P.J. (1976) Nucl. Inst. & Meth. 133 247
19. Breare, J.M., Nandi, B.C., Tait, I.D. (1976) Nucl. Inst & Meth. (in preparation)

CHAPTER FIVE

OPERATION OF THE MODIFIED FLASH TUBE CHAMBER ON A POSITRON BEAM

5.1 INTRODUCTION

Having found the optimum working conditions of the Ne-He-CH_4 tubes (chapter 4), the modified flash tube chamber containing these tubes was tested in a positron beam at the Daresbury Laboratory.

These tests were similar to those done earlier in the positron beam using the prototype chamber (1, 2) (see chapter 3), and included investigations into the optimum working rate and efficiency of the chamber, together with the detection of electromagnetic showers produced by positrons of a few GeV in energy. However, these later tests utilised a computer link in the sending and storage of data from the chamber.

A description of the initial tests done on the chamber in the laboratory, the set up of the chamber in the positron beam and the taking of data in the beam is given in this chapter (3).

The analysis of the electromagnetic shower data taken and the results obtained are presented in the following chapter.

5.2 INITIAL CHAMBER TESTS

Several modifications were made to the chamber in order to increase the digitisation pulse heights obtained from the flash tubes.

The modules were modified in order to provide good contact between tubes and H.T. plates. Thin aluminium foil was wrapped

around the edges of the H.T. plates nearest the digitisation probes and strips of thin rubber foam were added to the inside surfaces of the earth plates. The rubber foam exerted a small inward pressure on the tubes ensuring a good contact between them and the aluminium foil. Perspex spacers were also added to the insides of the modules to ensure that the H.T. plates remained central.

Small thin 7 mm. diameter aluminium discs were glued to the flash tube windows, in order to increase the effective probe diameters.

The digitisation pulse heights obtained from the modified modules were studied using cosmic rays. Each modified module was placed horizontally between two scintillators, a coincidence from which was used to trigger the chamber pulsing unit which applied a high voltage pulse to the H.T. plate. The resulting field was about 10 KV cm^{-1} and had a CR decay time of 5 μ sec. The integrated circuit boards were removed from the modules and the resulting digitisation pulse heights, obtained across a 5.6 KΩ resistor, were sampled from each module.

The digitisation pulse heights were all found to be greater than the 4 V threshold needed to set the latches in the chamber, average pulse heights of 20 or 30 V were obtained.

These large digitisation pulses meant that the integrated circuit boards had to be modified in order to protect the standard T.T.L. circuits. Five volt zener diodes were therefore connected across the inputs of the integrated circuit boards.

The modified integrated circuit boards were individually tested to ensure a set output voltage for a given input signal, and to ensure resetting on the application of a reset pulse.

The wiring of the reassembled chamber was then checked to ensure a one to one tube-probe correspondance. Digitisation inputs were manually set and the resulting outputs from the latches were observed using a 128 light emitting diode display.

The modified chamber was mounted on a traversing table in the positron test beam area at the Daresbury Laboratory, where the modules were aligned to within ± 0.5 mm.

5.3 THE POSITRON BEAM FACILITY AT THE DARESBURY LABORATORY

The positron beam is a low intensity, monochromatic beam of variable energy, produced by double conversion of the circulating electron beam of NINA the Daresbury synchrotron (4).

The positron beam passes through a beam pipe in the wall surrounding the main circulating electron beam and then enters the positron test beam area where the flash tube chamber was set up. Personnel can work in safety within the vicinity of the positron beam in this area.

The beam line elements producing the positron beam are shown in figure 5.1.

The positron beam can be obtained either from a "parasitic" or "bump" mode of extraction. In the former method, parasitic electrons which circulate the accelerator after the main electron beam has been targetted by other users, are used to produce the positron beam. These parasitic electrons deviate from the main circulating orbit and strike a tungsten target (target no. 4) at the beginning of the positron beam line.

In the bump mode of extraction, which is the method used in

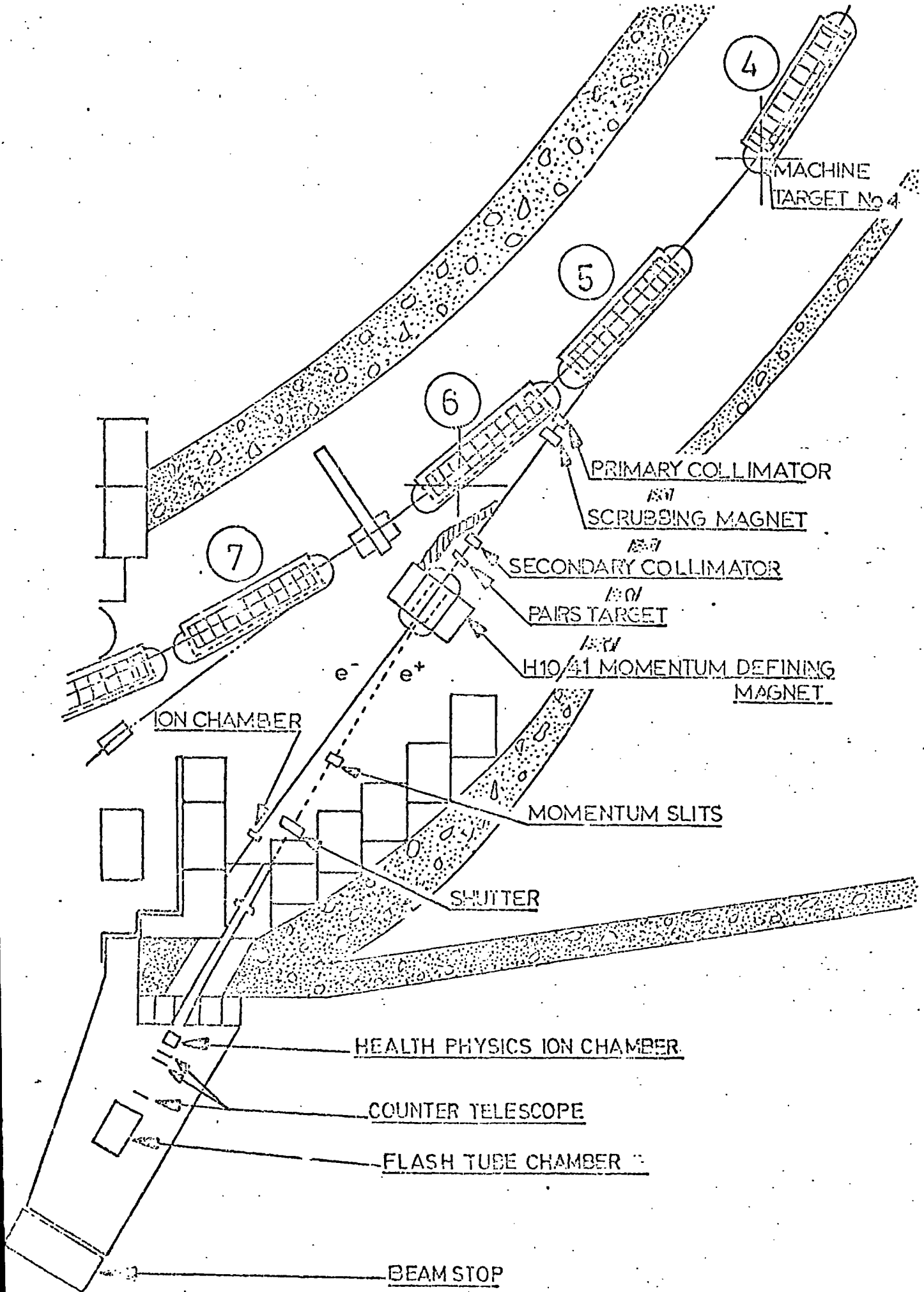

ig.5.1

The DNPL e^+ beam line and the Flash Tube Chamber.

testing the flash tube chamber, a small perturbation is introduced into the magnetic field of the circulating magnet no. 4. This causes some of the circulating electrons to leave their orbit and strike the tungsten target. This method of extraction is preferred in the testing of the chamber as continuously controllable beams are produced.

Electrons incident on the tungsten target produce a photon beam which is collimated and then stripped of charged particles by a permanent magnet. The "clean" beam is then collimated once more and made to impinge on a copper target where the photons are converted to electron-positron pairs. Positrons of the desired momentum are then selected by a bending magnet and a momentum slit. The positron beam emerges through a long square collimator in the main wall surrounding the synchrotron into the positron test beam area. On entering this area the positrons pass through an ionisation chamber monitoring system, which trips a shutter when the positron beam intensity exceeds a safe working level.

The resulting beam in the test beam area can consist of positrons having energy from about 200 MeV to about 4 GeV with a spread of $\pm 1.0\%$ or less.

The main circulating electron beam is accelerated and extracted every 19 msec., hence working in beam "bump" mode, a positron beam can be obtained in the test beam area about 50 times a second.

However, in the testing of the flash tube chamber, very low flashing rates were needed so the lowest extraction rate was used. This rate produced about one positron beam spill per second in the test beam area, the beam being produced by applying a

perturbing field or "bump" once every sixty acceleration cycles of the main beam. This extraction rate was effectively reduced by incorporating a paralysis unit in the logic of the data acquisition system.

The cycling times of the main beam and the position of the beam "bump" in time are shown in figure 5.2. The position of the beam "bump" with respect to the minimum field of the circulating magnets and the magnitude of the beam "bump", could be varied in order to produce the required positron beam intensity. The width of the beam "bump" can also be varied. A short "bump" lasting about 0.6 msec., or a longer one of 1.0 msec. can be applied.

In the short "bump" mode, positrons in a spill were found to be very bunched, with separation between some positrons being about 20 nsec. Such close bunching of particles produces multiple tracks in the chamber, however, in the long "bump" mode particle separations were found to be several μ sec. at the beginning of a spill, so this mode of operation was employed in testing the chamber.

The position and magnitude of the beam "bump" were varied to give about 30 positrons per spill in the test beam area. A 1.1 mm x 3.84 mm. momentum defining slit was also used to give a beam profile of several centimeters in diameter on the front module of the chamber.

5.4 DATA ACQUISITION SYSTEM

The path of the positron beam in the test beam area was located by means of a Geiger counter, and the position of the flash

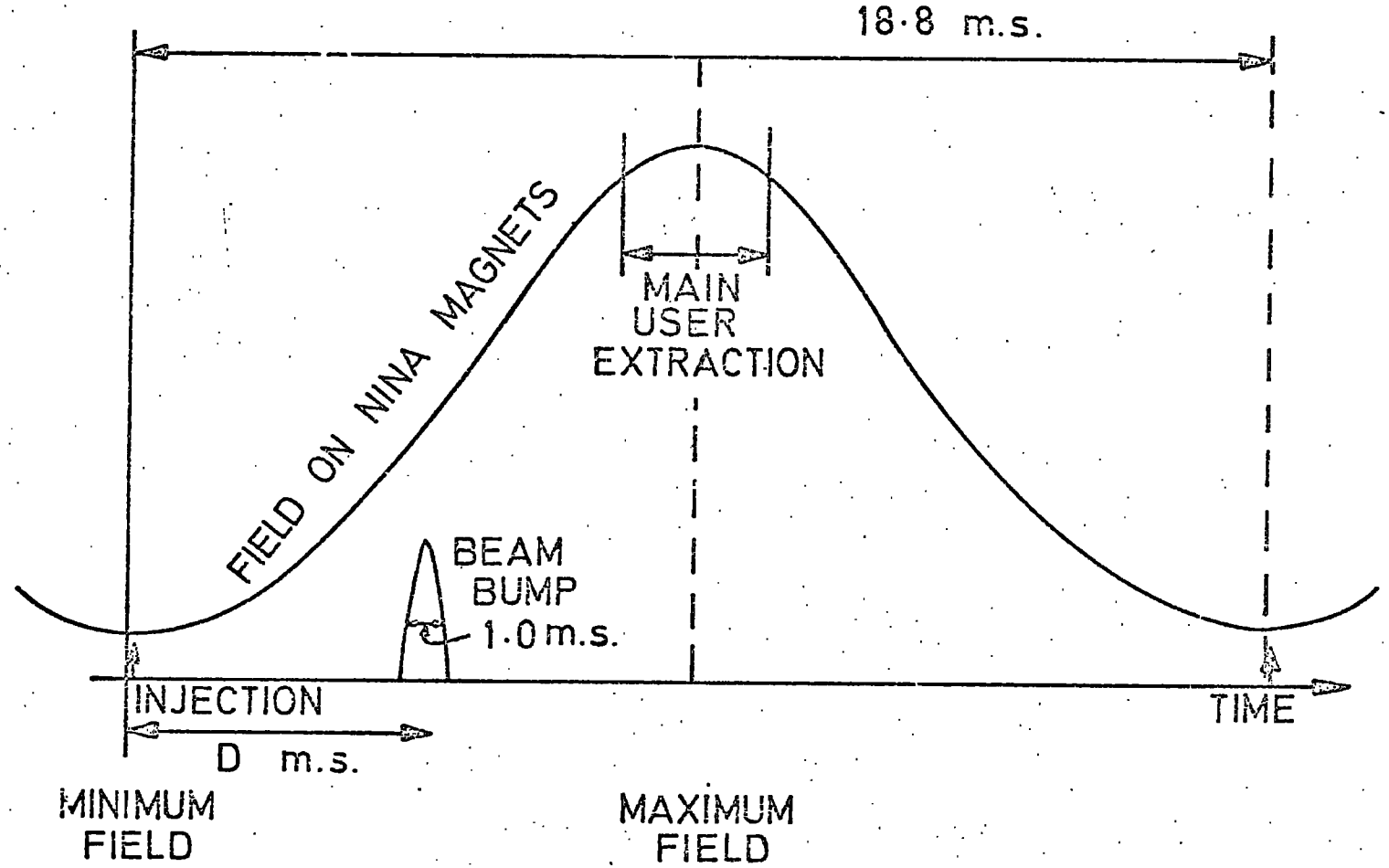

Fig.5·2 The beam cycling times .

tube chamber was varied until the beam was incident on its centre. Four scintillators were placed upstream of the chamber, the coincidences of which were used to define incident positrons (see figure 5.3).

Because of the bunching of positrons in the central regions of a beam spill, the coincidence circuit was gated off until a millisecond or so before the beginning of a beam spill, then enabled for about 5 msec. This meant that coincidences were obtained on well separated positrons at the beginning of a spill.

The timing of the coincidence circuit was done with respect to a scalar pulse, which was fed by cable to the test beam area from the main control room of the synchrotron. The scalar pulse, indicating that the main circulating magnets were at minimum field, was delayed for about (D - 1)msec. using an EG & G standard GG200 unit, and was then used to enable the scintillator coincidence circuit for about 5 msec. (c.f. figure 5.2 for definition of D).

A coincidence from this circuit then signified a single separate positron incident on the chamber. The coincidence signal was fanned out, one output going to a paralysis unit. This unit then disabled the coincidence circuit for a fixed period of time, usually several seconds, thus defining the event rate. This unit also disabled the dual trigger, DT3. This ensured that after the paralysis period the coincidence circuit was only enabled via a scalar pulse, thus preventing coincidences due to parasitically produced positrons or positrons in the centre of a spill.

A second output from the coincidence unit was used to trigger the high voltage pulsing unit mounted on the top of the flash tube chamber, which produced a high voltage pulse on the H.T.

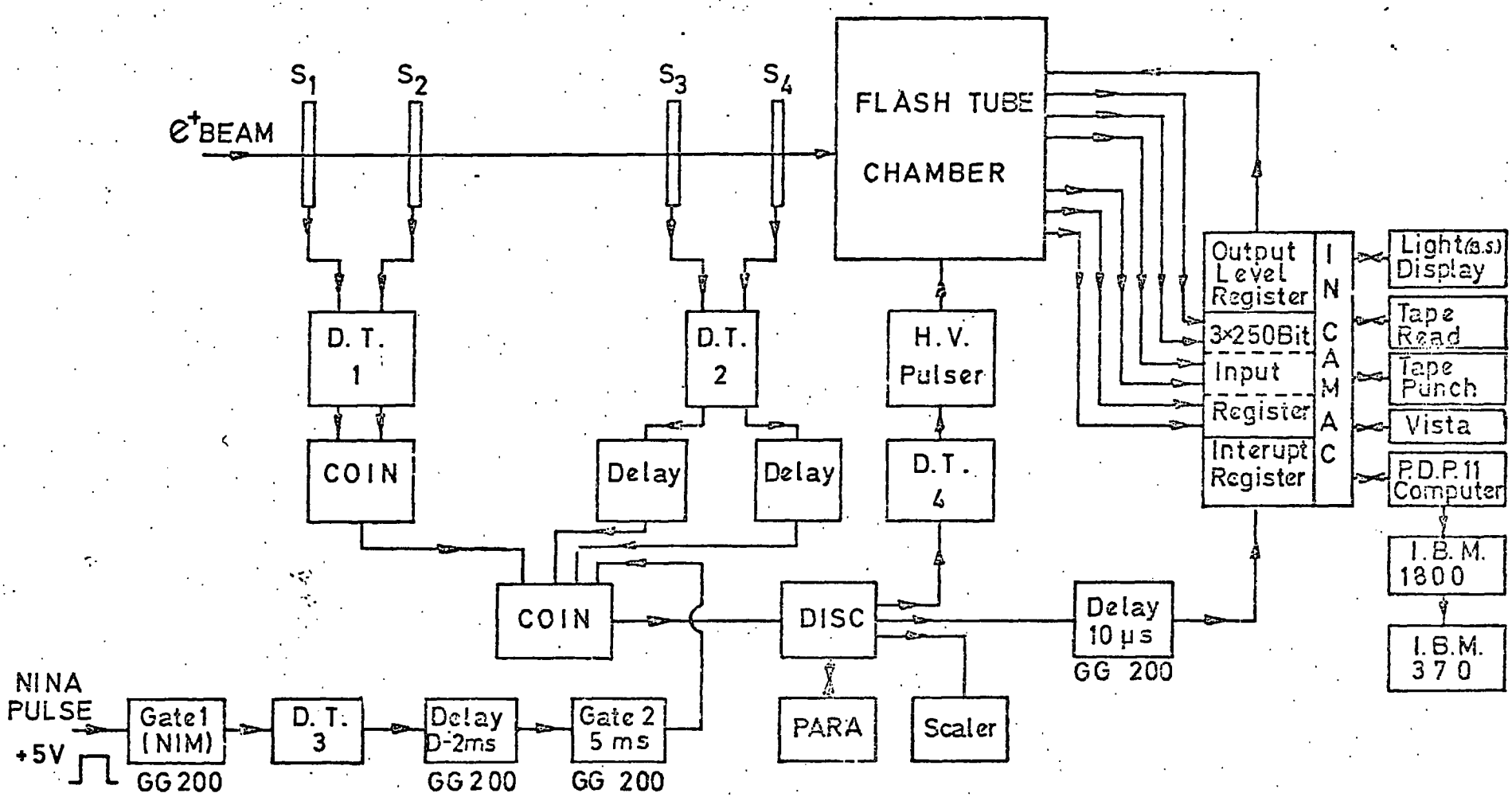

Fig.5.3 The data aquisition system .

plates of the modules. The delay between the passage of a positron through the chamber and the application of the high voltage pulse was about 300 nsec.

A third output from the coincidence unit was delayed for 10 μ sec. then fed to an interrupt register situated in the CAMAC system. This commenced the reading and storing of the outputs of the chamber latches by a PDP 11 computer via the six EMIHUS cables connected to the three 256 bit CAMAC input registers. The 10 μ sec. delay was introduced in order to allow the applied high voltage pulse to decay and the digitisation pulses from flashed tubes to set the latches.

Once the outputs of the latches were read and stored by the PDP 11 computer they were reset by the CAMAC output level unit.

The PDP 11 was programmed in Assembler language (5) and a flow diagram of the programme is shown in figure 5.4.

The PDP 11 computer stored two events, which could then be displayed on a vista screen connected to the computer system, or the events could be sent via a computer link to an IBM 370, depending on the commands given to the PDP 11 via the vista keyboard.

Once the data reached the IBM 370 by the computer link it was stored on disc. Two data runs were usually stored, each run containing several thousand events, then the data was copied to magnetic tape. The data on magnetic tape was then read and analysed using programmes written in FORTRAN.

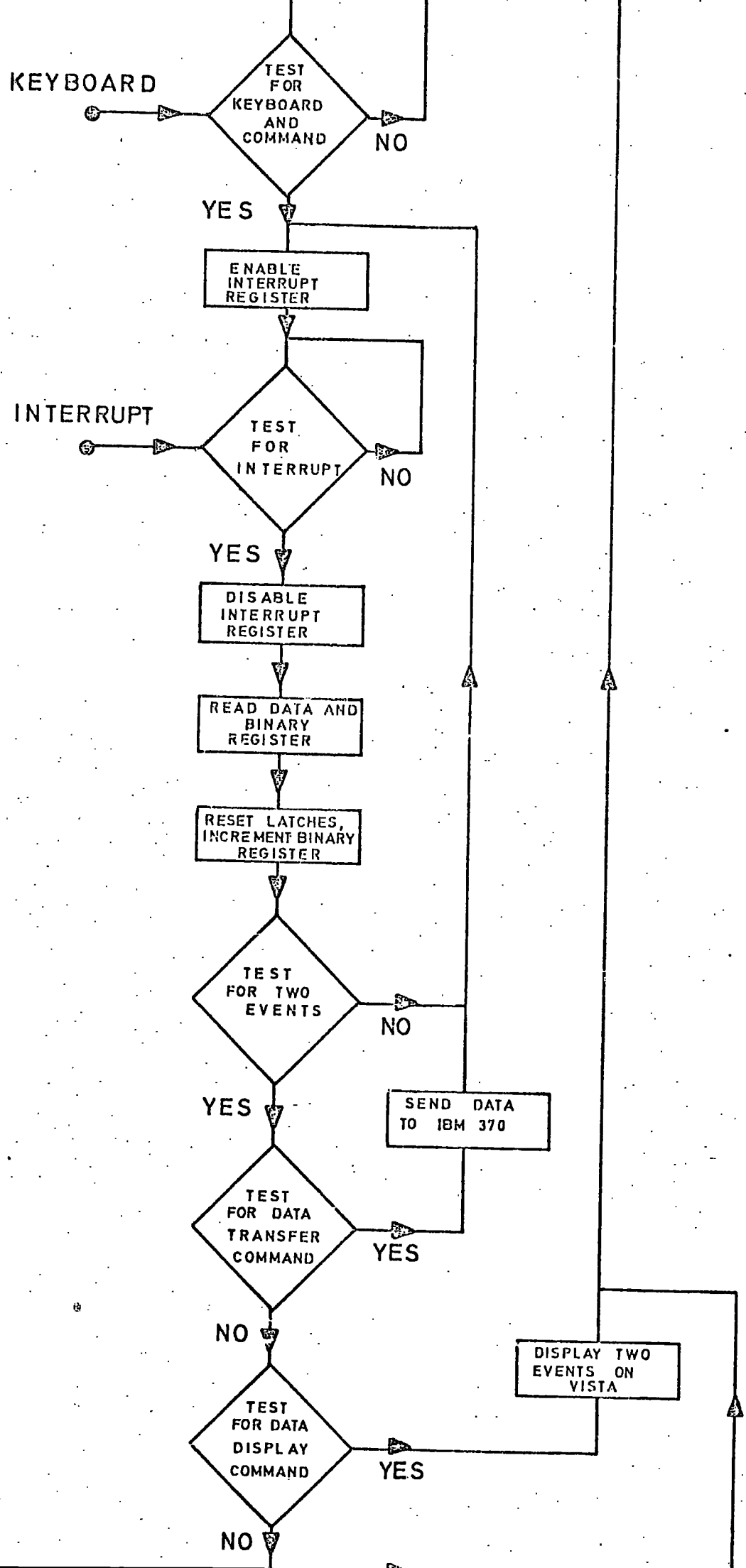

Fig. 5.4 A flow diagram of the data aquisition programme .

5.5 TESTS IN THE POSITRON BEAM

The main tests carried out in the positron beam were in order to find the capabilities of the chamber in the detection of electromagnetic showers, using fully digitised output.

However, several tests were done before the electromagnetic shower measurements were taken, in order to remove spurious and inefficient tubes and to find the optimum working voltage and rate.

In all the tests a 50 V (peak to peak) cm^{-1} alternating external clearing field was applied to the H.T. plates.

5.5.1 SPURIOUSLY FLASHING TUBES

The tubes used in the chamber were tested for spurious flashing by using a pulse generator to simulate coincidence signals in the scintillator coincidence circuit (see figure 5.3).

A high voltage pulse of 11 KV was applied on each simulated coincidence. This resulted in an applied field of about 10 - 11 KV cm^{-1} across the tubes, depending on which module they were in. This variation in applied field arose from the varying H.T.-earth plate separations, due to the addition of rubber foam.

The data obtained was sent down the computer link, copied to magnetic tape and analysed. A simple analysis programme was run, which counted the number of times each tube flashed and gave a frequency plot for all the tubes in the chamber. Spuriously flashing tubes were easily recognised, removed and replaced.

5.5.2 SCANNING OF THE CHAMBER

In order to check that the efficiencies of all the tubes were reasonably high, the chamber was scanned using the positron beam, with no lead target between the modules. Using the motorised traversing table on which it was mounted, the chamber was moved back and forth at a constant rate across the beam, ensuring that the total width of the chamber was traversed. While the chamber was being scanned, coincidences from the four fixed beam defining scintillators were used to trigger the high voltage pulsing unit, and the data obtained was sent down the computer link.

The data was analysed in the same way as the data obtained from the spuriously flashing tube tests. The tube ignition frequencies then gave indications of the efficiencies. Inefficient tubes were removed and replaced.

5.5.3 EFFICIENCY MEASUREMENTS

The flash tube chamber was positioned, without any lead target between the modules, so that the positron beam was incident on its centre. The layer efficiencies were then found from straight through positron tracks for various applied high voltage pulses. The data taking rate was very low, about several events per minute, in order to minimise induced clearing field effects.

The data was analysed using two computer programmes and some of the data was analysed by eye, in order to check the validity of the efficiencies given by the programmes.

One programme recorded whether or not a tube flashed in each

module for an incident positron. Summing over several thousand events, the individual module efficiencies and the layer efficiency of the chamber were obtained.

The second programme did a similar analysis, however information was only considered from tubes in a central, cylindrical region of the chamber, where one expected to find positron trajectories.

Any large differences between the results obtained from the two programmes would indicate spuriously flashing tubes.

A very good agreement was found between the results obtained by both computer analyses of the data and the data analysed by eye, for applied high voltage pulses less than 11 KV. The results obtained for the layer efficiency of the chamber for various applied high voltage pulses are shown in figure 5.5.

Because of the varying H.T.-earth plate separation, the working voltage varied from module to module. Some modules were very efficient for a 10 KV pulse, whereas others needed a pulse of 11 KV. This is seen as the rise in layer efficiency of the chamber as the applied high voltage pulse is increased from 10 to 11 KV in figure 5.5. However, for pulses greater than 11 KV some of the tubes began to flash spuriously. A working voltage of 11 KV was therefore chosen.

A display on the vista screen of two positron tracks through the chamber is shown in figure 5.6.

The layer efficiencies of the modules and of the chamber were also found for various event rates. The high voltage pulse was 11 KV and the data was analysed using the above mentioned computer programmes. The results obtained for the chamber layer efficiency

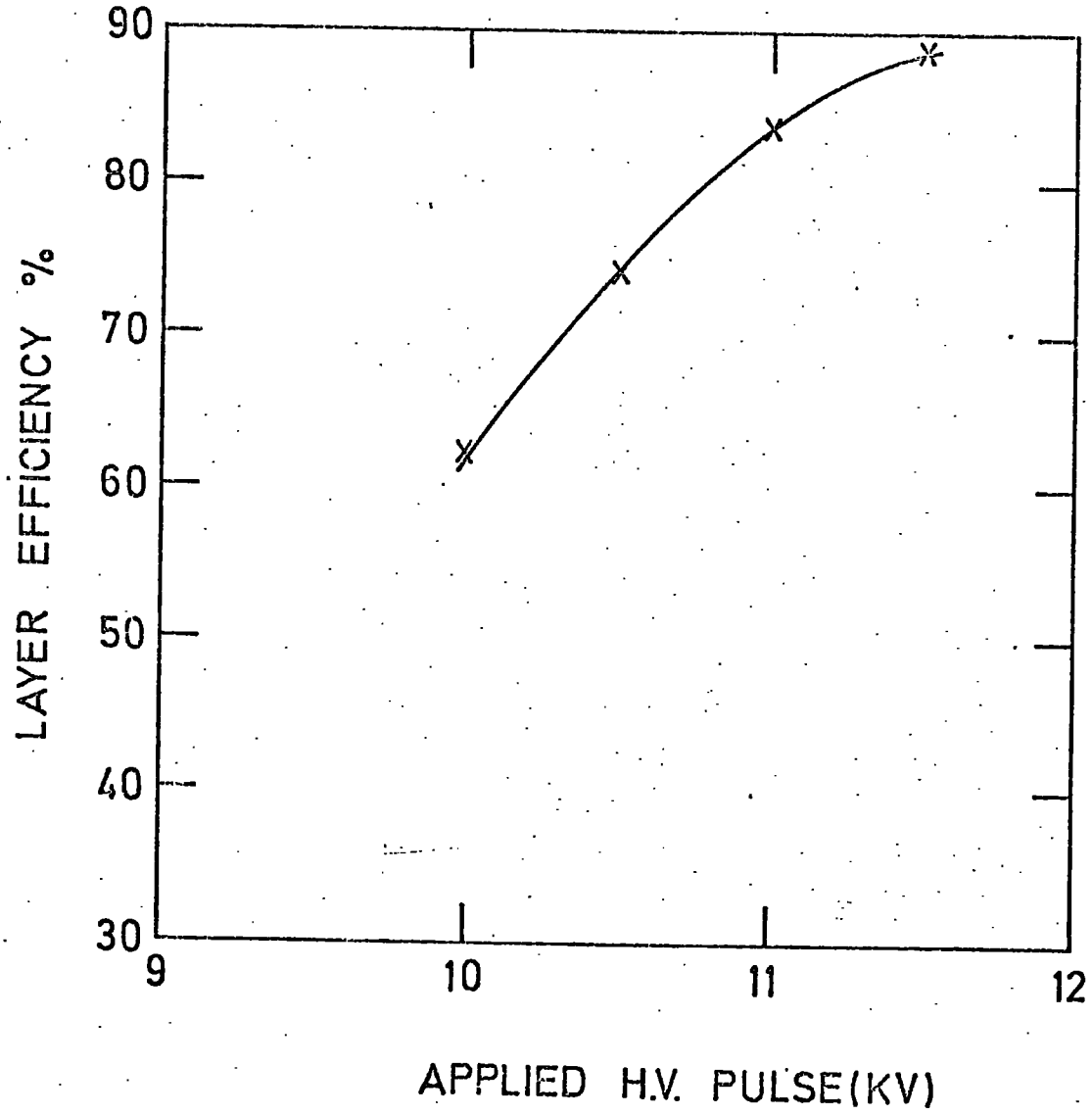

g. 5.5 Efficiency versus applied high voltage pulse .

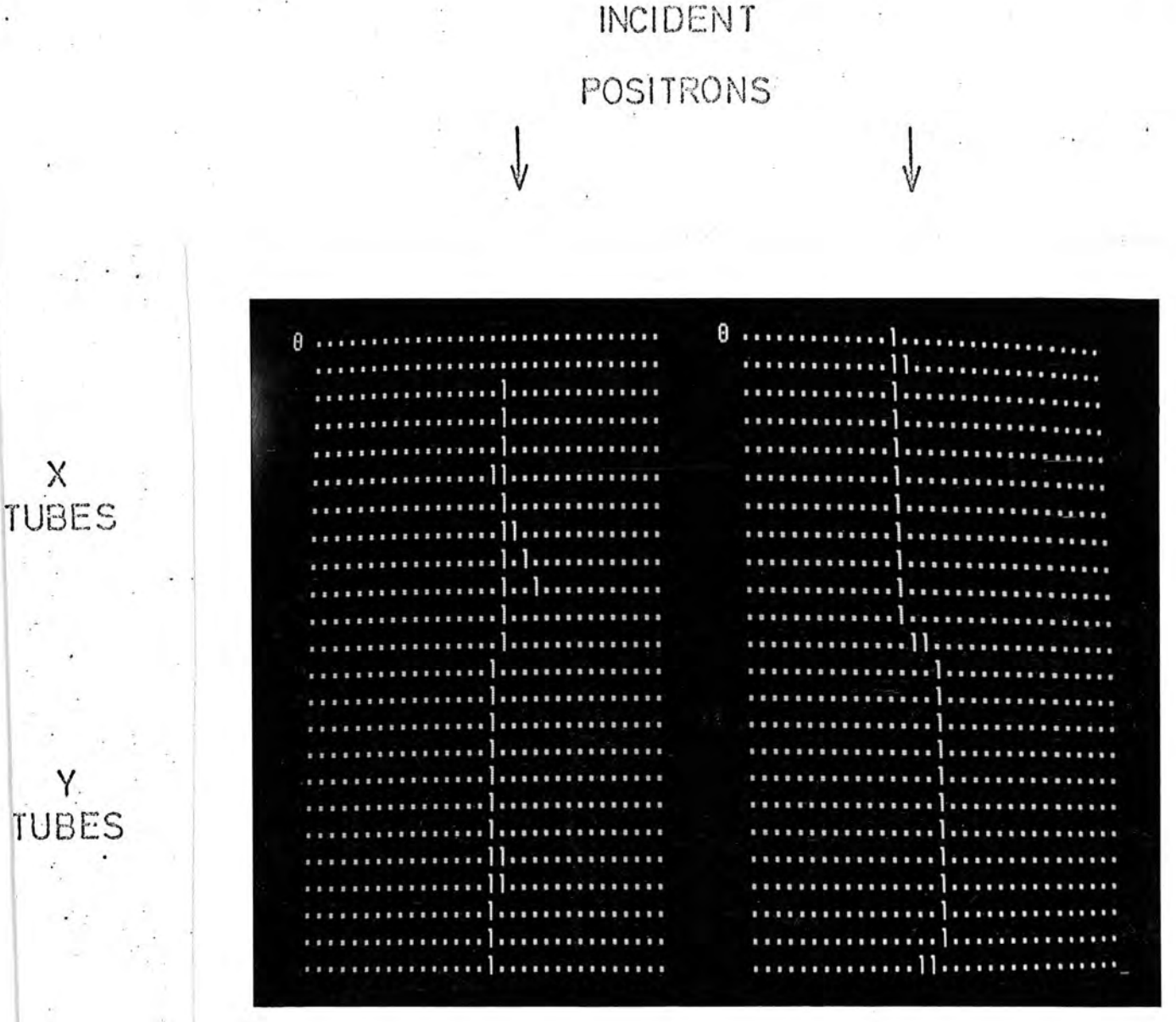

Fig.5.6 Tracks through the chamber without lead target as seen on the vista screen.

are shown in figure 5.7.

The layer efficiency of the chamber is seen to decrease fairly rapidly with rate, due to the reductions in the digitisation pulse heights resulting from the build up of large induced clearing fields (see chapter 4).

The module efficiencies obtained for various event rates are shown in figure 5.8. These also are seen to decrease with event rate, however, some modules decrease in efficiency faster than others, due to variations in H.T.-earth plate separation.

An event rate of about 11 per minute was chosen as a satisfactory one, producing a chamber layer efficiency of 83%. Higher event rates would have produced lower efficiencies, and lower event rates would have made data taking too long a process.

5.5.4 ELECTROMAGNETIC SHOWER MEASUREMENTS

Having decided on an event rate of about 11 per minute, and an applied high voltage pulse of 11 KV, the chamber was set up in order to take electromagnetic shower data.

The chamber was positioned so that positrons were incident on the centre of the first module, and lead target was placed between the modules. Three thicknesses of target were used, 0.6, 1.2 and 1.8 radiation lengths.

As an estimate of the spatial resolution of the chamber was to be made, the positions of incident positrons were needed. These were obtained from the position of a single flashed tube in the first module, which had no lead target in front of it.

The energy of the incident positron was varied between 0.5

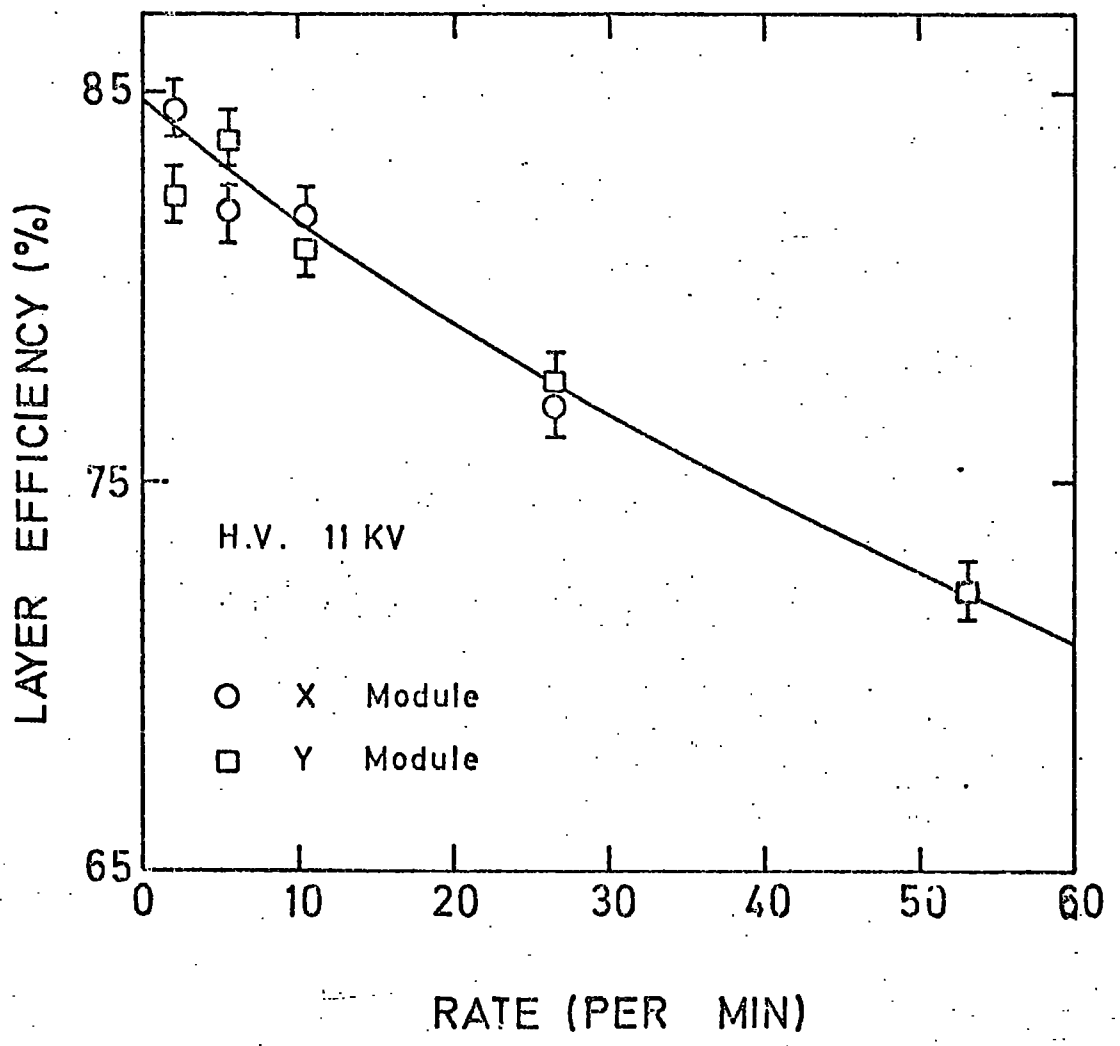

Fig. 5.7

Efficiency versus repetition rate .

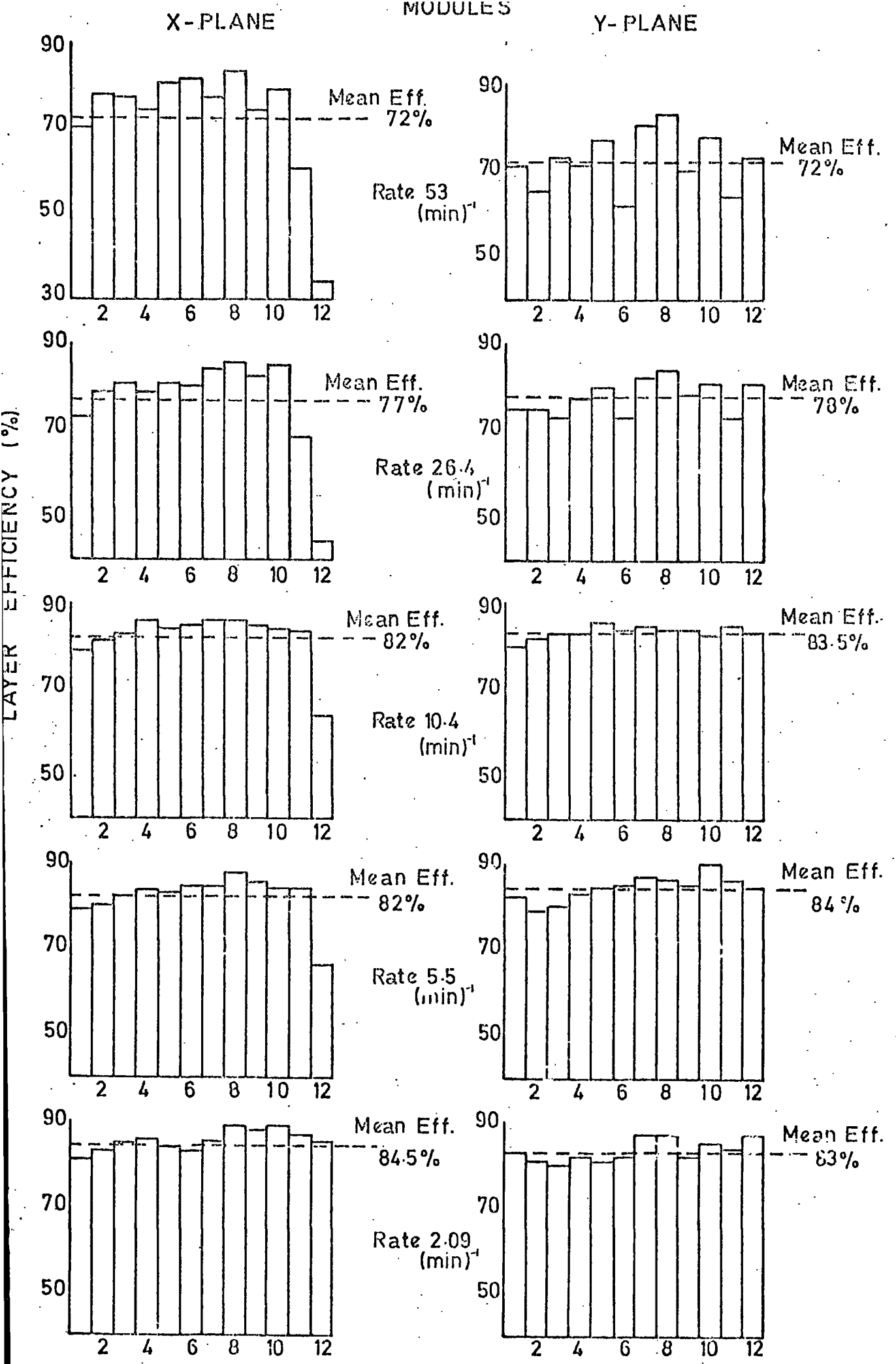

Fig.5.8 Module efficiencies at various repetition rates.

INCIDENT
POSITRONS

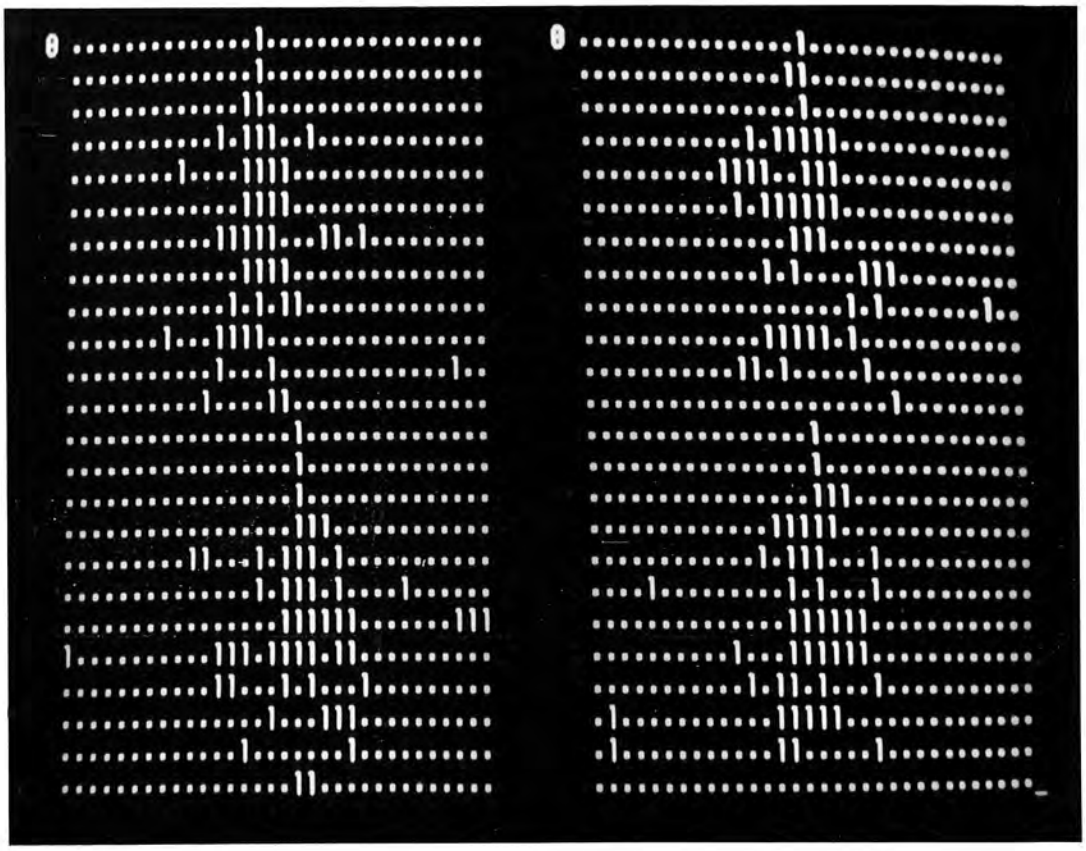

X
TUBES

Y
TUBES

Fig.5.9 Showers produced in the chamber as seen on the vista screen .

and 3.5 GeV and several thousand shower events were taken for each target configuration and incident energy.

A vista screen display of a typical shower event is shown in figure 5.9.

The results obtained from the electromagnetic shower tests are presented in the following chapter.

REFERENCES

1. Chaney, J.E., Breare, J.M. (1975) Nucl. Inst. & Meth. 124 61

2. Chaney, J.E. et al. (1975) Nucl. Inst. & Meth. 125 189

3. Breare, J.M. et al. (1976) Nucl. Inst. & Meth. (in preparation)

4. Aitken, T.W. (1970) Daresbury Nuclear Physics Laboratory Report, DNPL/TM70

5. Golding, F. (1975) Private Communication, Daresbury Nuclear Physics Laboratory

CHAPTER SIX

ELECTROMAGNETIC SHOWER DETECTION USING THE MODIFIED FLASH TUBE CHAMBER

6.1 ENERGY RESOLUTION

In order to estimate the energies of positrons incident on the chamber containing lead target, the shower data obtained was analysed using similar methods to those used in the analysis of the shower data obtained from the prototype chamber. The total number of ignited tubes was recorded for each shower produced for an incident positron of known energy. The total number of ignited tubes then gave a measure of the secondaries sampled in the shower which was proportional to the energy of the incident positron (see chapter 3, section 3.3.4).

The total numbers of secondaries expected by sampling electromagnetic showers produced in lead by incident electrons of varying energies are shown in figure 6.1.

The numbers are obtained from Monte Carlo simulations done by Messel and Crawford (1) and Volkel (2).

The samplings of the showers were taken at 0.6, 1.2 and 1.8 radiation length intervals for a threshold secondary energy of 2 MeV.

The total numbers of tubes which ignited in the chamber for given positron energies and target thicknesses were calculated, and the frequency distributions obtained for the integral energy runs

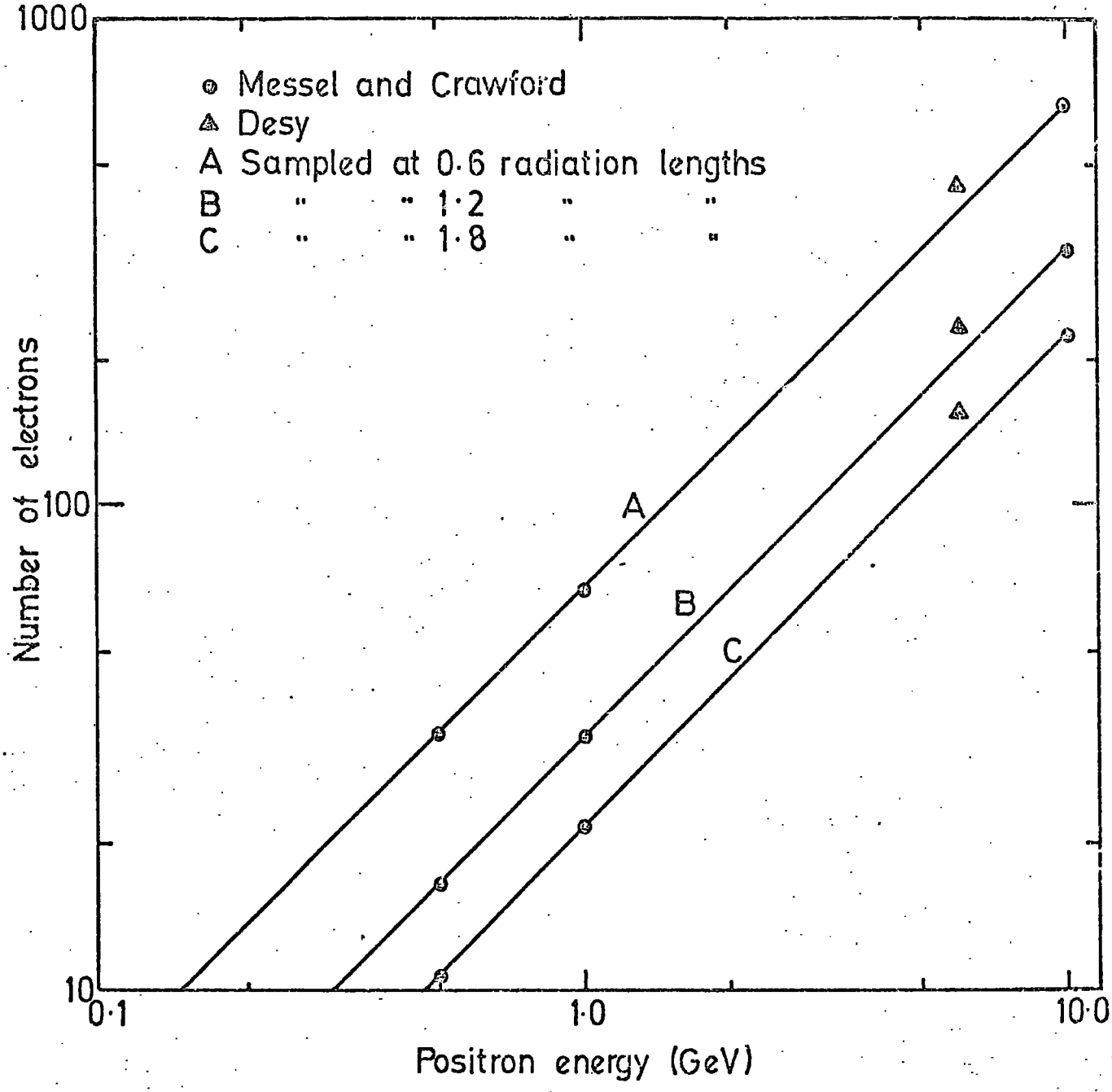

Fig. 6·1 The total number of electrons expected by sampling at 0·6, 1·2 and 1·8 radiation length intervals as a function of primary positron energy.

are shown in figure 6.2 for 0.6, 1.2 and 1.8 radiation lengths of lead target between each module.

From these distributions the mean total number of flash tube ignitions was found for various energies and target conditions, and the results are plotted in figure 6.3.

The curves deviate from the linear relationship one expects, however these deviations are not as pronounced as those present in the data obtained from the prototype chamber (see figure 3.6), due to the reduction in shower leakage and the increased electron sensitivity of the modified flash tube chamber.

The energy resolutions of the chamber were calculated by taking the FWHM of the tube ignition frequency distributions, as was done for the prototype chamber. The various resolutions obtained for the chamber for different working conditions are shown in figure 6.4.

For the lower energy runs the resolutions follow the $1/\sqrt{E}$ variation one expects, however, for the higher energy runs, where the electron insensitivity of the tubes becomes important together with shower leakage in the 0.6 radiation length runs, the resolution changes very little with increasing energy.

Using 1.2 radiation lengths of lead target between the modules, an energy resolution of about $\pm 10\%$ was obtained for positrons of 3 GeV.

6.1.1 SHOWER LEAKAGE

Shower leakage was also present in the modified chamber for the thinner target and higher energy runs, however the shower

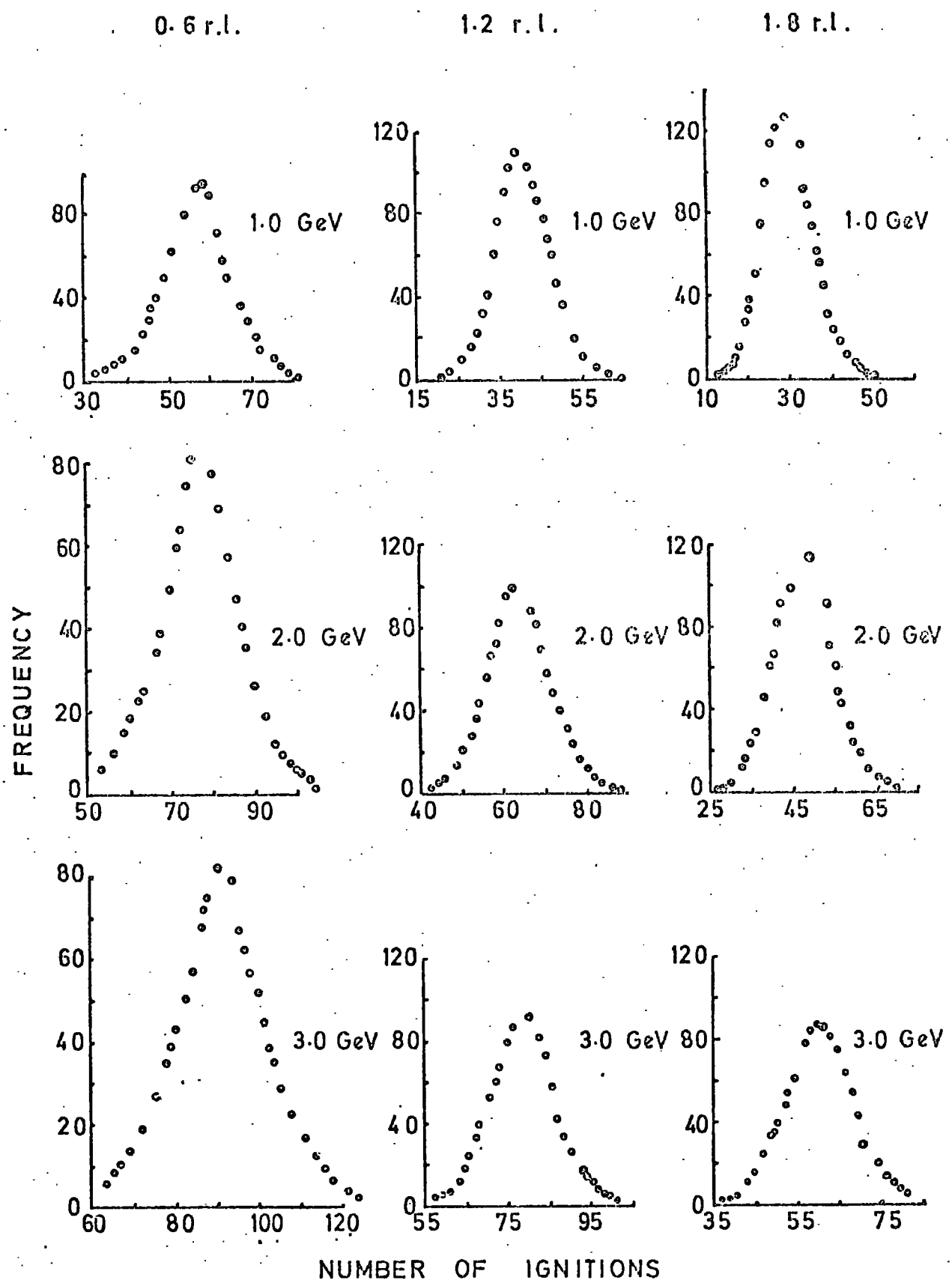

Fig.6·2 Flash tube ignition frequency distributions for various energy and target configurations .

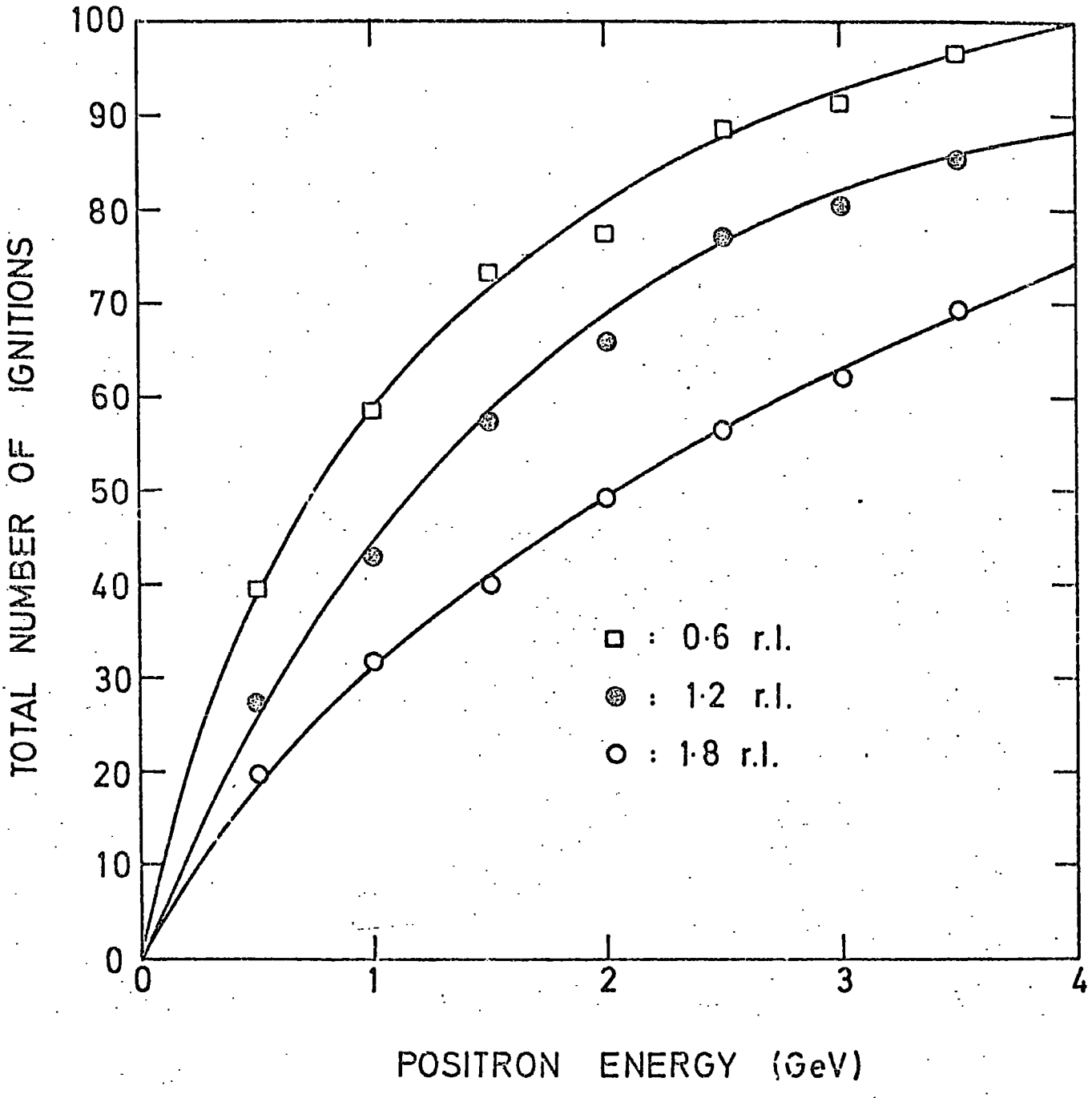

Fig. 6.3 Mean total number of tube ignitions for various positron energies .

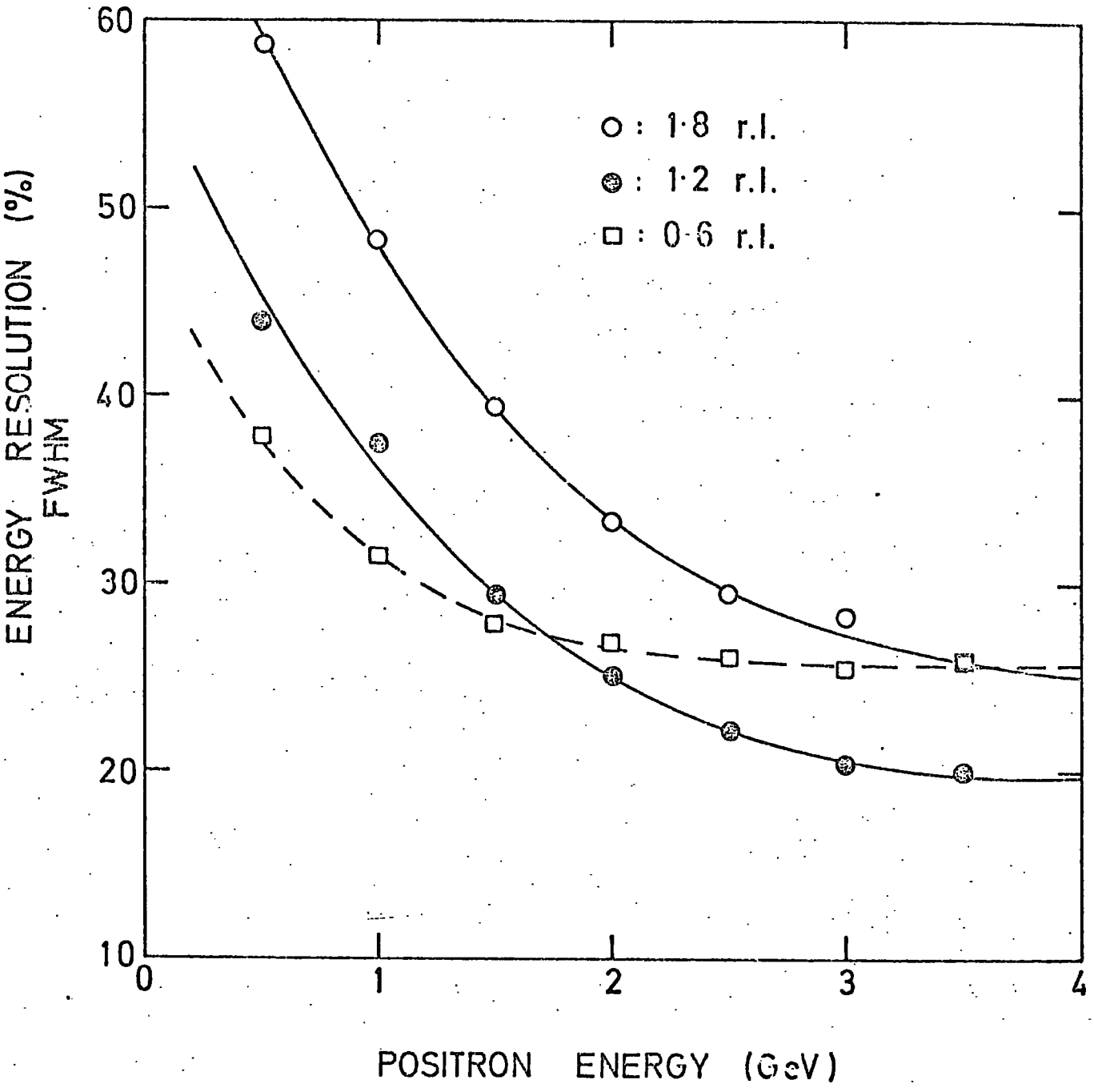

Fig.6.4 Energy resolution as a function of energy .

leakage was only present in the longitudinal direction with very little or no leakage in the lateral direction. This is clearly illustrated in figure 6.5, which shows the development of showers in the chamber produced from 3 GeV positrons. There was 0.6 radiation lengths of target between the modules. The shower shapes produced in each module are shown, tube ignition frequencies are plotted in the vertical direction for the respective tube numbers which are plotted in the horizontal direction. Irregularities in the heights of the distributions arise as all the modules were not operating at their optimum working voltages.

The mean number of tube ignitions for each of the modules in the Y direction is plotted for various target configurations and energy in figure 6.6. These curves show that longitudinal shower leakage is always present in the 0.6 radiation length runs and is also present at higher energies in the 1.2 radiation length runs.

Plots of the number of flashed tubes for various amounts of traversed lead target in the Y direction are shown in figure 6.7. These results are seen to follow the same behaviour as those obtained from Monte Carlo simulations by Messel and Crawford (1) (see chapter 3, figure 3.2). A fast initial rise in the number of electrons produced is seen, leading to a maximum value which is followed by a gradual decrease in the number with increasing target thickness. The positions of these maxima can be shown to be proportional to the logarithm of the incident positron energy (1). The positions of the maxima obtained using the chamber are plotted for various positron energies in figure 6.8. Results obtained from Monte Carlo simulations (1, 2) are also shown and are seen to give reasonable agreement with the results obtained from the chamber.

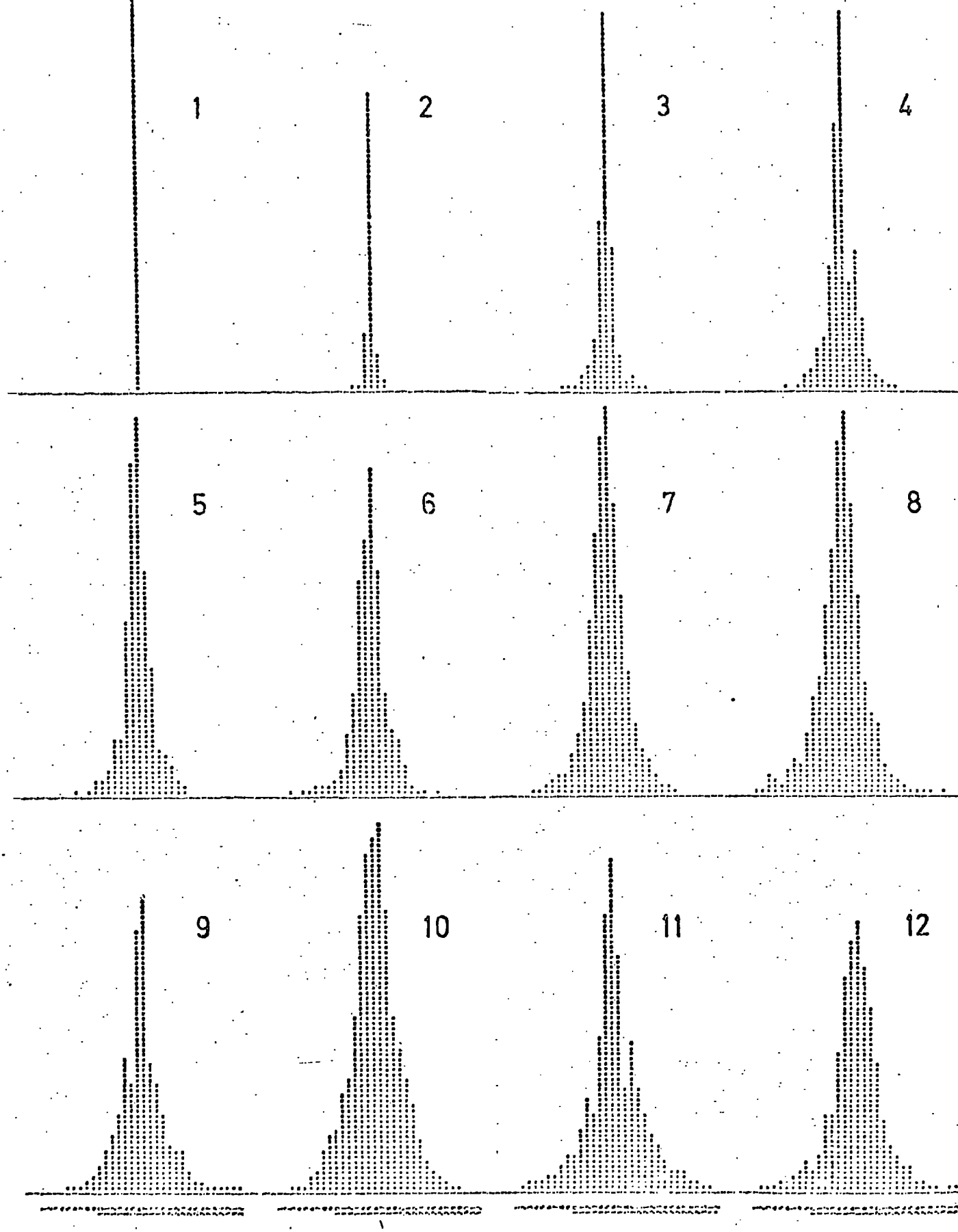

Fig. 6·5 Average shower development for 3·0 GeV positrons using 0·6r.l. of target between each module.

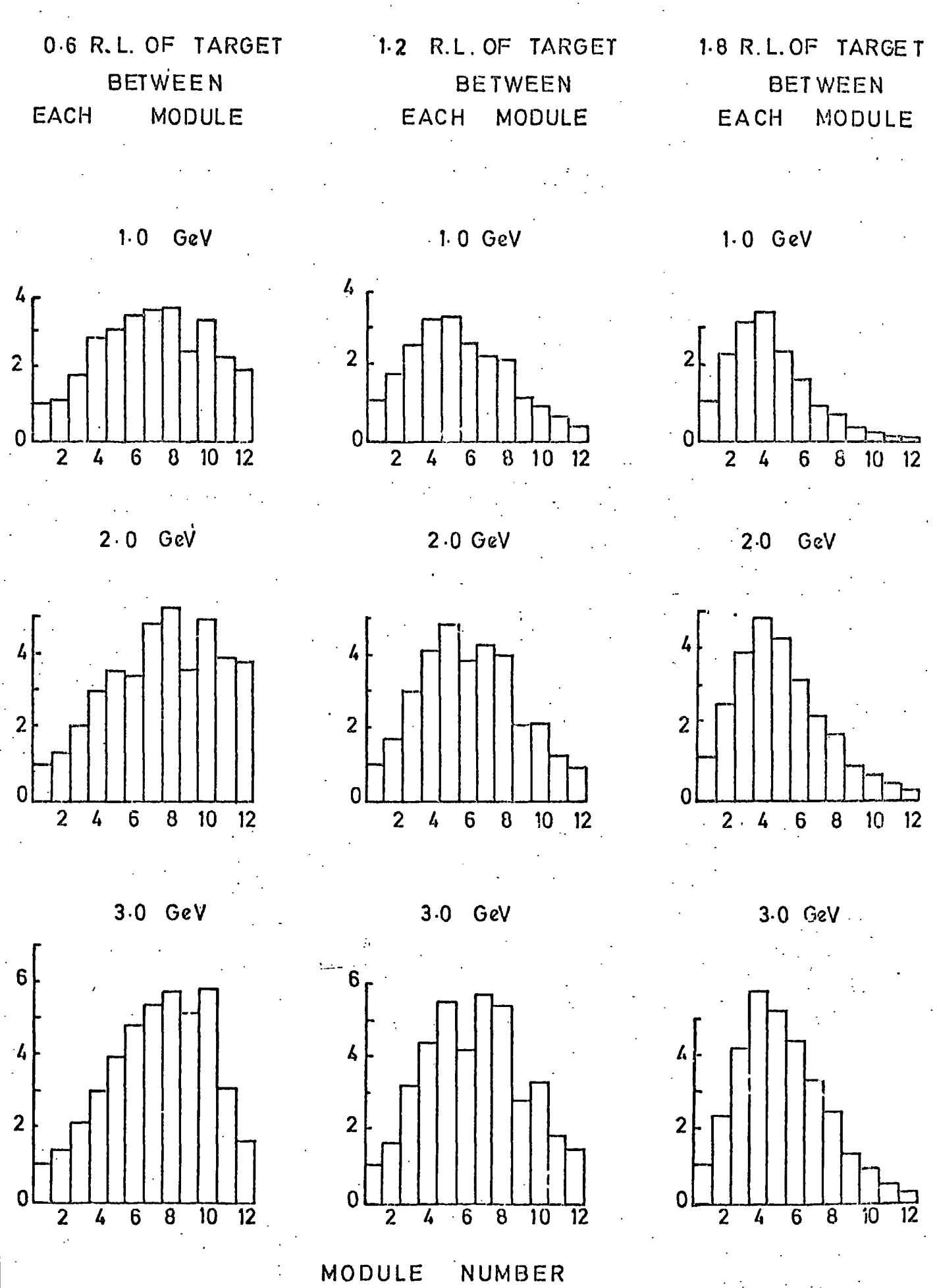

g.6.6 Mean number of tube ignitions in each module for various energy and target configurations.

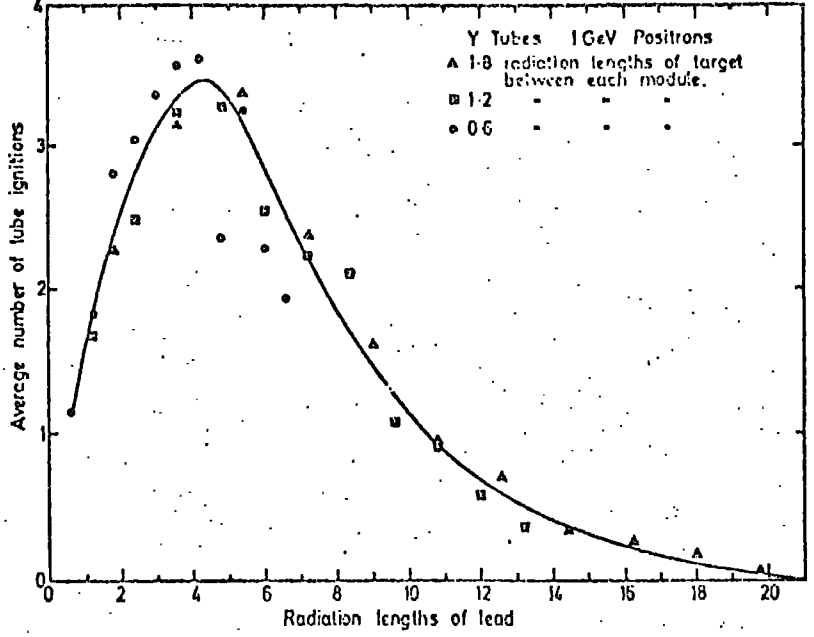

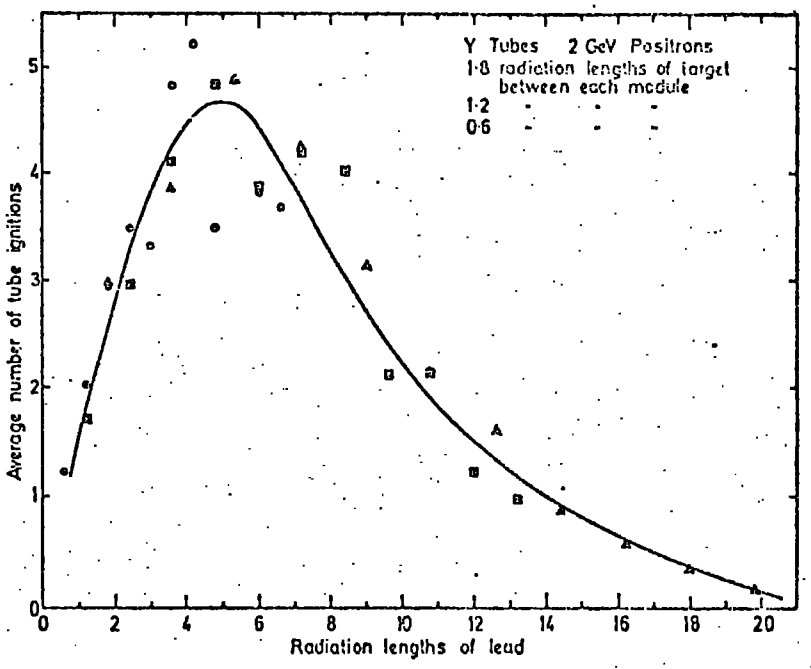

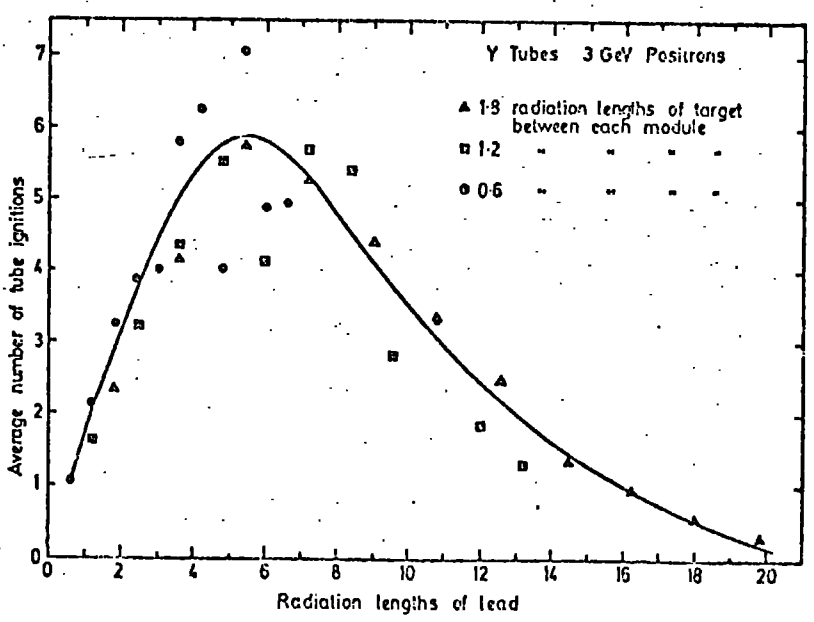

Fig 6·7 Mean total number of ignitions versus target depth for various energies.

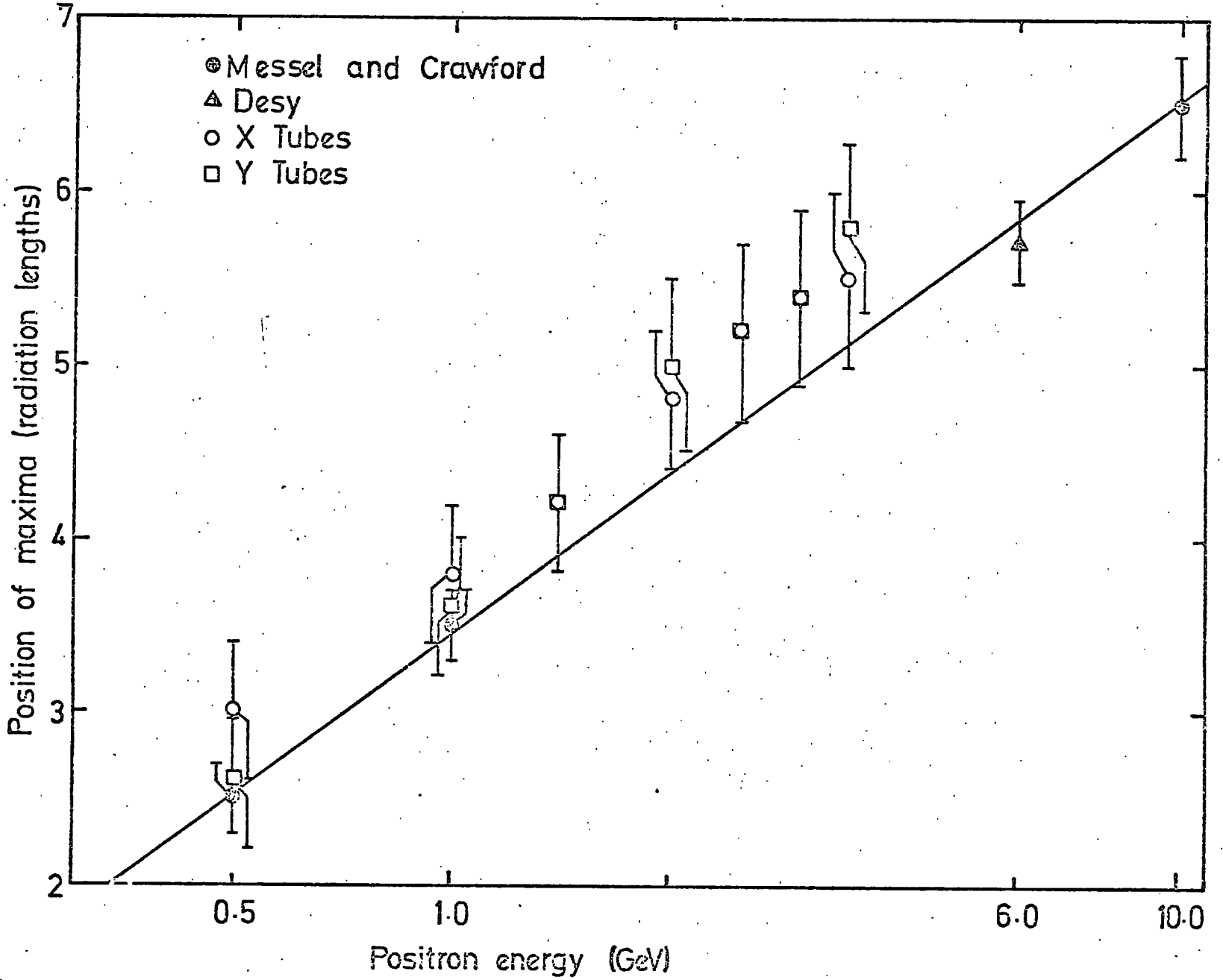

Fig.6·8 Shower maxima positions for various positron energies .

Using curves of the number of flash tube ignitions for various target thicknesses (see figure 6.7) corrections can be made for longitudinal shower leakage from the chamber encountered in the thinner target runs. The total number of flash tube ignitions for various incident positron energies have been estimated using these corrections and the results are shown in figure 6.9.

A considerable improvement in linearity is seen in the corrected results of the 0.6 radiation length runs, however, there is little change in the 1.2 radiation length runs, as most of the showers were contained in the chamber.

The longitudinally corrected curves still deviate from the linear; this is mainly due to the electron insensitivity of the tubes, that is, the inability of a tube to simultaneously detect the passage of more than one electron through it.

6.1.2 ELECTRON SENSITIVITY OF THE FLASH TUBES

The electron sensitivity of the tubes has been estimated using the theoretical numbers of sampled secondaries produced in an electromagnetic shower from Monte Carlo simulations (see figure 6.1). The results are presented in table I.

An estimate of the electron sensitivity of the flash tubes was made for the 0.5 GeV run only, in the 0.6 radiation length tests, as longitudinal shower leakage was quite considerable for incident positrons having energies greater than 0.5 GeV.

The results in table I can be compared with those obtained from the prototype chamber employing the larger diameter flash tubes (see chapter 3, table 1).

Values ranging from about 40% to 60% were obtained for the

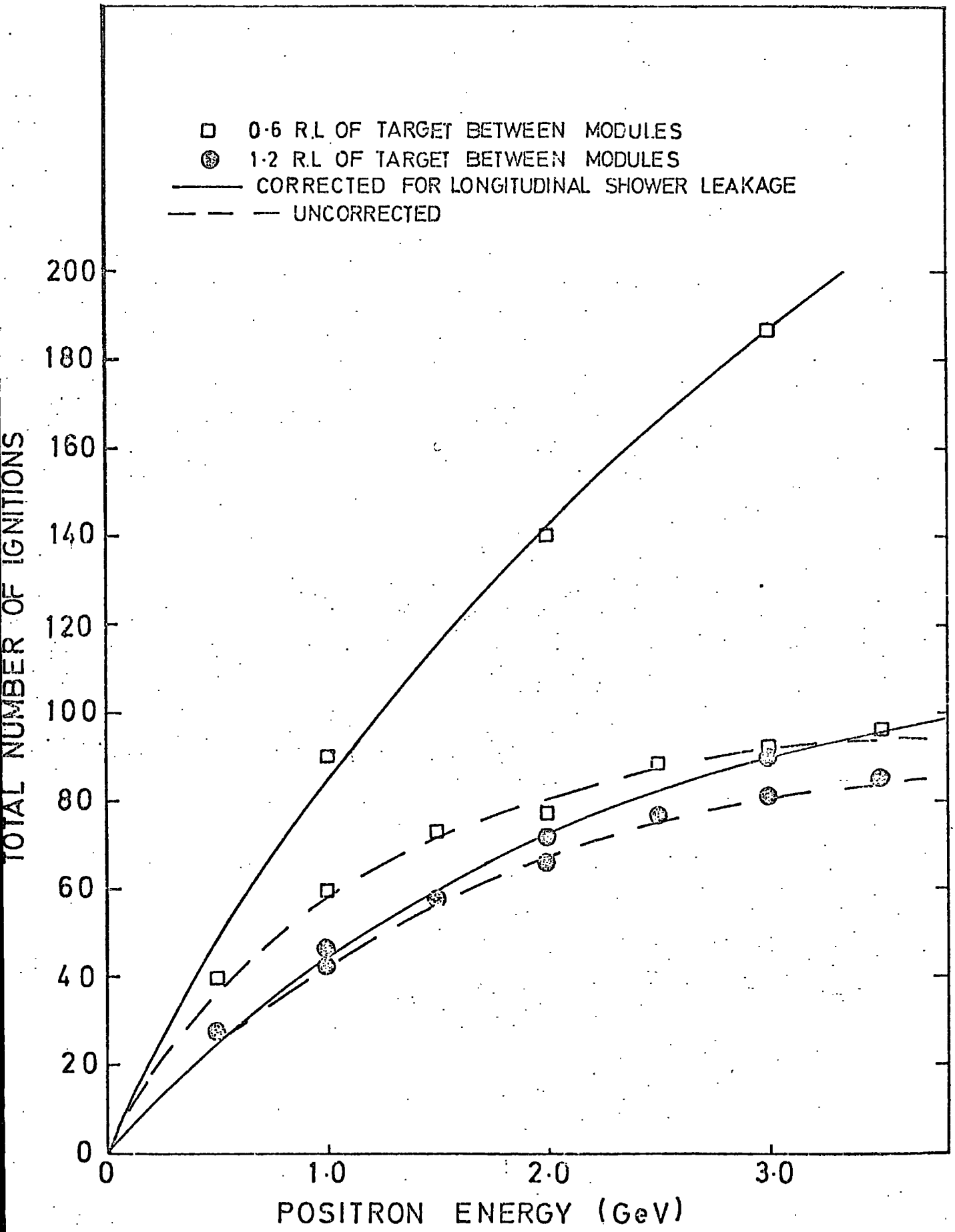

Fig.6.9 Mean total number of tube ignitions for various positron energies corrected for longitudinal leakage .

TABLE I

Positron energy (GeV)	Radiation Lengths of target between modules	Number of secondaries	Number of flash tube ignitions	Sensitivity (%)
0.5	0.6	33.6	20	60
0.5	1.2	16.5	14	85
1.0	1.2	33.2	22	66
1.5	1.2	49.9	29	58
2.0	1.2	66.7	33	49
2.5	1.2	83.5	39	47
0.5	1.8	10.8	10	93
1.0	1.8	21.8	16	73
1.5	1.8	32.8	20	61
2.0	1.8	43.9	25	57
2.5	1.8	55.1	29	53
3.0	1.8	66.3	31	47
3.5	1.8	77.5	35	45

electron sensitivity using the prototype chamber. The electron sensitivity has been greatly improved using the smaller tubes of the modified chamber, where values ranging from about 50% to 90% were obtained.

The electron sensitivity of the tubes is seen to improve with decreasing positron energy due to the formation of less dense electromagnetic showers. One way in which this sensitivity may be further improved at these higher energy runs is by increasing the module to module separation in the chamber and so enable showers produced in the chamber to widen in the lateral direction, producing less dense showers.

6.2 SPATIAL MEASUREMENTS

6.2.1 INTRODUCTION

The electromagnetic shower data obtained from the improved flash tube chamber was analysed with respect to spatial and angular information, in a similar manner to that obtained from the prototype chamber.

Estimates of the shower centres in each module were obtained using the symmetrical properties of developing showers. These shower centres were then used to obtain a first estimate of the shower axis.

Knowing the lateral distributions of the secondaries in each of the modules, the positions of ignited tubes were weighted according to their distances from the estimated shower axis, and a series of weighted shower centres was obtained. A better estimate

of the shower axis was then obtained by the weighted least squares fitting of a line to the weighted shower centres. Successive estimates of the shower axis were then obtained using the above method as an iterative process. The final estimate of the shower axis was taken after ten iterative loops. Estimates of the positions of incident positrons were then obtained by finding the positions of the intercepts of the final estimated shower axes on the first module. These intercept positions were then compared with the known positions obtained from the positions of the single flashed tubes in the first module.

"Apex deviation" distributions were found as for the prototype chamber, and from these distributions the spatial resolutions of the chamber were found.

The angular resolutions of the chamber were also found by comparing the angles of estimated shower axes with the known values of angles of incidence of positrons on the chamber.

6.2.2 LATERAL DISTRIBUTIONS OF SECONDARIES

The shower data was first analysed in order to obtain the shower profiles produced by the secondaries in each module, for various incident positron energies and target thicknesses. An example of the shower profiles thus obtained is shown in figure 6.5. The standard deviations (σ_i) or "shower widths" ($2\sigma_i$) were obtained for each of the profile distributions. Some shower widths are shown in figure 6.10.

For the i^{th} module the frequency distribution of secondaries was represented by:

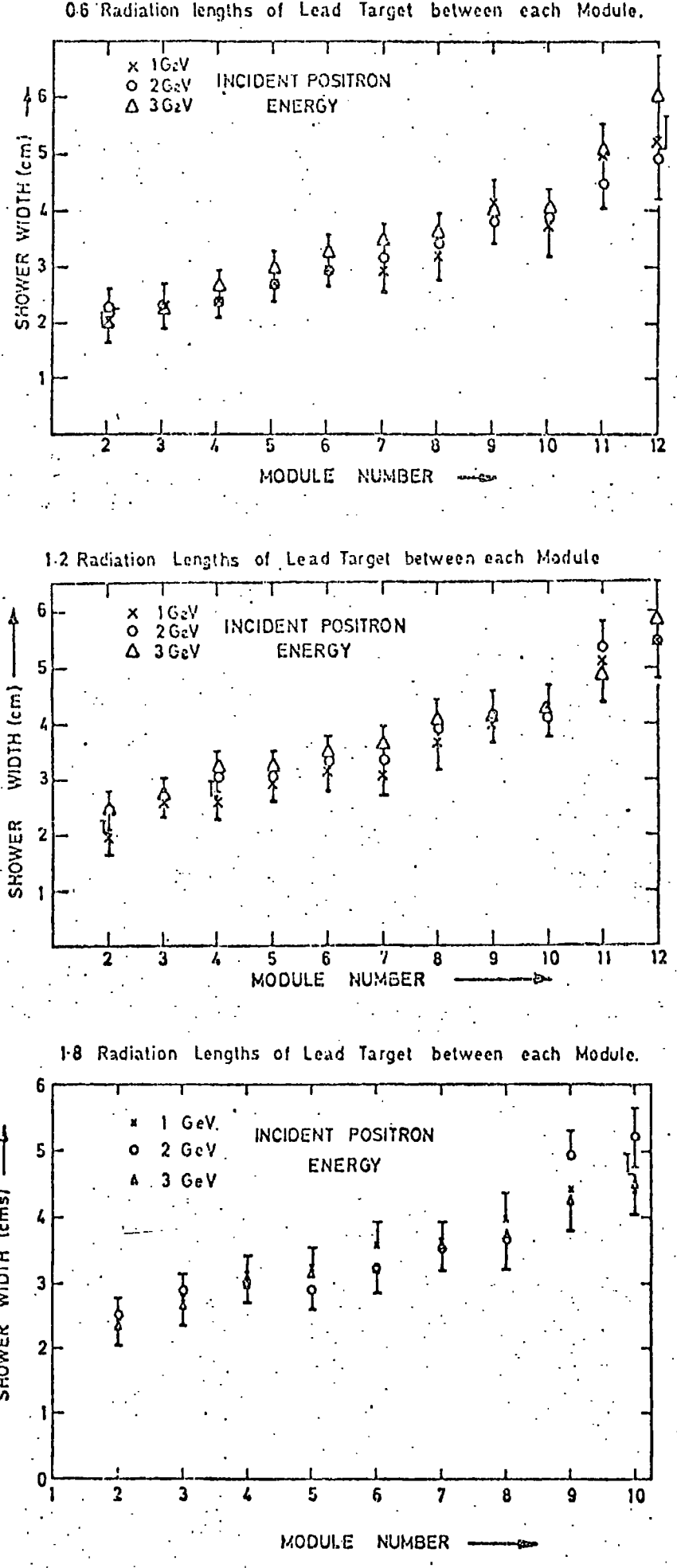

Fig. 6·10 Average shower widths for various energies and target configurations.

$$f_{ij}(y_{ij}) = \exp(-(q_{ij})^2)$$

where $$q_{ij} = \frac{(y_{ij} - y_i)\cos\phi}{K_i \sigma_i}$$

(using similar notation as in chapter 3, and K_i is a fitting parameter for module i)

The frequency distributions $f_{ij}(y_{ij})$ were fitted to the empirical shower profiles by varying the values of K_i. The values of K_i which gave the best fit to the empirical shower profiles are shown in figure 6.11.

6.2.3 LONGITUDINAL WEIGHTING OF THE DATA

Because of the fluctuations in electron positions and densities in a shower, which increased as the shower progressed further through the chamber, the shower data was weighted in the longitudinal direction when estimating shower axes.

The shower data was analysed using the iterative process and using various values of K_i, and various longitudinal weighting factors in the weighted least squares fitting of a line (shower axis) to the weighted shower centres.

The use of longitudinal weighting factors of $(1/\sigma_i)$ to varying powers was investigated. The values of σ_i were used because they gave some measure of the fluctuations in electron position and density in each module.

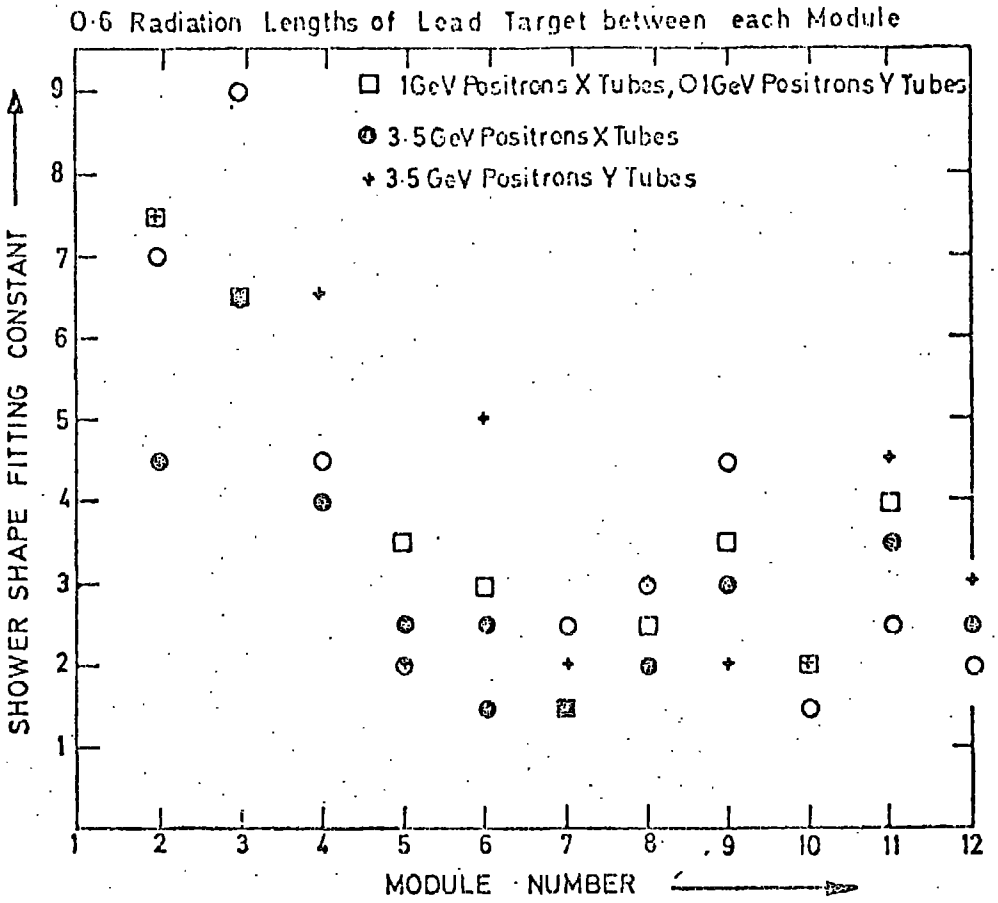

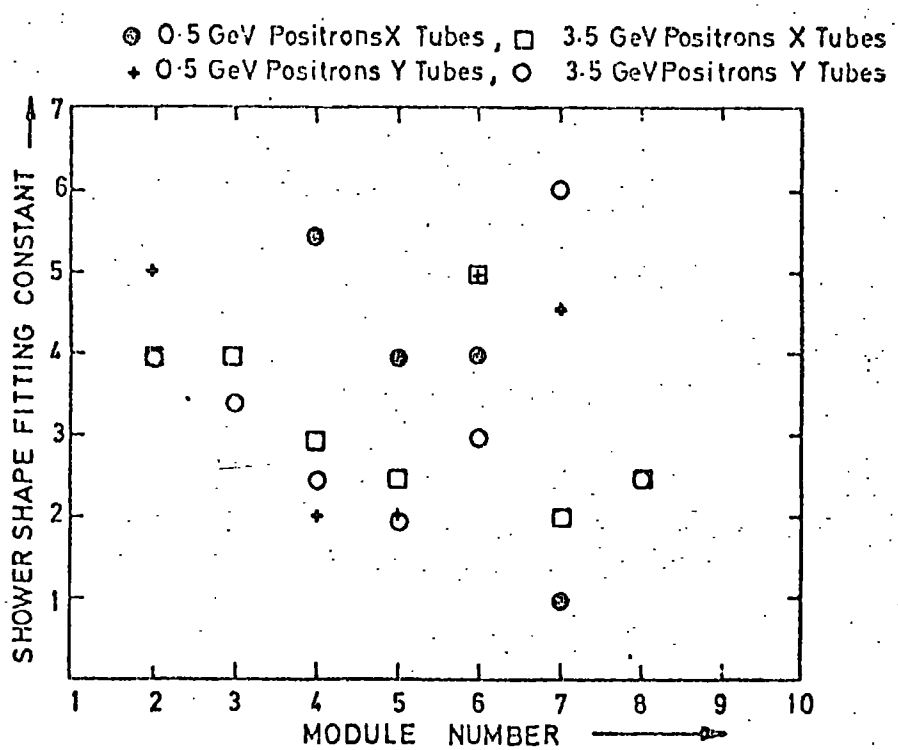

Fig.6·11 Shower shape fitting constants for various energies and target configurations.

Some of the results are shown in table II. The standard deviations of the resulting apex deviation distributions are shown. These give a measure of the spatial resolution of the chamber, which is seen not to be very dependent on the values of K_i used in the analysis.

Longitudinal weighting factors of $(1/L_i)$ to varying powers were also tried in the analysis of the data, where L_i was the amount of target traversed by secondaries in the shower before reaching module i. The resulting standard deviations of the apex deviation distributions are shown in table III.

The use of $1/(\sigma_i)^2$ in the analysis in weighting in the longitudinal direction gave the better spatial resolution. Because the values of σ_i were intrinsic to each module and were related to the individual module efficiencies whereas the L_i values were not, it was decided to use $1/(\sigma_i)^2$ in the final analysis of the data. However a check was first made in order to verify that all the flash tube information obtained from an event in the chamber was being usefully used in the analysis, and that the $1/(\sigma_i)^2$ weighting was not effectively "weighting out" data from the rear modules of the chamber in the analysis.

This check was performed by analysing the shower data using the information from various numbers of modules. The data was analysed using 5, 7, 9 and 11 modules, and in all cases the resolution of the chamber improved as the number of modules used was increased, hence the $1/(\sigma_i)^2$ weighting appeared satisfactory and was used in the final analysis of the data.

TABLE II

"STANDARD DEVIATIONS" (D) OF APEX DEVIATION DISTRIBUTIONS (mm)

FOR 1 GeV POSITRONS AND 0.6 RADIATION LENGTHS OF TARGET BETWEEN MODULES

Longitudinal Weighting $\frac{1}{\sigma_i}$

K_i	0.5	3.5	
X tubes	8.8	8.7	
Y tubes	11.5	10.8	

Lonitudinal Weighting $\frac{1}{\sigma_i^2}$

				First 4 Modules	Rear 7 Modules
K_i	0.5	3.5	7.0	6.0	2.5
X tubes	7.4	6.9	6.8	7.5	
Y tubes	11.1	10.2	9.8	11.2	

Longitudinal Weighting $\frac{1}{\sigma_i^3}$

K_i	0.5	3.5	
X tubes	6.8	6.3	
Y tubes	11.7	10.3	

TABLE III

"STANDARD DEVIATIONS" (D) OF APEX DEVIATION DISTRIBUTIONS (mm)
FOR 1 GeV POSITRONS AND 0.6 RADIATION LENGTHS OF TARGET BETWEEN MODULES

Longitudinal Weighting Factors	$\frac{1}{\sigma_i}$	$\frac{1}{\sigma_i^2}$	$\frac{1}{\sigma_i^3}$	$\frac{1}{\sigma_i^4}$	$\frac{1}{L_i}$	$\frac{1}{L_i^2}$	$\frac{1}{L_i^3}$
X tubes	8.8	7.4	6.8	7.6	7.8	9.3	12.0
Y tubes	11.5	11.1	11.7	12.4	12.1	16.1	19.3

6.2.4 SPATIAL AND ANGULAR RESOLUTIONS

The shower data was analysed with respect to spatial and angular information, using a value of 3.5 for the lateral fitting constants K_i and using values of $1/(\sigma_i)^2$ for weighting in the longitudinal direction.

The analysis gave apex deviation distributions and shower axis angle distributions. The widths of these distributions were found and used to obtain estimates of the chamber resolutions, knowing the positions of incident positrons to ± one tube radius, and knowing that the angles of incident positrons were $0^o \pm 2^o$. The angles of incident positrons were found from straight tracks made in the chamber without any target placed between the modules.

The frequency distributions of the shower axis angles and apex deviations were not Gaussian like in shape, hence the widths of the distributions were estimated in a similar manner to those obtained from the prototype chamber.

Limits containing 75% of the data were found and the limit separations were taken as the widths of the distributions. The measure of resolution given by a distribution was then taken as ± (half the distribution width).

The resolutions obtained from the chamber were then found as before taking into account the improved estimate of the incident positron position from the single flashed tube, that is,

(spatial resolution obtained from apex deviation frequency distribution (mm))^2 ~ 16 + (spatial resolution of chamber (mm))^2

(angular resolution obtained from shower angle frequency distribution (degrees))^2 ~ 4 + (angular resolution of chamber (degrees))^2

The spatial and angular resolutions obtained for the chamber are shown in figure 6.12 and figure 6.13 respectively.

The spatial resolution is seen to improve with increasing energy and decreasing target thickness, giving values as good as ± 2 mm.

Similar trends are found for the angular resolution where values as good as ± 2° were obtained.

The data was also analysed without any weighting of the flash tube information. A considerable improvement in the spatial and angular resolutions of the chamber was found using weighted methods; typical results are shown in table IV.

TABLE IV

SPATIAL RESOLUTION OF THE CHAMBER (mm)

1 GeV POSITRONS, 0.6 RADIATION LENGTHS OF TARGET BETWEEN EACH MODULE

	K_i = 3.5, Longitudinal Weighting $1/(\sigma_i)^2$	Unweighted
X tubes	1.9	4.2
Y tubes	3.7	5.8

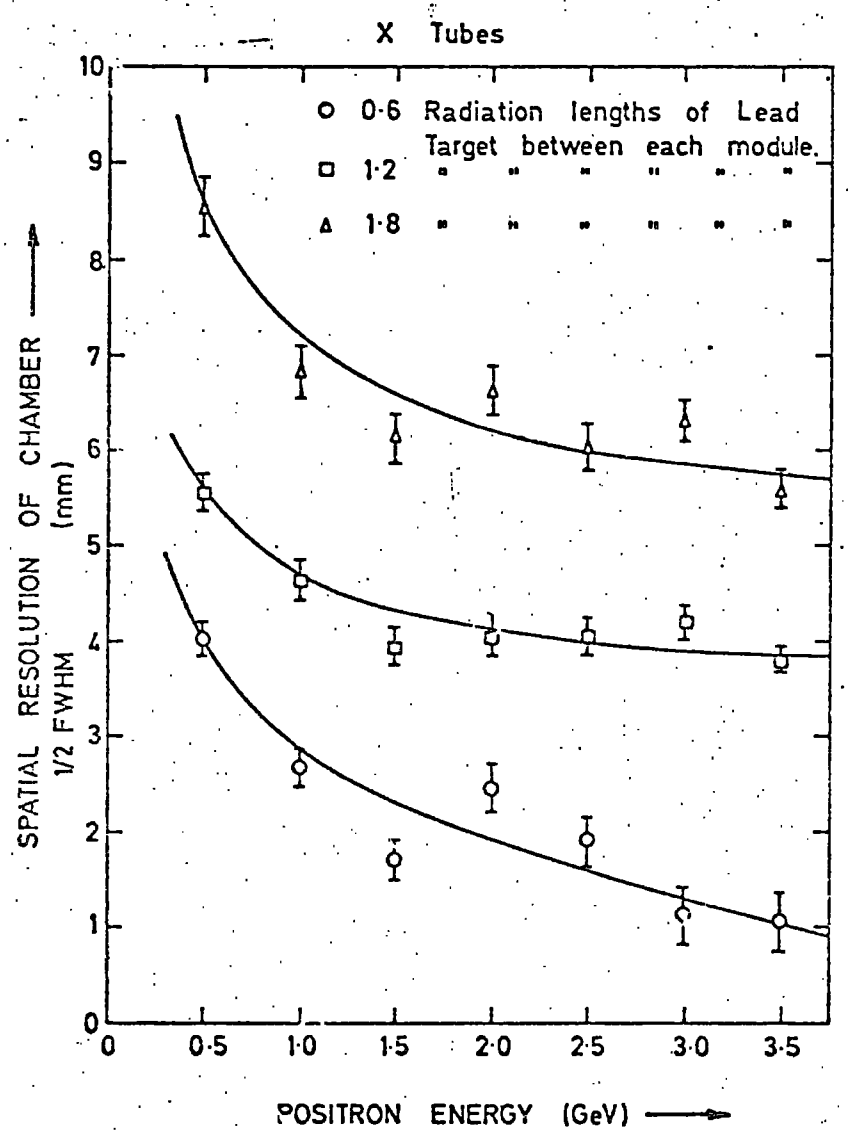

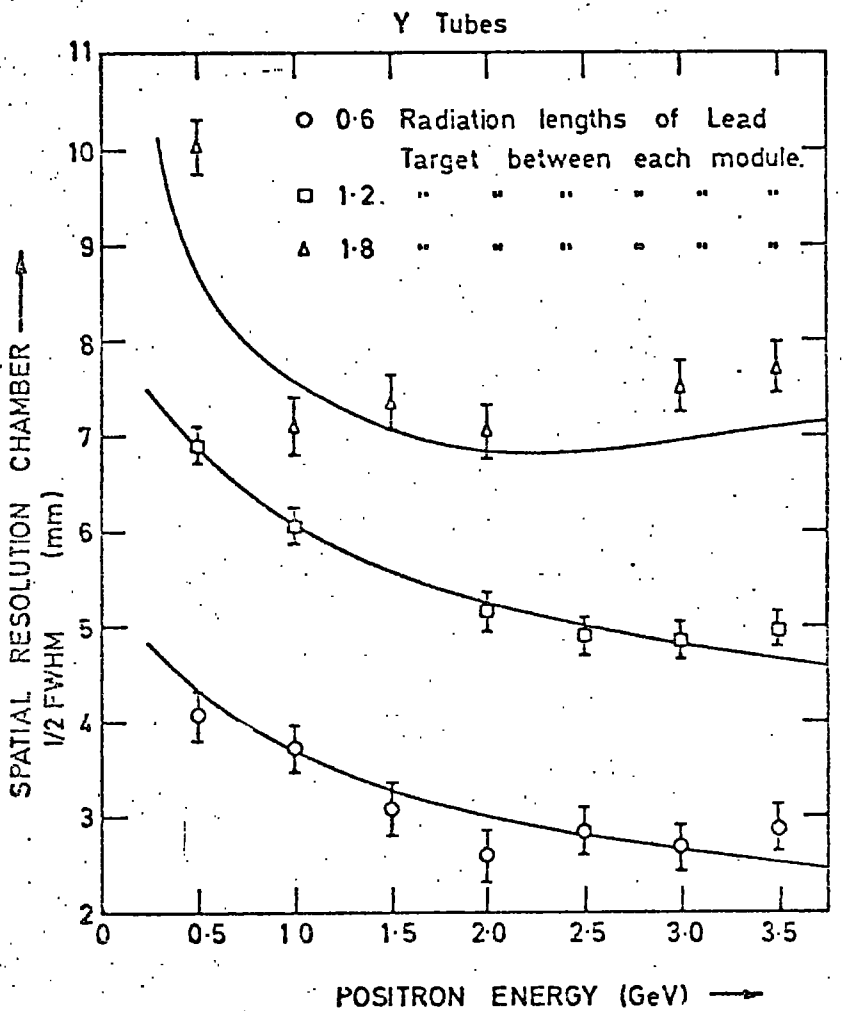

Fig.6·12 Spatial resolution versus energy.

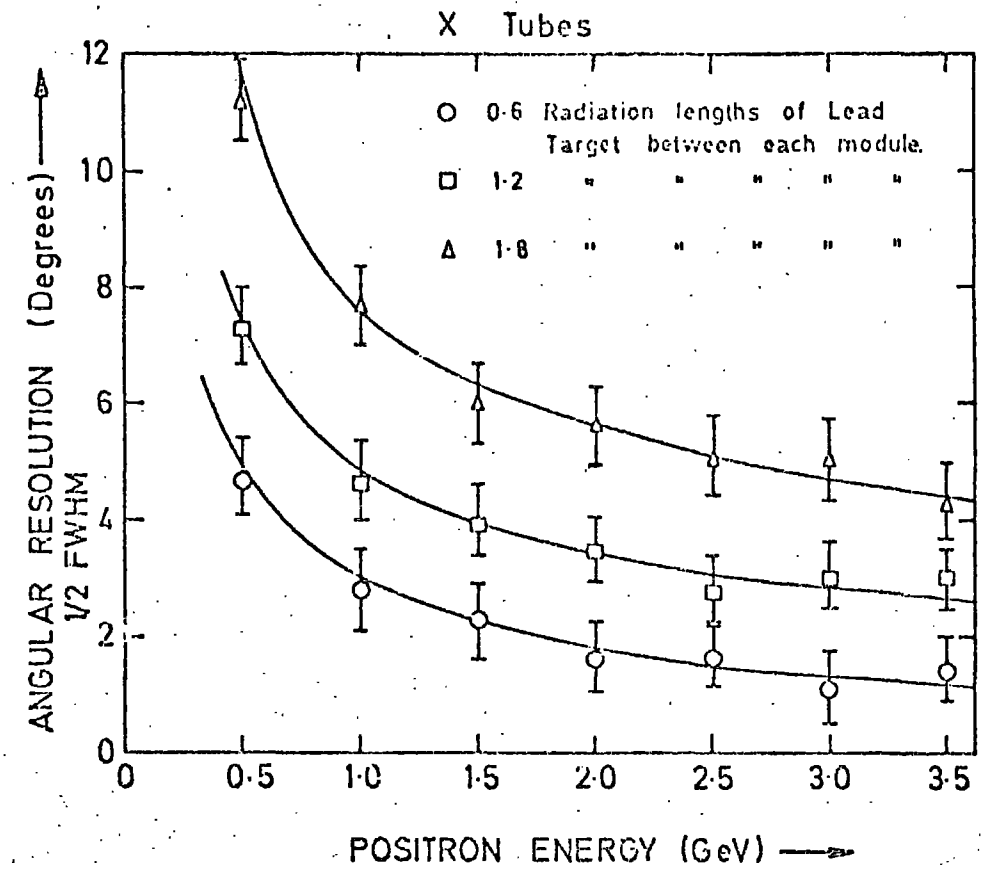

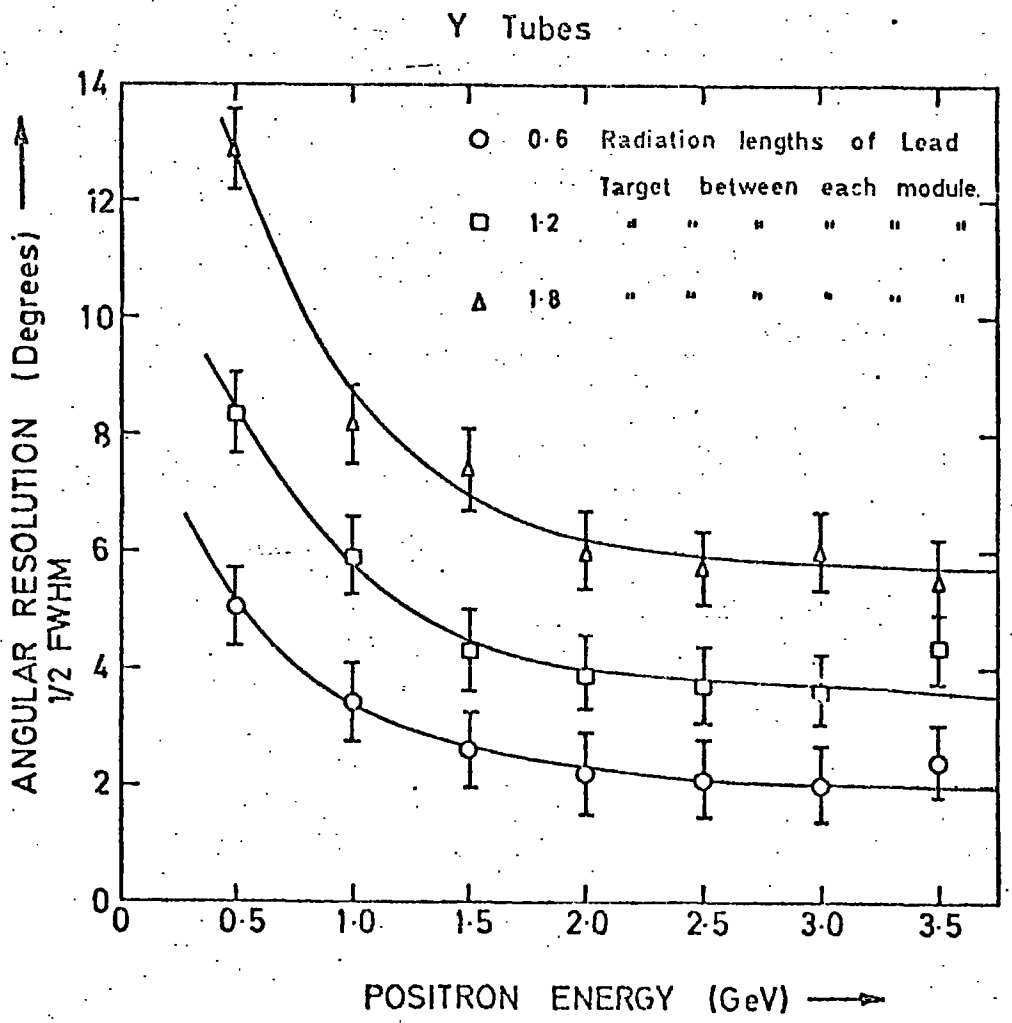

Fig. 6.13 Angular resolution versus energy.

6.3 CONCLUSIONS

From the series of tests carried out on the modified flash tube chamber in the positron beam, together with the results of the analysed shower data obtained from the chamber, the usefullness of the flash tube chamber in the detection of electromagnetic showers under accelerator conditions has been clearly illustrated.

The resolutions obtained using the modified chamber have considerably improved on those obtained from the prototype chamber employing the larger diameter flash tubes (see chapter 3).

Shower leakage from the chamber has been reduced and electron sensitivities as great as 90% have been obtained using the modified chamber. This has lead to a much better energy resolution, giving up to ± 10% for 3 GeV positrons incident on the chamber containing 1.2 radiation lengths of lead target between the modules.

The spatial resolutions of the modified chamber of up to ± 2 mm are a great improvement over those of the prototype chamber. However, angular resolutions have remained similar to those of the prototype chamber, where shower angles were found to within a few degrees.

A comparison between the energy resolution obtained from the modified flash tube chamber and those obtained by recent work employing electromagnetic shower detectors which give both spatial and energy information is shown in figure 6.14.

All the detectors give spatial resolutions of a few millimetres or less.

The results obtained by Basile et al. (3) were from an electromagnetic shower detector employing two six-gap thin plate

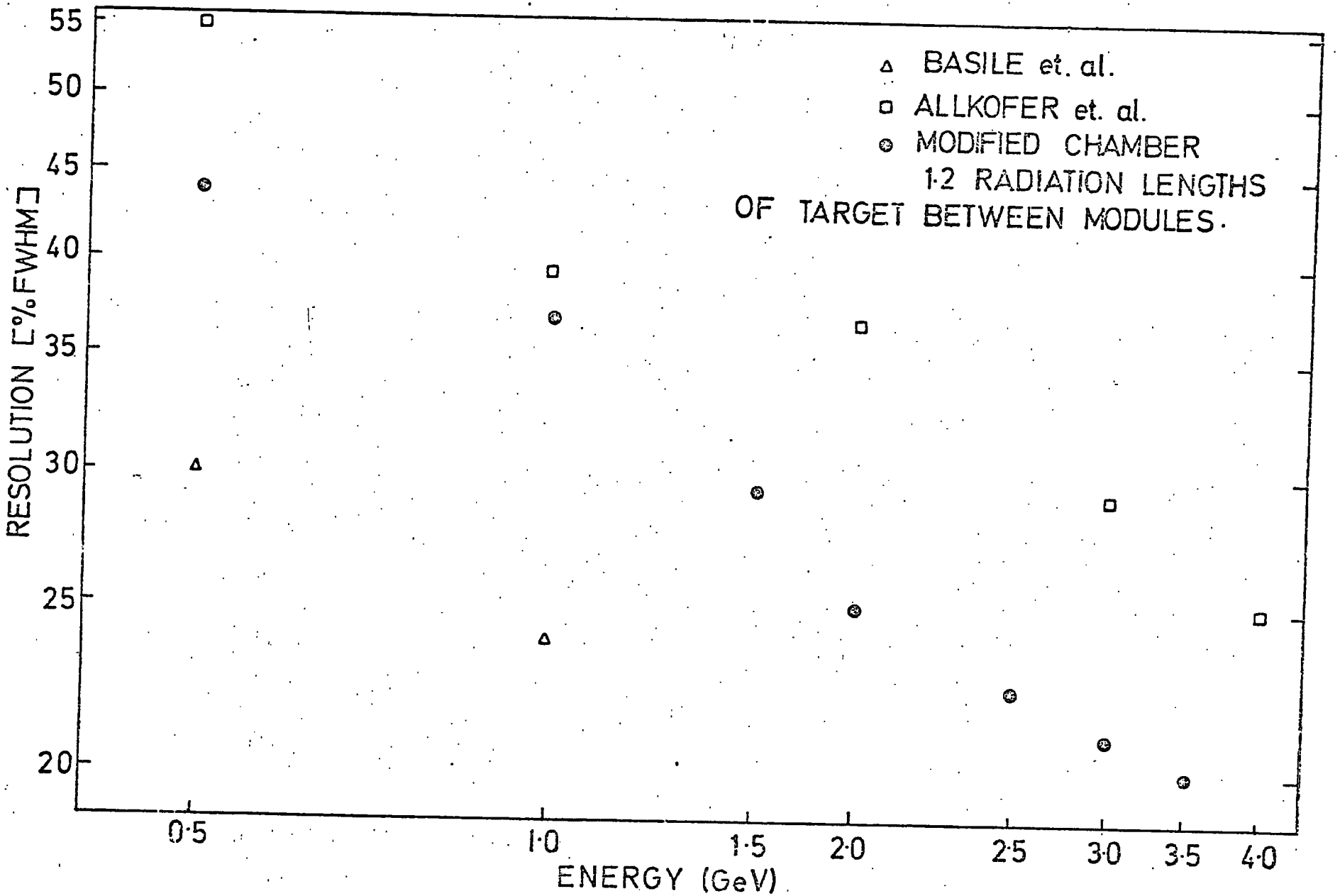

Fig. 6.14 A comparison of energy resolutions obtained using various detecting systems .

spark chambers and nine spark chamber-scintillator sandwiches. Electrons were used to produce the showers.

The results obtained by Allkofer et al. (4) were from a set of 21 glass spark chambers interspaced with iron plates, electrons were also used to produce the showers in this detector.

The energy resolution obtained using the modified flash tube chamber is seen to compare favourably with those results obtained by Basile et al. and Allkofer et al. The resolutions obtained by Basile et al. are rather better than those from the modified flash tube chamber. This results from the use of the plastic scintillators in the detector to determine the energy of the primary electron producing the shower. Without any information from the scintillators the energy resolution of the detector is increased by a factor of two.

However, the data obtained from the detectors used by Basile et al. and Allkofer et al. was recorded photographically; this meant tedious methods of analysis, counting sparks and fitting shower axes by eye, whereas the flash tube chamber produced fully digitised information which could be analysed "on line" during an experiment using "on line" computing techniques, or simply stored on disc or magnetic tape to be analysed at a later date using computational methods.

From the results obtained from the modified flash tube chamber, it is seen that the energy and spatial resolutions are comparable with those of conventional detectors, however the operation of the modified flash tube chamber is severely restricted to low repetition rates of about several events per minute. This rate may be satisfactory for certain accelerator experiments, but

the potential of the chamber would be greatly increased if higher repetition rates could be used.

The following chapter gives details of a method pursued at Durham in order to increase the working rate of the high pressure, methane doped tubes.

REFERENCES

1. Messel, H., Crawford, D.F. (1970) Electron Photon Shower Distribution Functions. Pergamon Press, New York

2. Volkel, U. (1965) Internal Report, DESY 65/6

3. Basile, M. et al. (1972) Nucl Inst. & Meth. 101 433

4. Allkofer, O.C., Dau, W.D., Grupen, C., Pischke, J., Stamm, W., Uhr, R. (1973) Proc. Int. Conf. Cosmic rays Denver 2761

CHAPTER SEVEN

A HIGH VOLTAGE PULSING SYSTEM FOR USE AT HIGH REPETITION RATES

7.1 INTRODUCTION

From the tests done on the small diameter, high pressure tubes filled with Ne(70%)-He(30%) + 2% CH_4 on the positron beam (see chapter 4), and on the modified chamber (see chapter 5), it was found that the flash tube digitisation pulse heights decreased with increasing flashing rate (1). This effect limited the operation of the chamber to repetition rates of several events per minute (2).

The decrease in digitisation pulse height with repetition rate was believed to be due to the build up of large induced clearing fields in the tubes after their discharging.

Tests were therefore carried out at Durham, where the digitisation pulse heights were studied using various modes of high voltage pulsing, with the aim of reducing the magnitude of the clearing fields, and so increasing the working rate of the tubes. The tests are described in this chapter.

7.2 ANOMALOUS EFFECTS ASSOCIATED WITH THE POLARITY OF THE APPLIED ELECTRIC FIELD

The digitisation pulse heights obtained from the tubes were studied using a similar test rig to that used in the positron beam tests (see figure 7.1 b).

The digitisation probe was a 6 BA screw placed in contact

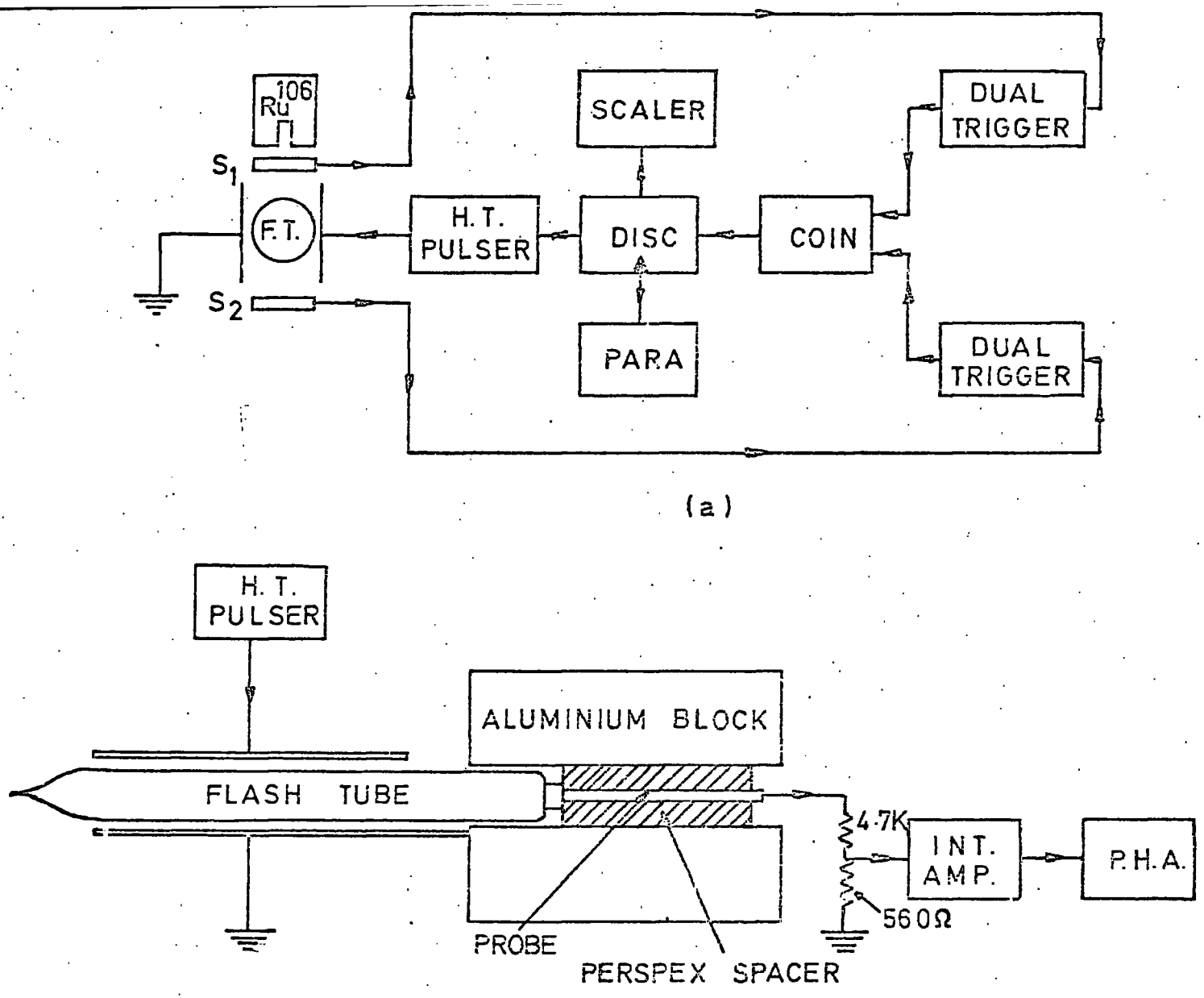

Fig. 7.1 Experimental and digitisation probe arrangement .

with the tube window to which a 7 mm. aluminium disc was adhered.

The probe impedance was 5.3 KΩ and consisted of a 4.7 KΩ resistor and a 560 Ω resistor connected in series. Digitisation pulses obtained across the 560 Ω resistor were fed into a pulse height analyser via an interface amplifier. This amplifier served two purposes; firstly it was used to amplify the pulses which were sometimes very small, and secondly, to invert pulses of negative polarity because of the unipole nature of the analyser input. The pulse height analyser was calibrated using a pulse generator.

Single β-particles from a Ru^{106} source were selected on passing through a flash tube, by means of a two fold coincidence of scintillation counters S_1 and S_2 (see figure 7.1 a).

The coincidence signals were used to trigger the high voltage pulsing unit which provided a pulsed field across the tube. The coincidence unit could be paralysed for a fixed period of time after each coincidence by means of a paralysis unit, hence the working rate of the tube could be varied.

The high voltage pulsing unit consisted of a CR decay system which was discharged using a trigatron spark gap (3). The spark gap was triggered by a -3 KV trigger pulse obtained from a hydrogen thyratron on the acceptance of a coincidence signal.

The trigatron spark gap was used so that the polarity of the applied high voltage pulse could be changed simply by changing the polarity of the high voltage supply.

The characteristics of the applied electric field are given in table I.

TABLE I

CHARACTERISTICS OF THE APPLIED ELECTRIC FIELD

Peak Value ($KV\ cm^{-1}$)	Delay Time (nsec.)	Width (RC time) (μsec.)	Rise Time (nsec.)
10 - 11	200	4.5	60

7.2.1 THE EFFECT OF THE FLASHING RATE ON THE DIGITISATION PULSE HEIGHTS

The digitisation pulse heights associated with the small diameter, methane doped tubes, had been studied at very low flashing rates, of several events per minute using cosmic rays, and at higher rates, up to about 240 events per minute, using a positron beam (see chapter 4). The digitisation pulse heights were studied for intermediate flashing rates of up to 90 events per minute using the Ru^{106} source and using applied fields of different polarities.

The digitisation pulses were obtained for both negative and positive applied electric fields of different magnitudes and for various flashing rates. About 1000 pulse heights were recorded for each flashing rate and applied field. Almost 30% of the two-fold coincidences obtained were due to β-particles which produced a discharge in the tube on the application of the pulsed electric

field. The remainder of the coincidences were due to the high background of gamma-rays also emitted by the source. The times, therefore, between the genuine β-particle coincidences which produced discharges accompanied by digitisation pulses, were not constant, and the flashing rate mentioned throughout this chapter, unless otherwise stated, was the average flashing rate of the tube and not the rate of coincidences. The mean and standard deviations of each of the digitisation pulse height distributions were calculated and the results are plotted in figure 7.2 and 7.3 for negative and positive applied fields respectively.

The variations in digitisation pulse height with flashing rate using a negative applied field agree quantitatively with those found in the positron beam tests (see figure 4.12). However, a very different trend was found when a positive applied field was used, the decrease in digitisation pulse height with flashing rate being a much more gradual process, which resulted in considerably larger digitisation pulse heights at the higher flashing rates.

As the magnitude of the digitisation pulse heights depends strongly on the size of the remanent clearing field in the tube, these results suggest that the time constants for the decay of the induced fields are smaller when positive electric fields are applied.

The size and decay constants of the induced fields were estimated for various applied fields.

7.2.2 INTERNAL CLEARING FIELDS

The digitisation pulse height distributions were measured for different polarities and various magnitudes of applied fields

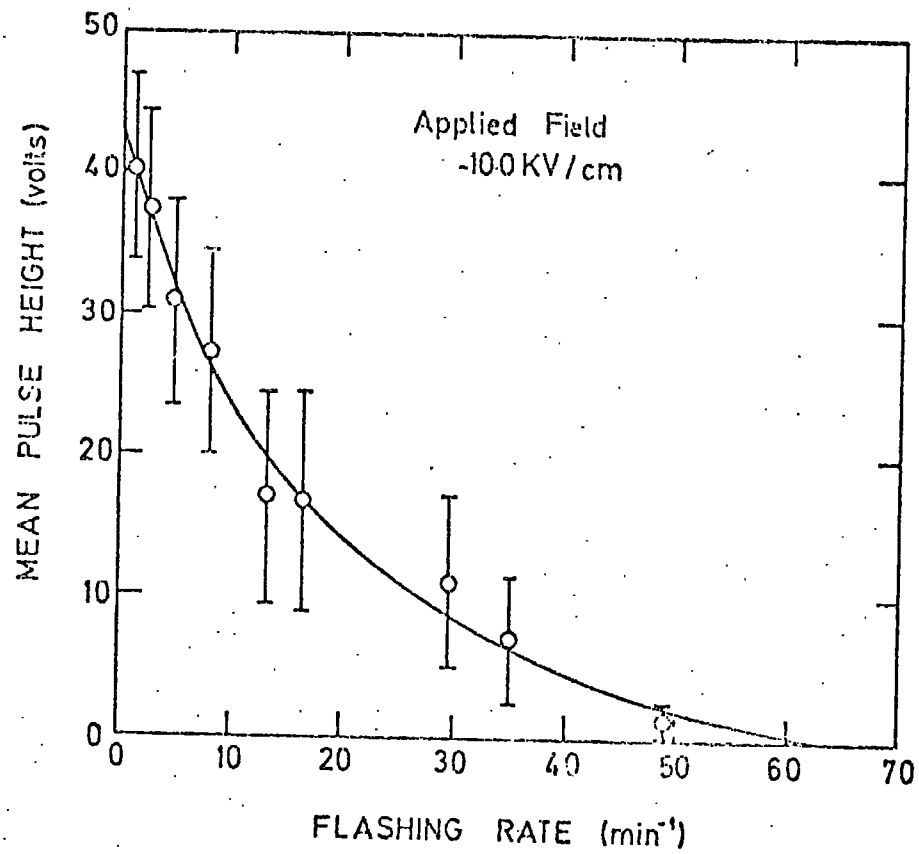

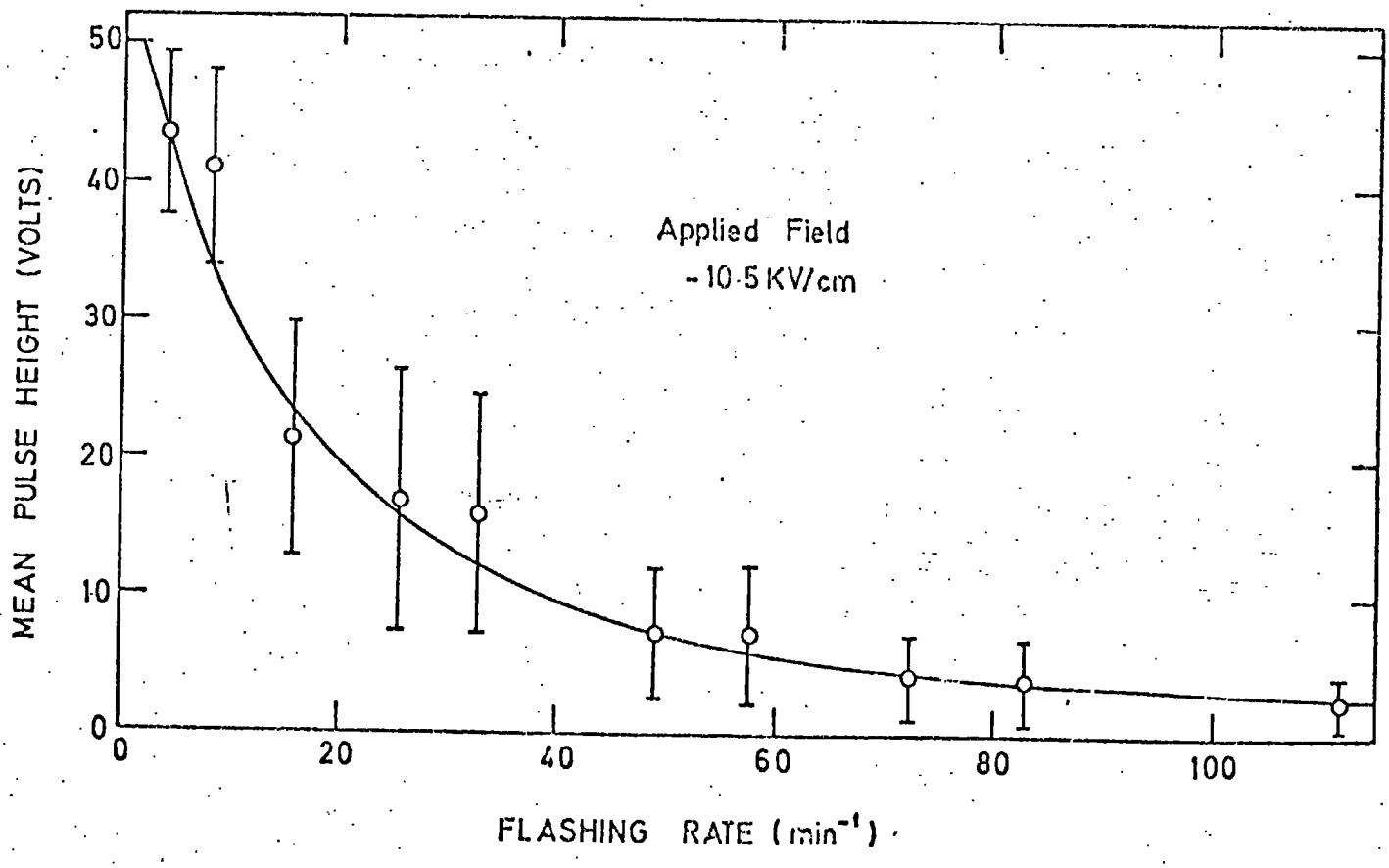

Fig. 7.2 Digitisation pulse height versus flashing rate for negative applied fields.

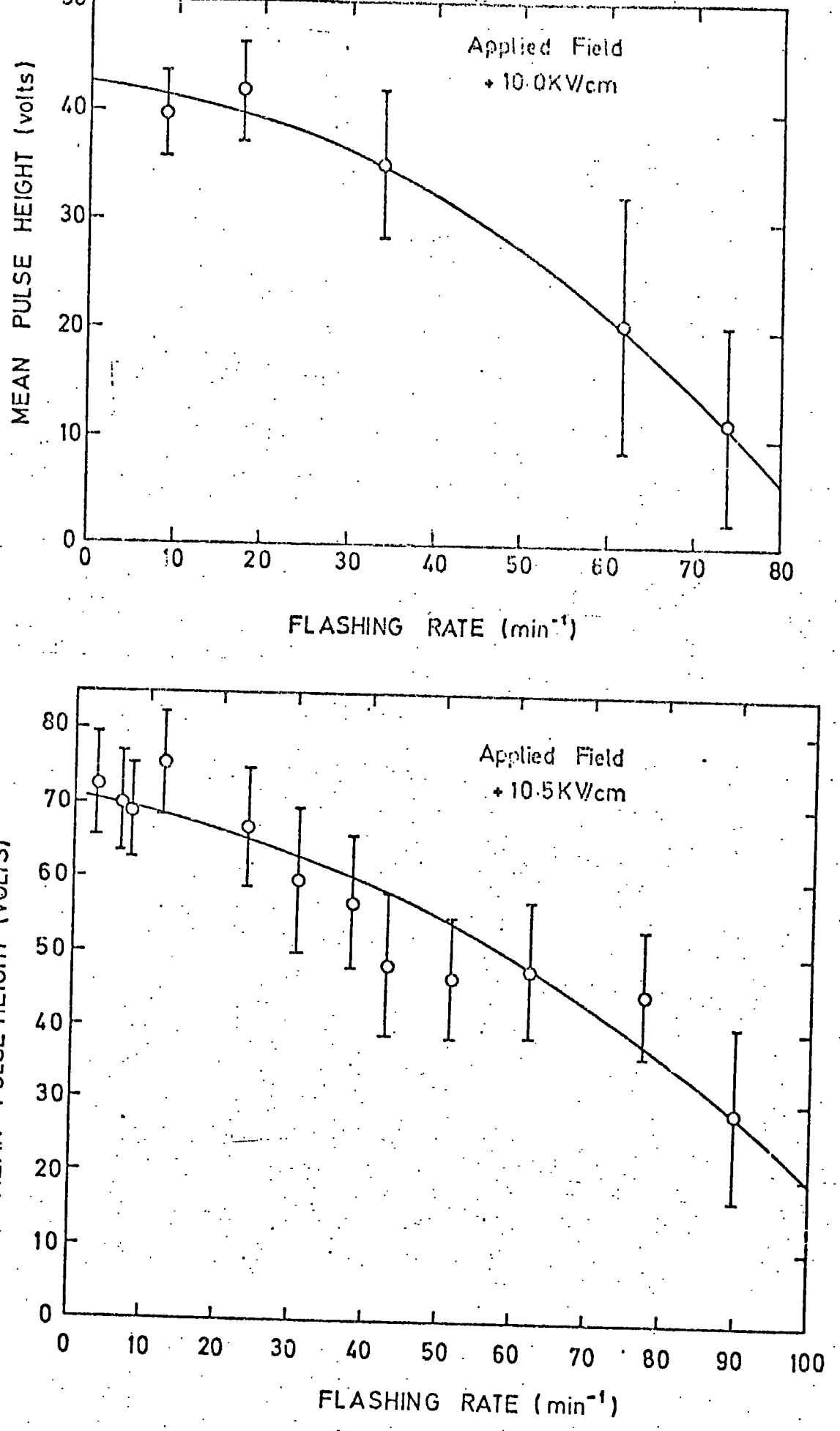

ig. 7.3 Digitisation pulse height versus flashing rate for positive applied fields .

at very slow flashing rates, so that clearing field effects could effectively be neglected.

The results obtained for negative and positive applied fields are shown in figure 7.4. A linear relationship had been found in previous tests using negative applied fields (4), and this was also found for both the negative and positive applied fields as shown in figure 7.4.

The points in this figure are the means of the pulse height distributions, and the errors associated with each of the points are the standard deviations of the respective pulse height distributions.

The results in figures 7.2 and 7.3, together with the results from the graphs in figure 7.4 were used to estimate the magnitudes of the induced clearing fields at various flashing rates, for applied fields of different polarities.

For a given flashing rate and applied field, the resulting digitisation pulse height was found from either figure 7.2 or 7.3. The effective applied field for the resulting pulse height was then found from figure 7.4. The magnitude of the internal clearing field was then taken as the difference between the applied electric field, and the corresponding effective applied field at that flashing rate.

The resulting estimates obtained for the magnitudes of the remanent clearing fields are shown in figure 7.5. The magnitude of the applied field was 10 KV cm^{-1}.

The decay times of the induced fields are seen to be very different for the different polarities of applied fields. The decay constants of the induced fields, measured from the linear portions of the curves, are found to be 27.7 sec. and 0.6 sec. for the

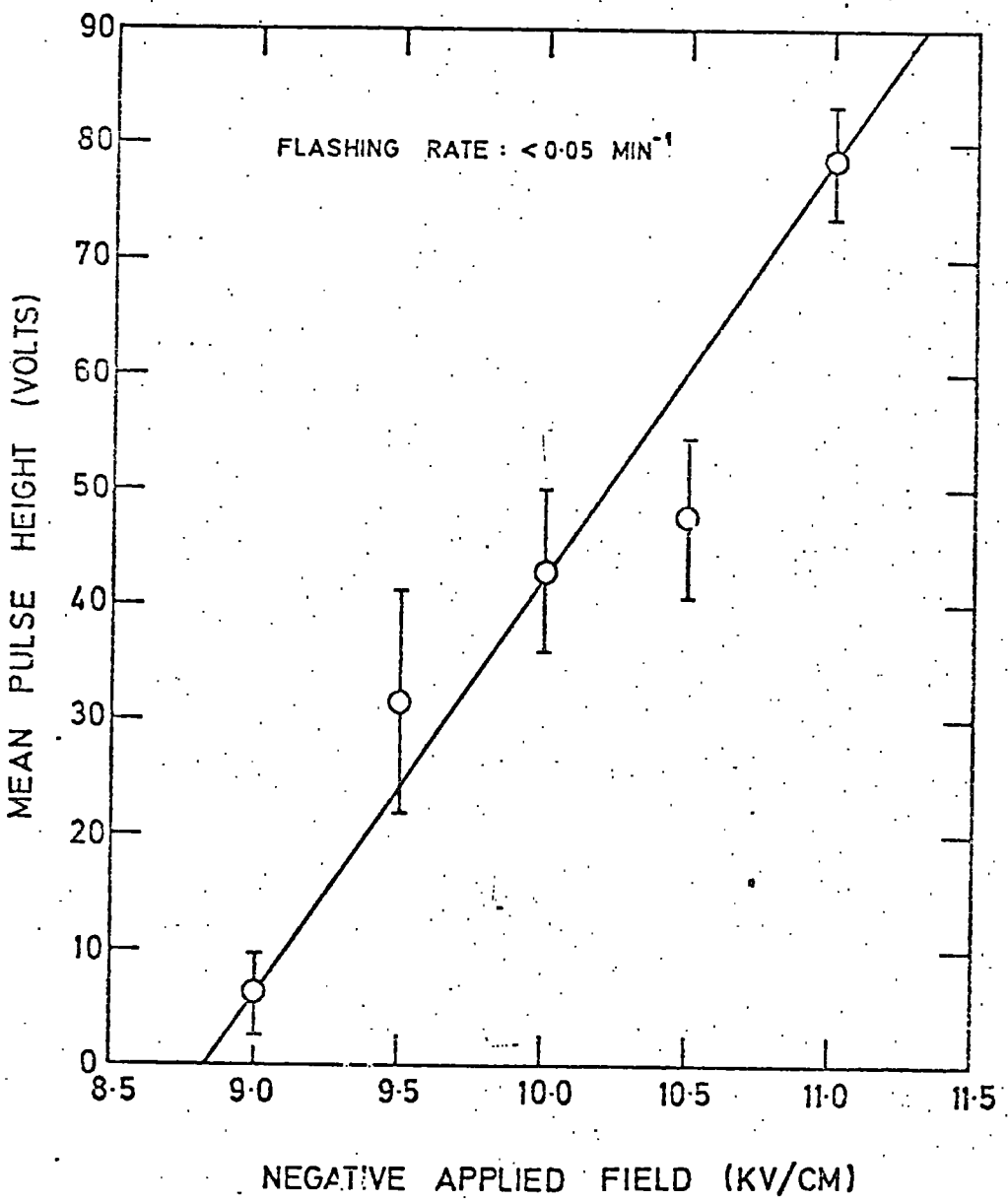

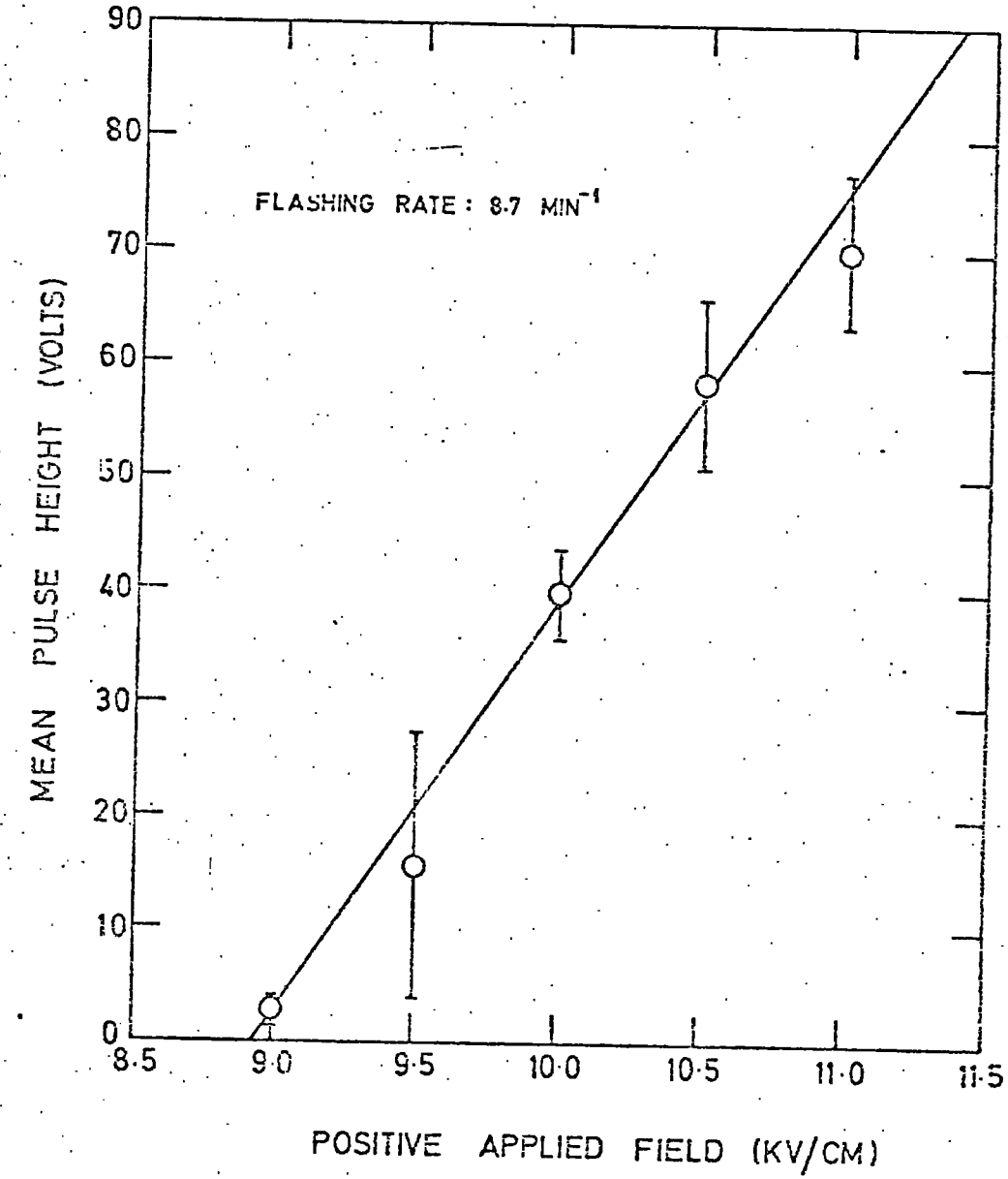

Fig. 7·4 Digitisation pulse height versus applied field.

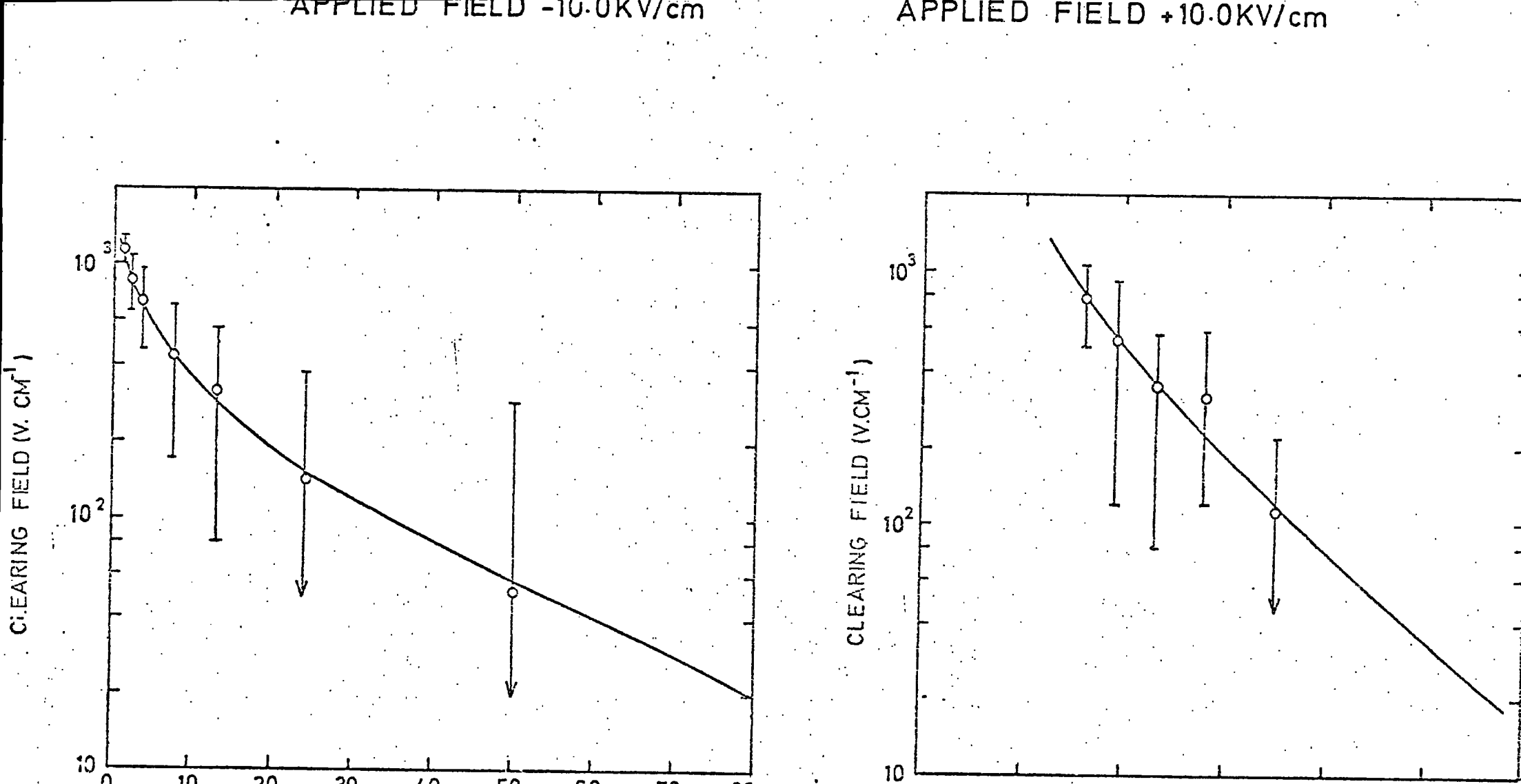

Fig. 7.5 The magnitudes of the induced clearing fields as a function of time .

negative and positive polarities respectively.

From the curves in figure 7.5 it is seen that there are two distinct gradients associated with the decay of the internal fields. The curved portion at the beginning of the curves indicates a varying decay constant immediately after the discharge, which then remains constant in the later part of the curves.

Similar trends in the decay constants of induced fields were found by Ashton et al. (5), using low pressure flash tubes made of S95 soda glass, however the decay constants were different, which suggests that they depend a great deal on the type of tube being used.

Further evidence of the magnitude of the remanent clearing field depending on the polarity of the applied electric field was found in sensitive time measurements of the tubes (see section 7.4.3).

7.3 TWO DISCHARGE MECHANISMS

For the faster flashing rate runs the digitisation pulse height distributions were found to separate into two quite distinct distributions (see figure 7.6). This effect was also observed during the lower flashing rate runs, when smaller applied fields were used (see table II).

The two separate distributions indicate that there are two quite distinct discharge processes, giving rise to the digitisation pulses. It is believed that the two processes responsible may be Townsend and Streamer discharge mechanisms (6), the streamer discharges, of very high charge densities, occurring for effective applied fields greater than about 9.5 KV cm^{-1}, producing the larger

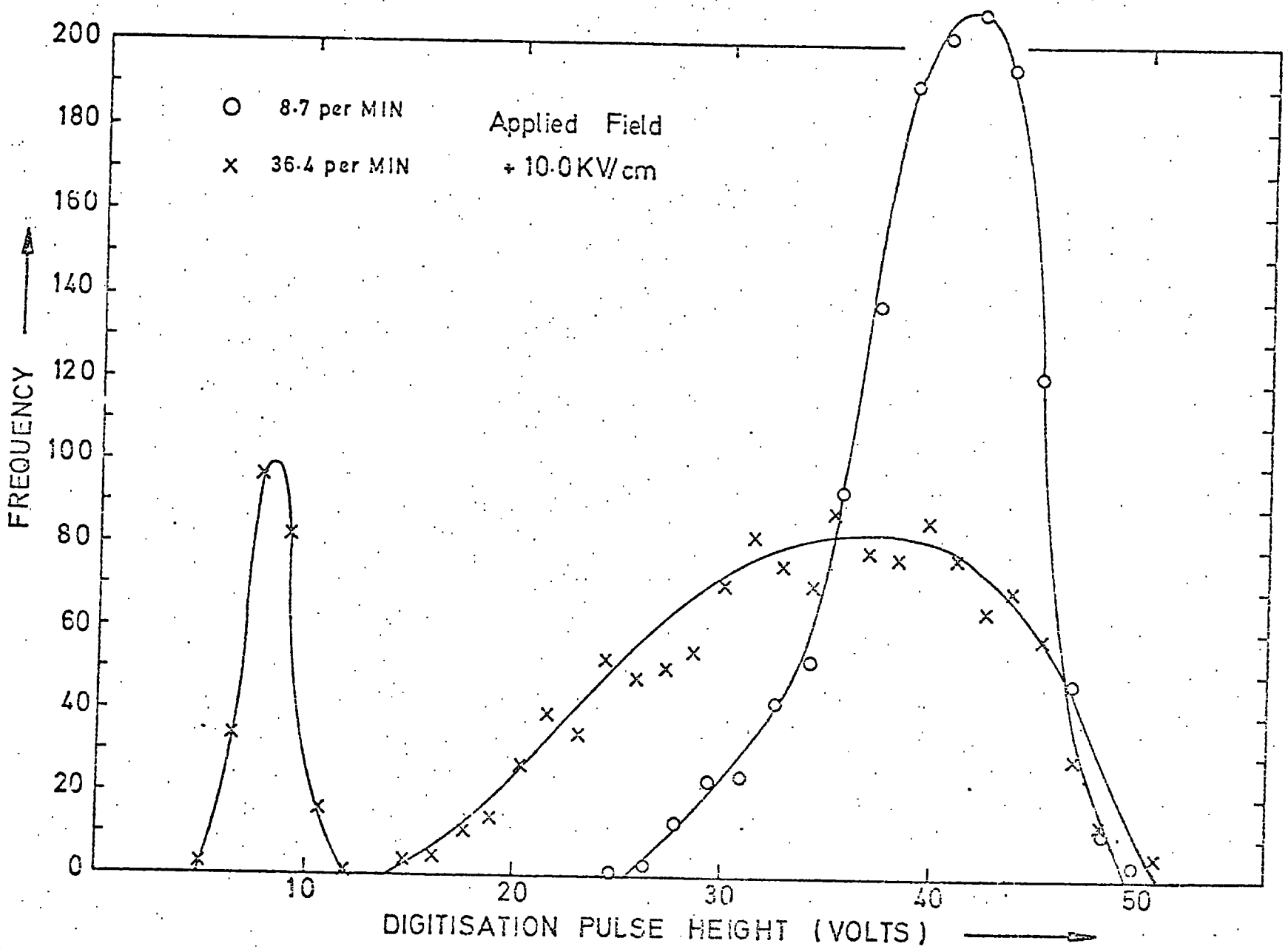

Fig. 7·6

Digitisation pulse height distributions.

TABLE II

Fields ($KV\ cm^{-1}$)	Peaks in Distributions (Volts)	Number of Events in each Distribution (%)	Flashing Rate (Min^{-1})
-10.0	1	26	33
	6	74	
-10.0	0.5	69	41
	5	31	
+ 10.0	7	13	36
	37	87	
+ 10.0	7	39	62
	25	61	
+ 10.0	5	66	74
	20	34	
+ 9.5	5	55	7
	27	45	
-9.0	0.5	50	4
	6	50	

digitisation pulses. At the faster flashing rates the induced fields reduce the effective applied fields. This results in Townsend discharges, of lower charge densities, producing smaller digitisation pulse heights.

7.4 APPLIED FIELDS OF ALTERNATE POLARITIES

In order to reduce the build up of the induced clearing fields at faster flashing rates, a double pulsing system was constructed, which applied alternate polarity high voltage pulses on successive particle coincidences. This entailed the coupling of two opposite polarity high voltage pulsing units to the flash tube H.T. plate, the units being triggered and the coupling controlled by a logic unit incorporated in the system. A diagram of the experimental arrangement employing the double pulsing system is shown in figure 7.7.

The two high voltage pulsing units were coupled to the H.T. plate using two high voltage reed switches, (type DTA-812, manufactured by Flight Research Ltd.).

Two spark gaps were used to produce exponential CR high voltage pulses of alternate polarities.

In the operation of the double pulsing system a + 24 V two way relay in the logic unit (see figure 7.7 b) is closed to provide power for one of the high voltage reed switch coils. Consider the case when the reed coil for spark gap 1 is powered. The logic unit, on recieving a coincidence signal, sends a trigger signal to spark gap 1 which then switches. The spark gap 1 reed coil is powered hence its associated reed switch is closed, so a high voltage pulse of positive polarity is obtained on the flash

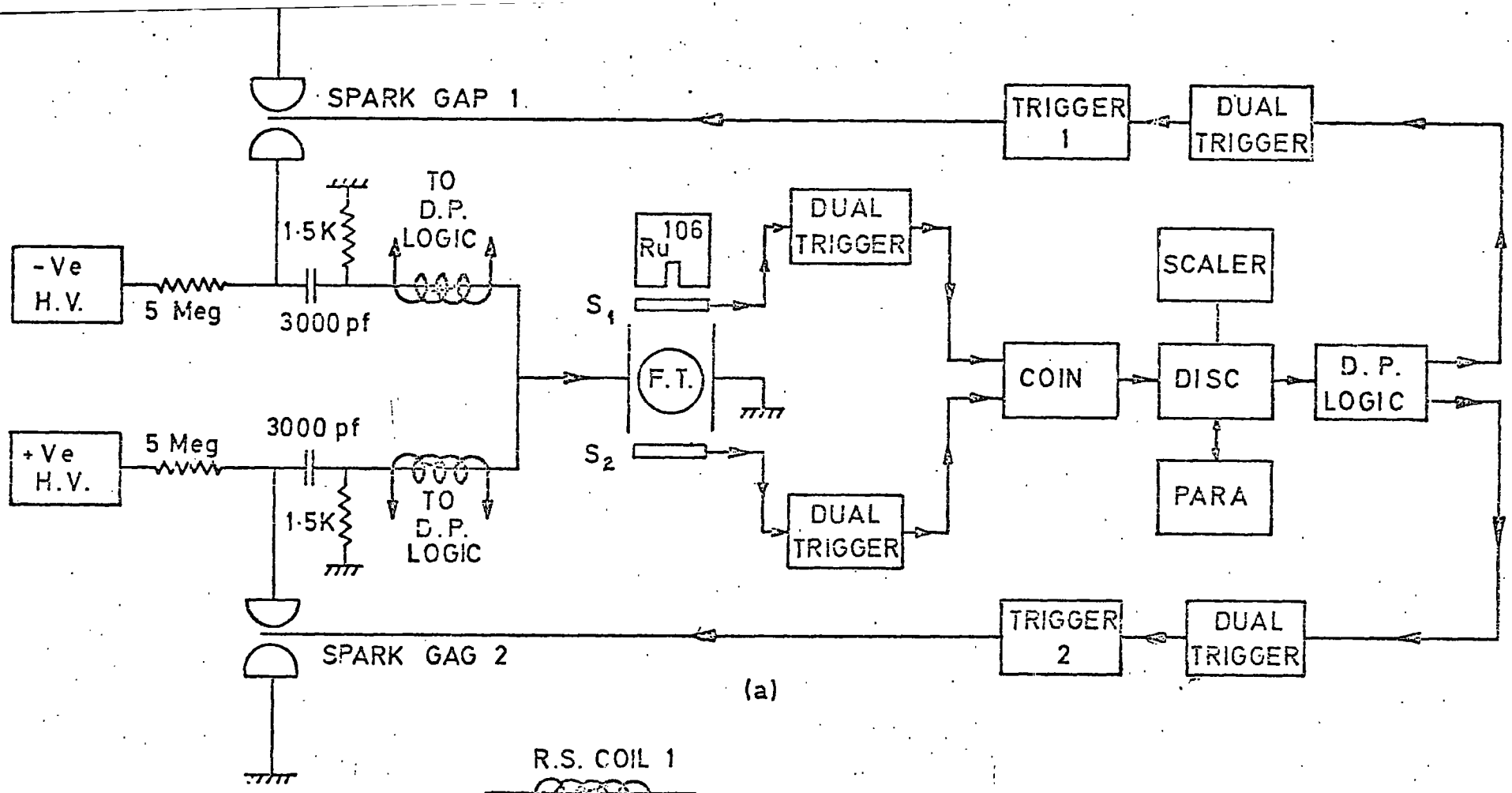

Fig.7.7 Experimental arrangement used to apply H.V. pulses of alternate polarity

tube H.T. plate. After a delay of about 400 μ sec. from the switching of spark gap 1, the relay position changes to provide power for the spark gap 2 reed coil. A coincidence signal fed to the logic unit then sends a trigger signal to spark gap 2, the resulting high voltage pulse of negative polarity appears on the H.T. plate. In this way high voltage pulses of opposite polarity are fed to the flash tube H.T. plate on successive coincidence signals.

The logic unit was made from standard TTL integrated circuits, and a circuit diagram is shown in figure 7.8. The unit was housed in a standard N.I.M. module. It recieves + 5 V scalar signals at the coincidence input and produces N.I.M. standard signals alternately at outputs P_1 and P_2 on successive coincidence inputs. The N.I.M. outputs from P_1 and P_2 are fed to high voltage thyratron pulsing units, which are used to trigger the spark gaps. The + 24 V line is switched between outputs R_1 and R_2 after a delay of about 400 μ sec. on recieving input signals.

A schematic diagram of the logic unit is shown in figure 7.9. The + 5 V scalar input signals change the state of a J-K flip flop (7470), the output levels of which pass through a NAND (7910), which gives "clean" edges to the changing levels.

Each level from the NAND is then fed to a monostable (74121), which triggers on a positive rising edge, producing both a N.I.M. signal across 50 Ω at P_1 or P_2, and a logic signal which is delayed for about 400 μ sec. by two similar monostables. The delayed logic signals are then fed to a set-reset latch (74118), the output of which is used to switch a transistor (BC109). The transistor operates a + 6 V relay which switches the + 24 V line between outputs R_1 and R_2.

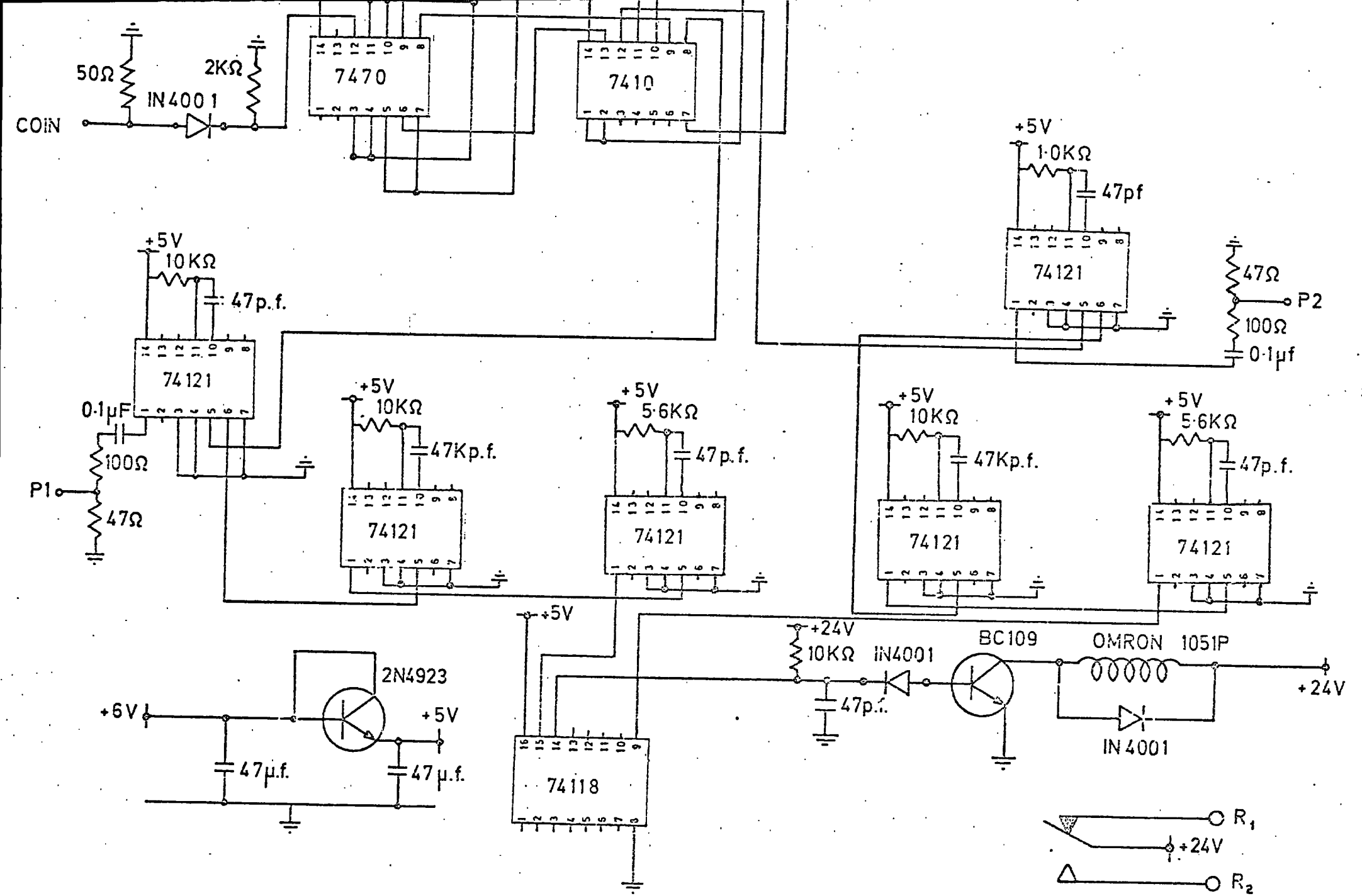

Fig. 7.8 Circuit diagram of the double pulsing logic unit

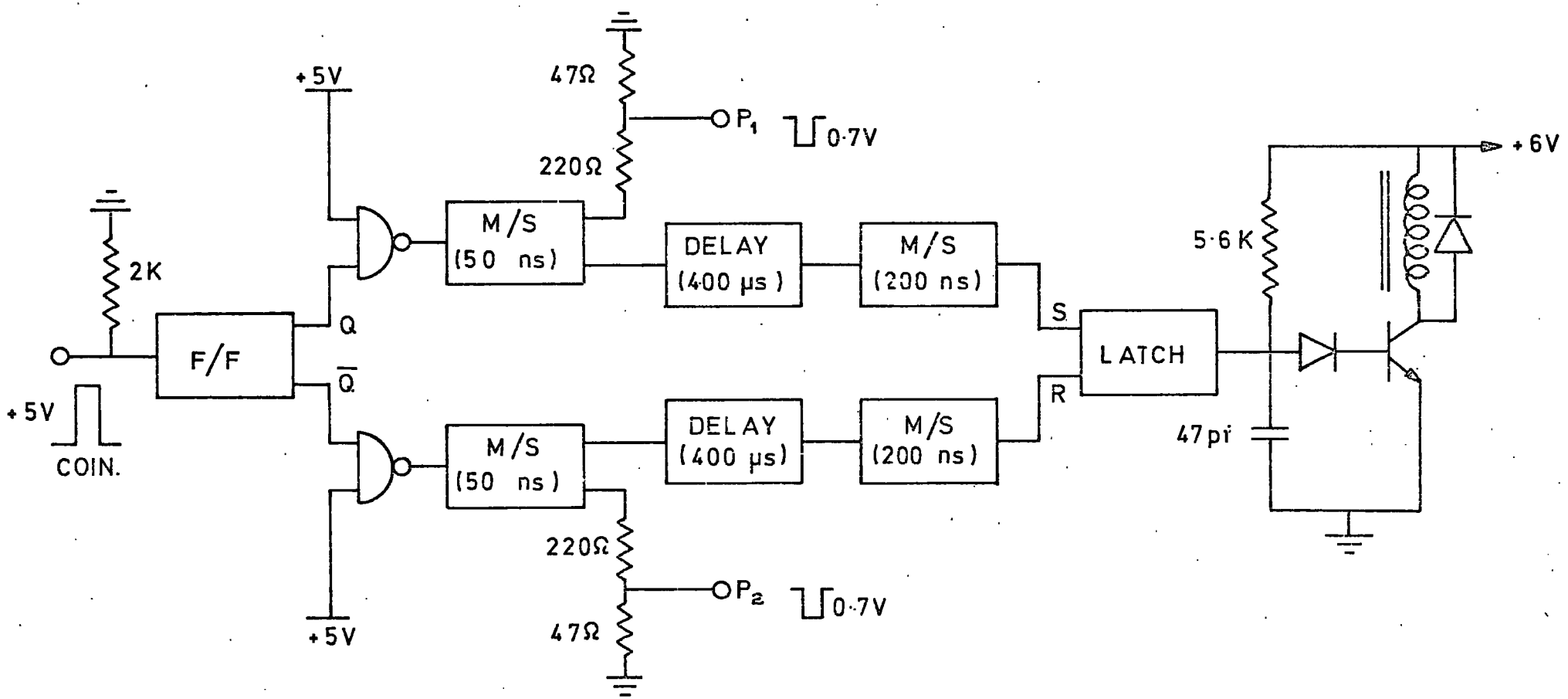

Fig.7.9 Schematic diagram of the double pulsing logic unit .

The double pulsing system was set up as shown in figure 7.7, the Ru^{106} source being used to provide coincidence signals as in the previous tests.

The digitisation pulse heights were recorded as in the single pulsing tests.

7.4.1 VARIATIONS IN DIGITISATION PULSE HEIGHT WITH FLASHING RATE USING THE DOUBLE PULSING SYSTEM

Using the experimental arrangement described in the previous section, the effect of applying alternate polarity fields on successive coincidences was investigated. The digitisation pulse heights were measured for each polarity separately, for various flashing rates, and the mean pulse heights obtained are shown in figure 7.10, for negative and positive applied fields.

The mean pulse heights are seen to remain roughly constant up to a flashing rate of 90 min^{-1}. The pulse height distributions are found to widen as the flashing rate is increased, this is indicated in the figures by the increase in the error bars associated with each point.

The widening of the pulse height distributions at the higher flashing rates is due to the presence of the gamma-ray background produced by the radioactive source, giving rise to coincidences resulting in the application of high voltage pulses without the discharging of the tube. In the ideal case when the tube flashes on consecutive coincidences resulting from β-particles, then the digitisation pulse resulting from a second discharge is larger than that accompanying the first discharge.

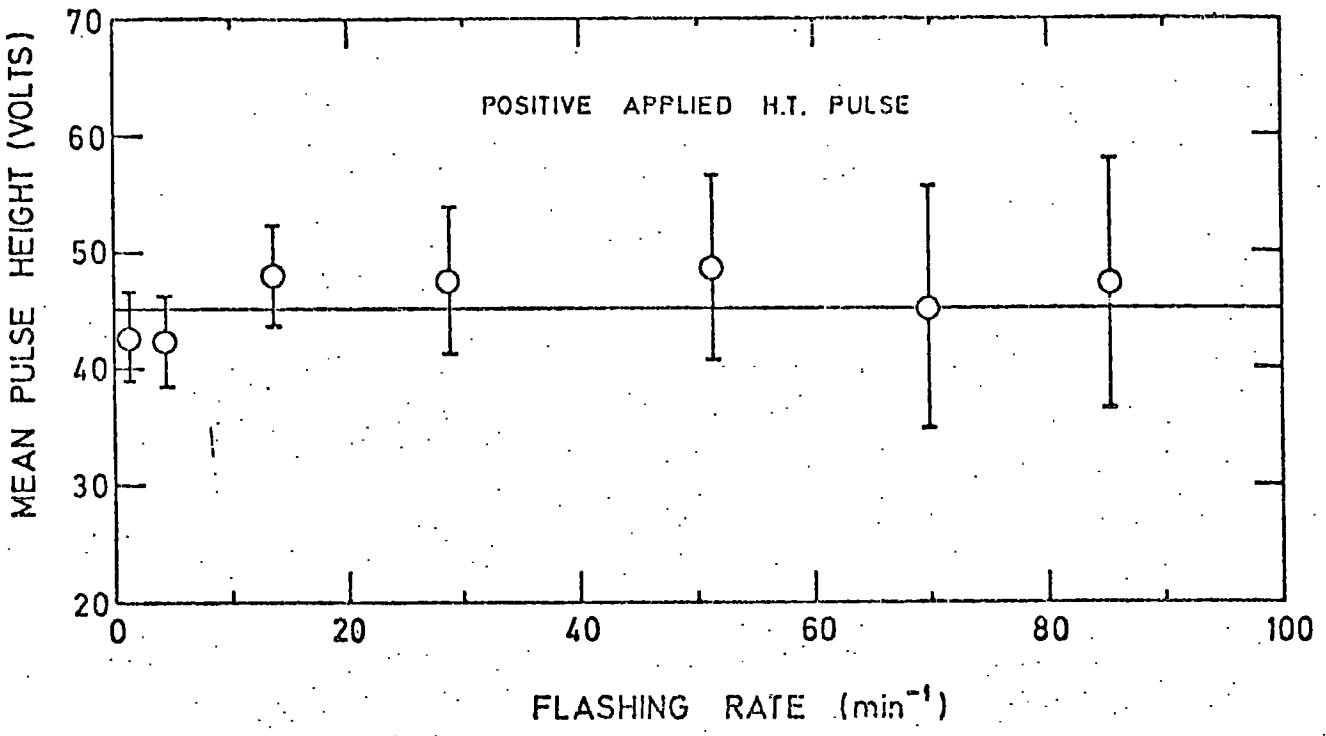

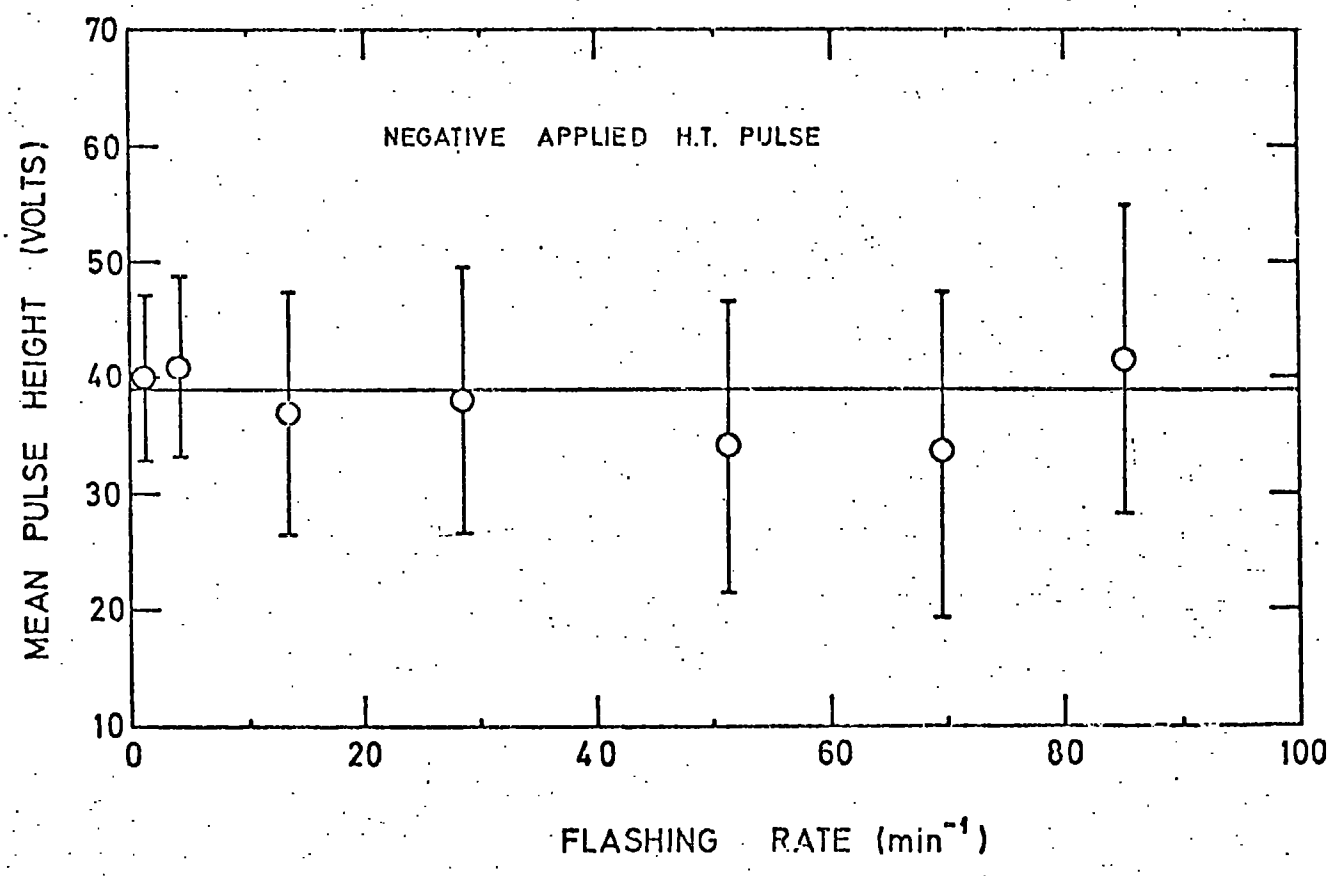

Fig. 7.10 Digitisation pulse heights as a function of flashing rate using the modified pulsing system.

This is because the charges deposited on the tube walls from the first discharge enhance the second applied high voltage pulse.

However, consecutive discharges arising from similar polarity applied high voltage pulses give rise to smaller digitisation pulses, because of the backing off of the applied pulse by the deposited charges on the tube walls.

Hence the gamma-ray background, which causes consecutive discharges to be produced from varying polarity high voltage pulses, causes variations in digitisation pulse heights at higher flashing rates, where the remanent clearing fields are much larger.

The standard deviations of the pulse height distributions obtained using the double pulsing system, for various flashing rates, are shown in figure 7.11. The standard deviations increase initially with rate, however they appear to remain constant for flashing rates greater than about 70 min^{-1}.

The constant distribution widths may be due to there being little chance of accumulating charge on the tube walls, when fields of both polarities are applied alternately.

7.4.2 SPURIOUS FLASHING

As mentioned in chapter 4 it was found that spurious flashing of the high pressure methane doped tubes occurred for applied fields of more than about 10 KV cm^{-1}, and the amount of spurious flashing was found to increase if the applied field was increased.

The possibility of spurious flashing therefore arises during double pulsing tests, as the applied field may be enhanced

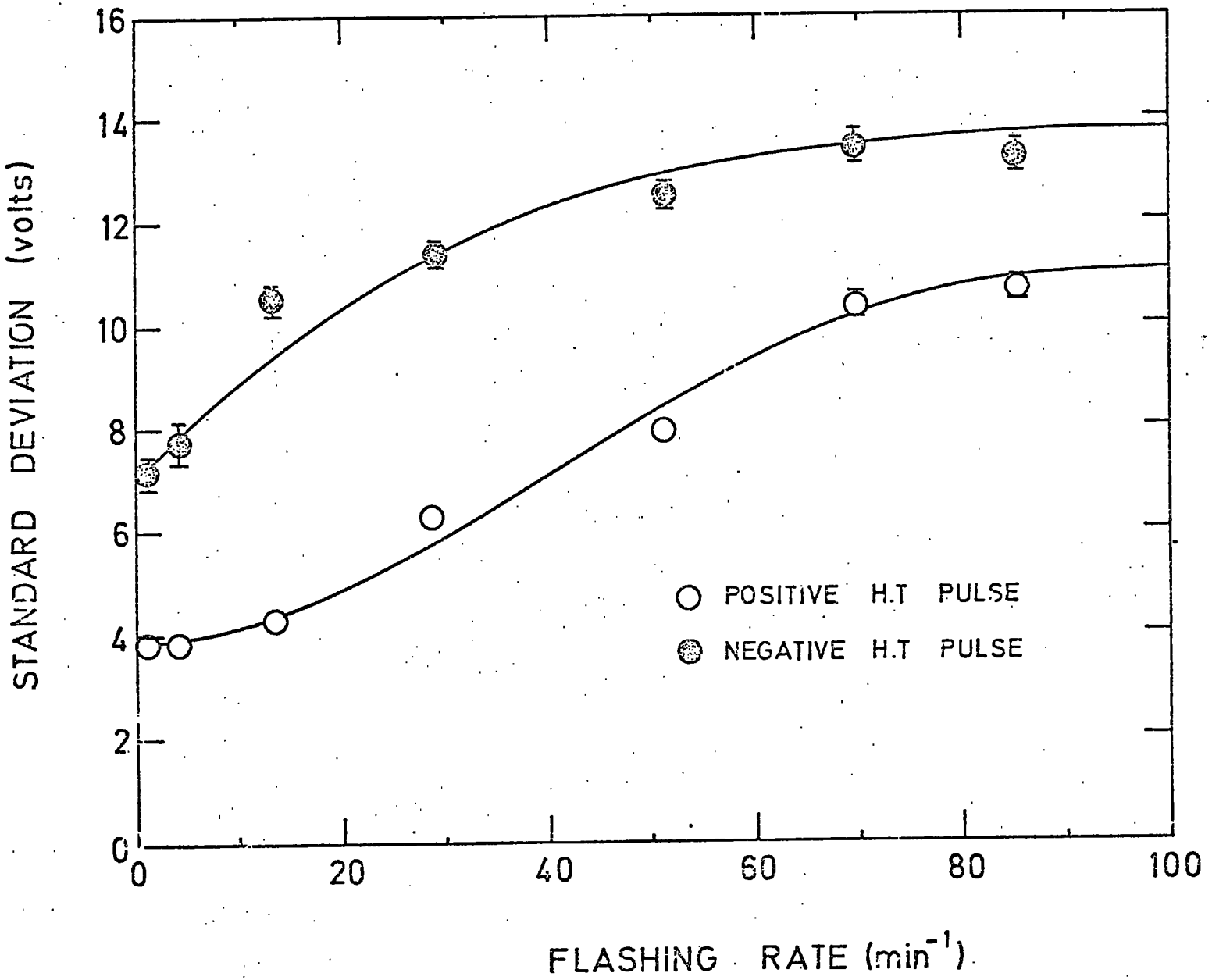

Fig.7.11 Standard deviation of the digitisation pulse height distribution as a function of flashing rate

by the presence of an internal clearing field.

A measure was made of the amount of spurious flashing during the double pulsing tests by calculating the "flashing efficiency" of the tube,

$$\text{ie.} \left[\frac{\text{Number of tube discharges}}{\text{Number of applied high voltage pulses}} \right] \times 100\%$$

for various pulsing rates.

The results obtained for applied fields of $\pm$ 10 KV cm^{-1} are shown in figure 7.12. It is seen that the flashing efficiency remains almost constant for various pulsing rates using the double pulsing system, and hence the amount of spurious flashing can be considered negligible.

The fall in flashing efficiency at the higher pulsing rates for the single pulsing run of -10 KV cm^{-1} is attributed to the large build up of the clearing field, which reduces the effective applied field.

However, similar measurements were made for applied fields of 10.5 KV cm^{-1} and 11.0 KV cm^{-1}, and the flashing efficiencies were found to increase with pulsing rate, see figure 7.13. The figures give evidence of spurious flashing, so the applied field must be carefully chosen, in order to work at higher flashing rates without the occurrence of spurious flashing.

7.4.3 SENSITIVE TIMES

The variation of layer efficiency of the tubes with time

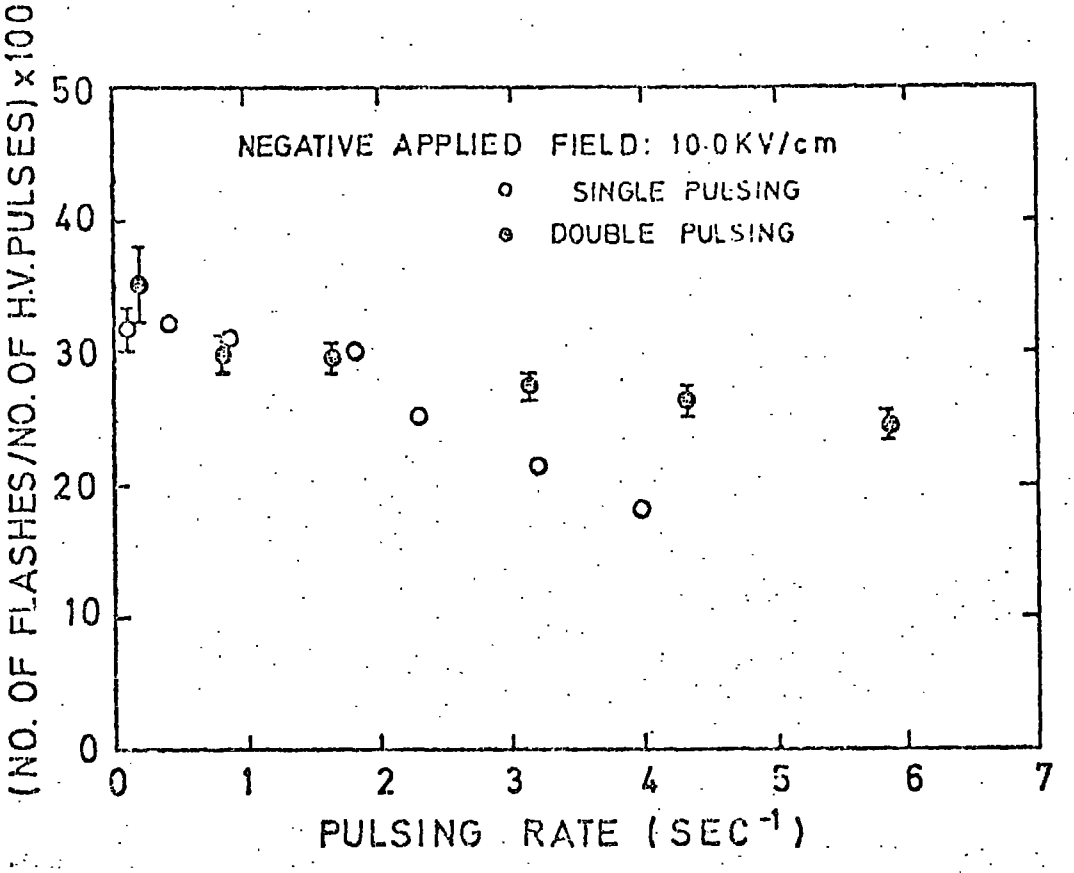

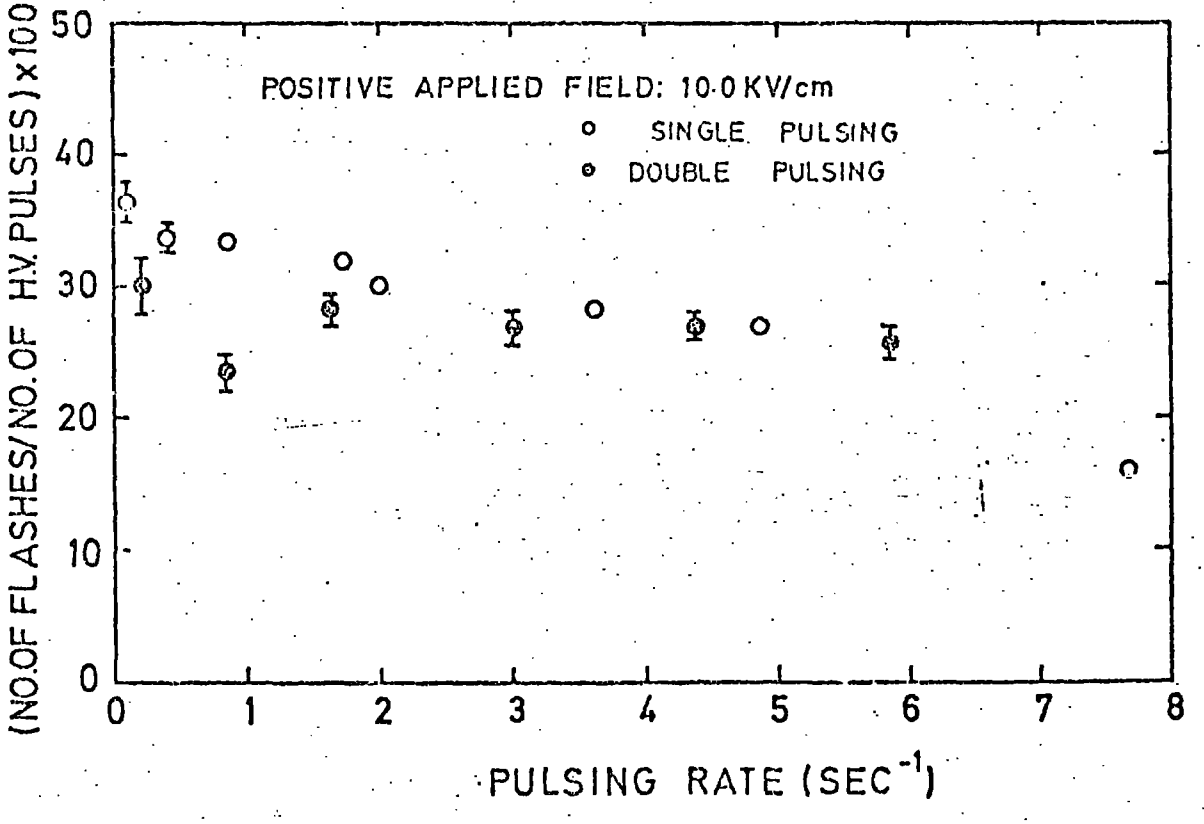

Fig. 7.12

Flashing efficiency versus pulsing rate for applied fields of 10·0 KV/cm.

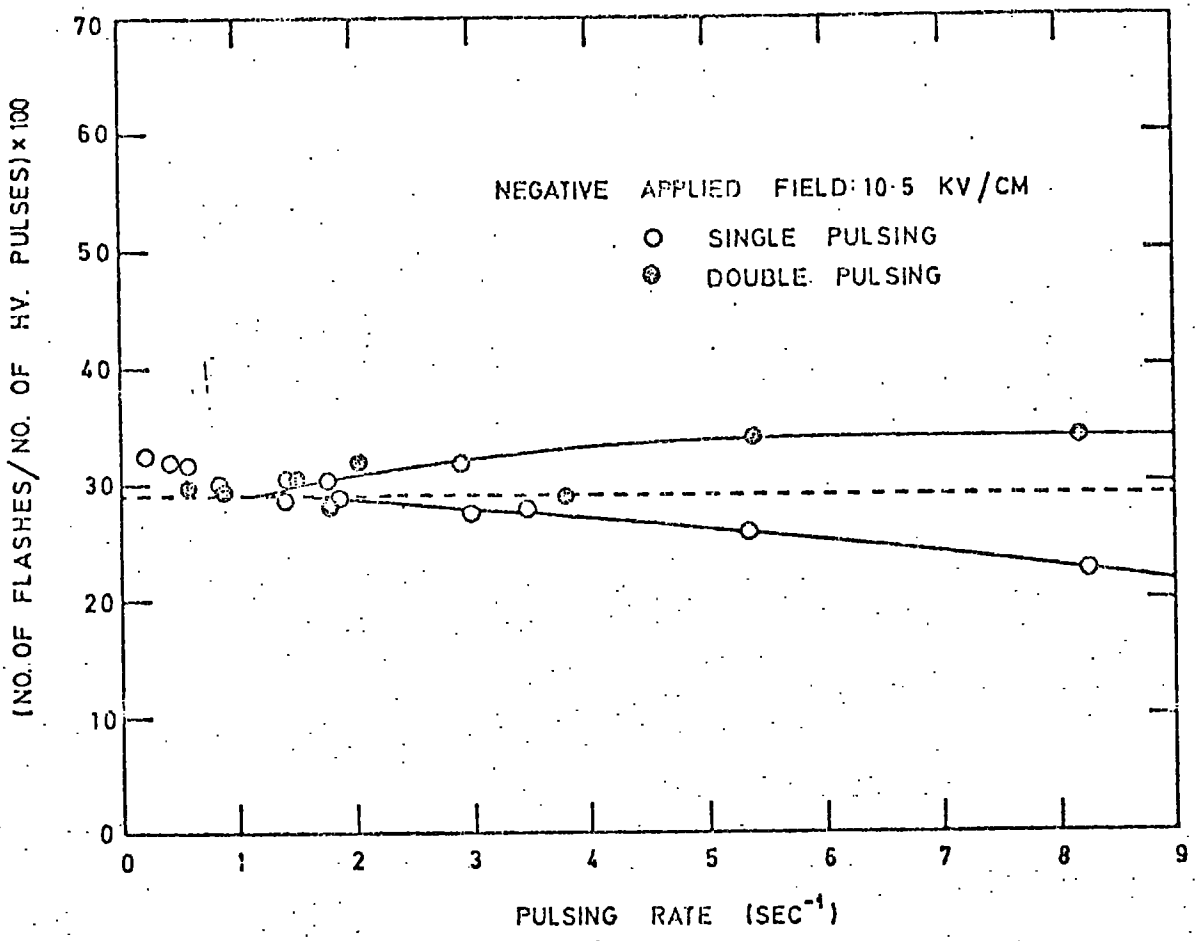

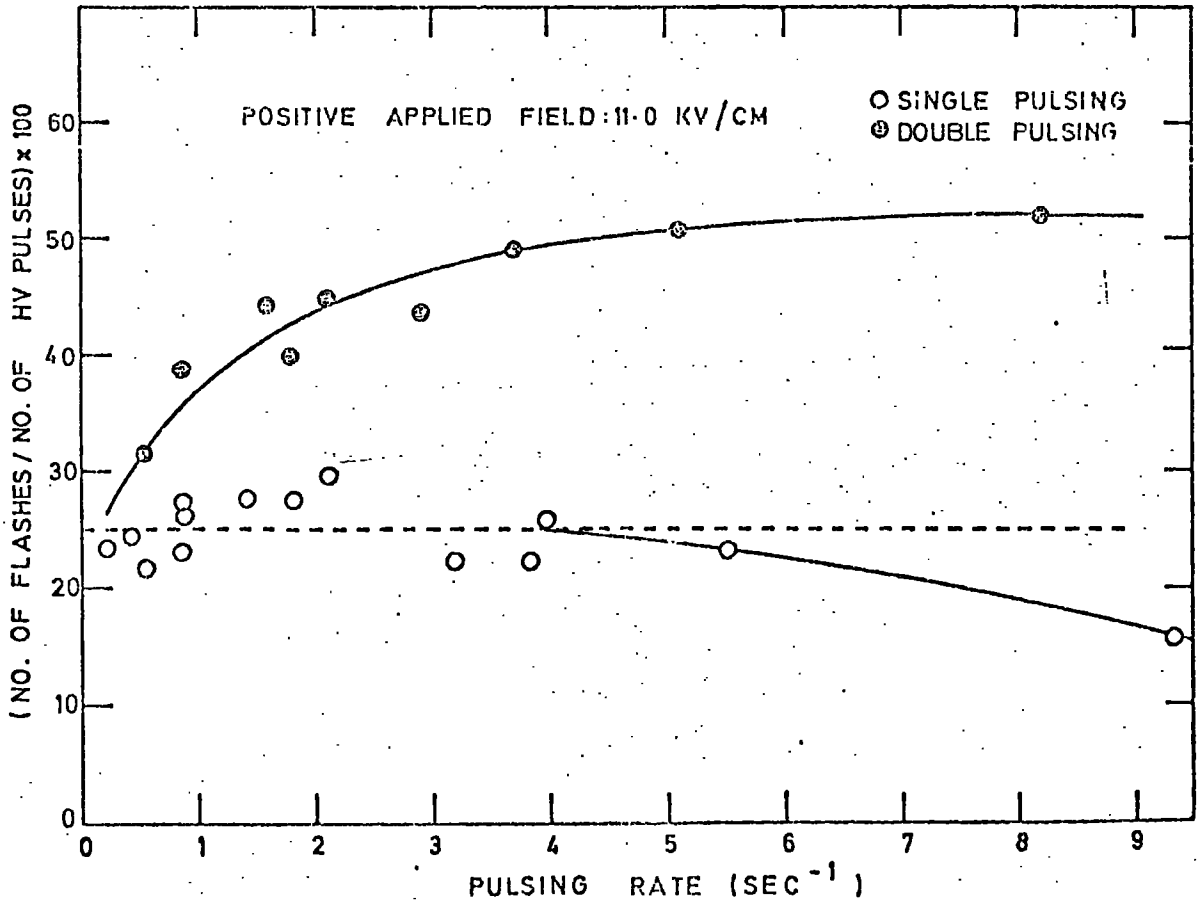

Fig. 7.13 Flashing efficiency versus pulsing rate for applied fields greater than 10.0 KV/cm .

delay was measured using the double and single pulsing systems. The measurements were made for single cosmic muon traversals through an array of three layers of tubes, separated by earth and H.T. plates. The passage of a muon through the array being registered by a two fold coincidence of plastic scintillators placed above and below the array. A diagram of the apparatus is shown in figure 7.14.

The dependence of the layer efficiency on time delay obtained from single pulsing of the array is shown in figure 7.15, for positive and negative polarity fields. An externally applied clearing field was not used. From these curves the sensitive times of the tubes were found to be 27 μ sec. and 7 μ sec. for positive and negative applied fields respectively.

The shorter sensitive time for the negative applied field is further evidence of the remanent clearing fields taking a longer time to decay for negative applied fields. The clearing fields then sweep any primary ionisation produced by an ionising particle in a tube, away from the sensitive volume, leading to a reduction in the sensitive time of the tubes.

The variation of the layer efficiency as a function of time delay was also investigated using the double pulsing system, and using different applied alternating square wave clearing fields working at 100 Hz.

The coupling of the clearing field arrangement to the H.T. plates of the array is shown in figure 7.14. The value of the resistor R_1 was taken as 2 MΩ ($R_1 \gg R_2$), providing a high resistance link to ground for the charging capacitors (C_1). The value of C_2 was 0.1 μF, which presented a low impedance path to ground for the high voltage pulse, thus protecting the clearing field assembly. The

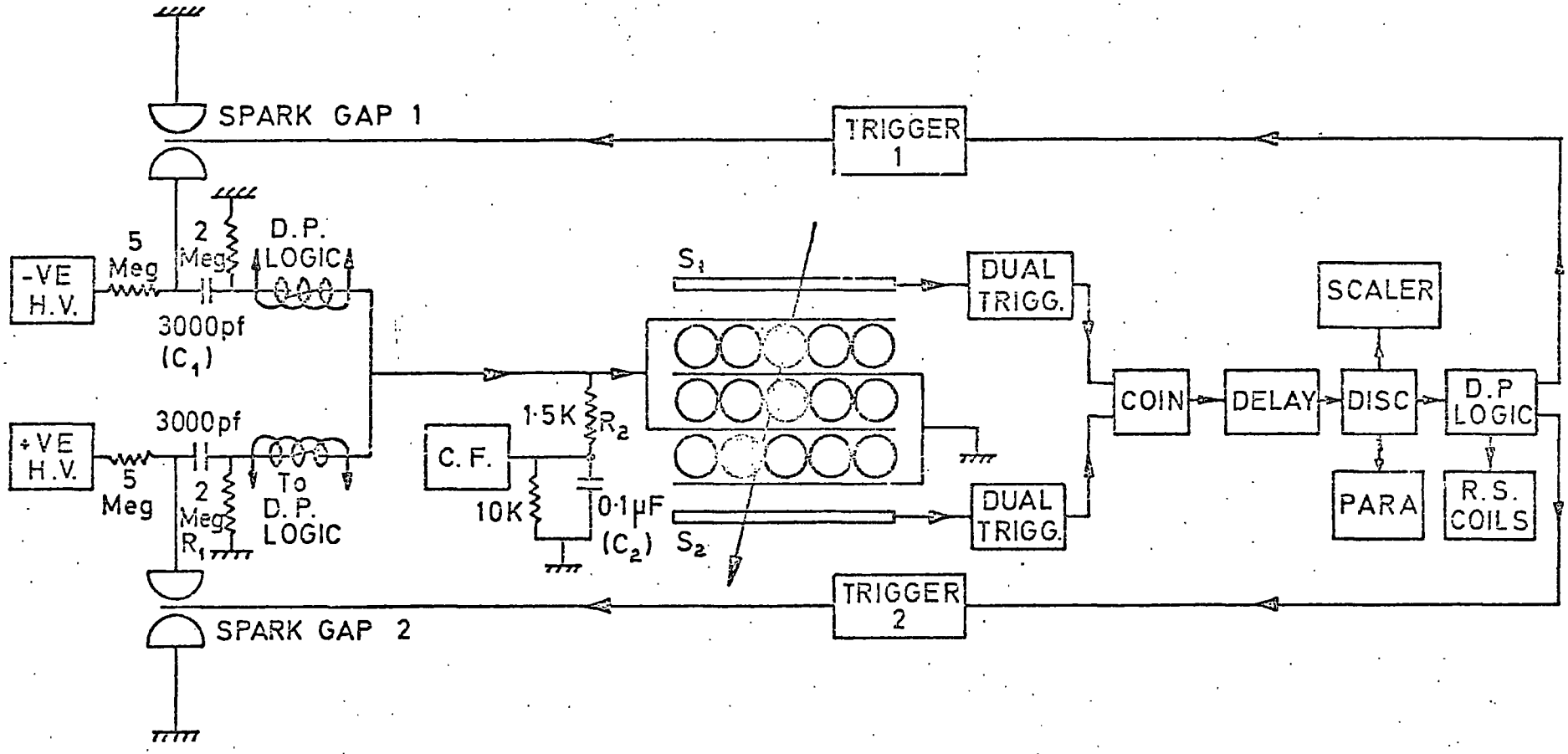

Fig. 7·14 The high voltage pulsing and clearing field arrangement .

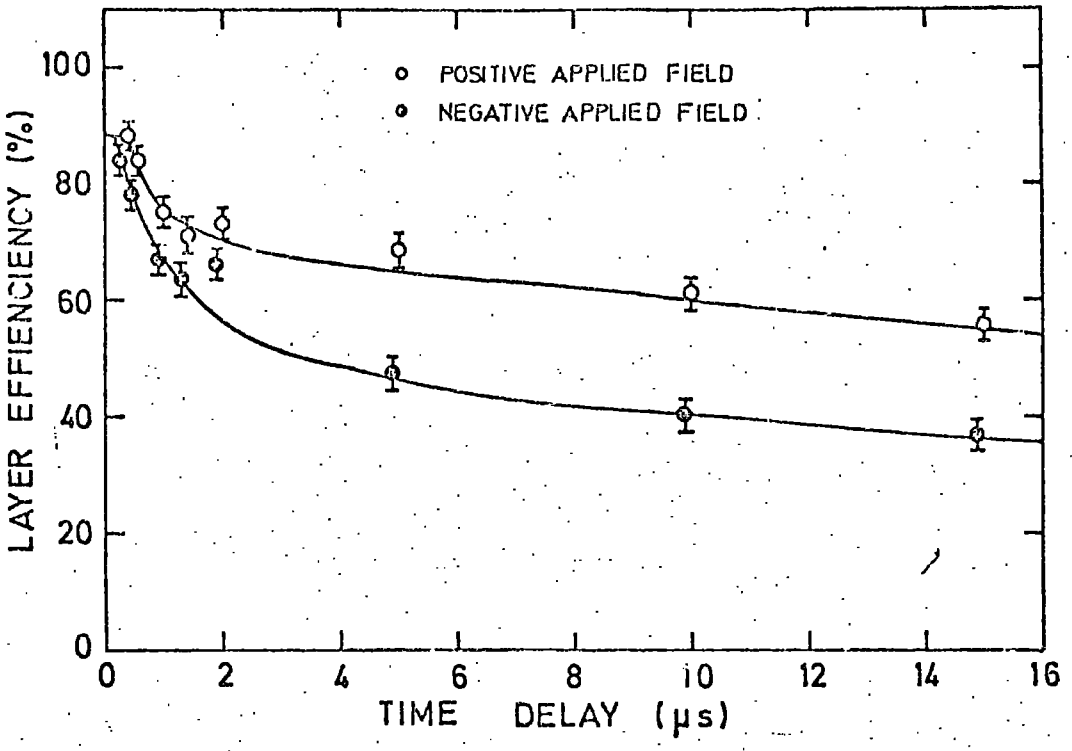

Fig. 7.15 Efficiency versus time delay for different polarities of the applied field.

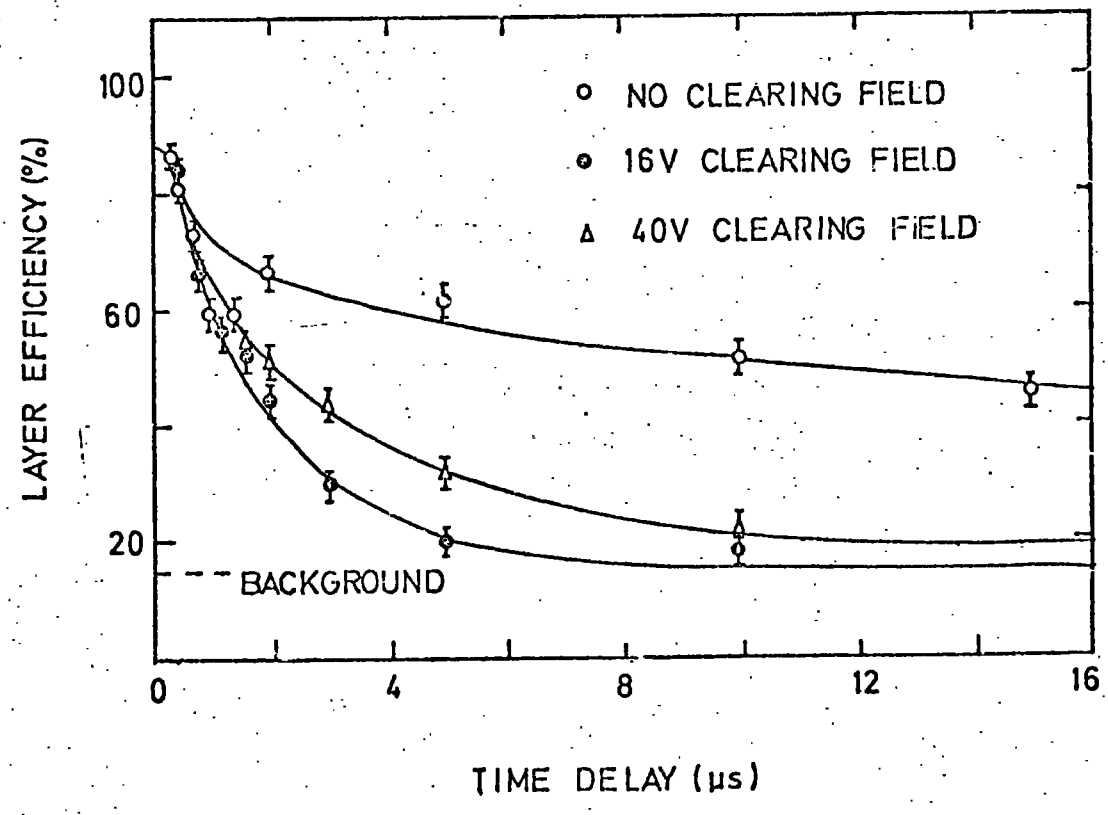

Fig. 7.16 Efficiency versus time delay for different applied clearing fields and using the modified pulsing system.

results obtained are shown in figure 7.16, and the sensitive times obtained are shown in table III.

TABLE III

Clearing Field (V cm^{-1})	Sensitive Time (μsec.)
0	1.8
16	2.7
40	1.8

7.5 CONCLUSIONS

The results presented in this chapter (7), together with the results given in chapter 4 (1), prove conclusively the presence of remanent clearing fields in the small diameter, high pressure, methane doped flash tubes.

The measurements of the digitisation pulse heights for various flashing rates given in this chapter show that very large clearing fields are built up after a discharge; these fields then decay with time, the rate of decay depending on the resistance and capacitance of the tubes.

The rates of decay of the induced fields were estimated from the digitisation pulse heights and were found to be very dependent on the polarity of the applied field. The decay constant for the induced field resulting from a negative applied high voltage pulse was found to be about 30 sec., more than an order of

magnitude greater than that obtained for a field resulting from a positive applied high voltage pulse. The existance of these effects was also supported by the results obtained on the tube layer efficiencies for various time delays, where the sensitive time of the tubes for a negative applied field was found to be about three times smaller than the value obtained for positive applied fields.

These polarity effects probably result from the outside surface conductivity of the tubes contributing to the decay process of the induced fields.

The decay constants of the induced fields were found to be very small immediately after the discharge. These small values may be due to the surface conductivity of the inside surfaces of the tubes being greatly modified by the presence of the gas plasma, an effect observed by Fowler and Sakuntala (8).

The effects of the residual clearing fields on the operation of the flash tubes can be greatly reduced if a pulsing system is employed which alternately applies fields of negative and positive polarity. The mean digitisation pulse heights obtained using such a pulsing system are found to remain constant for flashing rates up to 1.5 sec^{-1}.

The suitability of the pulsing system at higher flashing rates has yet to be tested in a particle beam.

REFERENCES

1. Breare, J.M., Nandi, B.C., Tait, I.D. (1976) Nucl. Inst. & Meth. in the Press

2. Breare, J.M., Chaney, J.E., Doe, P.J., El Disouki, W, Nandi, B.C., Tait, I.D. (1976) Nucl. Inst. & Meth. in preparation

3. Stubbs, R.J. (1971) Ph.D. Thesis, University of Durham

4. Breare, J.M., Nandi, B.C., Tait, I.D. (1976) Nucl. Inst. & Meth. 133 415

5. Ashton, F., Breare, J.M., Holroyd, F.W., Tsuji, K., Wolfendale, A.W. (1971) Lett. Nuovo Cim. 2 707

6. Raether, H. (1964) Electron Avalanches and Breakdown in Gases. Butterworths, London.

7. Breare, J.M., Nandi, B.C., Tait, I.D. (1976) Nucl. Inst. & Meth. in preparation

8. Fowler, R.G., Sakuntala, M. (1957) Jour. Chem. Phys. 27 824

CHAPTER EIGHT

CONCLUSION AND FUTURE WORK

8.1 CONCLUSION

In this thesis the analysis of the results obtained using a prototype flash tube chamber on a positron beam, in the detection of electromagnetic showers, has been described, and an account of the investigations made into the characteristics of small diameter, methane doped tubes, developed for a modified chamber is presented, together with details of the subsequent development of this detector.

The prototype chamber was tested in a beam, where positrons having energies between 0.5 and 3.5 GeV were made to produce electromagnetic showers in the chamber, which proved very satisfactory in the detection of these showers, and functioned without any deterioration in efficiency at repetition rates up to 50 Hz (1). For incident positrons of energy 2.5 GeV, the chamber gave an energy resolution of $\pm$ 13%, a spatial resolution of $\pm$ 8 mm. and an angular resolution of $\pm 2^{o}$ (2). These results were very promising, as relatively large diameter flash tubes were used (1.6 cm. internal diameter) and the resolutions obtained were comparable with those of present methods of electromagnetic shower detection.

In order to increse the working rate and improve spatial and energy resolutions, small diameter (0.8 cm. internal diameter) tubes, doped with methane, were designed by Chaney et al. (1) to be

used in a modified chamber.

The characteristics of these tubes were studied in great detail, the results leading to several alterations in the design of the modified chamber.

Unlike conventional small diameter, high pressure flash tubes, the methane doped tubes designed by Chaney et al. required very stringent operating conditions.

Due to the quenching effect of the methane on the discharge of a tube, they required very high electric fields of about 9-10 KV cm^{-1}, having rise times of 70 nsec. or less (3).

The digitisation pulse heights obtained were found to be very dependent on the tube-H.T. plate separation. A good contact between a tube and the H.T. plate was found to produce greatly increased digitisation pulse heights. This lead to the re-design of the H.T. plates of the modified chamber to ensure good tube-H.T. plate contact.

The tubes were doped with methane to give recovery times of less than 0.6 msec. (1) so that high repetition rates were possible. However, due to the build up of very large internal clearing fields resulting from the deposition of charge inside the tubes after a discharge, the working rate was severely restricted to several events per minute per tube (4).

The modified flash tube chamber containing the small diameter, methane doped tubes was tested in a positron beam, as was the case with the prototype chamber, however, at very low repetition rates.

The modified chamber proved very satisfactory in the detection of the electromagnetic showers produced in it by the positrons,

giving greatly improved resolutions, most notably in the higher energy range where the prototype chamber suffered severe shower leakage. The resolutions obtained were comparable to those of present very complex and expensive detecting systems.

For 2.5 GeV positrons the modified chamber gave an energy resolution of ± 11% (5), a spatial resolution of ± 3 mm. and an angular resolution of ± 2^{o} (6).

The very low repetition rates neccessary to ensure satisfactory operation of the small diameter, methane doped tubes greatly restricts the use of the tubes in accelerator experiments, however, a method of increasing their working rate using a modified pulsing system was pursued.

The polarity of the field applied to a flash tube was changed after each application of the field. This greatly reduced the magnitude of the induced clearing fields built up, thereby increasing the possible working rate.

Much information was gained on the magnitude and decay time of the induced fields from data obtained using the modified pulsing system.

Using this system the tubes operate satisfactorily up to 1.5 Hz (7), however, the system has yet to be tested at higher repetition rates on a positron beam.

The magnitudes of the induced clearing fields were measured from the digitisation pulse heights, and were found to be greater than 500 V one second after the discharge.

The rates of decay of the induced fields were also found to depend on the polarity of the applied field; CR decay constants of 28 sec. and 0.6 sec. were obtained for negative and positive

applied fields respectively. The outside surfaces of the tubes are thought to be responsible for these polarity effects.

8.2 FUTURE WORK

Work to be done in the near future will involve investigations into reductions of the induced fields built up inside the small diameter, methane doped flash tubes. This reduction may be achieved using the double pulsing system mentioned in the previous section. This may involve investigations into the shape of the applied high voltage pulse if very high repetition rates are required, where a pulse shape giving maximum tube efficiency together with minimum charge deposition would be found.

Another possible method is the treatment of the flash tubes in order to produce surfaces less susceptible to charge build up. The use of a glass other than Jena 16B in the flash tube manufacture may provide a solution.

Further development has also to be done on the modified flash tube chamber. If a double pulsing system is found satisfactory in the reduction of the induced clearing fields, then the integrated circuitry which records the digitisation pulses will have to be modified to accept pulses of either polarity.

The chamber frame can also be re-designed in order that the the chamber may be variably extended in the longitudinal direction, with the view of increasing the electron sensitivity together with the upper limit in energy detection. Optimum target thicknesses and module separations for given energy ranges could be investigated. Monte Carlo simulations of shower development in the chamber can

be done and the resolutions obtained compared with those from experiment.

Work can be done on the handling of the data from the chamber. "On line" computer links used at present are very complex; the possible use of magnetic tape drive units coupled directly to the chamber could be investigated. The use of microprocessors linked to the chamber, giving direct measurements of shower energies and axes can also be looked into.

Once the successful operation of the modified chamber at high repetition rates has been achieved, then work can begin on longer, small diameter tubes with the aim of building a flash tube chamber capable of covering large detecting areas.

REFERENCES

1. Chaney, J.E., Breare, J.M. (1975) Nucl. Inst. & Meth. 124 61

2. Chaney, J.E., Breare, J.M., Tait, I.D. (1975) Nucl. Inst. & Meth. 125 189

3. Breare, J.M., Nandi, B.C., Tait, I.D. (1976) Nucl. Inst. & Meth. 133 415

4. Breare, J.M., Nandi, B.C., Tait, I.D. (1976) Nucl. Inst. & Meth. In the Press

5. Breare, J.M., Chaney, J.E., Doe, P.J., El Disouki, W., Nandi, B.C., Tait, I.D. (1976) Nucl. Inst. & Meth. in preparation

6. Breare, J.M., Chaney, J.E., Doe, P.J., El Disouki, W., Nandi, B.C., Tait, I.D. (1976) Nucl. Inst. & Meth. in preparation

7. Breare, J.M., Nandi, B.C., Tait, I.D. (1976) submitted to Nucl. Inst. & Meth.